

**“INVESTIGATION OF THIN LAYER ACTIVATION IN
STRATEGICALLY IMPORTANT RARE EARTH MATERIALS”**

A Thesis Submitted to the
University of Petroleum and Energy Studies

For the Award of
Doctor of Philosophy
in
Department of Mechanical Engineering

By
VARUN VIJAY SAVADI
June – 2022

SUPERVISORS

DR. D. P. SINGH

DR. SHYAM PANDEY



Mechanical Cluster
(Department of Mechanical Engineering, SOES)
University of Petroleum & Energy Studies
Dehradun – 248007, Uttarakhand

**“INVESTIGATION OF THIN LAYER ACTIVATION IN
STRATEGICALLY IMPORTANT RARE EARTH MATERIALS”**

A Thesis Submitted to the
University of Petroleum and Energy Studies

For the Award of
Doctor of Philosophy
in
Engineering

By
VARUN VIJAY SAVADI
(SAP ID: 500073886)
June – 2022

Supervisor
Dr. D. P. Singh
Associate Professor
University of Petroleum & Energy Studies
Dehradun 248007

Co-Supervisor
Dr. Shyam Pandey
Principal
Yogoda Satsang Mahavidyalaya
Ranchi -834004, Jharkhand



Mechanical Cluster
(Department of Mechanical Engineering, SOES)
University of Petroleum & Energy Studies
Dehradun – 248007, Uttarakhand

December-2022

DECLARATION

I declare that the thesis entitled “**Investigation of Thin Layer Activation in Strategically Important Rare Earth Materials**” has been prepared by me under the guidance of Dr. D. P. Singh, Associate Professor, Department of Physics University of Petroleum & Energy Studies. Dr Shyam Pandey, External Supervisor, Principal, Yogoda Satsang Mahavidyalaya. No part of this thesis has formed the basis for the award of any degree or fellowship previously.

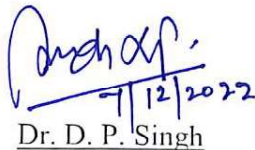


Varun Vijay Savadi
School of Engineering [SOE],
University of Petroleum & Energy Studies.
Dehradun-248007, Uttarakhand

Decemeber-2022

CERTIFICATE

I certify that Varun Vijay Savadi has prepared his thesis entitled “Investigation of Thin Layer Activation in Strategically Important Rare Earth Materials”, for the award of PhD degree of the University of Petroleum & Energy Studies, under my guidance. He has carried out the work at School of Engineering, University of Petroleum & Energy Studies.



7/12/2022

Dr. D. P. Singh

School of Engineering,

University of Petroleum & Energy Studies

Dehradun -248007, Uttarakhand

Date: 7-12-2022



Yogoda Satsanga Mahavidyalaya

(Established in 1967)

NAAC Accredited B++ (CGPA 2.89)

Affiliated to Ranchi University & registered under 2 (F) & 12 (B) of UGC Act



December-2022

CERTIFICATE

I certify that Varun Vijay Savadi has prepared his thesis entitled “Investigation of Thin Layer Activation in Strategically Important Rare Earth Materials”, for the award of PhD degree of the University of Petroleum & Energy Studies, under my guidance. He has carried out the work at School of Engineering, University of Petroleum & Energy Studies.

Dr. Shyam Pandey

External Supervisor,

Yogoda Satsang Mahavidyalaya

Ranchi -834004, Jharkhand

Date: 7-12-2022

Jagannathpur, Dhurwa, Ranchi 834004, Jharkhand

Email: y:m.principal@y:ei.edu.in, Web: www.ysmranchi.net

Under the auspices of YOGODA SATSANGA SOCIETY OF INDIA

Founder: SRI SRI PARAMAHANSA YOGANANDA • President: SRI SRI SWAMI CHIDANANDA GIRI



ABSTRACT

Recently there has been steady increase in the global energy demands over past couple of decades due to rapid advancement in technology and modern society. Rising energy demands with focus on developing green technologies to address global climate challenge is inevitably coupled with surface degradation phenomena like friction and wear. Increased greenhouse gas emissions from presently available non-renewable sources have resulted in global shift towards a foreseeable advancement in renewable technologies in coming few decades. Advancement of newer technologies will certainly comprise of multiple mating components, machineries and equipments for increased efficiency and output. Investigation of precise friction, wear and other surface degradation process leading to economic loss is need of concern in coming days. There are several well established tools and techniques for monitoring performance of machine components subjected to friction and wear phenomena. Tribology forms the backbone for investigation of frictional and wears losses in industry. Several tribology set-ups such as pin-on-disc, pin-on-plate, ball on disc, twin disc, continuous abrasion, taber abrasion, tumbler, jet impingement etc coupled with electrical set-ups and sensors have been successfully tested and used for estimating amount of wear induced in various industrial applications. The existing research and industries have come up with many tools (hard-ware and software) coupled to the tribological investigation set-ups for improvised monitoring of surface degradation in materials subjected to friction and wear. Acoustic emission signal analysis has been a success in monitoring tool wears condition in machining operations such milling and turning. Even with availability of many tools and techniques there is a need of new solution which can be helpful in monitoring surface degradation very easily across multidisciplinary fields and various materials. Investigation of wear by a new technique capable of ousting these issues is needed and is demand of current scenario. Thin Layer Activation is a very new tool and approach for estimating precise amount of wear in any industrial component or material subjected to surface degradation phenomena. Thin

Layer Activation has gained a significant importance in past few years due to its precise and accurate measurement of wear and other surface phenomena in various industries. In the present work, an attempt has been made to explore feasibility of a very new approach of measuring surface activity in some strategically important rare earth materials viz; Terbium, Thullium & Tantalum alongwith Nickel material having wide range of industrial applications and significance. Irradiations with these materials were done to observe nuclear interactions and systematics through direct measurement method in which stacks of respective target materials have been irradiated with heavy ion Oxygen beam available at one of the national laboratory which is Inter University Accelerator Center, New Delhi, India for carrying out irradiation studies. The standard beam energy range available at accelerator facility was $\approx 70-110$ MeV. Data obtained through irradiations have been further used to explore the feasibility of TLA based applications to identify specific reaction products in a very thin layer of the material. The results showed that the proposed methodology of measuring surface activity in materials is feasible with high accuracy, precision and can be used in industrial applications to estimate surface degradation phenomena's ranging from few micrometers to nanometers. By using TLA, surface degradation in materials can be estimated in few hours as compared to that of the conventional techniques in which component or material specimen are subjected for longer cycles of operation to deduce results. The proposed methodology uses offline γ -spectroscopy arrangement coupled with High Purity Germanium Detector set-up for detection of worn out fraction mass of particles after irradiation. The relative activity induced across the overall thickness of target materials after beam irradiation is the rate of interaction. The rate of interaction between beam and material further estimates the maximum yield and surface activity distribution in material across the entire depth of stack. Results showed the maximum depth of interaction in the form of activity ranges from 12-16 μm in rare earth materials specimen of Terbium, Thullium, Tantalum in standard operating accelerator conditions using Oxygen beam & 25 μm in Nickel material while using Alpha beams.

I Dedicate My Ph.D. Thesis to

My Loving Parents, Family, Friends and My Guide

Dr. D. P. Singh

&

Dr. Shyam Pandey

for their endless support, blessings and guidance

Acknowledgment

I bow my head humbly to pay heartfelt regards to Almighty God for giving me the strengths and blessing in completing this thesis.

Foremost, I would like to express my sincere gratitude to my PhD thesis supervisors Dr. D. P. Singh and Dr. Shyam Pandey, for picking me up as a student at the critical stage of my career and the continuous support of my Doctoral study and research, for their patience, motivation, enthusiasm, and immense knowledge. Their guidance helped me in all the time of research and writing of this thesis.

Besides my supervisors, I would like to thank the University of Petroleum and Energy Studies for their encouragement, suggestions and valuable support for my research work. I would like to thank Cluster Heads of Mechanical Engineering & Applied Science Departments, Dr. Ajay Kumar, Dr. Ashish Karn, Dr. Manish Garg, Dr. Rakesh. K, Dr. Santosh Dubey, Dr. S. K. Joshi, Dr. Kailash Pandey, Dr. Prashant Rawat and Dr. S. M. Tauseef and all colleagues in the University for their insightful comments, encouragement feedback and cooperation. I would also like to extend my special thanks to Nuclear Physics Group, Aligarh Muslim University for providing data regarding nuclear interactions and their continuous support.

Further, I extend my sincere thanks to Dr. D. K. Avasthi, Dean (R&D) & Dr Gurvinder Singh Virk, Dean (SOES) for their constant guidance and support which helped me in staying motivated and organized for completion of doctoral research work.

Finally, I would like to express my gratitude to my family for all of the love, support, encouragement, and prayers they have sent my way along this journey. I am eternally indebted to my loving parents and in-laws for all the sacrifices they have made on my behalf. I would like to express sincere gratitude to my parents who believed in me and provided encouragement during challenging times. Your unconditional love and support in the moments when there was no one to answer my queries has helped me immensely.

TABLE OF CONTENT

DECLARATION	iii
CERTIFICATE (INTERNAL)	iv
CERTIFICATE (EXTERNAL)	v
ABSTRACT	vi
ACKNOWLEDGEMENT	ix
TABLE OF CONTENT	x
LIST OF FIGURES	xiii
LIST OF TABLES	xviii
CHAPTER 1: INTRODUCTION	1
1.1 Background	1
1.2 Activation Methods	10
1.2.1 Bulk Neutron Activation	10
1.2.2 Recoil Nuclei Implantation (UTLA)	13
1.2.3 Radioactive Ion Implantation	15
1.2.4 Thin Layer Activation Method (TLA)	17
1.3 Literature Review	19
1.4 Rare Earth & strategically important materials for our research & their importance	24
1.5 Motivation, Research Gap & Objectives	29
References	31
CHAPTER 2: THIN LAYER ACTIVATION METHODOLOGY	39
2.1 TLA Mechanism	39
2.2 TLA Theory	39
2.3 Advantages of TLA compared to conventional techniques	41
2.4 Measurement Methods	42
2.4.1 Direct Measurement Technique	42
2.4.2 Indirect Measurement Technique	43
2.5 Pre-requisites for TLA investigations	44

2.5.1 Radioactivity Detection	44
2.5.2 Detectors selection	46
2.5.2.1 Scintillation detectors	47
2.6 TLA Electronics for Detection	47
References	48
CHAPTER 3: EXPERIMENTAL METHODOLOGY	51
3.1 Pelletron Accelerator at IUAC	51
3.2 Sample Preparation	53
3.2.1. Rolling Technique	53
3.2.2. Thickness measurement using α -transmission method....	56
3.3 Stack foil activation technique	58
3.4 Irradiation	61
3.5 Post-irradiation analysis	62
3.5.1 Calibration and Efficiency Determination of HPGe	62
3.5.2 Identification of Reaction Products	64
3.5.3 Determination of the nuclear reaction production cross-section	65
3.5.4 Experimental Uncertainties; Error Analysis	69
References	70
CHAPTER 4: MEASUREMENTS & RESULTS	
4.1 Thin Layer Activation (TLA) investigations using Oxygen & Alpha ion beams	72
4.2 Stack Foil Activation details	74
4.3 TLA reactions initiated using Oxygen (heavy ion) beam	78
4.3.1 TLA investigations in spectroscopically pure ($\approx 99\%$) Terbium	78
4.3.1.1 Measurement of Cross-Section and Yield Curves	79
4.3.1.2 Measurement of Activity and Calibration Curves	83
4.3.2 TLA investigations in spectroscopically pure ($\approx 99\%$) Thulium	87
4.3.2.1 Measurement of Cross-Section and Yield Curves	88
4.3.2.2 Measurement of Activity and Calibration Curves	92

4.3.3 TLA investigations in spectroscopically pure (\approx 99 %) Tantalum	97
4.3.3.1 Measurement of Cross-Section and Yield Curves	97
4.3.3.2 Measurement of Activity and Calibration Curves	102
4.3.4 Comparative study in different Rare Earth Materials using Oxygen (heavy ion) beam	106
4.3.4.1 Measurement of Cross-Section and Yield Curves	106
4.3.4.2 Measurement of Activity and Calibration Curves	114
4.4 TLA reactions initiated using Alpha (heavy ion) beam	127
4.4.1 TLA investigations in natural Nickel material using Alpha ion beam	127
4.4.2 Measurement of Cross-Section and Yield Curves	129
4.4.3 Measurement of Activity and Calibration Curves	133
4.5 Results & Discussions	136
References	137
CHAPTER 5: CONCLUSIONS AND FUTURE PERSPECTIVES	140

FIGURES

CHAPTER 1: INTRODUCTION		
Fig 1	Classification of Engineering Material	2
Fig 2	Ball On Disc Setup (BOD)	4
Fig 3	Block On Ring Setup (BOR)	4
Fig 4	Pin On Disc Setup (POD)	5
Fig 5	Taber Abrasion Setup	5
Fig 6	Four Ball Tester (FBT)	6
Fig 7	Twin Disc Tribometer Setup	7
Fig 8	Jet Impingement Tester	7
Fig 9	Characteristics of different Ion Beams	9
Fig 10	Recoil Nuclei Implantation	13
Fig 11	Calibration curve $A/A_0 = f(x)$ with ^{56}Co nuclei implantation into nickel (16 MeV protons, tubular geometry and acceptance cone $[30^\circ-38^\circ]$)	15
Fig 12	Principle of the ^7Be implantation	16
Fig 13	^7Be distribution in a PTFE target	17
Fig 14	Working principle of charged particle activation	17
Fig 15	Experimental measurements for the $^{\text{nat}}\text{Fe}(p,n)^{56}\text{Co}$ Cross Section up to 50 MeV bombarding energy	19
Fig 16	Example for a measured activity-versus-depth distribution of ^{56}Co in an iron alloy	19
Fig 17	Rare Earth Materials	25
Fig 18	Rare Earth Materials Applications	25
Fig 19	Global REE Consumption Sector Wise	26
Fig 20	US REE Consumption (2018) Sector Wise	26
Fig 21	Industrial sector wise consumption of Terbium	28
Fig 22	Industrial sector wise consumption of Tantalum	28
CHAPTER 2: THIN LAYER ACTIVATION METHODOLOGY		
Fig 2.1	Illustration of TLA mechanism (Courtesy A. Kleinrahm).	38

Fig 2.2	TLA calibration curve (total activity versus material depth)	39
Fig 2.3	Schematic illustration of Direct Measurement Technique.	42
Fig 2.4	Schematic illustration of Indirect Measurement Technique.	43
Fig 2.5	Schematic illustration of TLA electronics system.	47
CHAPTER 3: EXPERIMENTAL METHODOLOGY		
Fig 3.1	A schematic diagram of IUAC Pelletron Accelerator	52
Fig 3.2	Rolling Machine 1 at IUAC (a)	54
Fig 3.2	Rolling Machine 1 at IUAC (b)	55
Fig 3.3	Evaporator Machine at IUAC	56
Fig 3.4	Block diagram of α -transmission thickness measurement set-up	56
Fig 3.5	α -spectroscopy thickness measurement set-up at target laboratory, IUAC	57
Fig 3.6	Stack foil activation using offline energy degradation technique	59
Fig 3.7	Illustration of random target sample stack calculations using energy degradation technique	60
Fig 3.8	Side view of General Purpose Scattering Chamber (GPSC) (a) at IUAC	62
Fig 3.8	Inside view of General Purpose Scattering Chamber (GPSC) (b) at IUAC	62
Fig 3.9	Geometry dependent efficiency curves as a function of γ -ray energy at source-detector separations $d=1$ cm. Solid lines represent the best polynomial fit.	63
Fig 3.10	Experimentally observed decay curve; the count-rates have been plotted on semi-log graph as a function of lapse time, which indicates the half-life of corresponding residue produced in $^{16}\text{O} + ^{181}\text{Ta}$ system.	64

CHAPTER 4: MEASUREMENTS & RESULTS		
Fig 1	Yield curves of reaction products $^{172,171,170}\text{Ta}$ in Terbium material	81
Fig 2	Yield curves of reaction products $^{171,170}\text{Hf}$ in Terbium material	81
Fig 3	Yield curves of reaction products $^{171,170,169}\text{Lu}$, ^{165}Tm in Terbium material	83
Fig 4	Calibration curves of reaction products $^{172,171,170}\text{Ta}$ in Terbium material	84
Fig 5	Calibration curves of reaction products $^{171,170}\text{Hf}$ in Terbium material	86
Fig 6	Calibration curves of reaction products $^{171,170,169}\text{Lu}$, ^{165}Tm in Terbium material	87
Fig 7	Yield curves of reaction products $^{182,181}\text{Ir}$ in Thulium material	89
Fig 8	Yield curves of reaction products $^{182,181}\text{Os}$ in Thulium material	90
Fig 9	Yield curves of reaction products $^{182,178}\text{Re}$, ^{175}Hf , ^{172}Lu in Thulium material	92
Fig 10	Calibration curves of reaction Products $^{182,181}\text{Ir}$ in Thulium material	93
Fig 11	Calibration curves of reaction products $^{182,181}\text{Os}$ in Thulium material	95
Fig 12	Calibration curves of reaction products $^{182,178}\text{Re}$, ^{175}Hf , ^{172}Lu in Thulium material	96
Fig 13	Yield Curves of isotopes $^{194,193,192}\text{Tl}$ in Tantalum material	98
Fig 14	Yield Curves of isotopes $^{193,192}\text{Hg}$ in Tantalum material	99
Fig 15	Yield Curves of isotopes $^{192,191,190}\text{Au}$ in Tantalum material	101
Fig 16	Calibration Curves of isotopes $^{194,193,192}\text{Tl}$ in Tantalum material	102
Fig 17	Calibration Curves of isotopes $^{193,192}\text{Hg}$ in Tantalum	104

	material	
Fig 18	Calibration Curves of isotopes $^{192, 191, 190}\text{Au}$ in Tantalum material	105
Fig 19	Relative Yield curves of isotopes ^{172}Ta , ^{182}Ir , ^{194}Tl from Tb, Tm & Ta material	109
Fig 20	Relative Yield curve of isotopes ^{171}Ta , ^{181}Ir , ^{193}Tl from Tb, Tm & Ta material.	109
Fig 21	Relative Yield curves of isotopes ^{170}Ta & ^{194}Tl from Tb & Ta material.	110
Fig 22	Relative Yield curves of isotopes ^{171}Hf , ^{181}Os & ^{193}Hg from Tb, Tm & Ta material.	110
Fig 23	Relative Yield curves of isotopes ^{170}Hf & ^{192}Hg from Tb & Ta material.	111
Fig 24	Relative Yield curves of isotopes ^{171}Lu & ^{181}Re from Tb & Tm material.	112
Fig 25	Relative Yield curves of isotopes ^{170}Lu & ^{192}Au from Tb & Ta material.	113
Fig 26	Relative Yield curves of isotopes ^{169}Lu & ^{192}Au from Tb & Ta material.	113
Fig 27	Relative Yield curves of isotopes ^{178}Re & ^{190}Au from Tm & Ta material.	114
Fig 28	Calibration curves of isotopes ^{172}Ta , ^{182}Ir , ^{194}Tl from Tb, Tm & Ta materials at incident energies ranging from 95 to 70 MeV	116
Fig 29	Calibration curves of isotopes ^{171}Ta , ^{181}Ir , ^{193}Tl from Tb, Tm & Ta materials at incident energies ranging from 95 to 70 MeV.	118
Fig 30	Calibration curves of isotopes ^{170}Ta & ^{194}Tl from Tb & Ta materials at incident energies ranging from 95 to 70 MeV	119
Fig 31	Calibration curves of isotopes ^{171}Hf , ^{181}Os & ^{193}Hg from Tb, Tm & Ta materials at incident energies ranging from	120

	100 to 70	
Fig 32	Calibration curves of isotopes ^{170}Hf & ^{192}Hg from Tb & Ta materials at incident energies ranging from 100 to 70 MeV	122
Fig 33	Calibration curves of isotopes ^{171}Lu & ^{181}Re from Tb & Tm materials at incident energies ranging from 95 to 65 MeV	122
Fig 34	Calibration curves of isotopes ^{170}Lu & ^{192}Au from Tb & Ta materials at incident energies ranging from 100 to 65 MeV	125
Fig 35	Calibration curves of isotopes ^{169}Lu & ^{192}Au from Tb & Ta materials at incident energies ranging from 100 to 65 MeV	125
Fig 36	Calibration curves of isotopes ^{178}Re & ^{190}Au from Tm & Ta materials at incident energies ranging from 100 to 70 MeV.	127
Fig 37	Relative Yield curves for $^{58\text{nat}}\text{Ni}$ Material	131
Fig 38	Relative Yield curves for $^{60\text{nat}}\text{Ni}$ Material	132
Fig 39	Relative Yield curves for $^{61\text{nat}}\text{Ni}$ Material	132
Fig 40	Calibration curves for $^{58\text{nat}}\text{Ni}$ at incident energies ranging from 10-40 MeV	134
Fig 41	Calibration curves for $^{60\text{nat}}\text{Ni}$ at incident energies ranging from 10-40 MeV	134
Fig 42	Calibration curves for $^{61\text{nat}}\text{Ni}$ at incident energies ranging from 10-40 MeV.	135

TABLES

CHAPTER 1: INTRODUCTION		
Table 1	List of Deuteron induced TLA reactions in various Metals / Elements	21
Table 2	List of Proton induced TLA reactions in various Metals / Elements	22
Table 3	List of He & α induced TLA reactions on various Metals / Elements	23
Table 4	Important properties for Terbium, Thulium, Tantalum and Nickel material	29
CHAPTER 3: EXPERIMENTAL METHODOLOGY		
Table 1	Sample stack thickness calculations by SRIM / TRIM	59
Table 2	A list of γ -ray energies and absolute intensities of some of the prominent γ -rays from standard γ -source ^{152}Eu .	63
CHAPTER 4: MEASUREMENTS & RESULTS		
Table 4.1	List of systems for which cross-sections, beam energy range and activation threshold energy measured	73
Table 4.2	Decay data of reaction products identified through reactions in Terbium material	76
Table 4.3	Decay data of reaction products identified through reactions in Thulium material	76
Table 4.4	Decay data of reaction products identified through reactions in Tantalum material	77
Table 4.5	Decay data of reaction products identified through reactions in nickel material with alpha beam.	78
Table 4.6	Measured cross-sections at different energies for reaction products identified in $^{16}\text{O} + ^{159}\text{Tb}$ through XN reaction channels for application in thin layer activation technique	80
Table 4.7	Measured cross-sections at different energies for reaction products identified in $^{16}\text{O} + ^{159}\text{Tb}$ through PXN reaction	80

	channels for application in thin layer activation technique	
Table 4.8	Measured cross-sections at different energies for reaction products identified in $^{16}\text{O} + ^{159}\text{Tb}$ through α -reaction channels for application in thin layer activation technique	82
Table 4.9	Residual Activity range distribution range in Terbium material for xn reaction channels using 16 Oxygen beam in energy range 70-95 MeV	85
Table 4.10	Residual Activity range distribution range in Terbium material for pxn reaction channels using 16 Oxygen beam in energy range 70-95 MeV	85
Table 4.11	Residual Activity range distribution range in Terbium material for alpha reaction channels using 16 Oxygen beam in energy range 70-95 MeV	86
Table 4.12	Measured cross-sections at different energies for reaction products identified in $^{16}\text{O} + ^{169}\text{Tm}$ through XN reaction channels for application in thin layer activation technique	88
Table 4.13	Measured cross-sections at different energies for reaction products identified in $^{16}\text{O} + ^{169}\text{Tm}$ through PXN reaction channels for application in thin layer activation technique	90
Table 4.14	Measured cross-sections at different energies for reaction products identified in $^{16}\text{O} + ^{169}\text{Tm}$ through alpha reaction channels for application in thin layer activation technique	91
Table 4.15	Residual Activity range distribution range in Thulium material for xn reaction channels using 16 Oxygen beam in energy range 70-95 MeV	94
Table 4.16	Residual Activity range distribution range in Thulium material for pxn reaction channels using 16 Oxygen beam in energy range 70-95 MeV	94
Table 4.17	Residual Activity range distribution range in Thulium material for alpha reaction channels using 16 Oxygen beam in energy range 70-95 MeV	96

Table 4.18	Measured cross-sections at different energies for reaction products identified in $^{16}\text{O} + ^{181}\text{Ta}$ through xn reaction channels for application in thin layer activation technique	98
Table 4.19	Measured cross-sections at different energies for reaction products identified in $^{16}\text{O} + ^{181}\text{Ta}$ through pxn reaction channels for application in Thin Layer Activation technique	100
Table 4.20	Measured cross-sections at different energies for reaction products identified in $^{16}\text{O} + ^{181}\text{Ta}$ through alpha reaction channels for applications in Thin Layer Activation technique	
	Residual Activity range distribution range in Tantalum material for xn reaction channels using 16 Oxygen beam in energy range 70-100 MeV	100
Table 4.21	Residual Activity range distribution range in Tantalum material for pxn reaction channels using 16 Oxygen beam in energy range 70-100 MeV	103
Table 4.22	Residual Activity range distribution range in Tantalum material for alpha reaction channels using 16 Oxygen beam in energy range 70-100 MeV	105
Table 4.23	Residual Activity range distribution range in Terbium, Thulium & Tantalum materials for 3N reaction channels using 16 Oxygen beam in energy range 70-110 MeV	115
Table 4.24	Residual Activity range distribution range in Terbium, Thulium & Tantalum materials for 3N reaction channels using 16 Oxygen beam in energy range 70-110 MeV	117
Table 4.25	Residual Activity range distribution range in Terbium, & Tantalum materials for 5N reaction channels using 16 Oxygen beam in energy range 70-110 MeV	118
Table 4.26	Residual Activity range distribution range in Terbium, Thulium & Tantalum materials for P3N reaction channels	120

	using ^{16}O Oxygen beam in energy range 70-110 MeV	
Table 4.28	Residual Activity range distribution range in Terbium & Tantalum materials for P4N reaction channels using ^{16}O Oxygen beam in energy range 70-110 MeV	121
Table 4.29	Residual Activity range distribution range in Terbium & Thulium materials for 2P2N reaction channels using ^{16}O Oxygen beam in energy range 70-110 MeV	123
Table 4.30	Residual Activity range distribution range in Terbium & Tantalum materials for αn reaction channels using ^{16}O Oxygen beam in energy range 70-110 MeV	124
Table 4.31	Residual Activity range distribution range in Terbium & Tantalum materials for $\alpha 2n$ reaction channels using ^{16}O Oxygen beam in energy range 70-110 MeV	126
Table 4.32	Residual Activity range distribution range in Thulium & Tantalum materials for $\alpha 3n$ reaction channels using ^{16}O Oxygen beam in energy range 70-110 MeV	126
Table 4.33	Spectroscopic properties of isotopes $^{60}, ^{61}\text{Cu}$ & $^{62}, ^{63}\text{Zn}$ used in Stack Foil Activation technique	130
Table 4.34	Maximum surface activity induced in Terbium material	136
Table 4.35	Maximum surface activity induced in Thulium material	136
Table 4.36	Maximum surface activity induced in Tantalum material	136
Table 4.37	Maximum surface activity induced in Nickel material	137

CHAPTER 1

INTRODUCTION

1.1 BACKGROUND

Role of materials has been pivotal in progress of human civilizations right from the beginning of Stone Age followed by Bronze & Steel Age. Influence of physical properties of any material affecting the thermodynamic characteristics in an atomic structure has led to development of metallurgical sciences through mining in 19th century [1-2]. Rapid progress in science and space technology has resulted in development of modern materials for industries like space, defense, power etc. Advancement of materials has a significant role in development of science & technology at faster rate. The swift progresses in evolvement of materials have improved our lives from all aspects through improvisation and development of existing products and new technologies [3-4]. Any material in use today is made of combination through several elements existing in nature [5-6]. These elements in the purest form lack the required physical, chemical, mechanical, thermal, electric and magnetic etc. properties which serve as a pre-requisite for selection of appropriate material before any practical application. Hence, it is very important to understand properties and classification of materials depending upon the applications. Engineering materials can be broadly classified into two main categories known as Metals and Non-Metals. Further sub-classification of these categories is presented in Fig. 1[5-6]. Recent advancement in Science & Technology has led to a positive shift towards establishment and growth of industries such as heavy engineering, conventional and/or nuclear power plants, manufacturing & processing industries. Machines and equipments used in industries like power plants, process & transportation systems are substantially influenced by surface degradation phenomena's such as erosion, corrosion and wear in materials, limiting the endurance and performance

reliability [7–10]. The functioning of the conventional power plants at elevated temperatures for increased efficiency and demand is often coupled with challenges such as degradation of structural materials subjected to extreme temperature and pressure operating conditions [8–10]. The materials used in pipelines in the nuclear power plants are often subjected to accelerated flow corrosion and thinning of welds at heat affected zones leading to failure of systems [11].

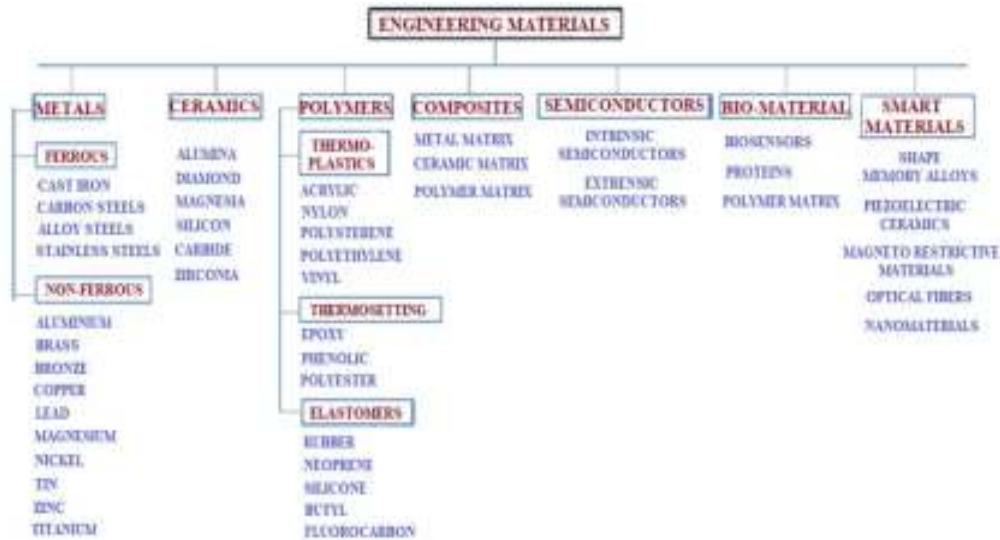


Fig. 1. Classification of Engineering Materials

Electric power industry and plants have been reported an estimated loss of around 150 million US\$ in a year in terms of efficiency, forced outages and repair costs due to solid particle erosion resulting mainly due to degradation of materials in use [12]. Various conventional non-destructive methods and techniques are available but with limitations to measure the material properties and surface defects occurring in various industries like; aerospace, manufacturing, process industries, military and defence, nuclear industry etc. [13]. Installation of offshore wind plants due to climate change has gained importance over a couple of years [14]. The materials used in monopile foundation and its components are subjected to varying wind currents leading to surface degradation and wear. Determination of reliable measurement methods for analysing material performance in such fluctuating conditions in offshore wind plants is an emerging challenge [14]. Some of the commonly

adopted non-destructive methods are visual inspection, microscopy, radiography, dye penetrant, ultrasonic, magnetic particle testing, eddy current for metals, acoustic emission testing etc [15]. New developments and sustainable solutions in medical field such as artificial joints replacement are gaining significant importance. In one of the recent studies, wear evaluation of artificial hip joints for wear couples of 28 mm CoCrMo femoral heads, against conventional and X-linked Ultra-High Molecular Weight Polyethylene acetabular cups were subjected to more than several million cycles to get desired results using gravimetric analysis [16]. Studies employing gravimetric analysis for measurement of wear in knee implants subjected to as many as 3 million working cycles for effective results [17]. In case of visual inspection and microscopy only macroscopic and small surface flaws can be detected. Radiography and dye penetrant testing are not suitable for porous materials. For ultrasonic testing material subjected under test necessarily needs to be good conductor of sound. Magnetic particle testing is applicable to its best only with ferromagnetic materials. Eddy current is limited only for metals and acoustic emission involves cost implications for testing of a component [18]. Assessment of non-contacting optical methods was carried out and successfully developed technique for measurement of wear up to 0.0001 mg in ceramics [19].

A very high sensitive and reliable tool technique is required to investigate the near surface phenomenon. Strategically important industries such as space, defense, power and other process industries comprise of various equipments and mating components. The materials with which parts of such components are fabricated are often subjected to friction and wear conditions. These working conditions account for considerable amount of economic losses which can be avoided by adapting newer technologies and appropriate tribological set-ups. Ever increasing population, globally growing energy demands coupled with control in CO₂ emissions have recently led to lot of progress in surface technology, lubricants, smart materials and tribological set-up designs to overcome losses incurred due to wear and friction in industries. Some of the widely used tribological set-ups for analysing performance,

characteristics and properties of materials subjected to different operating conditions are listed below;

BALL ON DISC [BOD] SETUP

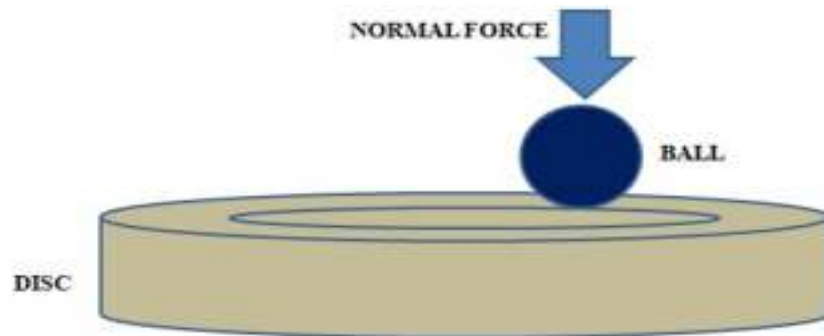


Fig. 2. Ball On Disc Setup (BOD)

In this setup, a ball of size as per the set standards is subjected to rolling/sliding motion against the rotating disc. The speed and force can be varied according to required testing conditions. Components such as drive splines on drive shafts, wheels at the lug bolt interface, and cylinder head gaskets which are often subjected to fretting wear due to varying thermal stresses under cyclic loading operated conditions can be tested with the help of BOD [20-24].

BLOCK ON RING [BOR] SETUP

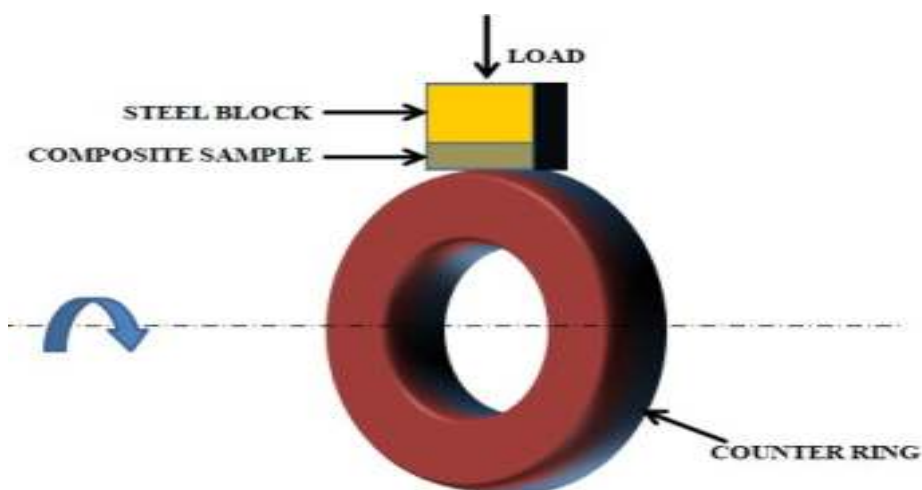


Fig. 3. Block On Ring Setup (BOR)

BOR is another form of tribological setup used for investigating wear studies in rollers, bearings, tyres, camshafts, pulleys with varying load, speed, temperature and other parameters etc [25-28].

PIN ON DISC (POD) SETUP

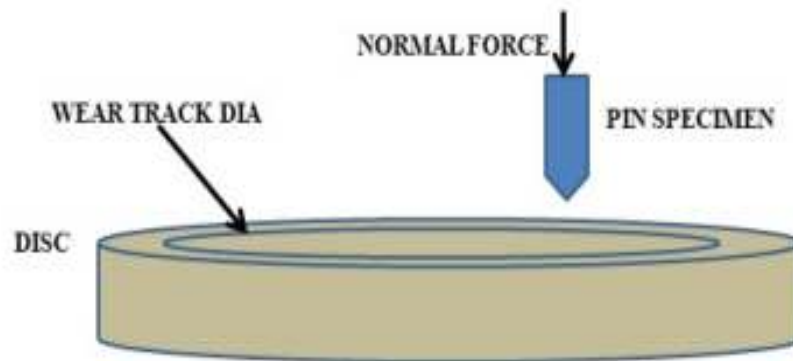


Fig. 4. Pin On Disc Setup (POD)

POD setups are generally used for estimating amount of wear incurred between two materials subjected to sliding action. Parameters influencing wear such as speed, velocity, lubricants properties, friction, temperature etc can be studied with the help of POD. Wear studies in wet clutch system, brake pad material, Diamond like Coating materials subjected to different kinds of loads and speeds are effectively measured with the help of POD setup [29-32].

TABER ABRASION TEST (TA)

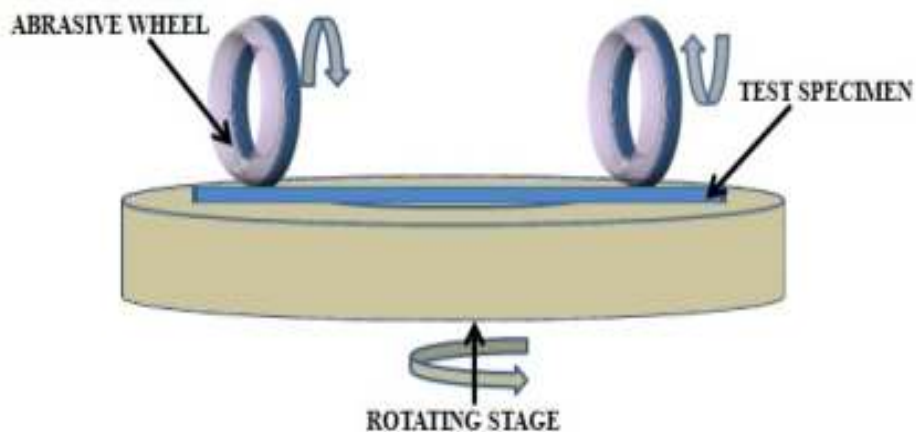


Fig. 5. Taber Abrasion Setup

TA or Abrasion Resistance Tester (ART) is a machine that consists of two abrasive wheels with a rotating stage. Materials and coatings have gained significant importance in various industries to cut down costs due friction and wear. With the help of TA, testing the resistance of materials and coatings subjected to abrasion wear can be done. Test specimens can be circular or square in shape [33-36].

FOUR BALL TESTER (FBT)

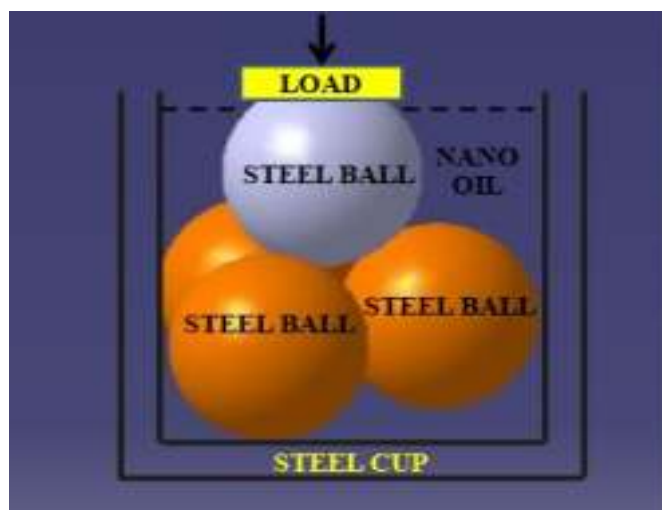


Fig. 6. Four Ball Tester (FBT)

FBT also known as Ball on 3 Balls tester (B3B) is a Tribology set-up used for determination of wear scar properties and coefficient of friction of lubricating grease. Different kinds of lubricants can be tested for the wear resistance properties under high load operating conditions. The set-up consists of 4 balls; one ball is rotated against 3 lubricated stationary steel balls under specified testing conditions to evaluate wear resistant properties of various lubricants and grease applicable in extreme pressure conditions. Steel bearings under different load, temperature and operating conditions have been tested for wear scar properties using B3B set-up [37-40].

TWIN DISC TRIBOMETER

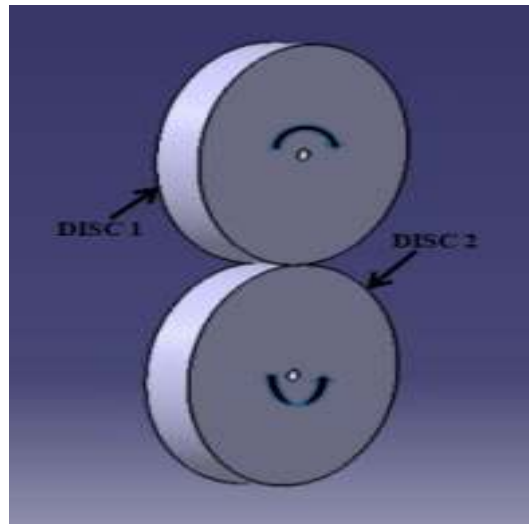


Fig.7. Twin Disc Tribometer Setup

TDT consists of two similar kinds of disc samples which are subjected to motion under different load and operating conditions. This kind of set-up is mostly used for investigating of wear between rail wheels and track. Since set-up involves symmetrical discs, even various materials can be investigated for wear behaviour and performance [41-44].

JET IMPINGEMENT TESTER (JIT)

JIT set-up consists of ejector & nozzle typically used for measuring corrosion wear studies on various materials applicable in flow accelerated environments. Behaviour of various materials especially used in flowing medium like slurry & pipeline industry can be investigated for corrosion studies under different set of operating conditions [45-48].

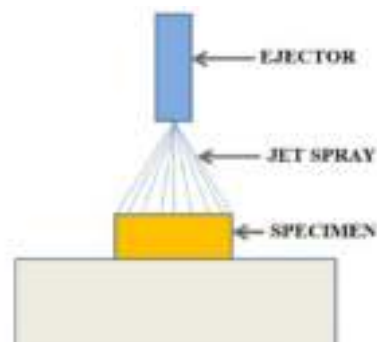


Fig.8. Jet Impingement Tester

Researchers have carried out myriad studies for investigation of materials, coatings, lubricants and other mechanical properties of various metals subjected to wear conditions using above mentioned setups. Though so many customised wear monitoring set-ups existing, it is very difficult to estimate actual wear occurring in components when they are subjected to real time operating conditions as these setups are designed with scale down approach and simulations. Effective monitoring, detection and measurement of such processes are of great importance. Improvised detection and monitoring techniques can prevent catastrophic and breakdown losses which are inevitable during installation & operational phase in industries of strategic importance. Complex engineering structures are often not so easy to access & monitor efficiently on regular basis. In such situations, nuclear techniques such as Charged Particle Activation Analysis (CPAA) and Neutron Activation Analysis (NAA) are of great importance to effectively monitor and measure surface degradation in components due to wear and corrosion [49]. In activation analysis technique, a small part or a component prone to wear or corrosion is subjected to irradiation using suitable charged particles. Post irradiation characteristic γ -rays are captured using detector set-up. Neutron activation is carried out by placing the whole component or machine in nuclear reactors, where a homogenous distribution of activity is produced in the whole component. One of advantages of this process is that any component, equipment of interest can be activated in bulk under real operating conditions. Since it is bulk activation, the activity produced is far more as compared to that of measurable quantity of activity produced in the desired part of the component leading to excess radioactivity distribution [50]. With the help of charged particle activation, this excess amount of radioactivity distribution can be taken care of by selectively activating or irradiating a small desirable surface of component by using appropriate beams available at national & international accelerator facilities. This method known as Thin Layer Activation (TLA) or Surface Layer Activation (SLA) helps in increased sensitivity, precise measurements & accurate monitoring while keeping radioactivity levels very low. Surface layers of thickness in range of few

micrometres of the desired part or component to be tested can be activated using TLA [51]. Modern industries are constantly progressing in adapting newer and efficient radiotracer techniques for monitoring of wear and corrosion. Activation analysis depends on choice & properties of materials of interest. In case of polymers, CPAA is not feasible due to crystal structure and physical properties. In such cases, alternative methods like; isotope diffusion, recoil range activation, radioactive implantation, thermal spraying, galvanic deposition etc can be used [52-53].

Modern times have led to increased demands in adapting newer technologies with high precision, safety and accuracy to fulfil the quality and safety requirements in industries of strategic importance. This has led to shift of research focus on TLA based studies employing light & heavy ion beams. A comparative analysis of TLA using all three viz; light ions, heavy ions and neutron beams with their characteristics have been presented in Fig 9.

LIGHT ION BEAMS	HEAVY ION BEAMS	NEUTRONS
Sensitivity ranges from mm to few microns	Carbon, Oxygen, Fluorine, Lithium etc.	Plutonium, Polonium, Americium etc.
Less energy is penetrated in a given surface area of activation	Sensitivity ranges from microns to nanometers	Sensitivity is high
Requires more thickness to get better results from activated surface	More energy is induced in a given surface area of activation	Penetration power is very high
Precision & accuracy is less as compared to that of heavy ions	Requires less thickness to get better results from activated surface	Proper radiation shielding is must for using such sources
	Precision and accuracy is more as compared to that of light ions	Applicable across wide range of industries

Fig. 9. Characteristics of different Ion Beams

1.2 ACTIVATION METHODS

1.2.1 BULK NEUTRON ACTIVATION

NAA has been employed to effectively monitor wear components with the help of suitable radioactive isotopes generated through nuclear reaction post irradiation. It has been established process over couple of decades in which complete component or machine is activated inside the nuclear reactor. As the activation is carried out in bulk, it is also known as bulk neutron activation. Since, it is achieved by using research reactors, operating costs are less as compared to that of accelerators and as homogenous activity distribution achieved throughout the component, multiple parts of a component can be activated and tested in a single run. It is cost effective, precise and accurate which can measure wear rates less than 1 nm/h depending upon the specific activities induced and total fluid volume of test system [49].

Research reactors came into existence from mid 19th century. Since then, neutron activation analysis has been successfully employed for testing of engine components. Engine components to be tested for wear analysis are seal packed inside water-tight canisters. These engine components are then subjected to neutron flux of the order 10^{12} - 10^{13} neutrons / cm^2 / seconds by lowering the canisters or placing it in front of reactor core. Neutrons do not possess any charge which keeps them unaffected from the electron clouds and can easily penetrate through the desired component or material subjected to activation analysis. In this process, fraction of thermal neutrons interacts with atomic nuclei of the material through nuclear collisions. If the kinetic energy imparted through collisions is sufficient enough, it further results in nuclear reaction. Depending upon the target nucleus, specific reaction and resulting radioisotope are produced. One of the most widely used alloy material in manufacturing and fabrication of engine components is steel. Steel has maximum fraction of ^{58}Fe (Iron) by weight. When thermal neutrons react with ^{58}Fe , resulting nuclear reaction is given by Eqn. (1).



For any nuclear reaction to be feasible for further applications or measurements, most important parameters are the half-life of the produced radio-isotope, cross-section and γ energy abundance. ${}^{59}\text{Fe}$ has a half-life of 44.5 days and emits two useful high energy gamma rays (1099 keV & 1291 keV), when it decays [50]. Cross-section is measurement of interaction probability of thermal neutron with ${}^{58}\text{Fe}$ in a given unit area per unit time in this typical case. Specific and total activity induced can be calculated by taking into consideration all the input parameters such as neutron flux, irradiation time, material elemental composition for the component undergoing test conditions. It can be stated with the help of Eqn. (2)

$$A = \frac{m}{w} * \theta * 6.023 * 10^{23} * \sigma * \phi * [1 - e^{-\lambda * t_{irr}}] \quad (2)$$

Where,

A = activity (dps)

m = total element mass in irradiated sample (g)

w = atomic weight

θ = isotope abundance

σ = cross-section (barns)

ϕ = neutron flux (n/cm²/sec)

λ = decay constant (0.693/t_{1/2})

t_{1/2} = isotope half-life (hours)

t_{irr} = irradiation time (hours)

Due to bulk activation of the entire component, the whole component becomes radioactive. It is thus very difficult to discretize or measure the loss of activity from a specific part of the component due to high signal-to-noise ratio resulting from the surplus amount of radioactivity induced [51]. Hence, it is very important in case of neutron activation analysis, to use indirect method of measurement collected through accumulation in flow through systems.

There are several factors which have to be taken into account for setting up of experiments for wear analysis. These include:

- ✚ Awareness of regulatory norms;
- ✚ Knowledge of amount of expected activity to be induced;
- ✚ Operational cost;
- ✚ Metallurgical properties of testing component;
- ✚ Exposure time;
- ✚ Irradiation hours;
- ✚ Detectors & Nuclear Electronics efficiency;
- ✚ Volume of the fluid system.
- ✚ Spectroscopic details (Half-life, γ -energy & abundance, cross-section, reaction residues)

Nuclear data collected through gamma spectroscopic arrangement can be converted to useful wear analysis & measurements of various engineering components & systems with the help of calibration. Relative measurements can be also carried out, in which calibration is not so necessary. By making appropriate time decay corrections, direct comparison can be done by considering counts per unit time obtained. By pre-calibrating the detection and measurement set-up, experimental errors can be minimized for each specific parameter taken into consideration [52-55]. For efficient calibration, a prototype set-up can also be prepared in which the material of component placed inside the reactor is subjected to similar operating parameters and conditions. From comparative analysis between the two set-ups, radioactivity induced and amount of wear, corrosion are determined by monitoring loss of activity obtained through counts collected over a period of fixed time intervals. Series of such experiments can be repeated for measurement of collective wear, corrosion induced in the component with high level of precision and accuracy [56-57]. A linear regression is performed on the curve to determine the calibration factor.

1.2.2 RECOIL NUCLEI IMPLANTATION

Rapid advancement and competitiveness in industries like power, automobile & transportation, metallurgy has led to continuous improvement on quality of the products on one hand alongwith productivity of production lines. In race of achieving better quality and quantity, use of new and innovative materials which are wear and corrosion resistant plays a vital role in endurance and durability of components by minimizing the losses from very early stages. To monitor such losses efficiently with high level of precision and accuracy, a very high sensitive technique which can measure material loss in few nanometers range is required. It is not feasible to radioactively label or activate some materials like plastics or some ceramics using NAA and CPAA. In such cases, Ultra Thin Layer Activation (UTLA) method is adapted to monitor losses with precision in nanometric scale. UTLA is achieved through implantation of heavy radioactive nuclei on a small area or piece of material which is further subjected to wear or corrosion in real operating conditions. A very thin foil of thickness ranging in few micrometers is subjected to irradiation with proton, deuteron or alpha ion beams. This can be explained through nuclear reaction as stated in Eqn. (3)



Where,

A - Primary target material of the thin foil

(a, b) - Ion beam and reaction channel

B* - Final resultant radio-isotope produced

Resultant kinetic energy due to transfer reaction ranges from few hundreds of keV to MeV which further leads to recoil of some of the radioactive nuclei B* generated out of the target made of thin foils. Exposed material thus gets implanted by this sufficient excess kinetic energy possessed by recoil nuclei. Effective implantation is achieved by placing mask and maintaining tubular or annular geometry. Recoiling nuclei are implanted on material of interest by maintaining a fixed solid angle [Φ_{\min} , Φ_{\max}], where Φ is the angle between the

velocity vector of the radioactive nucleus and the primary beam. Further the incident beam is completely brought to rest by collecting all the radioactive nuclei generated in a Faraday cup [58-59] moving in forward direction kept at a fixed distance from thin target foils.

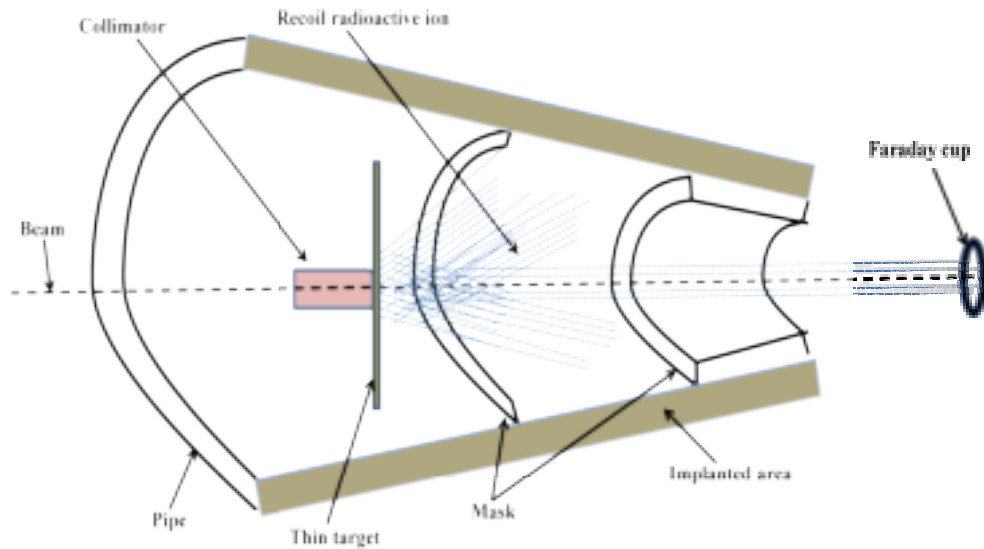


Fig. 10. Recoil Nuclei Implantation [58].

After ion implantation or activation of the desired surface or material, the specimen is taken out and subjected further to real time operating conditions. Loss of residual activity induced against the test time is estimated through direct measurement method. Further calibration curves are deduced into wear rate by measuring and estimating the reduction in loss of activity over a period of testing or run time. For testing of materials, several such thin films having thickness of few micrometers are prepared on substrates by physical vapor deposition (PVD) technique. Thickness of each film is measured with the help of Rutherford Backscattering Spectroscopy (RBS) technique [60]. By subjecting these thin films to similar operating conditions and maintaining same angle of incidence $[\Phi_{\min}, \Phi_{\max}]$, ratio of relative loss of total activity A to the initial activity A_0 i.e. (A/A_0) against the depth of activation or cumulative thickness X is obtained. Correlation between the residual activity induced and surface loss incurred is determined through irradiation of various such stacks of thin films Fig. 10.

The long step of measurement of the calibration curve could be considered as a brake of the extension of UTLA applications. An appropriate computer simulation code (IRIS: Ion Recoil Implantation Simulation) is given in literature to calculate $A/A_0 = f(X)$ [61-63].

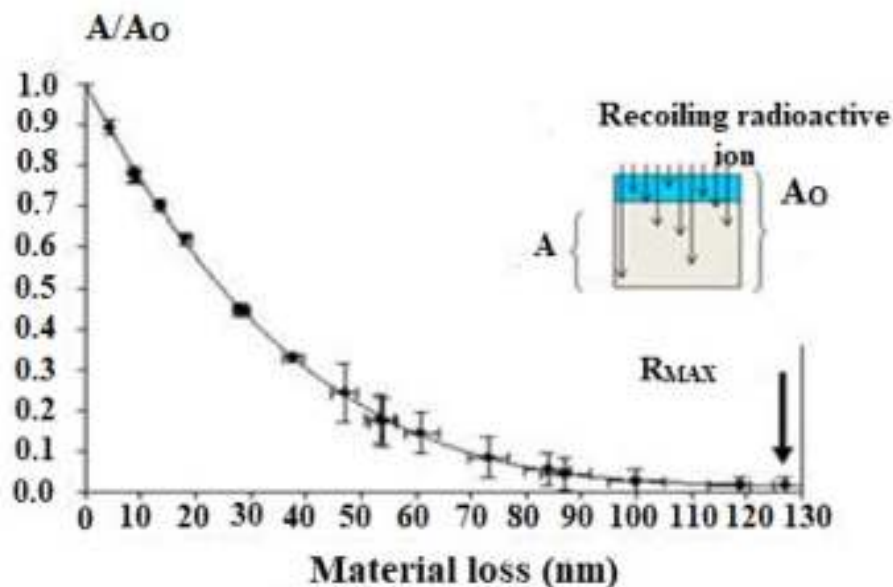


Fig. 11. Calibration curve $A/A_0 = f(x)$ with ^{56}Co nuclei implantation into nickel (16 MeV protons, tubular geometry and acceptance cone $[30^\circ\text{-}38^\circ]$) [52].

The procedure is as follows:

- Thin layer of material deposited on substrate;
- Thickness ($< 1\mu\text{m}$) of film is measured by RBS;
- Irradiation of samples;
- Measurements of the total activity A_0 of the film-substrate pair;
- Chemical dissolution of film to measure A.

1.2.3 RADIOACTIVE ION IMPLANTATION

Polymer materials like PTFE, LDPE, HDPE, PP, and PVC so on, are very highly sensitive to radioactivity and thus require very less exposure of radioactivity levels when compared to that of metallic materials. In such cases,

radioactive labelling by using proton, deuterons and alpha beams is not possible. Through radioactive implantation, activation or labelling of such materials can be achieved. ^7Be ion beam is the most preferred for implantation in polymer and polymer composite materials as it has nearly 8 orders of less magnitude radioactivity affect when compared with charged particles like proton, deuteron and alpha ion beam. Since, the magnitude is so small, wear characteristics of the material remains unaffected [64] as the thickness of activation ranges in few microns. With the advancement and ease in accelerator technology, it is now possible to ^7Be ions through Lithium material by bombarding protons in accelerators. ^7Be has a measurable half-life of 53.3 days and a single characteristic γ -energy peak at 478 keV. Cathode ion-source prepared through chemical and mechanical process is used for sputtering of target material. Target specimen is placed inside vacuum chamber and then ^7Be ions produced and accelerated upto 8 MeV are impinged on target specimen. Typical arrangement of radioactive ion beam implantation is shown in Fig. 12, while Fig. 13 illustrates typical implantation depth and activity induced in range of few micrometers for PTFE material [65]. The activity levels of radioactive ion implantation are far below the free-handling limit. The handling of such parts is very easy and no license is required for such handling. There are no other radioisotopes in the sample than the implanted one. Typical total activities of ^7Be implanted into e.g. a bearing are 200 to 400 kBq.

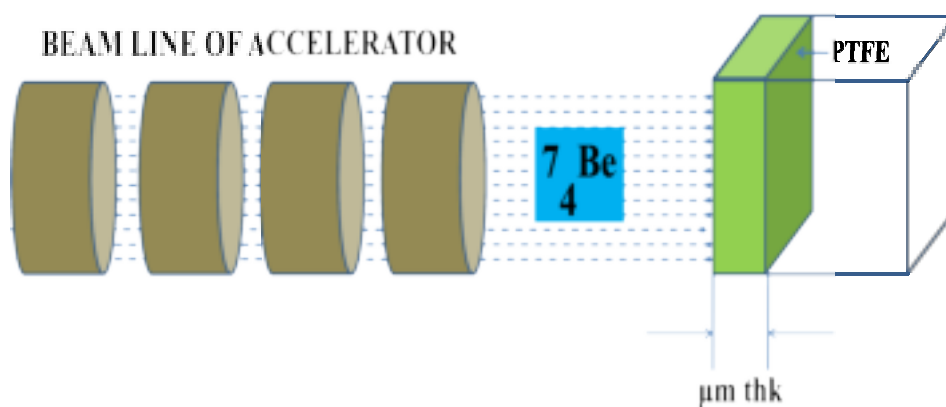


Figure. 12. Principle of the ^7Be implantation [65].

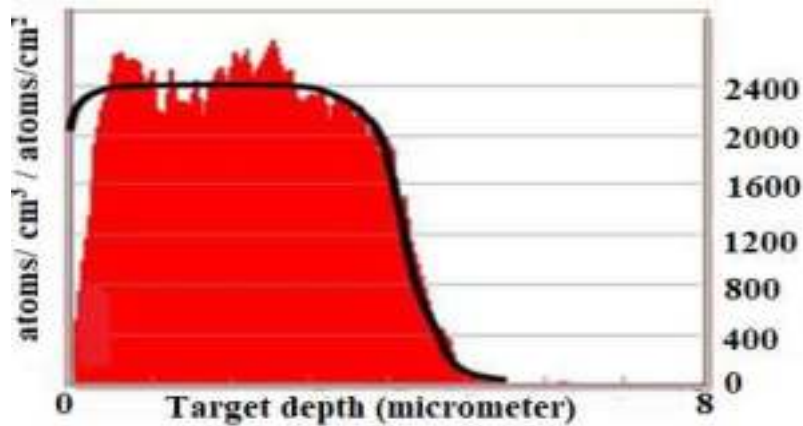


Figure 13. ${}^7\text{Be}$ distribution in a PTFE target [65].

1.2.4 THIN LAYER ACTIVATION METHOD (TLA)

Wear or corrosion in metallic materials and alloys can be easily determined by using TLA technique. TLA is achieved by using suitably charged particles like ${}^1\text{H}$, ${}^2\text{H}$, ${}^3\text{He}$ and ${}^4\text{He}$ for activation of desired surface of a component or machine to be investigated. Considering a typical case of ${}^{56}\text{Fe}$ which forms main constituent by % wt fraction in all kinds of steel alloys, by employing TLA using charged particles like protons and deuterons typical nuclear reaction induced is as shown in Eqn. (4) respectively.

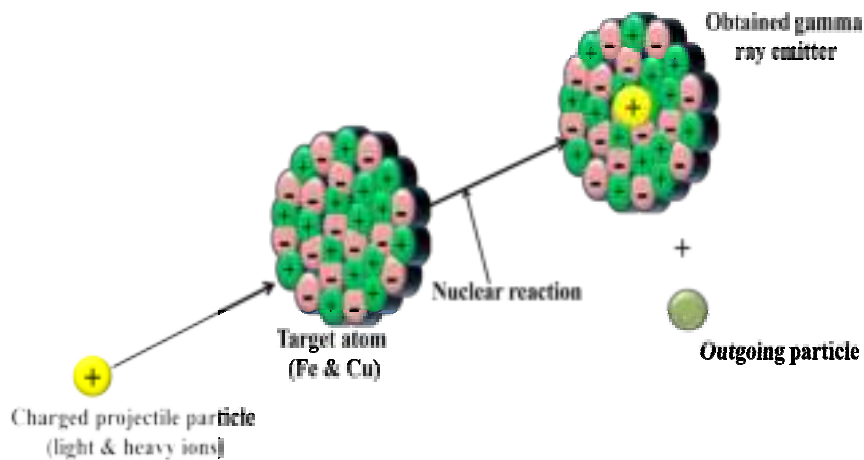


Fig. 14. Working principle of charged particle activation [66].

The probability of nuclear interaction (cross-section) depends upon the amount of energy imparted by projectile on target specimen. TLA analysis can be done by activating surface or machine component directly and subjecting to real operating conditions or through off-line measurement using stacks of thin target foils backed by appropriate thickness of catcher foils. With the help of TLA, it is also possible to measure wear and corrosion during in-situ operations without affecting the operational parameters. For accurate and precise measurement, it is very important to achieve homogenized activity distribution alongwith length of linear activation region. Figure 8 presents an example for a measured activity-versus-depth distribution of ^{56}Co in an iron alloy [68].

All metallic alloys used in engineering components having elemental traces of Al, Co, Cu, Cr, Mo, Ni, Pb, Sn, Ti, V, W, Zn etc can be activated by using TLA for measurement of wear and corrosion. Each element when interacts with charged particles will result into different nuclear reaction and a radio-isotope will be produced through nuclear decay. Cross-section of each element at varying energy obtained through nuclear interactions will vary. For efficient monitoring and precise measurement of wear and corrosion, it is necessary that cross-sections obtained across various energy points are measurable enough (typically ranging above 10 mbarns) alongwith measurable half-life and intense γ -energy lines. Depth of activation and activity distribution in thick target of activated surface is determined through yield and calibration curves. Range of activation may vary from few microns to millimeters. The necessary amount of activity for a given task of wear measurement can be estimated by knowing the main parameters of the measurements (detector type, detector-source distance, machine wall thickness and material, expected wear rate, expected wear depth, etc).

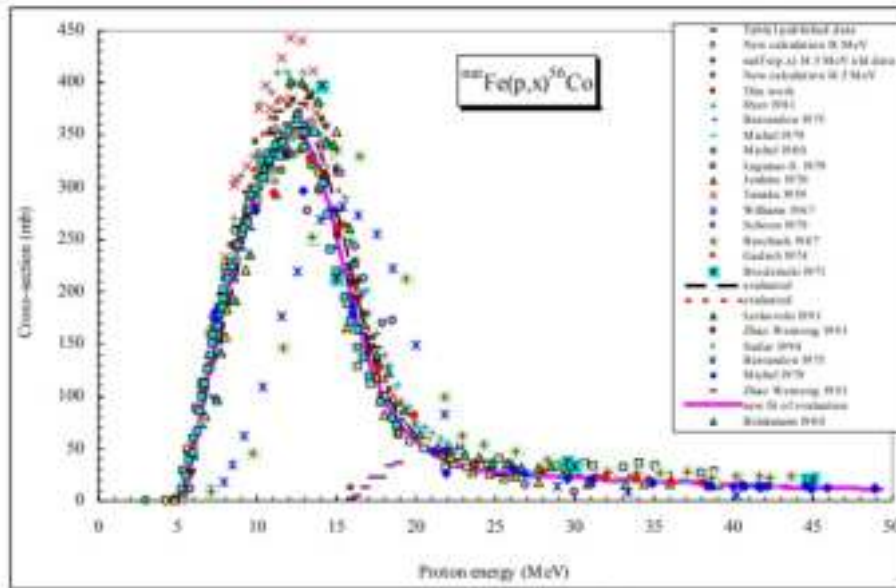


Fig. 15. Experimental measurements for the $^{nat}\text{Fe}(p,n)^{56}\text{Co}$ Cross Section up to 50 MeV bombarding energy [67].

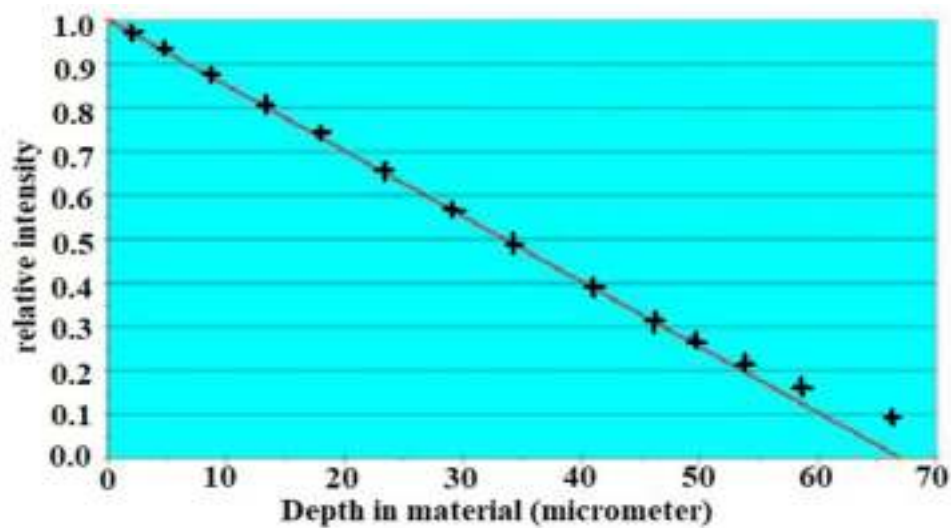


Figure 16. Example for a measured activity-versus-depth distribution of ^{56}Co in an iron alloy [68].

To produce this activity in a given materials (metal, alloy, etc.) a deep physical knowledge is necessary.

1.3 LITERATURE REVIEW:

For a couple of years, TLA using charged particles has been preferred over conventional surface phenomena measurement methods due to many advantages [69–72]. With the help of TLA, surface degradation of multiple

components can be measured in a single go without influencing the operating conditions of system. It is also economically more feasible with increased level of sensitivity and reduced amount of radioactivity leading to easy handling of samples. The precision of TLA ranges from several hundred micrometers to few tens of nanometers [70–72]. Activity has been measured using heavy ions up to 110 MeV in a Cu target for determination of surface wear induced in a very thin layer (up to nanometers) [73]. Studies conducted in Titanium alloys using TLA with different beams viz; (Nitrogen, Carbon and light ions) lead to conclusion that wear measurement by TLA are more precise than conventional gravimetric analysis in Titanium and Chromium alloys [74]. With the availability of cutting edge research in the accelerator technology, it is now possible to activate the desired surface of the material with the help of light and/or heavy charged particles such as Proton, Deuterons, Alpha particles, Oxygen beams etc [75–77]. Since the charge particles quickly lose their kinetic energy as a consequence of intense interaction with the target atoms in a very thin layer, it is known as TLA and can be achieved either by activity loss measurement or collected activity measurement [75–77]. Wear analysis employing TLA with the help of light ions (Proton, Deuteron and Alpha particles) in Molybdenum was carried out, which is used as alloying elements in Steel to increase corrosion resistance [78]. TLA was employed for measurement of wear induced in piston ring and cylinder of automobile [79]. In one of the investigation conducted, it was concluded that Platinum and Platinum alloys can be activated in a very thin layer with most suitable radioisotopes being ^{197}Au & ^{196}Au [80]. In of the studies, TLA was employed to study pseudoelasticity effect on Nickel-Titanium alloys used for orthodontic applications [81]. Recent studies conducted in Niobium alloys could be employed in TLA by measuring cross sections as Niobium alloys are commonly used in industries like nuclear and medicine [82]. For investigation of wear and erosion specimens containing Tungsten it was concluded that ^{183}Re and ^{184}Re are the most suitable ones by employing TLA [83]. In one of the studies conducted, calibration curves were deduced indicating amount residual activity induced in Rhodium & Rhodium alloys [84].

Table 1 List of Deuteron induced TLA reactions in various Metals / Elements

SL NO	METAL/ ELEMENT	REACTION	ENERGY RANGE (MeV)
1	B	$^{nat}\text{B}(\text{d},\text{x})^7\text{Be}$	2-9
2	C	$^{nat}\text{C}(\text{d},\text{x})^7\text{Be}$	22-61
3	Al	$^{22}\text{Al}(\text{d},\text{x})^{22}\text{Na}$	19-58
		$^{27}\text{Al}(\text{d},\text{x})^{24}\text{Na}$	8-50
4	Ti	$^{nat}\text{Ti}(\text{d},\text{x})^{48}\text{V}$	2-41
		$^{nat}\text{Ti}(\text{d},\text{x})^{46}\text{Sc}$	2-49
5	V	$^{nat}\text{V}(\text{d},\text{x})^{51}\text{Cr}$	3-46
6	Cr	$^{nat}\text{Cr}(\text{d},\text{x})^{51}\text{Cr}$	2-13
		$^{nat}\text{Cr}(\text{d},\text{x})^{54}\text{Mn}$	2-49
7	Fe	$^{nat}\text{Fe}(\text{d},\text{x})^{57}\text{Co}$	2.2-21
8	Ni	$^{nat}\text{Ni}(\text{d},\text{x})^{56}\text{Co}$	3-48
9	Co	$^{59}\text{Co}(\text{d},\text{x})^{60}\text{Co}$	0.8-47.8
		$^{59}\text{Co}(\text{d},\text{x})^{58}\text{Co}$	14-58
10	Cu	$^{nat}\text{Cu}(\text{d},\text{x})^{65}\text{Zn}$	4-47
11	Zn	$^{nat}\text{Zn}(\text{d},\text{x})^{65}\text{Zn}$	2-47
12	Zr	$^{nat}\text{Zr}(\text{d},\text{x})^{92\text{m}}\text{Nb}$	3-48
		$^{nat}\text{Zr}(\text{d},\text{x})^{91\text{m}}\text{Nb}$	2-20
13	Nb	$^{93}\text{Nb}(\text{d},\text{x})^{92\text{m}}\text{Nb}$	1-38
		$^{93}\text{Nb}(\text{d},\text{x})^{91\text{m}}\text{Nb}$	28-48
14	Mo	$^{nat}\text{Mo}(\text{d},\text{x})^{96}\text{Tc}$	4.5-37
		$^{nat}\text{Mo}(\text{d},\text{x})^{88}\text{Zr}$	29-49
15	Rh	$^{103}\text{Rh}(\text{d},\text{n})^{102\text{g}}\text{Rh}$	1-39
		$^{103}\text{Rh}(\text{d},\text{n})^{103}\text{Pd}$	4-39
16	Pd	$^{nat}\text{Pd}(\text{d},\text{x})^{110\text{m}}\text{Ag}$	4.5-20
17	Ag	$^{nat}\text{Ag}(\text{d},\text{x})^{105\text{g}}\text{Ag}$	26-48

18	Yb	$^{nat}\text{Yb}(d,x)^{175}\text{Yb}$	4-20
		$^{nat}\text{Yb}(d,x)^{173}\text{Lu}$	4-47
19	Ta	$^{181}\text{Ta}(d,p)^{182}\text{Ta}$	6-39
20	W	$^{nat}\text{W}(d,x)^{183}\text{Re}$	6-49
		$^{nat}\text{W}(d,x)^{184}\text{Re}$	6-49
21	Re	$^{nat}\text{Re}(d,x)^{185}\text{Os}$	9-38
22	Os	$^{nat}\text{Os}(d,x)^{192g}\text{Ir}$	5.2-20.5
23	Ir	$^{nat}\text{Ir}(d,x)^{191}\text{Pt}$	5.8-21
		$^{nat}\text{Ir}(d,x)^{192g}\text{Ir}$	2-37
24	Pt	$^{nat}\text{Pt}(d,x)^{195g}\text{Au}$	7-38
		$^{nat}\text{Pt}(d,x)^{196}\text{Au}$	6-38

Table 2 List of Proton induced TLA reactions in various Metals / Elements

SL NO	METAL/ ELEMENT	REACTION	ENERGY RANGE (MeV)
1	Al	$^{27}\text{Al}(p,x)^{22}\text{Na}$	26-50
2	Ti	$^{nat}\text{Ti}(p,x)^{48}\text{V}$	5-50
3	V	$^{nat}\text{V}(p,x)^{51}\text{Cr}$	1.6-33
4	Cr	$^{nat}\text{Cr}(p,x)^{52}\text{Mn}$	5-29
5	Mn	$^{55}\text{Mn}(p,x)^{54}\text{Mn}$	9.3-50
6	Fe	$^{nat}\text{Fe}(p,x)^{56}\text{Co}$	5.2-35
7	Ni	$^{nat}\text{Ni}(p,x)^{57}\text{Ni}$	13-49
		$^{nat}\text{Ni}(p,x)^{57}\text{Co}$	7-64
8	Co	$^{59}\text{Co}(p,x)^{57}\text{Co}$	15-74
		$^{59}\text{Co}(p,x)^{58}\text{Co}$	11.7-50
9	Cu	$^{nat}\text{Cu}(p,x)^{65}\text{Zn}$	2-50
10	Zn	$^{nat}\text{Zn}(p,x)^{65}\text{Zn}$	11-42
11	Y	$^{89}\text{Y}(p,2n)^{88}\text{Zr}$	9.7-50

12	Zr	$^{nat}\text{Zr}(p,x)^{92m}\text{Nb}$	2-18
13	Nb	$^{93}\text{Nb}(p,x)^{92m}\text{Nb}$	10-51
14	Mo	$^{nat}\text{Mo}(p,x)^{96}\text{Tc}$	4.5-37
		$^{nat}\text{Mo}(p,x)^{88}\text{Zr}$	20-79
15	Rh	$^{103}\text{Rh}(p,n)^{103}\text{Pd}$	3-39
16	Pd	$^{nat}\text{Pd}(p,x)^{105}\text{Ag}$	5-50
		$^{nat}\text{Pd}(p,x)^{110m}\text{Ag}$	3-36
17	Ag	$^{nat}\text{Ag}(p,x)^{105g}\text{Ag}$	23-78
18	Cd	$^{nat}\text{Cd}(p,x)^{114m}\text{In}$	3.6-18.5
19	In	$^{nat}\text{In}(p,x)^{113}\text{Sn}$	2.5-19.5
20	Sn	$^{nat}\text{Sn}(p,x)^{124g}\text{Sb}$	3-34
21	Sb	$^{nat}\text{Sb}(p,x)^{121g}\text{Te}$	3-23
22	Te	$^{nat}\text{Te}(p,x)^{126}\text{I}$	3-20
23	W	$^{nat}\text{W}(p,x)^{183}\text{Re}$	6.5-38.5
		$^{nat}\text{W}(p,x)^{184}\text{Re}$	7-50
24	Re	$^{nat}\text{Re}(p,x)^{185}\text{Os}$	4-21.5
25	Pt	$^{nat}\text{Pt}(p,x)^{195g}\text{Au}$	7-27
		$^{nat}\text{Pt}(p,x)^{196}\text{Au}$	6-45
26	Tl	$^{nat}\text{Tl}(p,x)^{202}\text{Tl}$	15-44
27	Pb	$^{nat}\text{Pb}(p,x)^{206}\text{Bi}$	8-51
		$^{nat}\text{Pb}(p,x)^{205}\text{Bi}$	17-48

Table 3 List of Alpha induced TLA reactions in various Metals / Elements

SL NO	METAL/ ELEMENT	REACTION	ENERGY RANGE (MeV)
1	Be	$^9\text{Be}(^3\text{He},\alpha n)^7\text{Be}$	5-26
2	C	$^{nat}\text{C}(^3\text{He},x)^7\text{Be}$	12-27
3	Al	$^{27}\text{Al}(^3\text{He},x)^{22}\text{Na}$	8-50
		$^{27}\text{Al}(a,x)^{22}\text{Na}$	7.5-48.5

4	Ti	${}^{\text{nat}}\text{Ti}({}^3\text{He},x){}^{48}\text{V}$	4.5-37.5
		${}^{\text{nat}}\text{Ti}(a,x){}^{51}\text{Cr}$	5-48
5	Fe	${}^{\text{nat}}\text{Fe}(a,x){}^{58}\text{Co}$	7.5-48.5
6	Cu	${}^{\text{nat}}\text{Cu}(a,x){}^{65}\text{Zn}$	15-43
		${}^{\text{nat}}\text{Cu}(a,x){}^{67}\text{Ga}$	15-50
7	Cd	${}^{\text{nat}}\text{Cd}(\alpha,x){}^{113}\text{Sn}$	11-50
8	Sn	${}^{\text{nat}}\text{Sn}(\alpha,x){}^{121\text{g}}\text{Te}$	12-37
		${}^{\text{nat}}\text{Sn}(\alpha,x){}^{121\text{m}}\text{Te}$	15-37
9	Ta	${}^{181}\text{Ta}(a,2n){}^{183}\text{Re}$	15.5-44.5

Reactions produced with various Metals/ Elements with the light ion beams viz; Deuteron, Proton, ${}^3\text{Helium}$ & Alpha with their respective energy range have been mentioned Table 1-3 respectively [85]. Further the factors affecting the TLA and its applications have been discussed in detail in later sections. It is clearly evident from the tabulated data that there are several studies carried out with TLA using light ion beams.

1.4 RARE EARTH & STRATEGICALLY IMPORTANT MATERIALS FOR OUR RESEARCH & THEIR IMPORTANCE

REE, metals or oxides are group of seventeen metallic elements. In these 15 elements are classified as Lanthanides alongwith Scandium and Yttrium [86]. REE's have diverse range of industrial applications and form an essential part in fabrication and production of high-tech devices such as lasers, mobiles, phosphors, magnets, hybrid vehicles and other industrial processes. REE's also play vital role in industries of strategic importance such as defense applications which include radar & sonar systems, missile guiding systems and other electronic devices such as capacitors and display units. Since it is very difficult to find traces of these elements naturally like iron and aluminium which are present in abundance, properties and characteristics of these elements are not so familiar. One of the most extensive applications of lightweight rare earth element Neodymium is in production and manufacturing of REM's which forms part of hybrid vehicles and wind turbines has been of

great importance from research and industrial applications point of view [87]. Over a couple of years, there has been an increasing demand in consumption of REE's due to their unique properties and unparalleled application advantages.

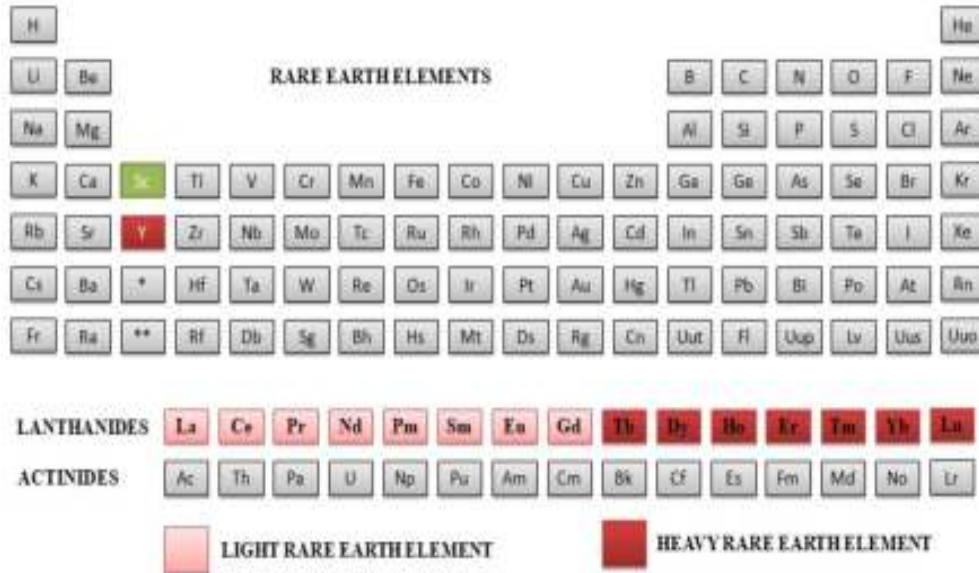


Fig. 17. Rare Earth Materials

(Ref: <https://sciencenotes.org/rare-earth-elements/>)

Major consumption of REE's globally has been found in manufacturing of catalyst and REM's. Applications of various REE's sector wise is shown in Figure 18 and their consumption globally have been presented with the help of Pie Charts as shown in Figure 11[88] & 12 [89] respectively.

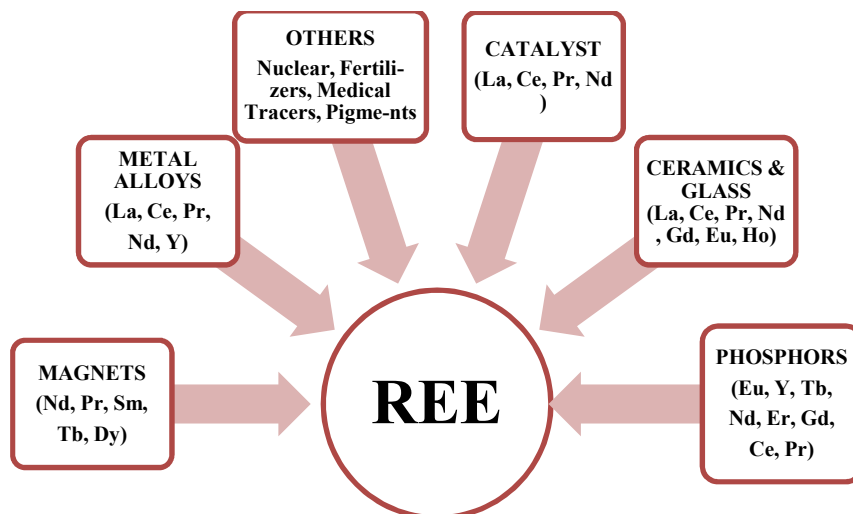


Fig 18. Rare Earth Materials Applications

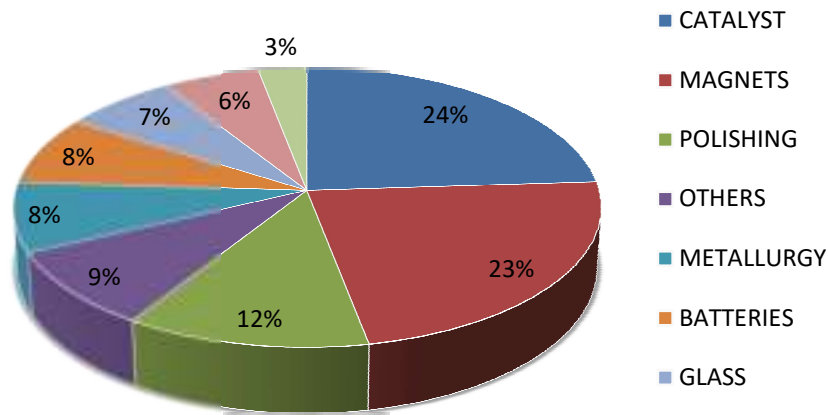


Fig. 19. Global REE Consumption Sector Wise

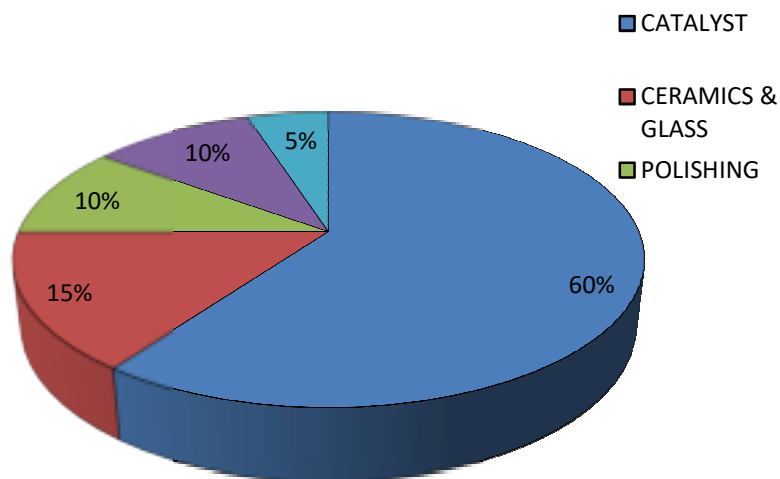


Fig. 20. US REE Consumption (2018) Sector Wise

Fig. 20 represents rare earth materials consumption in various industrial sectors by United States for year 2018. Current research work reports investigation of TLA in spectroscopically pure ($\approx 99\%$) Terbium, Thulium, Tantalum and natural Nickel material. Terbium and Thulium are classified as rare earth materials while Tantalum and Nickel are of great significance in various industrial applications due to their attractive physical and mechanical properties [90-93]. Details and significance of these materials has been discussed in further sections.

Nickel is one of the most widely used alloying elements due to its attractive temperature and corrosion resistant properties. Pure or natural nickel in the form of coatings is plated on metal parts to protect them from chemical attacks, high temperature and resist surface degradation in material. Toasters & Electric Ovens use Nichrome alloy which is combination of Nickel and Chromium alongwith small amounts of Silicon, Manganese and Iron to resist corrosion even when red hot conditions are achieved. In desalination plants, while conversion of seawater into fresh water, material surfaces in direct contact with fluid medium are prone to corrosion and erosion due to presence of salt and other impurities. In order to resist these phenomena, materials made of Copper-Nickel alloy are preferred. Weapons and armours use Nickel coatings to resist corrosion. Turbine blades and propeller shafts used in cruise ships are subjected to accelerated flow erosion and corrosion phenomena which are minimized by using appropriate Nickel alloys. Nickel in hybrid batteries prevents from high temperature acidic corrosion conditions. Terbium is REM mostly used in solid-state devices. Calcium Fluoride, Calcium Tungstate and Strontium Molybdate are doped with Terbium in order to improve performance of solid-state devices. Due to its advantageous fluorescence properties, terbium salts are used in laser devices, light bulbs, mercury lamps and in improvement of medical x-rays with reduced radioactivity exposure. Sound boxes are prepared with alloy consisting of Iron, Dysprosium and Terbium which forms basis of audio in speakers. Thulium is also a REM having good fluorescence properties, which is used in medical x-rays, lasers and surgical applications. Tantalum is one of the strategically important materials having wide range of applications in electronic, defense, space, medical, aerospace and metallurgical industries due to its excellent thermal, mechanical and chemical properties. Due to its high capacitance, Tantalum has been successful in finding its applications in form protective coatings in capacitors used in space technology. As Tantalum is non-toxic, it has also found significant importance in surgical instruments, implants, repair of muscles wear and tear in the form of foil or wire.

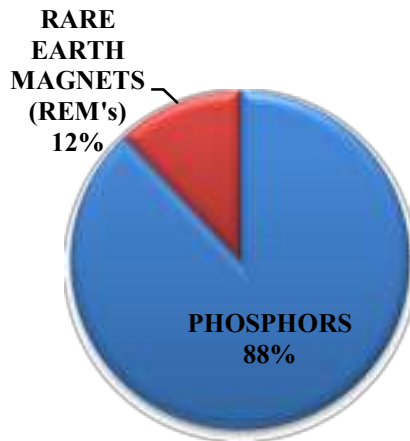


Fig. 21. Industrial sector wise consumption of Terbium

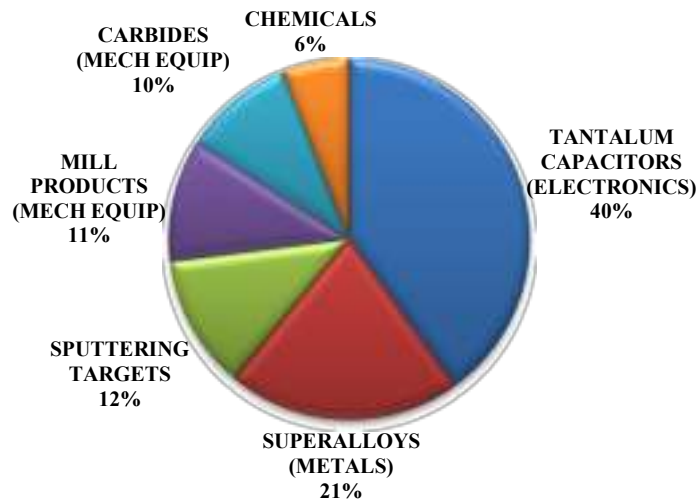


Fig. 22. Industrial sector wise consumption of Tantalum

Tantalum alloys are extremely temperature and corrosion resistant alongwith good mechanical strength which makes them suitable candidate materials for nozzles, turbine blades and nose caps for supersonic aircrafts [94-96]. Some of important mechanical, thermal, physical properties of these materials have presented in Table 4.




Table 4 Important properties for Terbium, Thulium, Tantalum and Nickel material

PROPERTIES	TERBIUM (Tb)	THULIUM (Tm)	TANTALUM (Ta)	NICKEL (Ni)
Atomic number	65	69	73	28
State at 20°C	Solid	Solid	Solid	Solid
Melting point	1359°C, 1632 K	1545°C, 1818 K	3017°C, 3290 K	1455°C, 1728 K
Boiling point	3230°C, 3503 K	1950°C, 2223 K	5455°C, 5728 K	2913°C, 3186 K
Density (g cm ⁻³)	8.23	9.32	16.4	8.90
Specific heat capacity (J kg ⁻¹ K ⁻¹)	182	160	140	444
Young's modulus (GPa)	55.7	74	185.7	≈ 200-220
Bulk modulus (GPa)	38.7	44.5	-	≈ 177-187
Shear modulus (GPa)	22.1	30.5	69.2	≈ 76-84

1.5 MOTIVATION, RESEARCH GAP & OBJECTIVES

Significance and applications alongwith its attractive properties of the materials chosen for our research work has been already discussed in previous sections. To capitalize and fulfil the global energy demands through advanced technology and shifting from Carbon based to Green Energy solutions, it is very necessary to figure out efficient and durable materials for smooth functioning of industries having strategic importance. Terbium, Thulium, Tantalum and Nickel have unique blend of characteristic advantages and it is

also very difficult to find a reliable substitute of these materials due to their enhanced physical, chemical and mechanical properties. It is also noteworthy to investigate the material performance with newer and more efficient detection techniques like TLA clubbed with other conventional techniques for more reliable results. Industries such as defense, space, power etc are very critical and small defect in functioning of materials might lead to huge economic losses coupled with catastrophic effects. To make effective utilisation of modern accelerator technology for TLA based studies, it is very important to primarily estimate the amount of residual or remnant activity thickness in the material of choice through calculated cross section and obtained yield. Till date activity measurement using nearly 100 charged particle beams on more than 50 elements has been successfully carried out. Most of the TLA based studies are carried using light ion beams. In current research work, Terbium, Thulium and Tantalum have been irradiated with HI Oxygen beam and Nickel with α beam. Activity measurement has been done in completely new set of energy range and other standard operating conditions. Till date there are no literatures reported for activity measurement of the above mentioned materials in the energy range, we have achieved by using HI beams. These results in completely new set of nuclear data to be used for TLA based studies in such materials having vital role in wide range of industries. Based on extensive literature and identified research gap, motivation of investigating activity distribution in such significant materials using heavy ion beams is carried out with the help of following objectives as mentioned below;

-  To investigate TLA feasibility in Terbium, Thulium (Rare Earth Materials) and Tantalum, Nickel having strategic importance from industrial perspective using Heavy Ion beams.
-  To measure Cross-Section and Yield in Terbium, Thulium, Tantalum and Nickel materials for Thin Layer based studies.
-  To measure residual activity distribution and maximum depth of penetration in above mentioned materials for TLA applications.

REFERENCES

- [1] William. D. Callister, David G. Rethwisch, “*Materials Science and Engineering: An Introduction*”, 8th Edition, ISBN-13: 978-0470419977, John Wiley and Sons (2010).
- [2] J. E. Gordon, “*The New Science of Strong Materials: Or Why You Don't Fall Through the Floor*”, Second Edition, ISBN- 978-0-14-013597-8, Penguin Science, (1991).
- [3] James Shackelford, “*Introduction to Materials Science for Engineers*”, 8th Edition, ISBN-13 -978-0133826654, Pearson Publisher, (2014).
- [4] William Smith and Javad Hashemi, “*Foundations of Materials Science and Engineering*”, 5th Edition, ISBN-13: 978-0073529240, McGraw-Hill Education, (2019).
- [5] O.P. Khanna, “*Material Science and Metallurgy*”, ISBN-10: 8189928317, Dhanpat Rai Publisher, (2010).
- [6] Robert Dehoff, “*Thermodynamics in Material Science*”, Second Edition, ISBN-13: 978-0849340659, CRC Press, (2006).
- [7] V Chawla, A Chawla, D Puri, S Prakash, PG Gurbuxani, BS Sidhu, “*Journal of minerals and materials characterization and Engineering*” 10 (04), (2011), 367
- [8] O.O. Daramola, B.O. Adewuyi, I.O. Oladele, “*Journal of minerals and materials characterization and Engineering*” Vol.10 No.10, August 10, (2011).
- [9] P.V. Ananthapadmanabhan , K.P. Sreekumar, K.V. Muraleedharan, N. Venkatramani, “*Surface & Coating Technology*”, Vol. 49, (1991), pp 62-66.
- [10] John Stringer, “*Proceedings International conference on corrosion*”, ‘CONCORN’, December 3–6, Mumbai, India, (1997), pp 13–23.
- [11] G. V. Tomarov, A. A. Shipkov and T. N. Komissarova, “*Thermal Engineering*”, (2019), 66, 138–147
- [12] Kevin J. Stein, Brian S. Schorr, Arnold R. Marder, “*Wear*”, Vol. 224, (1999), pp 153-159.
- [13] Sandeep Kumar Dwivedi , Manish Vishwakarma , Akhilesh Soni, “*Materials Today: Proceedings*”, 5, 3690–3698 (2018).

- [14] Aziah North, “*IEEE Underwater Technology*”. (UT) 1874 (1861) (2019).
- [15] Report on NDT; ndt.net, 7th European Conference on Non-destructive Testing, 2018.
- [16] Zikai Hua, Pingchuan Dou, Haili Jia, Fei Tang, Xiaojing Wang, Xin Xiong, Leiming Gao, Xiuling Huang and Zhongmin Jin, “*Frontiers in Mechanical Engineering*” 05 April (2019).
- [17] Anke Turger, Jens Kohler , Berend Denkena , Tomas A Correa , Christoph Becher and Christof Hurschler, “*BioMedical Engineering OnLine*”, (2013), 12:84
- [18] Daniyal, Sabih Akhtar, “*Journal of Building Pathology and Rehabilitation*”, 5 (2020) 1.
- [19] Naomi C Green, James Bowen, David WL Hukins, Duncan ET Shepherd, “Part H: *Journal of Engineering in Medicine*”, 229 (3) (2015) 245–254.
- [20] Wang, Q., Wang, Y., Wang, H., Fan, N., and Yan, F., “*Tribology International*”, Volume 104, (2016), pp.73–82.
- [21] Bjorling, M., Miettinen, J., Marklund, P., Lehtovaara, A., and Larsson, R. “*Tribology International*”, Volume 83, (2015), pp. 114–119.
- [22] ISO 20808: Fine ceramics (advanced ceramics, advanced technical ceramics) - Determination of friction and wear characteristics of monolithic ceramics by ball-on-disc method. ISO Standards, (2016).
- [23] Bjorling, M., Larsson, R., Marklund, P., and Kassfeldt, E., “*Proceedings of the Institution of Mechanical Engineers, Part J: Journal of Engineering Tribology*”, Volume 225, (2011), no. 7, pp. 671–681.
- [24] ISO 7148: Plain bearings -- Testing of the tribological behavior of bearing materials. ISO Standards, (2012).
- [25] ASTM G137-97, Standard Test Method for Ranking Resistance of Plastic Materials to Sliding Wear Using a Block-On-Ring Configuration. ASTM International, (2017).
- [26] ASTM D2714-94, Standard Test Method for Calibration and Operation of the Falex Block-on-Ring Friction and Wear Testing Machine. ASTM International, (2014).

- [27] ASTM G176-03, Standard Test Method for Ranking Resistance of Plastics to Sliding Wear Using Block-on-Ring Wear Test—Cumulative Wear Method, ASTM International, (2017).
- [28] ASTM D3704-96, Standard Test Method for Wear Preventive Properties of Lubricating Greases Using the (Falex) Block on Ring Test Machine in Oscillating Motion. ASTM International, (2012).
- [29] Djoufack, M. H., May, U., Repphun, G., Brogelmann, T., and Bobzin, K. “Tribology International”, Volume 92, (2015), pp. 12–20.
- [30] Nuraliza, M. H. F. N., Syahrullail, S., “*Journal of Tribology*”, Volume 9, (2016), pp. 45–59.
- [31] Marklund, P., and Larsson, R., “*Tribology International*”, Volume 41, (2008), no. 9–10, pp. 824–830.
- [32] ASTM International, ASTM G99: Standard Test Method for Wear Testing with a Pin-on-Disk Apparatus. *ASTM Standards*, Volume G99, (1995), pp. 1–5.
- [33] Rossi, S., Deflorian, F., and Risatti, M., “Surface and Coating Technology”, Volume 201, (2006), pp. 1173–1179.
- [34] Cambuzzi, A., Rossi, S., and Deflorian, F., “*Wear*”, Volume. 258, (2005), pp. 1696–1705.
- [35] Suzuki S., and Ando E., “*Thin Solid Films*”, Volume: 340, (1999), pp. 194–200.
- [36] Jumahat, M., Kasolang S., “*Journal of Tribology*”, Volume 6, (2015), pp. 24–36.
- [37] Danzer, R., Harrer, W., Supancic, P., Lube, T., Wang, Z., and Borger, A., “*Journal of the European Ceramic Society*”, Volume 27, (2007), pp. 1481–1485.
- [38] Hu, K.H., Liu, M., Wang, Q.J., Xu, Y.F., Schraube, S., and Hu, X.G., “*Tribology International*”, Volume 42, (2009), pp. 33–39.
- [39] Talib, N., Md. Nasir, R., and Abd. Rahim, E., “*International Journal of Integrated Engineering*”, Volume 10(3), (2018).
- [40] Li, J., Xu, X., Wang, Y., and Ren, T., “*Tribology International*”, Volume 43, (2010), pp. 1048–1053.

- [41] ASTM G181-11. Standard Test Method for Conducting Friction Tests of Piston Ring and Cylinder Liner Materials Under Lubricated Conditions. ASTM International, (2011).
- [42] Olander, P., Hollman, P., and Jacobson S., “*Wear*”, Volume 302, (2013), pp. 1345–1350.
- [43] Soderfjall, M., Almqvist, A., and Larsson R., “*Tribology International*”, Volume 104, (2016), pp. 57–63.
- [44] Ali, M.K.A., Xianjun, H., Mai, L., Qingping, C., Turkson, R.F., and Bicheng C. “*Tribology International*”, Volume 103, (2016), pp. 540–554.
- [45] Zhao, W., Wang, C., Zhang, T., Yang, M., Han, B., and Neville, A., “*Wear*”, Volume 362–363, (2016), pp. 39–52.
- [46] Fujisawa, N., Yamagata, T., and Wada, K., “*Annals of Nuclear Energy*”, Volume 88, (2016), pp. 151–157.
- [47] Hossain, J., and Hossain, N., “*Procedia Engineering*”, Volume 56, (2013), pp. 690–695.
- [48] Gant, A.J. Gee, M.G. and Plint G., “*Wear*”, Volume 263, (2007), pp. 284–288.
- [49] G.L. Molnar (Ed). Handbook of prompt gamma activation analysis with neutron beams. Kluwer Academic Publishers, Dordrecht, (2004) ISBN 1402013043, 423 pages
- [50] Richard B. Firestone, Coral M. Baglin, S. Y. Frank Chu, Table of Isotopes: 1999 Update, 8th Edition, ISBN: 978-0-471-35633-2 August (1999) 224 Pages
- [51] D.D. Sood, A.V.R. Reddy, N. Ramamoorthy, ‘Fundamentals of Radiochemistry’, IANCAS, Mumbai, India, (2000)
- [52] Reference neutron Activation Library, IAEA Technical Document TECDOC-1285 (2002) Vienna, Austria
- [53] F. de Corte, A. Simonits, Recommended nuclear data for use in the k_0 -standardization of neutron activation analysis, Atomic Data Nuclear Data Tables 85 (2003) 47–67
- [54] M.J.J. Koster-Ammerlaan, M.A. Bacchi, P. Bode, E.A. De Nadai Fernandes, “*Applied Radiation and Isotopes*”, 66 (2008) 1964–1969

- [55] R.M. Lindstrom, R. Zeisler, R.R. Greenberg, “*Journal of Radioanalytical and Nuclear Chemistry*”, 271 (2007) 311–315
- [56] G.P. Westphal, “*Journal of Radioanalytical and Nuclear Chemistry*”, 275 (2008) 677–685.
- [57] Joint Committee for Guides in Metrology, Evaluation of measurement data — Guide to the expression of uncertainty in measurement (2008) JCGM 101:2008 (ISO/IEC Guide 98-3).
- [58] Treuhaft. M. B, Eberle. D. C, The Use of Radioactive Tracer Technology to Measure Real-Time Wear in Engines and Other Mechanical Systems, (2007).
- [59] Lacroix. O, Sauvage. T, Blondiaux. G, Methodological aspects of recoil nuclei implantation technique applied in tribology or corrosion studies. Fourteenth Int. Conf. Appl. Accel. Res. Ind., vol. 392, AIP Publishing; (1997), p. 969–72.
- [60] Lacroix O, Sauvage T, Blondiaux G, Guinard L, “*Nuclear Instruments and Methods for Physics Research Section B*”, (1997); 122:262–8.
- [61] Wang Y, Nastasi. M. A, Handbook of modern ion beam materials analysis. Warrendale, Pennsylvania: *Materials Research Society*; (2009).
- [62] Vincent L, Sauvage T, Lacroix O, Saillard M, Blondiaux G, Guinard L. “*Nuclear Instruments and Methods in Physics Research Section B, Beam Interact with Matter Atoms*”, (2002); 190:831–4.
- [63] Vincent L, Sauvage T, Lacroix O, Fradin J, Saillard M., “*Nuclear Instruments and Methods in Physics Research Section B, Beam Interact with Matter Atoms*”, (2000); 161:115–9.
- [64] O. Koskelo, U. Koster. B. C, I. Riihimaki. D, J. Raisanen. A, “*Diamond & Related Materials*”, 17 (2008) 1991–1993.
- [65] Hoffmann M, Abbas K, Sauvage T, Blondiaux G, Vincent L, Stroosnijder M, “*Nuclear Instruments and Methods in Physics Research Section B, Beam Interact with Matter Atoms*”, (2001);183:419–24.
- [66] Ditroi F, Takacs S, Wopelka T, Jech M, Lenauer C. Investigation of wear process by using radioactive tracers. 20th Int. Conf. Wear Mater., Toronto: (2015), p. 145.

- [67] Ditroi F, Takacs S, Tarkanyi F. Evaluation of reaction cross section data used for thin layer activation technique. Int. Conf. Nucl. Data Sci. Technol. St. Fe, NM, USA, 26 Sept. - 1 Oct., 2004 AIP Conf. Proc. 769 (2005)1654, 2005.
- [68] ZAG Zyklotron AG measurement during quality control (internal communications) 2010.
- [69] Imam Kambali and Hari Suryanto, “*Journal of Engineering and Technological Sciences*”, 48 (4) (2016) 482–494.
- [70] IAEA report on The thin layer activation method and its applications in industry.
- [71] Devendra P. Singh, Vijay R. Sharma, Abhishek Yadav, Pushpendra P. Singh, Unnati, M. K. Sharma, H. D. Bhardwaj, B. P. Singh and R. Prasad, “*Journal of Nuclear Physics, Material Sciences, Radiation and Applications*”, (JNPMSRA), Vol. 1, No. 1, (2013) pp. 13–24.
- [72] Syed M. Qaim, Ingo Spahn, Bernhard Scholten and Bernd Neumaier, “*Radiochimica Acta*”, 104 (9) (2016) 601–624.
- [73] D.P. Chowdhury, R. Guin b, S.K. Saha, M. Sudersanan, “*Nuclear Instruments and Methods in Physics Research B*” 211 (2003) 288–296.
- [74] G. Dearnaley, J. Asher, A.T. Peacock, S.J. Allen, R.E.J. Watkins, “*Surface & Coatings Technology*”, 201 (2007) 8070–8075.
- [75] D. P. Chowdhury, J. Datta, A. V. R. Reddy, ““*Radiochimica Acta*”, 100, (2012), 139–145.
- [76] Biswal J, Thakre G. D, Pant H, Samantray J. S, Arya P. K, Sharma S. C, Gupta A. K ““*Nuclear Instruments and Methods in Physics Research B*”, 399: (2017) 69–73.
- [77] R. Verma, K. K. Swain, P. S. Remya Devi, Aditi A. Dalvi, Nicy Ajith, M. Ghosh, D. P. Chowdhury, J. Datta and S. Dasgupta, “*BARC Report External BARC/2016/E/004*”.
- [78] F.Ditroi, F.Tarkanyi, S.Takacs, “*Nuclear Instruments and Methods in Physics Research Section B: Beam Interactions with Materials and Atoms*”, 290 (2012) 30–38.
- [79] E. Corniani, M. Jech, F. Ditroi, T. Wopelka, F. Franek, “*Wear*”, 267 (2009) 828–832.

- [80] F. Tarkanyi, F. Ditroi, S. Takacs, J. Csikai, A. Hermanne, M. S. Uddin, M. Hagiwara, M. Baba, Yu. N. Shubin, A. I. Dityuk, “*Nuclear Instruments and Methods in Physics Research Section B*”, 226 (2004) 473–489.
- [81] M. Cioffi, D. Gilliland, G. Ceccone, R. Chiesa, and A. Cigada, “*Acta Biomaterialia*, vol. 1, no. 6, pp. 717–724, 2005.
- [82] F. Ditroi a, F. Tarkanyi, S. Takacs, A. Hermanne, A.V. Ignatyuk , “*Nuclear Instruments and Methods in Physics Research Section B*”, 373 (2016) 17–27.
- [83] F. Tarkanyi, S. Takacs, F. Szelecsenyi, F. Ditroi, A. Hermanne, M. Sonck, “*Nuclear Instruments and Methods in Physics Research Section B*”, 252 (2006) 160–174.
- [84] Ditroi F., Tarkanyi F., Takacs S., Hermanne A., Yamazaki H., Baba M., Mohammadi A., Ignatyuk A. V, “*Nuclear Instruments and Methods in Physics Research Section B: Beam Interactions with Materials and Atoms*”, 269 (2011)18: 1963-1972.
- [85] <https://www-nds.iaea.org/tla/index.html>
- [86] Nomenclature of Inorganic Chemistry, IUPAC Recommendations, 2005.
- [87] Haxel G.; Hedrick J.; Orris J et al; "Rare Earth Elements—Critical Resources for High Technology", United States Geological Survey. USGS Fact Sheet: 087-02. (2002).
- [88] Zhou, Baolu; Li, Zhongxue; Chen, Congcong, "Global Potential of Rare Earth Resources and Rare Earth Demand from Clean Technologies", *Minerals*. 7(11): 203. (October 25, 2017).
- [89] Mineral Commodity Summaries. 2019. p. 132, (doi:10.3133/70202434.)
- [90] W. M. Haynes, ed., CRC Handbook of Chemistry and Physics, CRC Press/Taylor and Francis, Boca Raton, FL, 95th Edition, Internet Version 2015, accessed December 2014.
- [91] Tables of Physical & Chemical Constants, Kaye & Laby Online, 16th edition, 1995. Version 1.0 (2005), accessed December 2014.
- [92] J. S. Coursey, D. J. Schwab, J. J. Tsai, and R. A. Dragoset, Atomic Weights and Isotopic Compositions (version 4.1), 2015, National Institute of Standards and Technology, Gaithersburg, MD, accessed November 2016.

- [93] T. L. Cottrell, *The Strengths of Chemical Bonds*, Butterworth, London, 1954.
- [94] John Emsley, *Nature's Building Blocks: An A-Z Guide to the Elements*, Oxford University Press, New York, 2nd Edition, 2011.
- [95] Thomas Jefferson National Accelerator Facility - Office of Science Education, *It's Elemental - The Periodic Table of Elements*, accessed December 2014.
- [96] *Periodic Table of Videos*, accessed December 2014.

CHAPTER 2 THIN LAYER ACTIVATION METHODOLOGY

2.1 TLA MECHANISM

TLA mechanism has been illustrated in Fig 2.1 with industrial application in automobile industry. TLA has been employed to detect wear or erosion between piston rings and piston cylinder arrangement. A thin layer of interest near Top Dead Center (TDC) of the cylinder is activated with the help of suitable charged particles. Iron being one of major elemental constituent leads to typical nuclear reaction when protons obtained from accelerator interacts with the surface of material. As a result of which characteristic γ -emissions are obtained from the activated thin layer. Amount of wear or erosion is determined by monitoring residual activity induced in the activated zone with the help of detector by capturing γ -emissions placed at appropriate distance. Fig 2.2 represents simplified activity [calibration curve] obtained through interaction of charged particles with activated material surface.

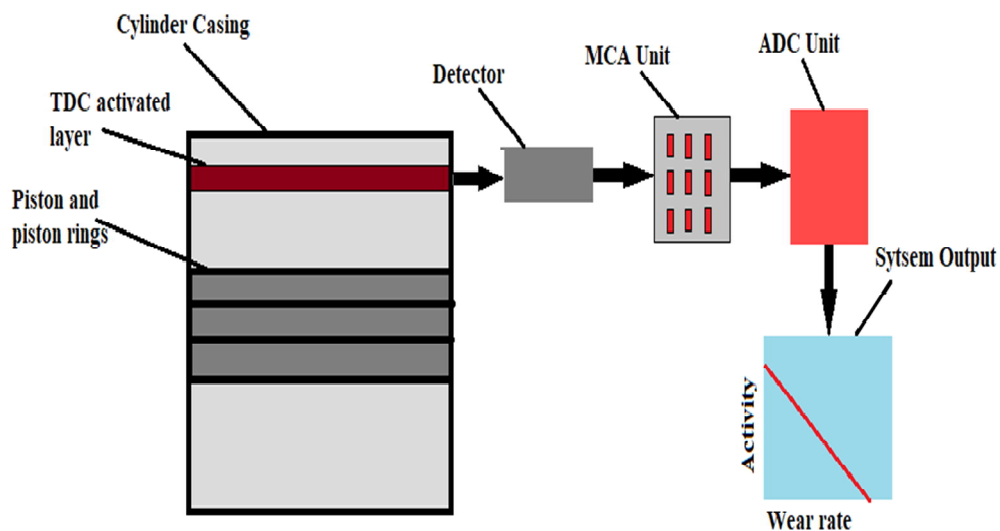


Fig. 2.1 Illustration of TLA mechanism [1].

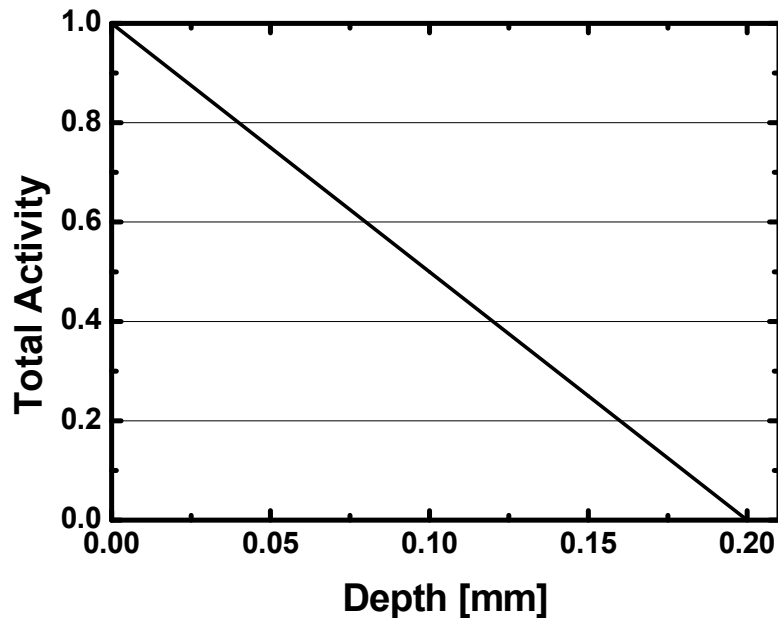


Figure 2.2 TLA calibration curve (total activity versus material depth) [1].

2.2 TLA THEORY

When a material is subjected to irradiation of charged particles obtained from accelerator, particles interact as result of transfer of kinetic energy. It is but obvious that at a certain depth of thickness, interaction probability between the material surface and ion beam will completely come to rest as loss of kinetic energy due to attenuation in charged particles. Interaction of charged particles with various elements present in a material surface, results in production of radio-isotopes having very less concentration with very low radioactivity levels typically ranging from 100 kBq to few MBq [2]. To make effective use of TLA for industrial applications, it is very important to be aware of certain basic factors influencing total activity levels induced in sample materials. Factors such as elementary composition of material, choice of ion beam, threshold energy and range of ion beam interactions, radionuclides produced, nuclear reaction maximum yield, irradiation time and measurement method needs to be taken care of well in advance for TLA based investigations.

Interaction of charged particles in different elements is well known to ensure feasibility of the TLA based investigations while considering all the above mentioned factors [3]. To address a specific problem, suitable charged particles can be used for creation of specific radio-isotope or reaction product through which desired levels of activity and depth of activation can be achieved. Range of ion beam interaction in elements, compounds and alloys can be obtained through Braggs's formula [4]. Other factors influencing TLA such as threshold energies, depth of interaction, Q-value of reaction can be referred through tabulated data available in literature [5]. When a charged particle interacts with an element or alloy, various nuclear reactions can be initiated. In order to determine the most suitable reaction for TLA applications, yield of reaction needs to be determined [6-9]. Unit of yield Y is expressed in μAh which can be obtained through eqn (1-2).

$$Y = \frac{A_o}{I} \frac{\lambda}{1 - e^{-\lambda t_i}} \quad (2.1)$$

Where:

λ = decay constant (s^{-1})

I = beam intensity (μA)

A_o = activity of reaction product after irradiation

t_i = irradiation time (s)

Maximum Yield which is the measure of TLA feasibility in a particular alloy is expressed through eqn 2,

$$Y_{\Sigma} = Y_i \times \eta_i i \frac{R_{\Sigma}}{R_i} \quad (2.2)$$

Y_{Σ} = yield obtained from the alloy

Y_i = yield obtained from pure element i

$\eta_i i$ = proportional weigh of element i in comparison to that of alloy.

2.3 ADVANTAGES OF TLA COMPARED TO CONVENTIONAL TECHNIQUES

Most widely adopted methods across various industries for monitoring and detection of wear, erosion, corrosion and surface degradation phenomenon is achieved through dimensional and visual inspections. In this method, dimensional checks are done before and after testing of materials or components after being subjected to long running cycles. Amount of loss in material or component before and after testing is identified through dimensional checks, but one cannot be sure about the exact occurrence of these degradation phenomena's with respect to different time scale in one testing cycle. The amount of loss determined is measure of total loss for complete duration of total operating hours.

Even the best monitoring techniques have limited efficiency and accuracy to detect the loss upto few tens of micrometers. Materials and components fitted in complex engineering structures and applications are already assembled with very less tolerance fits to get maximum efficiency while operating. To monitor loss through conventional methods, these complex parts needs to be dismantled first for checks and again needs to be assembled back to operate. While doing so, it may lead to more human errors and also lower the precision and accuracy of monitoring techniques. Through TLA, this can be overcome, as it is a non-destructive remote monitoring technique. Activation technique has also added advantage of simultaneously monitoring multiple parts or material surface of interest for measurement and detection of surface degradation. Operations in critical industries such as nuclear, space technology, transportation and others cannot be stopped at intermediate levels. In such cases components or material coatings used in these industries can be monitored effectively while being operational. Through activation technique, monitoring of complete cycle can be achieved at very regular time intervals without disturbing the operating conditions which is almost impossible to achieve through conventional methods. Precision and accuracy in detection of loss upto nanometers can be achieved by using TLA. It is possible to exactly

trace the origin of loss occurred, while fast changing transient conditions, without affecting the operational stability through activation technique. For conventional methods, it is necessary to develop a prototype bench test rigs for monitoring of wear, erosion or corrosion etc. By making use of activation technique, optimization of this testing time can be achieved which further reduces overall operating costs, otherwise usually is not possible to achieve through conventional methods.

2.4 MEASUREMENT METHODS

2.4.1 DIRECT MEASUREMENT TECHNIQUE

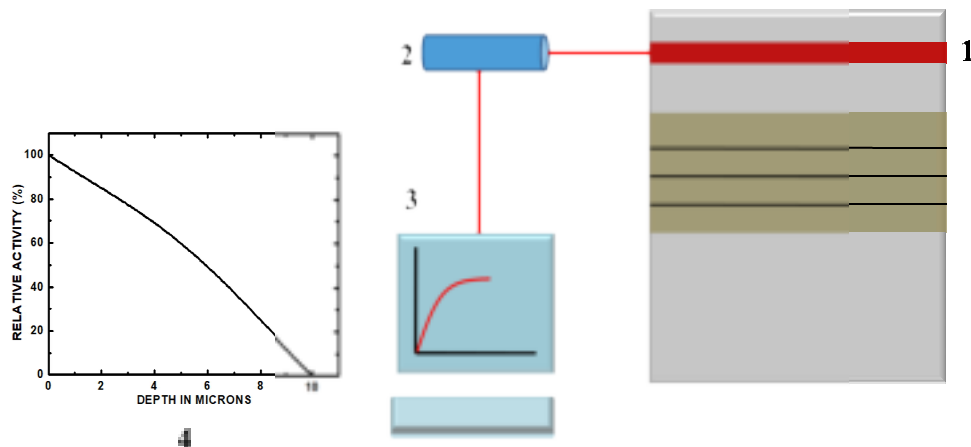


Fig. 2.3 Schematic illustration of Direct Measurement Technique. [10]

Figure 2.3 is simplified illustration for direct measurement set-up is represented having four major steps of monitoring the activity.

- ✚ In this step material surface area of concern for investigation and monitoring for amount of surface degradation is identified and activated with suitable charged particles obtained through the accelerator.
- ✚ After irradiation, precalibrated detector is used to capture the emitted characteristic γ -radiations from the activated surface.

- ✚ Using measured cross-section values and maximum yield obtained per unit thickness, resulting mass or volumetric loss when subjected to operations are measured with respect to time.
- ✚ Finally calibration curves are obtained for specific reaction of interest by observing the rate of activity induced through yield of the reaction. Plot of activity with respect to thickness of the material surface is the final measure of amount of loss (mass or volumetric).

Direct measurement method is advantageous in the sense that for measurement and monitoring flowing fluid chamber is not required. Limitation is that this can be applied only in monitoring of those surfaces or components which are subjected to dry abrasive, erosive or corrosive surface degradation.

2.4.2 INDIRECT MEASUREMENT TECHNIQUE

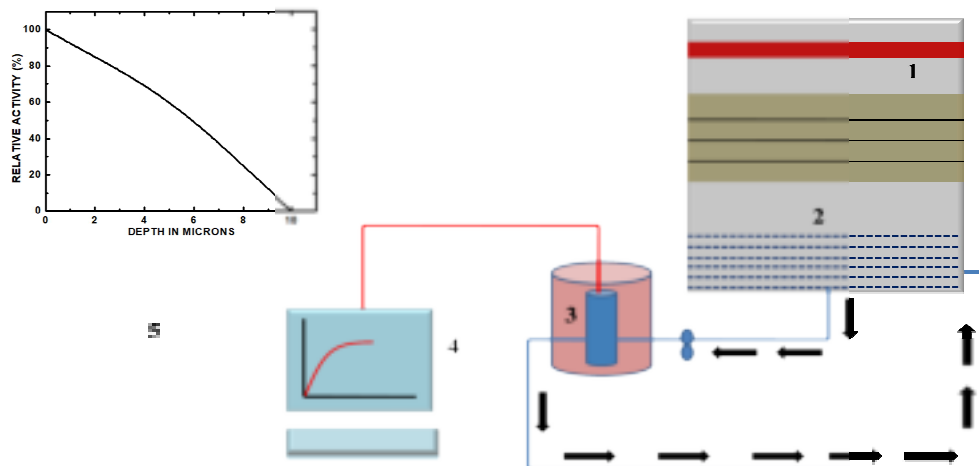


Fig. 2.4 Schematic illustration of Indirect Measurement Technique [11].

Figure 2.4 shows simplified illustration for indirect measurement set-up is having five major steps of monitoring the activity. In case of indirect measurement set-up, principle and monitoring of thin layer activated surface almost remains same other than a lubricant / cooling circuit.

- ✚ Apart from this ensuring the positioning of detectors at right distance from the surface and component is also a challenge as detectors are highly sensitive to the fluctuations in operational parameters.

- ✚ With the help of indirect measurement, this limitation can be overcome by providing additional flowing medium circuit in which detector of desired efficiency and accuracy is placed as shown above.
- ✚ In this case, the worn out particles flow along with the fluid medium and are collected in a detector gas chamber at regular intervals for detection activity induced with respect to thickness. Increase in the level of activity over a period of time is the measure of volumetric or mass loss.
- ✚ In this case, care needs to be taken off for regularly removing the accumulated worn out particles after each operating cycles so that the precision and efficiency remains high. This can be also done by installing appropriate filter in the flowing circuit to absorb gamma rays.

Eventhough precision and accuracy of higher order can be achieved through this method; utmost care needs to be taken while calculating specific activity influenced by variable parameters such as fluid medium, transportation, detector efficiency etc.

2.5 PRE-REQUISITES FOR TLA INVESTIGATIONS

2.5.1 RADIOACTIVITY DETECTION

TLA investigations can be achieved both through direct and indirect measurement methods. As discussed earlier, in industrial applications where dry surface degradation phenomena are prominent, direct measurement method is more suitable while in case lubrication parts or surfaces indirect measurement method turns out to be more effective. In both cases, challenge is to achieve precision and accuracy in capturing signals through detectors from the ionizing particles after irradiation of material samples. Range of penetration for α and β particles is poor as compared to that of γ -radiation that is why; it is the best choice for monitoring of surface degradation related measurements. Some of technical issues [12] which are to be taken into consideration in TLA investigation are as follows;

- 1) Background Irradiations: Remnants of naturally occurring radiations such as terrestrial, cosmic and radon background irradiation can influence the precision and accuracy while measuring the specific activity induced in the activated surface of material or components under investigation. This can be overcome by using a precalibrated detector set-up for measuring the radiation levels without and with source through comparative analysis.
- 2) Wear measurements through Calibration Curves: As discussed in previous chapter, activation of surface through charged particles results in a number of nuclear reactions which results in several reaction products. As a result of which, it is difficult to trace the one particular radiation being emitted after activation. Variable factors like position of detector from the activated surface, type of fluid, transportation and detector type and efficiency also influence the authenticity of obtained measurements. This can be managed through pre-calibration of the whole set-up using standard radiation sources.
- 3) Ion beam energy range: Gamma radiations obtained from irradiated material surface is one of primary input to check the feasibility of interaction probability and resulting amount of mass / volumetric loss. Gamma rays having less energy are not feasible as they will attenuate quickly in the shielding barriers and appropriate γ -energies might just pass the detector surface without any interaction. Hence, it is very important to consider threshold energy range of interaction between ion beam and material.
- 4) Detector intrinsic efficiency: Detector efficiency can be simple given by ratio of number of events captured to that of number of gamma rays emitted. This depends on the material of the detector, design and working principle. There are many commercially available detectors which can be used for measurements in such kind of set-ups. Details regarding material efficiency, positioning and energy of ion beams are available in the form of data sheets which can be considered before setting up of experiments [13].

2.5.2 DETECTORS SELECTION

For TLA based investigations, capturing of γ -rays of specific energy plays a vital role in analysis and measurement of surface degradation phenomena in

various industrial applications. This challenge can be addressed through spectroscopic analysis of characteristic gamma rays used to identify the specific reaction residue alongwith its sensitivity [14]. Detector setups are usually a complete line supported with electronic system either installed near to the equipmental set-up or may be at some distance away. During the operations, detector facility is also subjected to background irradiations, vibrations, temperature like variable parameters affecting the overall performance of the detection system. Thus it is very important that the detection facility turns out be cost-effective, reliable, sensitive coupled with high accuracy and precision. Commercially available detectors are mainly classified in two categories; inorganic scintillation and semiconductor technologies.

2.5.2.1 SCINTILLATION DETECTORS

Alkali Halides (NaI and CsI) or Bismuth Germanate ($\text{Bi}_4\text{Ge}_3\text{O}_{12}$ or BGO) based inorganic scintillators are widely used in various industrial applications. By mounting these detectors on Photo Multiplier Tubes (PMT) and conversion of scintillation light into electronic pulses is achieved. Bismuth Germanate is having higher density as compared to that of Sodium Iodide (NaI) but its energy resolution as compared to that of NaI turns out to be two times lower. One of main limitation with NaI is its low energy resolution, which cannot be used in such applications where multiple reactions are initiated after activation. NaI detectors turns out to be cost effective, and can be easily mounted on industrial test benches and also effective under vibrations and shocks and can be cooled at room temperature also. Some of new detector technologies with improved resolution are in demand coming from family of Lanthanum Halides $\text{LaCl}_3(\text{Ce})$ whose energy resolution is two times better in comparison to NaI but higher operational cost is one of the limitations at this stage.

2.5.2.2 SEMICONDUCTOR DETECTORS

As NaI are cost effective but offers very low energy resolution, High Purity Germanium detectors (HPGe) are one of its kind detector technologies with very energy resolution. These detectors are cooled with liquid Nitrogen which turns out to be little complicated while being in use at facilities. Advance portable commercially available electric cooled HPGe detectors are also available which can be used as a substitute for nitrogen cooled HPGe. Spectroscopic resolution of the detectors plays very vital role in indentifying properties of reaction products obtained post irradiation. In case of natural elements or simple alloy composition matrix, NaI detectors can be used for identification and analysis purpose. In case of complex composite matrix of material or alloy, lot of reactions are initiated through irradiation of charged particles. This results in overlapping of peaks through which identification of properties at specific time interval becomes very difficult for a given sample of material. HPGe detector turns out to be very effective in such industrial applications due to its high resolution.

2.6 TLA ELECTRONICS FOR DETECTION

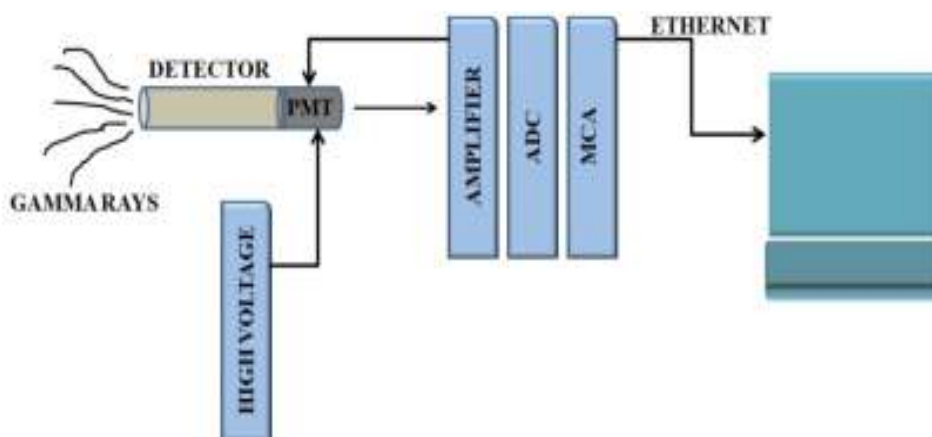


Fig. 2.5 Schematic illustration of TLA electronics system. [15]

Fig 2.5 illustrates electronic system set-up required for TLA investigations. Major electronics are detector, PMT, Amplifier, Analog to Digital Converter (ADC), Multi Channel Analyzer (MCA), high voltage source and system to

record output. Cost-effectiveness of this system depends upon the volume of experiments or TLA investigations and also the precision and accuracy needs of specific industry. In some cases, MCA can be replaced with Single Channel Analyzer in which specifically gamma emissions of one particular reaction can be recorded. High voltage source is connected to the detector set-up which is placed in front of the investigating sample to capture the γ -emissions obtained after activation. These γ -emissions are captured; pre-amplified and then amplified using amplifier. The signals recorded are in the form of pulse which is a unipolar output. This is further connected to MCA unit from which spectroscopic details of a particular reaction can be identified. This is finally connected to system output, which records the spectrum of reactions induced. For spectrum analysis, various in-house built software packages can be used for analysis of the captured data.

REFERENCES

1. Landolt-Bornstein Numerical Data and Functional Relationships in Science and Technology: Group 1 : Nuclear and Particle Physics Production of ... of Protons With Targets from I to Am), (2013), ISBN-13 : 978-0387560533
2. Maluhin VV, Konstantinov IO. Activation of construction materials on the cyclotron. *Isot v SSSR* 1975;44.
3. Dmitriev PP. The radionuclide yield in the reaction with protons, deuterons, alpha -particles and He-3 ions. Moscow: 1986.
4. Brown, A. & Suit, H. The centenary of the discovery of the Bragg peak. *Radiotherapy and Oncology*, **73**, 265–268, 2004.
5. Albert P, Blondiaux G, Debrun JL, Giovagnoli A, Valladon m. Thick target yields for the production of radioisotopes, Handbook on Nuclear Activation Data. Vienna (Austria): 1987.
6. Krasnov NN. Thick target yield. *Int J Appl Radiat Isot* 1974;25:223–7.
7. JECH M. Wear Measurement at Nanoscopic Scale by means of Radioactive Isotopes. Vienna University of Technology, 2012.

8. UNITED STATES NUCLEAR REGULATORY COMMISSION. NRC: 10 CFR 30.18 Exempt quantities. <http://www.nrc.gov/reading-rm/doc-collections/cfr/part030/part030-0018.html>. 2015.
9. EUROPEAN UNION. Council Directive 2013/59/Euratom of 5 December 2013 laying down basic safety standards for protection against the dangers arising from exposure to ionising radiation, Annex VII. 2013.
10. ZAG Zyklotron AG Brochure RTM Wear Diagnostics 2011:11.
11. ZAG Zyklotron, AG Broschure RTM Wear Measurement Technique 2012:2.
12. P. Thomas, K. Nester, KFK 2286, Abteilung Strahlenschutz und Sicherheit, Projekt Nukleare Sicherheit, Experimental determination of the atmospheric dispersion parameters over rough terrain: Part 2: Evaluation of Measurements, 1976.
13. Jech M, Lenauer C, Wopelka T, Novotny-Farkas F, Feitzinger T. Advances in wear measurement – piston rings in component test and engine environment. Int. Colloq. Tribol. -Tech. Akad. Esslingen, 2009.
14. David Jenkins, Radiation Detection for Nuclear Physics, Methods and industrial applications; ISBN: 978-0-7503-1428-2, IOP Publishing Ltd 2020.
15. Treuhaft MB, Eberle DC. The Use of Radioactive Tracer Technology to Measure Real-Time Wear in Engines and Other Mechanical Systems, 2007.

CHAPTER 3

EXPERIMENTAL METHODOLOGY

TLA (thin layer activation) is an important and unique nuclear technique through which analysis of material properties, behaviour and monitoring of surface degradation can be achieved which are of great importance in industrial applications. In TLA mechanism, when a beam of certain energy impinges on the material or target specimen, under investigations, initiates multiple nuclear reactions. This initiated nuclear reaction is in result of the interaction between various elements present in the target material with that of beam. Activation of thin layer of specific material under consideration, results in formation of completely new product through a specific reaction channel. Identification of various reaction products is done through γ -ray spectroscopy. By capturing specific γ - energies using high resolution detectors, the details of particular reaction product (corresponding to detected specific gamma energy) can be studied. Identification of reaction products may be done either using on-line or off-line measurement technique.

This thesis presents, the details of various experiments performed using the 15UD Pelletron Accelerator facility at Inter University Accelerator Center (IUAC), New Delhi, India. These irradiations in the selective materials were carried primarily for investigation of reaction dynamics. Experimental data obtained through irradiations has been further used to explore the yield and surface activity distribution which are very important parameters for TLA investigations. In section 3.1, details are provided on how the Pelletron Accelerator at IUAC is set up and operates. Details of target material preparation & further measurements have been discussed in section 3.2. Stack foil Activation technique is important, as large number of material samples can be irradiated in a single way. Samples of materials used are prepared in

stack and activation is achieved through stack foil activation. Details of stack arrangement and thickness are discussed in sections 3.3. Irradiation mechanism carried out alongwith post irradiation analysis, determining efficiency and calibration of HPGe detectors used, cross-section formulations and measurements with errors and uncertainties have been discussed in detail in sections 3.4 & 3.5. Overview of some of the simulation software and their functioning has been discussed in section 3.6.

3.1 PELLETRON ACCELERATOR AT IUAC

For a couple of years, the particle accelerators have been used in many research areas of sciences, engineering and medicine industries due to its multidisciplinary advantages and applications. Accelerator at IUAC, is a 15 UD Pelletron tandem accelerator. Particle as light as proton upto as heavy as Uranium can be accelerated through this accelerator independent of its charge and mass. The range of energy for acceleration varies from few tens of MeV to Hundreds of MeV. It is a vertical acceleration system constructed from a Stainless Steel tank with a diameter of 5.5 meters and a height of 26.5 meters. Since, accelerator is capable of producing million electric volts, it is maintained at $\approx 7-8$ atmospheric pressure by filling SF_6 di-electric constant gas for insulation and prevention of breakdown due to high potential. High voltage terminals are positioned in the center of the tank, which can support voltages between 4 and 16 million volts (MV). Pelletron accelerators work in a similar manner to Van-de Graff generators. Accelerator at IUAC is also known as Tandem Accelerator due to additional feature of utilizing its accelerating voltage twice before the particles interact with material. Once the terminal is fully charged to high voltage, any appropriate ion beam can be used to accelerate. Figure 3.1 is a schematic representation of the Pelletron accelerator. Working of acceleration of particles through Pelletron can be understood as follows [1-3].

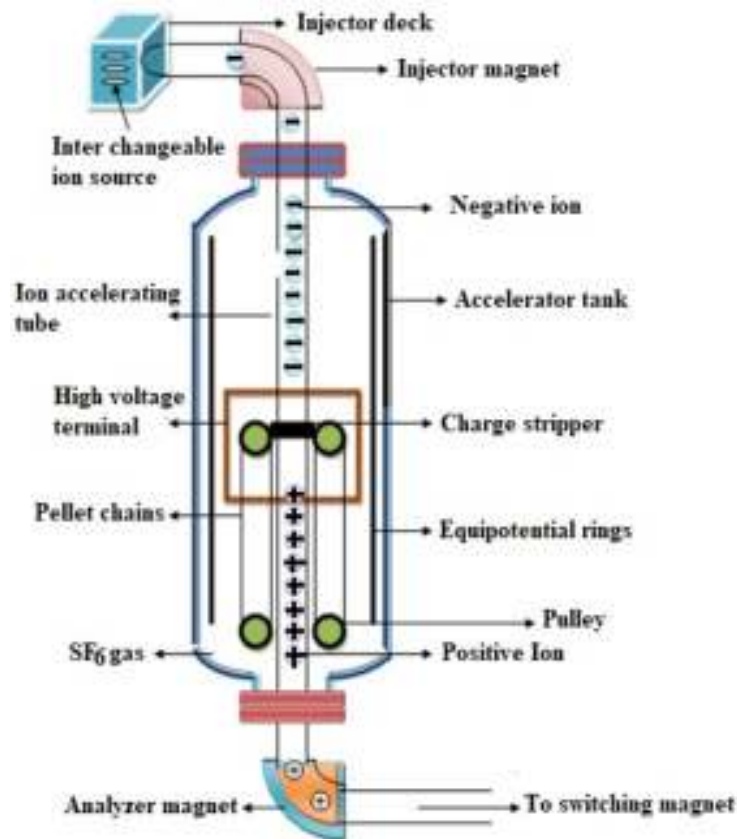


Figure 3.1: A schematic diagram of IUAC Pelletron Accelerator.

➡ Production of Negative Ion Source

Through addition of electron to neutrally charged ions, negative ion source are produced making use of Source of Negative Ions by Cesium Sputtering technique in which ion beams are generated by impacting cesium ions on cathode, which sputters out negative ions. These negatively charged ions are injected through injector deck at ground potential with the help of injector magnet from the top of tank. These beams are further accelerated towards a high positive potential fixed at the centre of tank.

➡ Stripping of the Negative Charge

The total energy gain by beam of particles is given by eV_t where (V_t is the terminal potential in MV). As the beam is accelerated towards positive

potential, it is made pass through charge a stripper which takes of the negative charge from the ion source, thus converting into positive charge.

➡ Acceleration due to same charge

As of now, the beam of charged particles are positively charged and the high voltage potential is also positive in charge, so the positive ions gets repelled and accelerated below the terminal to ground potential. If the charge state of positive ion after passing through the stripper at the terminal is q , then the energy gained in the acceleration below the terminal to the ground potential is qV_t . Therefore, after passing through the two stages of acceleration the final energy of the ion beam is given by,

$$E_{\text{final}} = E_0 + (q+1)V_t \quad (3.1)$$

where, E_0 = energy of ion before acceleration through terminal voltage V_t
 q = charge state of ion after stripping.

Since, initial energy before acceleration is infinitesimally small as compared to that of final energy after acceleration. The factor E_0 can be neglected in the above stated eqn and can be rewritten as,

$$E_{\text{final}} = (q+1)V_t \text{ MeV} \quad (3.2)$$

3.2 SAMPLE PREPARATION

Material samples for Terbium, Thulium and Tantalum systems for irradiation using Oxygen beam have been prepared through different techniques for measurement & analysis of cross-sections and activation depth achieved [4-6]. Details of techniques are described in following subsections.

3.2.1 ROLLING TECHNIQUE

Rolling machines were used in the target laboratory, IUAC, New Delhi, to prepare foils of Terbium, Thulium and Tantalum with ($\approx 99\%$ spectroscopic

purity) as shown in Figures 3.2 (a-b). With the help of these rolling machines, very thin foils of desired material can be prepared.



Fig. 3.2 (a) Rolling Machine 1 at IUAC

Foils of desired material is placed between the two mirror polished stainless steel rollers and then rolled through especially hardened rollers as shown in above figures. By applying appropriate pressure the gap between the rollers is gradually reduced to achieve foils as thin as possible. Thickness of foils ranging as low as $\approx 0.5\text{-}1\text{mg/cm}^2$ may be achieved through this technique. It is very efficient method having negligible loss in expensive materials used for fabrication [7-8].



Fig. 3.2 (b) Rolling Machine 1 at IUAC

Another technique which is used preparation of target samples which cannot be rolled or whose thickness is ranging in few tens of $\mu\text{g}/\text{cm}^2$ is achieved through evaporation technique. In this case, thin aluminium foils having thicknesses $1\text{-}1.5\text{ mg}/\text{cm}^2$ prepared by rolling are used as backing foils on which the material of choice in the powder form is deposited on this aluminium backing and then evaporated in vacuum chamber with pressure maintained in order of $\approx 10^{-6}$ bars using turbo molecular pump. Aluminium is deposited on glass slides using electron gun (2kW) bombardment technique, by maintain the vacuum conditions inside the chamber. Tantalum boats are used to generate maximum heat while evaporation in downward direction. Current used during evaporation ranges in between 100-170 mA. Evaporation process is monitored through quartz crystal set-up. After evaporation of thin foil is achieved on aluminium, it is allowed to cool for duration of 4-5 hours after which slides are carefully taken out. Thus the thin film of material deposited is removed through floating process in water and is taken further as sample material for performing experiments [7-8]. Schematic of evaporator used for preparation of thin aluminium backing has been presented in Figure 3.3.



Fig. 3.3. Evaporator Machine at IUAC

3.2.2. THICKNESS MEASUREMENT USING α -TRANSMISSION METHOD

Thickness of each sample foil is measured with the help of α -transmission method. In this α -particles having energy 5.486 MeV emitted through ^{241}Am source are allowed to pass through the sample foil to estimate energy loss of α -particles in sample thickness. Experimental set-up of thickness measurement is explained with the help of block diagram as shown in Figure 3.4

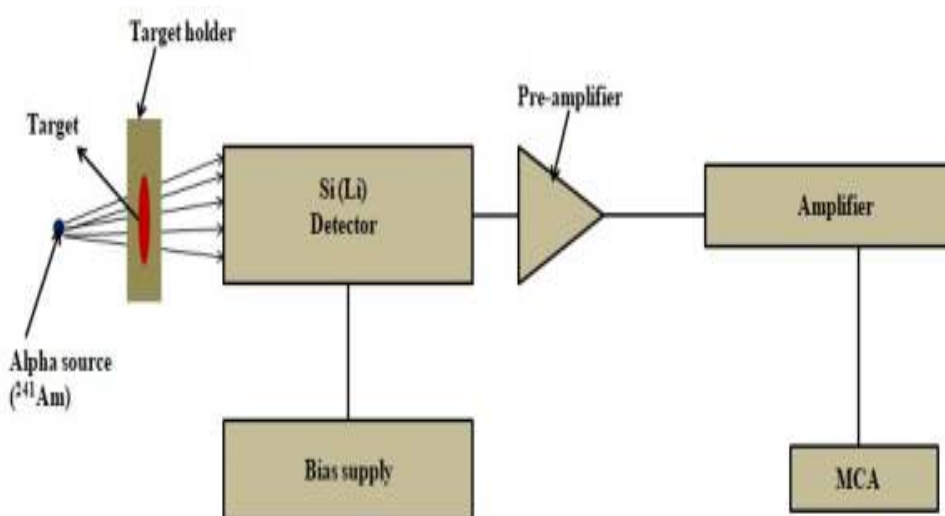


Fig. 3.4. Block diagram of α -transmission thickness measurement set-up

For determination of precise thickness of thin foils, α -spectrometer set-up is used. A pre- calibrated source of known strength i.e ^{241}Am is placed near the silicon detector. Thin foils obtained through rolling & evaporation techniques are mounted on target holder through which α -particles may pass. As they pass through thin foils, they lose an amount of energy (ΔE). The α -emissions are captured through detector, pre-amplifier and then amplifier in which peak fitting is carried out. This loss in energy ΔE across a thickness X of the material specimen is calculated through a parameter, known as stopping power which is estimated using SRIM calculation [9]. Thus, a very precise thickness measurement of samples in the form of thin foils can be determined through α -spectrometry set-up [10] as shown in Figure 3.5.



Fig. 3.5. α -spectroscopy thickness measurement set-up at Target Laboratory, IUAC

Detector, alpha source and target samples mounted on target holder are all kept in the vacuum chamber so as to avoid uncertainties in measuring γ -intensities. Multiple target samples can be mounted in one go on the slots provided on target holder thus reducing measurement and analysis time.

3.3 STACK FOIL ACTIVATION TECHNIQUE

Measurement and analysis of cross-sections for various reaction products have been done using stack foil activation technique. It is non-destructive technique used for determining the rate of interaction of material with the ion beam. Reactions initiated on stack of material results in formation of several reaction products through various reaction channels, due to nuclear interactions. Each of these reaction products can be identified individually through the emissions of characteristic γ -rays emitted and detected by HPGe detectors after activation. It is powerful technique to investigate reaction dynamics initiated after irradiation. In present work measurement and analysis of yield and surface activity in stacks of Terbium, Thulium, Tantalum and Nickel materials all backed by aluminium catcher foils of appropriate thickness which were initially irradiated for measuring nuclear interactions, has been further used for measuring cross-section and residual activity of a particular reaction using Oxygen and Alpha beams. Illustration of stack foil activation technique is shown in Figure 3.6. A charged particle beam of maximum energy obtained through accelerator is impinged on stack of target samples backed by Aluminium catcher foils as represented in above figure. As the beam traverse through thickness of complete stack, it keeps on losing its energy in each sample used in stack. This is also known as energy degradation technique through which, it is possible to activate same material samples in different energy regions using only one beam at fixed energy coming out of accelerator.

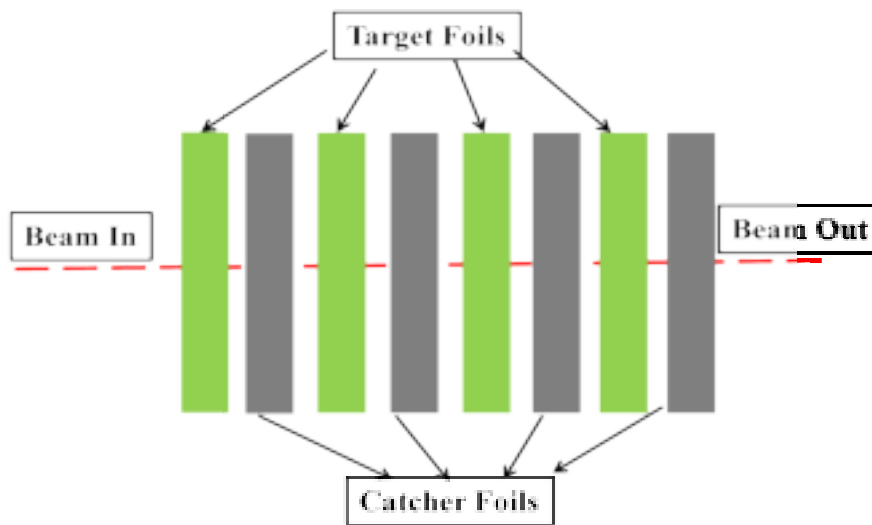


Figure 3.6. Stack foil activation using offline energy degradation technique

Advantage of this degradation technique is that activation can be achieved in multiple target samples simultaneously at varying thickness and energy regions using single beam, thus reducing the experimental time & cost [4-6].

Detailed discussion regarding calculations of thickness of target and catcher foils is illustrated with an example of stack calculation for any random material represented in figure 3.7 and table 3.1

Table 3.1. Sample stack thickness calculations by SRIM / TRIM

TARGET	THK (mg/cm ²)	CATCHER	THK (mg/cm ²)
STACK I			
T ₁	1.1	Al ₁	1
T ₂	1.3	Al ₂	1.1
T ₃	1.1	Al ₃	1
T ₄	1.11	Al ₄	1
STACK II			
T ₁	1.25	Al ₁	1.1
T ₂	1.5	Al ₂	1.2
T ₃	1.25	Al ₃	1.1

STACK III			
T ₁	1.2	Al ₁	1
T ₂	1.1	Al ₂	1.1
T ₃	1.2	Al ₃	1.1

Figure 3.6 is an illustration of general stack arrangement for target material with Aluminium backing. Thickness of each target sample with Aluminium catcher foil is presented in illustrated in Table 3.1. In the present studies Oxygen beam has been used for irradiation of the material with beam energies ranging from Coulomb Barrier (CB) upto 110 MeV, energy degradation or loss of energy observed between adjacent target and catcher arrangement is ranging from 3-5 MeV.

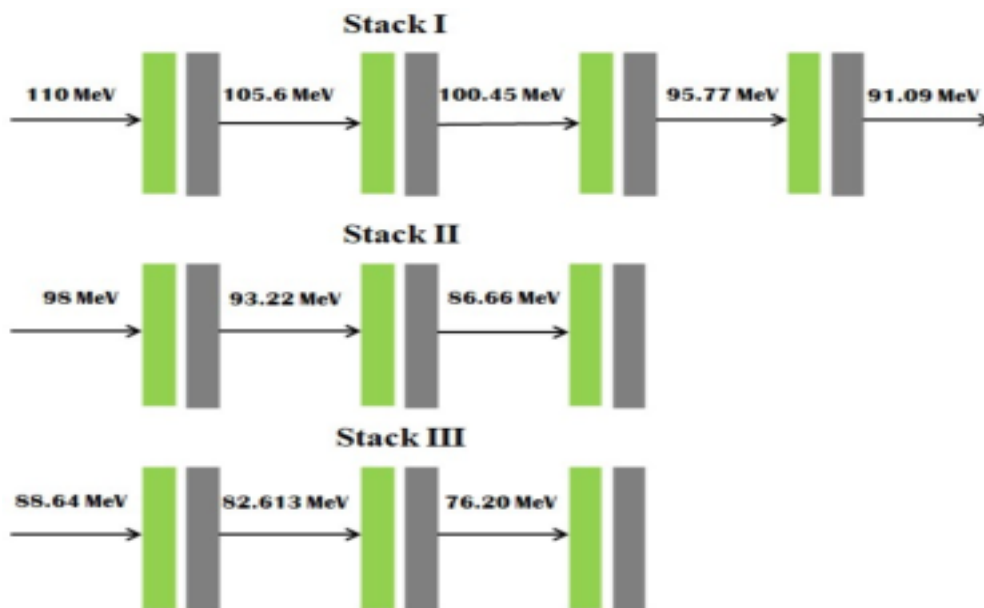


Figure 3.7. Illustration of random target sample stack calculations using energy degradation technique

Total energy points covered through single irradiation of stack are 11 as illustrated in figure 3.7. Loss of energy is calculated through dE/dX value obtained from SRIM calculations. Stack foil activation representation for target material having thickness in range of 1.1-1.5 mg/cm^2 with initial energy 110 MeV has been illustrated for understanding purpose.

As discussed earlier, in the present work, stacks of Terbium, Thulium and Tantalum which were irradiated initially to observe nuclear interactions have been further used for measuring residual activity distribution across thickness of material samples. Samples have been prepared and activated using Oxygen beam while natural Nickel material is activated using Alpha beams. For irradiation of Terbium system; two stacks containing four samples each was irradiated with beam energies 95 & 90 MeV respectively. For Thulium system; two stacks containing four samples each was irradiated with beam energies 95 & 92 MeV respectively. For Tantalum system; three stacks with four foils each was irradiated with beam energies 100, 98 & 88 MeV [4-6]. In case of $\alpha + {}^{nat}\text{Ni}$ system, single stack containing 8 foils was irradiated with 40 MeV α -beams [11]. Details of thickness of each target and catcher are discussed in next chapter 4

3.4 IRRADIATION

Primarily irradiations with Terbium, Thulium & Tantalum materials were carried out in General Purpose Scattering Chamber (GPSC) to investigate reaction dynamics and other parameters influencing around CB region [12-14]. Further these data has been extended in exploring measurement and analysis of yield and surface activity distribution which is an essential parameter for TLA based studies. GPSC is a stainless steel tank with 1.5 diameter housed with In-Vacuum Transfer (ITF) facility which allows transfer of stacks of target material without disturbing vacuum conditions inside tank. Using ITF lapse time can be reduced for counting the irradiated material and thereby detection of gamma radiations corresponding with short live reaction products. Beam line through the accelerator is connected to GPSC chambers equipped with powerful magnets and turbo molecular pump to maintain and guide the beam coming out from terminal potential of accelerator. Flux of the incident beam was measured through charge collected in the faraday up which is placed behind target catcher assembly. Stacks of target material samples were mounted on target catcher assembly whose position can be altered in

upward and downwards direction in order to align with the 90° incidence angle of beam. A pre-calibrated HPGe Detectors of 100 cc volume coupled to a PC

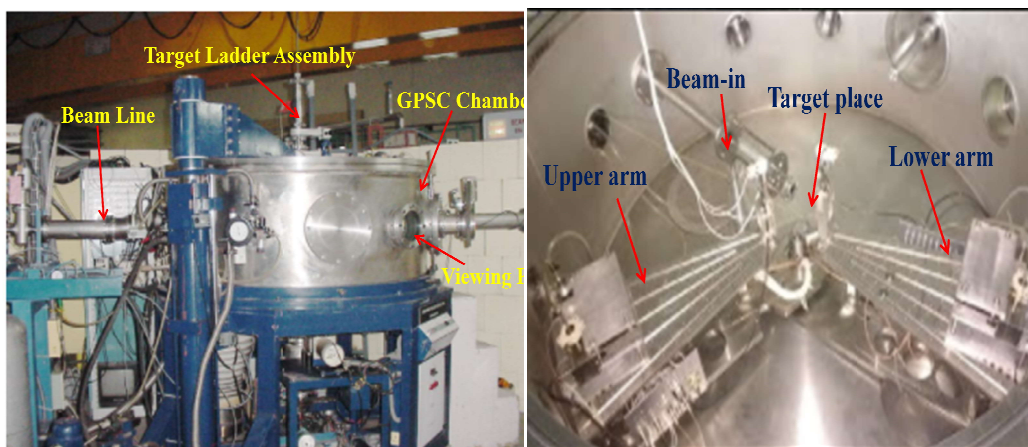


Figure 3.8. (a) Side view of GPSC at IUAC

Figure 3.8. (b) Inside view of GPSC at IUAC

through CAMAC based FREEDOM software was used to measure the amount of activity induced in target samples post irradiation. A typical side view and inside view of GPSC chamber is shown in Figures 3.8 (a-b) respectively.

3.5 POST-IRRADIATION ANALYSIS

In order to identify the characteristic γ -rays of evaporation residues in the complex γ -ray spectra, a detector of good resolution and proper calibration is required. The post irradiation analysis has been carried out using γ -ray spectrometer with a HPGe Detector.

3.5.1 CALIBRATION AND EFFICIENCY DETERMINATION OF HPGe DETECTOR

The HPGe detector was pre-calibrated both for energy as well as efficiency by using various standard γ -sources i.e., ^{22}Na , ^{60}Co , ^{133}Ba , ^{137}Cs and ^{152}Eu of known strengths. The prominent γ -rays of the standard ^{152}Eu source are given in Table 3.2, and have been used in the present measurements, both for energy calibration of the γ -ray spectrometer and for the determination of detector efficiency as a function of γ -ray energy

Table 3.2: A list of γ -ray energies and absolute intensities of some of the prominent γ -rays from ^{152}Eu .

γ -ray energy (keV)	Absolute Intensity (%)
121.78	28.58
244.69	7.58
344.27	26.54
443.96	2.82
778.90	12.94
867.37	4.24
964.07	14.60
1089.73	1.72
1112.07	13.64
1212.94	1.42
1299.14	1.62
1408.00	21.00

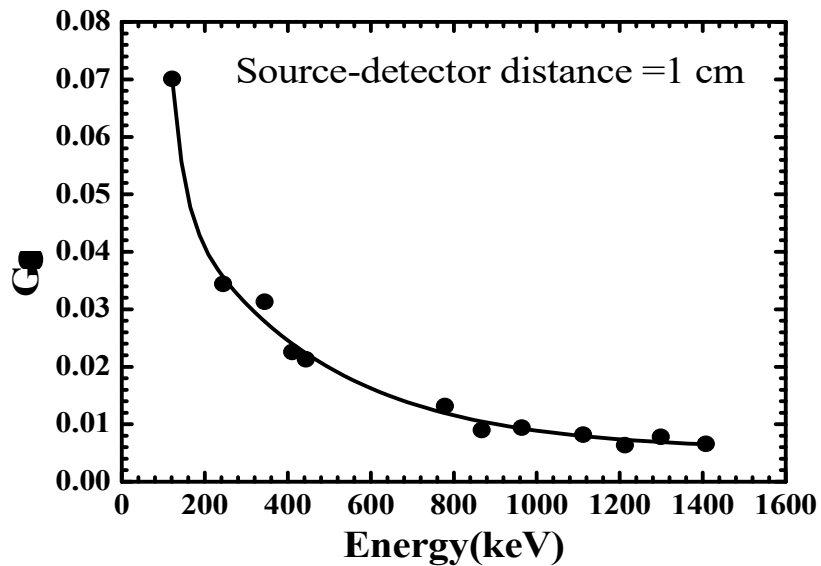


Figure 3.9: Geometry dependent efficiency curve as a function of γ -ray energy at source-detector separations $d=1$ cm. Solid lines represent the best polynomial fit.

The geometry dependent efficiency ($G\varepsilon$) of the HPGe detector at a given energy has been determined using the following expression;

$$G\varepsilon = \frac{N_0}{N_{a0}e^{(-\lambda t)\theta}} \quad (3.3)$$

where, N_o is the disintegration rate of the standard γ -source at the time of measurement, N_{ao} is the disintegration rate at the time of manufacture of the source, λ is the decay constant, t is the time lapse between the manufacture of the source and the start of the time of counting, and θ is the branching ratio of the characteristic γ -ray. In order to keep the geometry dependent detector efficiency same for standard γ -sources and samples/catchers, the standard γ -sources and the irradiated sample foils were counted in the same geometry. However, the source-detector separations for various irradiated samples were kept different, depending on the intensity of the induced activities, in order to keep the dead time of counting less than 10%. Typical geometry dependent efficiency as a function of γ -rays energy and for source-detector separations of 1 cm) are shown in Fig. 3.9. Further, the geometry dependent efficiency curves are found to be best fitted with a 5th order polynomial function of the type;

$$G_{\epsilon} = a_0 + a_1 E + a_2 E^2 + a_3 E^3 + a_4 E^4 + a_5 E^5 \quad (3.4)$$

where, E is the energy of the γ -ray and a_0, a_1, a_2, a_3, a_4 and a_5 are the coefficients having different values for each source-detector separation.

3.5.2 IDENTIFICATION OF REACTION PRODUCTS: DECAY CURVE ANALYSIS

Once the irradiation is done, the stacks of targets alongwith catcher foils were taken out of the GPSC with the help of ITF. The intensities of identified γ -peaks were recorded at increasing times to get their decay curves. The analysis of decay curves give the half-lives of the residues and thus confirmed their identification. This is a very specific way for the identification of reaction products because each radioactive isotope has a unique decay mode. As a representative case, a typical decay curve of ^{193g}Tl ($T_{1/2} = 21.6$ m) identified by 324.4 keV γ -ray is shown in Fig. 3.10. List of reaction products identified are given in Tables 4.2, 4.3, 4.4 and 4.5 in Chapter IV, alongwith their spectroscopic properties which have been taken from the Table of Isotopes.

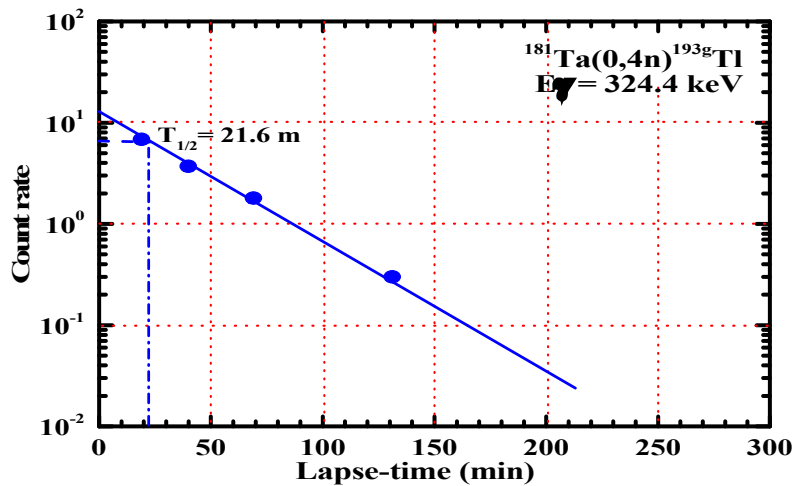


Fig. 3.10: Experimentally observed decay curve; the count-rates have been plotted on semi-log graph as a function of lapse time, which indicates the half-life of corresponding residue produced in $^{16}\text{O} + ^{181}\text{Ta}$ system.

3.5.3 DETERMINATION OF THE REACTION PRODUCTION CROSS-SECTION

For TLA investigation, yield of a particular reaction is measure of maximum probability of interaction of the given material with the ion beam at given set of conditions. Yield of a reaction depends upon production cross-section $\sigma_r(E)$ which is measure of probability of formation of a particular reaction product. On experimental basis, cross-section of a reaction $X(a,b)Y$ may be defined as total number of events occurring in per unit area and per unit target nucleus of material under investigation. Measuring unit for cross-section is expressed in barns. One barn equals to 10^{-28} m^2 . Mathematically, reaction cross-section may be represented as,

$$\sigma_r(E) = \frac{\text{Number of events of a given type } X(a,b)Y / \text{area}}{N_0 \Phi t} \quad (3.5)$$

where,

N_0 = Number of nuclei in the target,

Φ = incident beam flux

t = irradiation time

As represented in eqⁿ (3.5), for determining cross-section of any particular reaction, it is necessary to know the values of the quantities given in

denominator, while the quantities in expressed numerator, i.e. measurement of number of events of a given type needs to be determined. This is measured either by employing off-beam or in-beam techniques.

When a material sample is irradiated with the help of ion beams, it results in initiation of several nuclear reactions resulting in many reaction products through nuclear reactions. Determination of cross-sections for all such individual reaction products formed through activation analysis technique has been discussed in detail. Probability of formation of a particular reaction product initiated through nuclear reaction may be expressed by,

$$N = N_0 \phi \sigma_{X(a,b)Y} \quad (3.6)$$

where, $\sigma_{X(a,b)Y}$ is reaction cross-section or activation cross-section of a particular reaction product obtained through specific reaction channel. As discussed earlier there will be many reaction products initiated through nuclear reaction after ion beam material interaction, resultant products formed will be radioactive in nature and will keep on simultaneously decaying with respect to time. It is obvious with respect to increase in time after the stop of irradiation, rate of radioactivity will keep on decreasing. This disintegration rate can be expressed as,

$$\left[\frac{dN}{dt} \right]_t = N \frac{[1 - e^{(-\lambda t_1)}]}{e^{(\lambda t)}} \quad (3.7)$$

where,

t_1 = beam irradiation time and

λ = disintegration constant of induced activity which can be further expressed as,

$$\lambda = \frac{\ln 2}{t_{1/2}} \quad (3.8)$$

Decay of reaction products while irradiation of target material by a beam of incident particles is controlled by saturation factor $[1-\exp(-\lambda t_1)]$ which is also known as saturation correction. In a very small time dt , number of decays of induced radioactivity may be represented by,

$$dN = N \frac{[1-e^{(-\lambda t_1)}]}{e^{(\lambda t)}} dt \quad (3.9)$$

When the material is irradiated with ion beam, it is standard procedure to wait for some of highly radioactive products to completely disintegrate and then measure the data, so that the radioactivity levels reach well below the safety limits. As a result of which, a lapse time of interval t_2 is generated. If total measurement time of irradiated sample is given by t_3 , then the number reaction products decayed in time interval t_2 and $(t_2 + t_3)$ is expressed by,

$$C = N \frac{[1-e^{(-\lambda t_1)}][1-e^{(-\lambda t_3)}]}{\lambda \cdot e^{(t_2)}} \quad (3.10)$$

While performing experiments, the activity induced in the sample is recorded with the help of appropriate detector. For our experiments, detector used is gamma ray spectrometer of efficiency G_e , then absolute count rate C and observed counting rate A are expressed through relation as,

$$C = \frac{A}{\theta \cdot K \cdot G_e} \quad (3.11)$$

where,

A = Total number of counts of the induced activity during time interval t_3

θ = branching ratio of characteristic γ -ray indentified through spectrometer

G_e = Geometry dependent efficiency of detector.

K = Correction factor.

As irradiation of material takes place inside vacuum chamber, it is possible that small fraction of the γ -rays emitted after material irradiation gets absorbed

in the material itself across the varying thickness which is given as $K = [1 - \exp(-\mu d)]/\mu d$, where,

d = sample thickness in (gm/cm²)

μ = absorption co-efficient of gamma ray in material sample, (cm²/gm)

Thus overall cross-section of a nuclear reaction induced through irradiation of ion beam on selected target material can be expressed as,

$$\sigma_{X(a,b)Y}(E) = \frac{A.\lambda e^{(\lambda t_2)}}{N_0.\phi.K.G_\epsilon.[1-e^{(-\lambda t_1)}][1-e^{(-\lambda t_3)}]} \quad (3.12)$$

When irradiation stops at time $t = 0$, count rate $C_{t=0}$ is expressed by

$$C_{t=0} = \frac{A.\lambda e^{(\lambda t_2)}}{[1-e^{(-\lambda t_3)}]} \quad (3.13)$$

By making using of all the aforementioned equations and input parameters, final reaction cross-section $\sigma_{X(a,b)}$ is expressed as,

$$\sigma_{X(a,b)}(E) = \frac{C_{t=0}}{N_0.\phi.K.G_\epsilon.[1-e^{(-\lambda t_1)}]} \quad (3.14)$$

The above expression has been used to determine the reaction cross-sections using γ -spectroscopy in offline experiments carried with various materials terbium, thulium, tantalum & nickel materials which can be used for TLA investigations purposes in respective materials [15-16]. All these formulation are in built in PACE4 software which has been used to obtain the yield & calibration curves in above mentioned materials by measuring relative cross-sections and range of residual activity induced. A FORTRAN program EXP-SIGMA, based on the above formulations has been used for the determination of the reaction cross-sections of the reaction products.

3.5.4 EXPERIMENTAL UNCERTAINTIES; ERROR ANALYSIS

Since experimental set-up involves lot of prerequisite factors to be taken into consideration for obtaining results, some of the factors and errors associated while performing experiments are discussed as follows.

1. As discussed earlier that, irradiation with respective materials were carried out on stack of appropriate thickness on the basis of theoretical calculations. Since thickness of samples used are only few hundreds of milli-grams thickness, while rolling or evaporation of such thin foils may result in uncertainty and non-uniformity in stacks of respective samples. Although the sample thickness have been measured by highly sensitive α -transmission technique to reduce the errors introduced due to non uniformity, it has been still estimated that the error introduced in the target thickness is $\leq 1\%$.

2. The time of irradiation ranges from 8-12 hrs for almost all the selected target samples. It is possible that beam current may fluctuate in between while operating hours. Beam current influences the flux and thereby cross-section. Before carrying out experiments, many tests were performed to keep track of time-integrated beam fluctuations and errors resulting due to this were estimated to be not more than 4-5 % in measured cross-sections.

3. The errors resulting from solid angle defects accounts for less than 5%.

4. The attenuation in beam current when traversing foil thickness is estimated to cause errors of $\leq 2\%$.

5. In order to obtain accurate measurement of cross-sections, highly efficient HPGe detectors with spectrometry set-up to capture characteristic γ -rays was equipped. The efficiency of HPGe detectors was measured frequently during the run, using calibrated sources of ^{60}Co and ^{152}Eu . Dead time of detector was kept below 10% by properly adjusting the distance between source and detector. Statistical errors introduced were minimized through consideration of

large number of counts for comparatively longer times (≈ 5000 s). The uncertainty introduced due to curve fitting is estimated to be $< 3\%$. By taking into consideration of all the above mentioned uncertainties, maximum errors introduced in experimentally measured cross-sections is estimated to be less than 15%.

REFERENCES:

- [1] D. K. Avasthi; "Nuclear Physics News", Vol. 18, No. 1, 2008.
- [2] D. Kanjilal; 12TH International Conference on Heavy Ion Accelerator Technology, 2012
- [3] <https://www.iuac.res.in/>
- [4] D. P. Singh, Varun.V. Savadi, S.K.Joshi, Ishfaq Majeed, Md. Shuaib, V. R. Sharma, A. Yadav, P. P. Singh, Unnati, M. K. Sharma, R. Kumar, B. P. Singh and R. Prasad, "*Materials Today: Proceedings*", 17P1 (2019) pp. 266-270.
- [5] Varun .V. Savadi, D. P. Singh, S.K.Joshi, Ishfaq Majeed, Md. Shuaib, V. R. Sharma, A. Yadav, P. P. Singh, Unnat, M. K. Sharma, R. Kumar, B. P. Singh and R. Prasad, "*Materials Today: Proceedings*", 17P1 (2019) pp. 96-100.
- [6] Varun .V. Savadi, D. P. Singh, S.K.Joshi, Ishfaq Majeed, Md. Shuaib, V. R. Sharma, A. Yadav, P. P. Singh, Unnat, M. K. Sharma, R. Kumar, B. P. Singh and R. Prasad, "*Indian Journal of Pure and Applied Physics*", Vol.57 (2019) pp. 566-569.
- [7] S. R. Abhilash, J.Gehlot, Tathagata Banerjee, K. Selvakumar, Jasmeet Kaur & D. Kabiraj; "*Journal of Radioanalytical and Nuclear Chemistry*", vol 305, pp.749–753 (2015).
- [8] Abhilash S R and D Kabiraj; Proceedings of the DAE-BRNS Symp. on Nucl. Phys. 61 (2016).
- [9] Ziegler; James F; Biersack, Jochen P. "SRIM-2008, Stopping Power and Range of Ions in Matter".
- [10] H. Arora, Abhilash S. R, D. Kabiraj, G. R. Umamathy and B. R. Behera; Proceedings of the DAE Symp. on Nucl. Phys. 64 (2019).

- [11] Varun V Savadi, D P Singh, S K Joshi, A Yadav, P P Singh, M K Sharma, Unnati, M M Mustafa, B P Singh & R. Prasad, “*Indian Journal of Pure & Applied Physics*”, Vol. 59, May 2021, pp. 386-390.
- [12] Manoj Kumar Sharma , Unnati, B.P. Singh, Rakesh Kumar, K.S. Golda, H.D. Bhardwaj, R. Prasad, “*Nuclear Physics A*”, 776 (2006) 83–104.
- [13] Manoj Kumar Sharma, Unnati, B. K. Sharma, B. P. Singh, H. D. Bhardwaj, Rakesh Kumar, K. S. Golda, and R. Prasad, “*PHYSICAL REVIEW C*”, 70, 044606 (2004).
- [14] Devendra P. Singh, Unnati, Pushpendra P. Singh, Abhishek Yadav, Manoj Kumar Sharma, B. P. Singh, K. S. Golda, Rakesh Kumar, A. K. Sinha, and R. Prasad, “*PHYSICAL REVIEW C*”, 80, 014601 (2009).
- [15] Singh Bhanu Prakash; “Equilibrium and pre-equilibrium emission in alpha induced reactions at moderate excitation energies.” Ph.D. dissertation, Aligarh Muslim University, Aligarh, India, 1991.
- [16] Kumar, BP Ajith, “CANDLE. Collections and Analysis of Nuclear Data using Linux Network.” *DAE Symposium on Nuclear Physics*, Kolkata, India.

CHAPTER 4 MEASUREMENTS & RESULTS

4.1 THIN LAYER ACTIVATION (TLA) INVESTIGATIONS USING OXYGEN & ALPHA ION BEAMS.

TLA is a powerful technique used for monitoring surface degradation phenomena like wear, corrosion, erosion etc in various industrial applications by measuring cross-section, yields and residual activity induced in materials subjected to irradiation [1-6]. Measurements & results obtained for surface activity induced through oxygen beam in different rare earth materials like Tantalum, Terbium & Thulium, having great significance in critical industrial applications have been discussed in detail. Further measurements & results obtained for surface activity induced through α (Alpha) ion beam in natural nickel material by TLA investigations having extensive applications in the form of coatings and construction material across various industries has also been discussed in detail. In case of TLA, usually one nuclear reaction having the maximum cross-section and yields is taken into consideration for practical applications. Nickel based alloys and coatings have evolved mature subject of research and development from tribological applications point of view due to excellent anti wear & corrosion resistant properties [7-9]. To measure the activity induced by α -particles in Nickel material with energies between 10 and 40 MeV, stack foil activation procedure has been employed and irradiations of stacks were carried out at the Variable Energy Cyclotron Centre (VECC), Kolkata, India. Various reactions for which surface activity has been determined are $^{61}\text{Ni}(\alpha, 3n)^{62}\text{Zn}$, $^{61}\text{Ni}(\alpha, 2n)^{63}\text{Zn}$, $^{60}\text{Ni}(\alpha, p2n)^{61}\text{Cu}$, $^{60}\text{Ni}(\alpha, n)^{63}\text{Zn}$, $^{60}\text{Ni}(\alpha, 2n)^{62}\text{Zn}$, $^{58}\text{Ni}(\alpha, p)^{61}\text{Cu}$ and $^{58}\text{Ni}(\alpha, pn)^{60}\text{Cu}$ across different beam energies in $\alpha+^{\text{nat}}\text{Ni}$ system. Surface activity has been estimated through calibration curves of respective reaction products by measuring cross-sections.

Since, present research work is focussed on predicting the feasibility of TLA investigations in the above mentioned materials, all the reactions induced through different channels with measurable cross-section and half-life values have been considered for analysis [10-12]. Experiments were initially carried out for measuring nuclear interactions near coulomb barrier region in Terbium, Thulium & Tantalum material at Inter University Accelerator Center (IUAC), New Delhi. Through the data obtained from irradiations in these materials surface activity induced in thin layer of Terbium, Thulium & Tantalum materials using Oxygen beam has been determined.

Table 4.1 List of systems for which cross-sections, beam energy range and activation threshold energy measured are listed below

SL NO	Material	Ion Beam	Energy Range (MeV)	Activation threshold energy (MeV)
1.	Terbium	Oxygen	≈ 70-95	63.69
2.	Thulium	Oxygen	≈ 71-95	66.99
3.	Tantalum	Oxygen	≈ 70-110	70.09
4.	Nickel	Alpha	≈ 10-40	8.80

Table 4.1 lists the systems for which cross-sections, yields and range of activity have been measured, along with the energy range of activation and threshold energy for each system to obtain results. In the above mentioned systems, analysis has been performed from threshold energy activation and well above it for TLA investigation purposes. Cross-section and yield for all the systems are obtained by employing stack foil activation which has been discussed further in subsequent sections.

4.2 STACK FOIL ACTIVATION TECHNIQUE

Self supporting targets of ^{159}Tb spectroscopically (99.99% pure) having thickness $\approx 1.7 \text{ mg/cm}^2$ backed by Al-catchers of thickness $\approx 2 \text{ mg/cm}^2$ were prepared by rolling method. Targets of ^{169}Tm spectroscopically $\approx 100\%$ having $\approx 0.65 \text{ mg/cm}^2$ thickness were deposited on Al-backing of 1.5 mg/cm^2 thickness, using high vacuum-evaporation technique. Targets of ^{181}Ta of thickness $\approx 1.5 \text{ mg/cm}^2$ were deposited by electro deposition technique on Al-backing of thickness $\approx 1-1.5 \text{ mg/cm}^2$. In case of ^{159}Tb , two stacks containing four samples each were irradiated at energies 90 & 95 MeV respectively. In first stack, the thickness of four Tb samples were $\approx 1.65, 1.68, 1.57$ and 1.62 mg/cm^2 while corresponding catcher thickness were $\approx 1.71, 1.82, 1.69$ & 1.87 mg/cm^2 respectively. In second stack, the thickness of four Tb samples was $1.67, 1.72, 1.64$ and 1.81 mg/cm^2 while corresponding catcher thickness were $1.74, 1.86, 1.78$ & 1.94 mg/cm^2 respectively. The energy range covered in irradiating first stack of Tb was from 90 MeV to 65.5 MeV with intermediate energy points obtained at 83.2 MeV & 75.2 MeV respectively. Energy range covered in irradiating second stack of Terbium was from 95 MeV to 69.3 MeV with intermediate energy points obtained at 87.2 MeV & 78.7 MeV respectively. In case of ^{169}Tm , two stacks containing four samples each were irradiated at energies 92 & 95 MeV respectively. In first stack thickness of Tm samples were $\approx 0.83, 0.69, 0.57$ and 0.63 mg/cm^2 while corresponding catcher thickness were $1.42, 1.36, 1.29$ & 1.33 mg/cm^2 respectively. In second stack thickness of Tm samples were $\approx 0.71, 0.69, 0.73$ and 0.64 mg/cm^2 while corresponding catcher thickness were $1.41, 1.38, 1.47$ & 1.29 respectively. After irradiation, energy range covered was from 95 MeV to 71 MeV.

Further in case of ^{181}Ta , three stacks, with four foils, three foils and one foil respectively, were irradiated at 100, 98 & 88 MeV beam energies to cover a wide energy range. In the first stack, the thicknesses of four Ta samples were $1.25, 1.43, 1.42$ and 1.22 mg/cm^2 while the thicknesses of corresponding Al-catchers were $\approx 1.16, 1.76, 2.01$ and 1.24 mg/cm^2 respectively. In the second stack, the thicknesses of three Ta samples were $\approx 1.28, 2.03$ and 1.76 mg/cm^2

while the thicknesses of corresponding Al-catchers were ≈ 1.81 , 1.65 , and 1.47 mg/cm^2 respectively. However, in the third one containing single foil, the thickness of Ta sample was ≈ 1.22 mg/cm^2 while the thickness of corresponding Al catcher was ≈ 1.29 mg/cm^2 [10-12]. Backing with Al-catchers helped to serve as both energy degrader as well as catcher for residues recoiling out of target foil during the irradiations. α -transmission method was used to measure the thickness of each target. Measurement of energy lost by 5.487 MeV α -particles obtained from standard ^{241}Am source, while passing through the material of target is used to employ this technique. The targets were cut into the size of 1.2×1.2 cm^2 were pasted on Al holders having concentric hole of 1.0 cm diameter. Successive targets of the stack get irradiated at different energies. The energies of the incident ion on successive targets have been calculated using stopping power values obtained from code SRIM based on the range-energy formulations [13]. The stacks were placed normal to the beam direction, so that the recoiling products could be trapped in the catcher foil placed just behind the target and there would be no loss of activity. Beam current varying from ≈ 30 to 50 nA was used and the irradiations were carried out for ≈ 8 – 12 h duration for each stack. After the irradiation of the materials in different stacks, targets/ material samples along with catcher foils was taken out from the GPSC with the help of ITF. The evaporation residues populated in each target catcher foil assembly were identified by (characteristic γ -rays).

The activities induced in the irradiated samples were recorded using HPGe γ -ray spectrometer. The HPGe detector was pre-calibrated both for energy as well as efficiency by using various standard sources i.e, ^{60}Co and ^{152}Eu of known strengths. To obtain the residual activity measured cross sections of various reaction products were plotted at varying energies versus thickness of the target. Residual activity was calculated using remnant activity obtained from measured cross-section versus varying thickness of the target material. Further details regarding the experiment are given elsewhere [10–12].

Table 4.2 Decay data of reaction products identified through reactions in Terbium material

SL NO	System: $^{16}\text{O} + ^{159}\text{Tb}$				
	Reactions	Reaction Product	Half-Life	E_{γ} (keV)	Intensity (%)
1	$^{159}\text{Tb} (^{16}\text{O}, 3\text{n})$	^{172}Ta	36.8 m	213.9, 318.7	52, 49
2	$^{159}\text{Tb} (^{16}\text{O}, 4\text{n})$	^{171}Ta	23.3 m	152.2, 166.1	5.8, 19.8
3	$^{159}\text{Tb} (^{16}\text{O}, 5\text{n})$	^{170}Ta	6.76 m	860.4, 986.9	7.3, 3.3
4	$^{159}\text{Tb} (^{16}\text{O}, \text{p}3\text{n})$	^{171}Hf	12.1 h	122, 137.6	11.5, 12.7
5	$^{159}\text{Tb} (^{16}\text{O}, \text{p}4\text{n})$	^{170}Hf	16.01 h	120.1, 164.6	19, 33
6	$^{159}\text{Tb} (^{16}\text{O}, 2\text{p}2\text{n})$	^{171}Lu	8.24 d	667, 739.8	11, 48.1
7	$^{159}\text{Tb} (^{16}\text{O}, \alpha\text{n})$	^{170}Lu	2.0 d	193.1	2.07
8	$^{159}\text{Tb} (^{16}\text{O}, \alpha 2\text{n})$	^{169}Lu	1.41 d	191.2	20.7
9	$^{159}\text{Tb} (^{16}\text{O}, 2\alpha 2\text{n})$	^{165}Tm	1.25 d	242.8, 296.0	35, 23

Table 4.3 Decay data of reaction products identified through reactions in Thulium material

SL NO	System: $^{16}\text{O} + ^{169}\text{Tm}$				
	Reactions	Reaction Product	Half-Life	E_{γ} (keV)	Intensity (%)
1	$^{169}\text{Tm} (^{16}\text{O}, 3\text{n})$	^{182}Ir	15 m	126.9, 273.1	34.4, 43
2	$^{169}\text{Tm} (^{16}\text{O}, 4\text{n})$	^{181}Ir	4.90 m	107.6, 123.5	15.2, 8.7
3	$^{169}\text{Tm} (^{16}\text{O}, \text{p}2\text{n})$	^{182}Os	22.10 h	180.22, 263.29	34.7, 6.6
4	$^{169}\text{Tm} (^{16}\text{O}, \text{p}3\text{n})$	$^{181\text{g}}\text{Os}$	105 m	238.68, 826.74	44, 20.2
5	$^{169}\text{Tm} (^{16}\text{O}, 2\text{p}2\text{n})$	^{181}Re	19.9 h	360.7, 365.59	20, 57
6	$^{169}\text{Tm} (^{16}\text{O}, \alpha 3\text{n})$	^{178}Re	13.2 m	237.19	45
7	$^{169}\text{Tm} (^{16}\text{O}, 2\alpha\text{p}\text{n})$	^{175}Hf	70 d	343.4	87
8	$^{169}\text{Tm} (^{16}\text{O}, 3\alpha\text{n})$	^{172}Lu	6.70 d	1093.6	63.5

Table 4.4 Decay data of reaction products identified through reactions in Tantalum material

SL NO	System: $^{16}\text{O} + ^{181}\text{Ta}$				
	Reactions	Reaction Product	Half-Life	E_{γ} (keV)	Intensity (%)
1	$^{181}\text{Ta} (^{16}\text{O}, 3\text{n})$	$^{194}\text{Tl}^{\text{g}}$	32.8 m	636.1	99
2	$^{181}\text{Ta} (^{16}\text{O}, 3\text{n})$	$^{194}\text{Tl}^{\text{m}}$	33 m	636.1	15.3
3	$^{181}\text{Ta} (^{16}\text{O}, 4\text{n})$	$^{193}\text{Tl}^{\text{g}}$	2.1 m	365	90.1
4	$^{181}\text{Ta} (^{16}\text{O}, 4\text{n})$	$^{193}\text{Tl}^{\text{m}}$	21.6 m	324.4, 1044.7	15.2, 8.99
5	$^{181}\text{Ta} (^{16}\text{O}, 5\text{n})$	$^{192}\text{Tl}^{\text{g}}$	10.6 m	422.9	31.1
6	$^{181}\text{Ta} (^{16}\text{O}, 5\text{n})$	$^{192}\text{Tl}^{\text{m}}$	9.6 m	422.9	31.1
7	$^{181}\text{Ta} (^{16}\text{O}, \text{p}3\text{n})$	$^{193}\text{Hg}^{\text{g}}$	3.8 h	381.6, 539	11.0, 1.2
8	$^{181}\text{Ta} (^{16}\text{O}, \text{p}3\text{n})$	$^{193}\text{Hg}^{\text{m}}$	11.8 h	258.1	60
9	$^{181}\text{Ta} (^{16}\text{O}, \text{p}4\text{n})$	^{192}Hg	4.85 h	274.8	50
10	$^{181}\text{Ta} (^{16}\text{O}, \text{p}5\text{n})$	$^{191}\text{Hg}^{\text{g}}$	49 m	224.6, 241.2	17.4, 8.9
11	$^{181}\text{Ta} (^{16}\text{O}, \text{p}5\text{n})$	$^{191}\text{Hg}^{\text{m}}$	50.85 m	420.3, 578.7	17.9, 17
12	$^{181}\text{Ta} (^{16}\text{O}, \alpha\text{n})$	^{192}Au	4.94 h	295.5, 316.5	22.7, 58
13	$^{181}\text{Ta} (^{16}\text{O}, \alpha 2\text{n})$	^{191}Au	3.18 h	283.9, 399.8	6.3, 4.5
14	$^{181}\text{Ta} (^{16}\text{O}, \alpha 3\text{n})$	^{190}Au	42.8 m	295.9, 301.9	71, 25.1

Table 4.5 Decay data of reaction products identified through reactions in nickel material with alpha beam.

SL NO	System: $\alpha + {}^{58, 60, 61\text{nat}}\text{Ni}$				
	Reactions	Reaction Product	Half-Life	E_{γ} (keV)	Intensity (%)
1	${}^{58}\text{Ni}(\alpha, p)$	${}^{61}\text{Cu}$	3.33 h	475.0, 969.98	100
2	${}^{58}\text{Ni}(\alpha, pn)$	${}^{60}\text{Cu}$	23.7 m	364.6, 453.8	100
3	${}^{60}\text{Ni}(\alpha, p2n)$	${}^{61}\text{Cu}$	3.33 h	475.0, 969.98	100
4	${}^{60}\text{Ni}(\alpha, n)$	${}^{63}\text{Zn}$	38.47 m	627.10, 637.04	100
5	${}^{60}\text{Ni}(\alpha, 2n)$	${}^{62}\text{Zn}$	9.186 h	953.8, 850.8	100
6	${}^{61}\text{Ni}(\alpha, 3n)$	${}^{62}\text{Zn}$	9.186 h	953.8, 850.8	100
7	${}^{61}\text{Ni}(\alpha, 2n)$	${}^{63}\text{Zn}$	38.47 m	627.10, 637.04	100

Investigations and TLA analysis of reaction products for nearly 29 reactions initiated through Oxygen and Alpha beam on Terbium, Thulium, Tantalum and Nickel material have been measured.

4.3 TLA REACTIONS INITIATED USING OXYGEN (HEAVY ION) BEAM

4.3.1 TLA INVESTIGATIONS IN SPECTROSCOPICALLY PURE ($\approx 99\%$) TERBIUM MATERIAL USING OXYGEN (HEAVY ION) BEAM

Since Terbium is being used in solid state devices applied in nuclear plants; low energy light bulbs and mercury lamps; in medical X-ray imaging with reduced exposure time and also in laser devices in the form of terbium salts and in wind turbine blades, we had considered this material for study of surface activity induced over different energy ranges. Reaction cross-sections for several reaction products populated via different reaction channels;

$^{172}\text{Ta}(3\text{n})$, $^{171}\text{Ta}(4\text{n})$, $^{170}\text{Ta}(5\text{n})$, $^{171}\text{Hf}(p3\text{n})$, $^{170}\text{Hf}(p4\text{n})$, $^{171}\text{Lu}(\alpha)$, $^{170}\text{Lu}(\alpha\text{n})$, $^{169}\text{Lu}(\alpha 2\text{n})$ & $^{165}\text{Tm}(2\alpha 2\text{n})$ have been measured in $^{16}\text{O}+^{159}\text{Tb}$ system from threshold (≈ 70 MeV) to well above it (≈ 100 MeV).

4.3.1.1 MEASUREMENT OF CROSS-SECTION AND YIELD CURVES

Cross-sections obtained for various isotopes populated through various reaction channels across different energies are used to calculate the total yield and residual activity induced for application in thin layer activation technique. The yield curves of the isotopes, i.e., the variation of yield against the depth from the surface, are measured through stacked-foil irradiation using thin metal foils. The yield of the isotopes produced in each foil of the stack is obtained from the activity measured in the foils and a plot of the yield of the isotope against the depth at which the foil is located, generates the yield curve. The activities induced in each foil of the stack were used to deduce the yields of the isotopes of interest. The stopping power of ^{16}O beams has been used to obtain the incident energy on each foil. The yields of $^{172,171,170}\text{Ta}$, $^{171,170}\text{Hf}$, $^{171,170,169}\text{Lu}$ and ^{165}Tm isotopes have been obtained, from the intensity of characteristic γ -lines, at different energies of ^{16}O beam, i.e., at different depths from the experiment carried out for the measurement of the cross-sections of the reactions. The yield per micron thickness against the depth as well as incident energy for several nuclides is shown in Figures. 1-3 [10]. Table 4.6 represents details of 3 reaction products obtained by irradiation of Terbium material with Oxygen beam in the energy range of 70-95 MeV in xn reaction channels which can be used for TLA investigation purpose in various industrial applications. Total cross-section for reaction products $^{172, 171, 170}\text{Ta}$ obtained through 3n, 4n & 4n reaction channels respectively in Terbium material is measured by summing up of all individual cross-sections obtained at varying depths ranging from 0-16 microns and at varying energy range from 70-95 MeV incident Oxygen beam. Total cross-section values for $^{172, 171, 170}\text{Ta}$ is 136.144, 1140.33 & 925.09 mb respectively as represented in Table 4.6.

Table 4.6 Measured cross-sections at different energies for reaction products identified in $^{16}\text{O} + ^{159}\text{Tb}$ through xn reaction channels for application in TLA [15].

System: $^{16}\text{O} + ^{159}\text{Tb}$				
SL NO	Energy (MeV)	^{172}Ta	^{171}Ta	^{170}Ta
1	69.4 ± 1.0	0.3 ± 0.0		
2	75 ± 0.9	19.8 ± 3.3		
3	78.7 ± 0.9	34.8 ± 6.8	67.0 ± 11.8	
4	83.2 ± 0.8	48.14 ± 5.5	280.5 ± 47	64.9 ± 6.6
5	87.2 ± 0.8	12.6 ± 2.2	244 ± 43.3	100.2 ± 15.4
6	90 ± 1.0	11.8 ± 2.4	228.3 ± 39.2	263.4 ± 38.7
7	95 ± 0.7	8.53 ± 1.5	157.9 ± 28.5	390.1 ± 45.5

It has been discussed in earlier sections; cross-section is the measure of interaction probability between incident ion and material resulting in final yield of specific reaction product obtained. In Fig 1 yield curves have been obtained with polynomial order of 4 for smooth fitting. Maximum yield has been observed for reaction product ^{171}Ta obtained through 4n reaction channel.

Table 4.7 Measured cross-sections at different energies for reaction products identified in $^{16}\text{O} + ^{159}\text{Tb}$ through pxn reaction channels for application in TLA [15].

System: $^{16}\text{O} + ^{159}\text{Tb}$					
SL NO	Energy (MeV)	$^{171}\text{Hf}^{\text{cum}}$	$^{171}\text{Hf}^{\text{ind}}$	$^{170}\text{Hf}^{\text{cum}}$	$^{170}\text{Hf}^{\text{ind}}$
1	69.4 ± 1.0				
2	75 ± 0.9	13.6 ± 5.6			
3	78.7 ± 0.9	80.2 ± 19	11.01 ± 5		
4	83.2 ± 0.8	431.2 ± 86.2	141.4 ± 56.6	84.6 ± 10	19.2 ± 2.3
5	87.2 ± 0.8	322 ± 74.4	69.9 ± 29.9	177.3 ± 20	76.3 ± 11.8
6	90 ± 1.0	340.1 ± 73.4	104.3 ± 41.7	574.3 ± 68.8	308.2 ± 36.7
7	95 ± 0.7	205.4 ± 46.2	42.1 ± 18	427.3 ± 55	34.8 ± 10.8

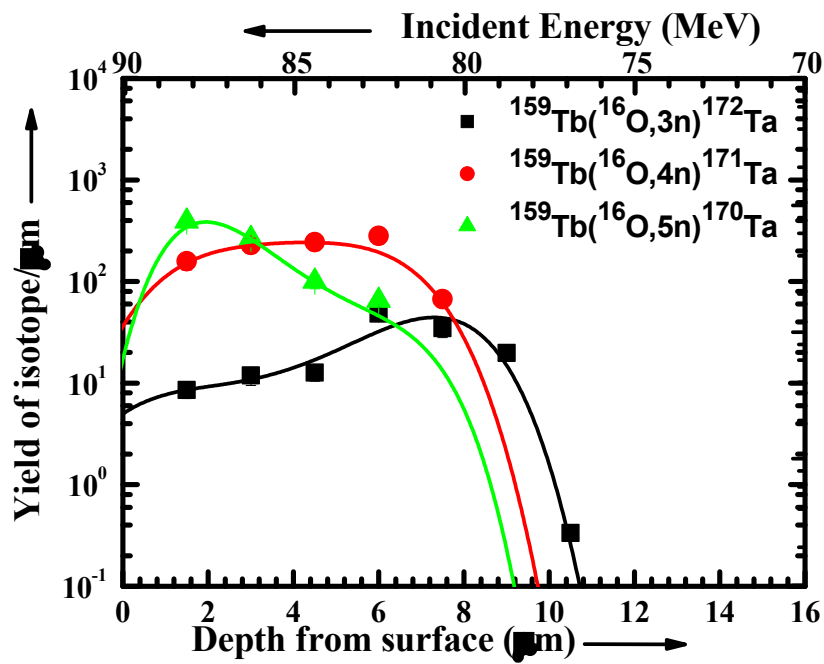


Fig 1 Yield curves of reaction products $^{172,171,170}\text{Ta}$ in Terbium material

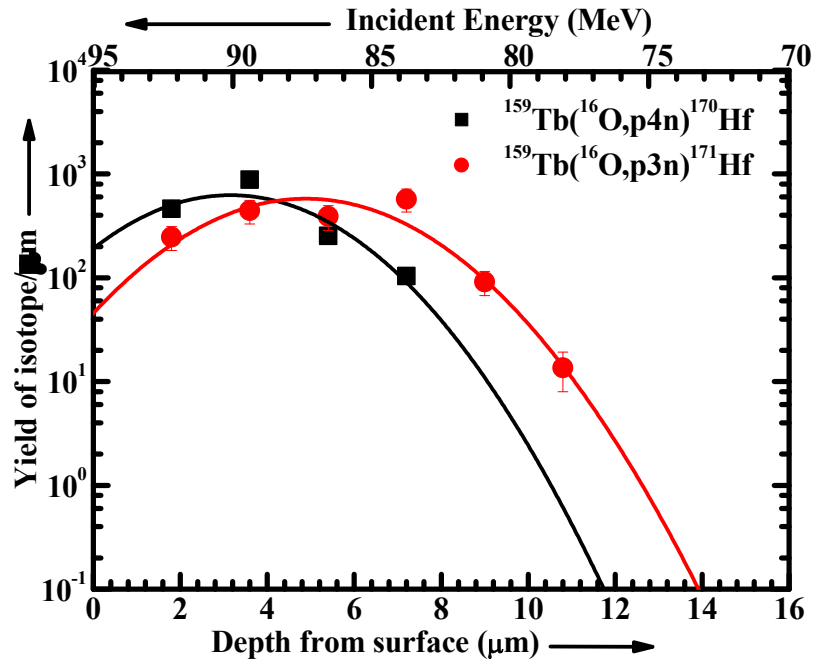


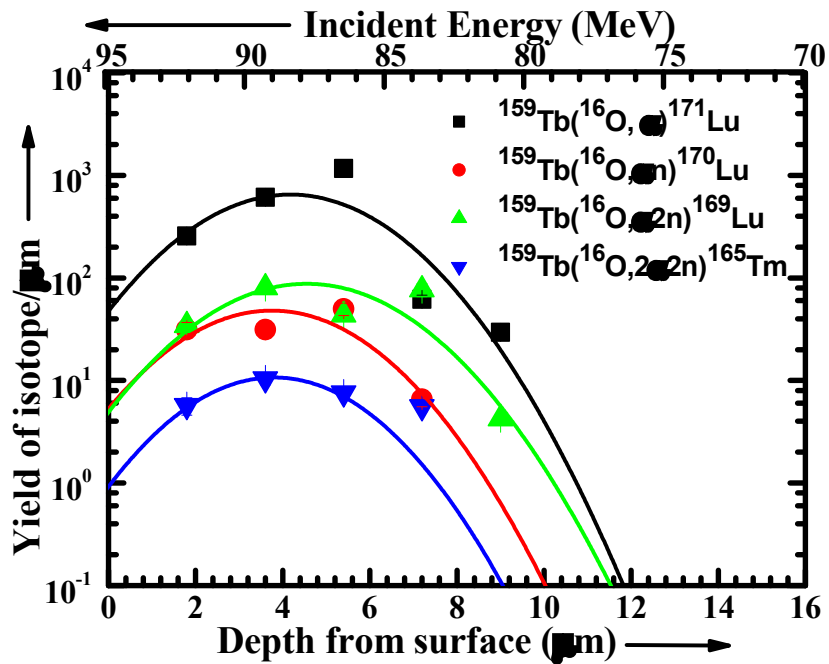
Fig 2 Yield curves of reaction products $^{171,170}\text{Hf}$ in Terbium material

Fig 2 illustrates plot of yield obtained through cross-section measurements for reaction products $^{171}, ^{170}\text{Hf}$ in p3n and p4n reaction channels of Terbium material respectively. Total cross-section values for $^{171}, ^{170}\text{Hf}$ is 2217.21 & 1917.4 respectively as represented in Table 4.7. Maximum yield has been observed for reaction product ^{171}Hf obtained through p3n reaction channel.

Table 4.8 Measured cross-sections at different energies for reaction products identified in $^{16}\text{O} + ^{159}\text{Tb}$ through α -reaction channels for application in TLA [15].

System: $^{16}\text{O} + ^{159}\text{Tb}$					
SL NO	Energy (MeV)	^{171}Lu	^{170}Lu	^{169}Lu	^{165}Tm
1	69.4 ± 1.0				
2	75 ± 0.9				
3	78.7 ± 0.9	29.5 ± 3.1		4.2 ± 0.4	
4	83.2 ± 0.8	61.6 ± 6.5	6.5 ± 1.0	76.8 ± 11.2	5.53 ± 0.58
5	87.2 ± 0.8	1167.62 ± 170.6	49.8 ± 6.7	43.4 ± 4.5	7.58 ± 0.8
6	90 ± 1.0	611.8 ± 64	31.3 ± 5.4	80.65 ± 9.4	10.36 ± 1.3
7	95 ± 0.7	255.8 ± 26.3	31.3 ± 5.4	34.4 ± 4.5	5.76 ± 1.1

Fig 3 illustrates plot of yield obtained through cross-section measurements for reaction products $^{171}, ^{170}, ^{169}\text{Lu}$ in α ; αn ; $\alpha 2n$ & ^{165}Tm in $2\alpha 2n$ reaction channels of Terbium material respectively. Total cross-section values for $^{171}, ^{170}, ^{169}\text{Lu}$ & ^{165}Tm is 2396.8, 137.64, 269.65 & 25.17 respectively as represented in Table 12. Maximum yield has been observed for reaction product ^{171}Lu obtained through α reaction channel.



**Fig 3 Yield curves of reaction products
^{171, 170, 169}Lu, ¹⁶⁵Tm in terbium material**

4.3.1.2 MEASUREMENT OF ACTIVITY AND CALIBRATION CURVES

The yield per micron thickness against the depth as well as incident energy for several nuclides is shown in Figures. (1-3). The calibration curve is then obtained by plotting the percentage of the remaining activity against the depth of material removed from the surface and the calibration curves so deduced from the yield curves are shown in Figs (4-6). Residual activity of radioisotopes populated via various xn, pxn and αxn channels were found to have contribution upto ≈ 13μm depth from the surface. The remnant activity induced in the Terbium material for several nuclides populated through various xn, pxn and αxn channels are as represented in Figures. (4-6) [10].

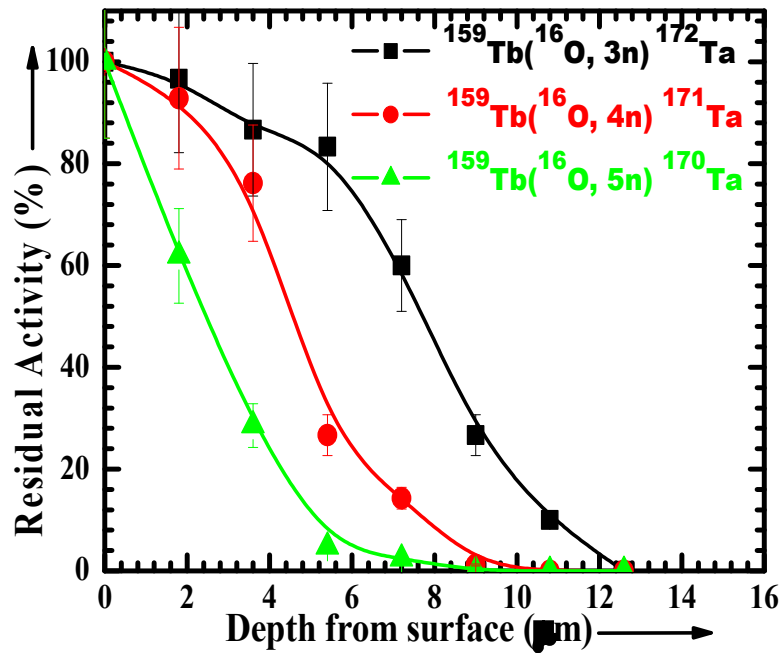


**Fig 4 Calibration curves of reaction products
 $^{172,171,170}\text{Ta}$ in terbium material**

Fig 4 illustrates plot of residual activity obtained through cross-section measurements for reaction products $^{172,171,170}\text{Ta}$ through 3n, 4n and 5n reaction channels of Terbium material respectively. Maximum activity has been observed in xn reaction products is approximately ranging upto 12.6 microns. At surface of material, it is obvious that beam will transfer all its intensity and as it traverses through thickness of nearly 13 microns, it will keep on attenuating unless it reaches zero. Fig 4 represents the distribution of activity for 3 reaction products ^{172}Ta , ^{171}Ta & ^{170}Ta individually highlighted with black squares, red circles, green triangles symbols and curves respectively from 100% intensity upto 0%. Fig 5 illustrates the plot of residual activity obtained through cross-section measurements for reaction products $^{171,170}\text{Hf}$ in p3n and p4n reaction channels of Thulium material respectively. Maximum activity observed for reaction products through pxn channels is approximately upto 9 microns for reaction product ^{171}Hf after which it is approaching towards zero. For reaction product ^{170}Hf least activity of 6.25% intensity is observed at nearly 7.2 micron thickness, beyond this

depth the intensity of beam is nearly 0. Detailed distribution of residual activity ranging from thickness 0 to 12 microns with respective intensities has been presented in Table 4.10

TABLE 4.9 Residual Activity range distribution range in Terbium material for xn reaction channels using ^{16}O beam in energy range 70-95 MeV as presented in Fig 4 [10].

Thickness Range (μm)	ACTIVITY INDUCED (%)		
	^{172}Ta	^{171}Ta	^{170}Ta
0	100	100	100
1.8	96.67	92.86	61.9
3.6	86.67	76.19	28.57
5.4	83.33	26.67	4.76
7.2	60	14.28	2.38
9	26.67	1.19	0
10.8	10	0	0
12.6	0	0	0

Fig 6 illustrates plot of residual activity obtained through cross-section measurements for reaction products $^{171}, ^{170}, ^{169}\text{Lu}$ in α ; αn & $\alpha 2n$ channels and ^{165}Tm through $2\alpha 2n$ reaction channel of Terbium material respectively.

TABLE 4.10 Residual Activity range distribution range in Terbium material for pxn reaction channels using ^{16}O beam in energy range 70-95 MeV as presented in fig 5 [10].

Thickness Range (μm)	ACTIVITY INDUCED (%)	
	^{171}Hf	^{170}Hf
0	100	100
1.8	95	87.5
3.6	75	68.75
5.4	55	18.75
7.2	17.5	6.25
9	5	0
10.8	0	0
12.6	0	0

Maximum activity observed for a reaction products obtained through pxn channels is approximately ranging upto 9 microns for reaction product ^{171}Hf after which it is approaching zero. For $^{171}, ^{170}, ^{169}\text{Lu}$ and ^{165}Tm , least activity is observed at nearly 9, 7.2, 9 & 7.2 micron thickness respectively. Beyond this depth the intensity of beam is nearly approaching towards 0. Detailed distribution of residual activity ranging from thickness 0 to 12 microns with respective intensities has been presented in Table 4.11.

TABLE 4.11 Residual Activity range distribution range in Terbium material for alpha reaction channels using ^{16}O beam in energy range 70-95 MeV as presented in fig 6 [10].

Thickness Range (μm)	ACTIVITY INDUCED (%)			
	^{171}Lu	^{170}Lu	^{169}Lu	^{165}Tm
0	100	100	100	100
1.8	92.3	84.1	91.7	87
3.6	73.1	72.7	69	61
5.4	46.2	36.4	47.61	22
7.2	9.62	0.9	16.7	11
9	1.92	0	1.1	0
10.8	0	0	0	0
12.6	0	0	0	0

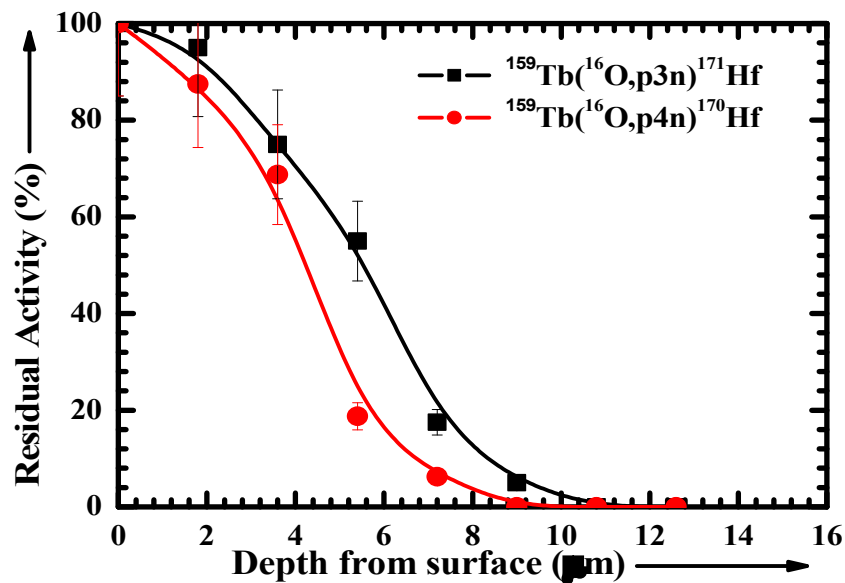


Fig 5 Calibration curves of reaction products $^{171,170}\text{Hf}$ in Terbium material

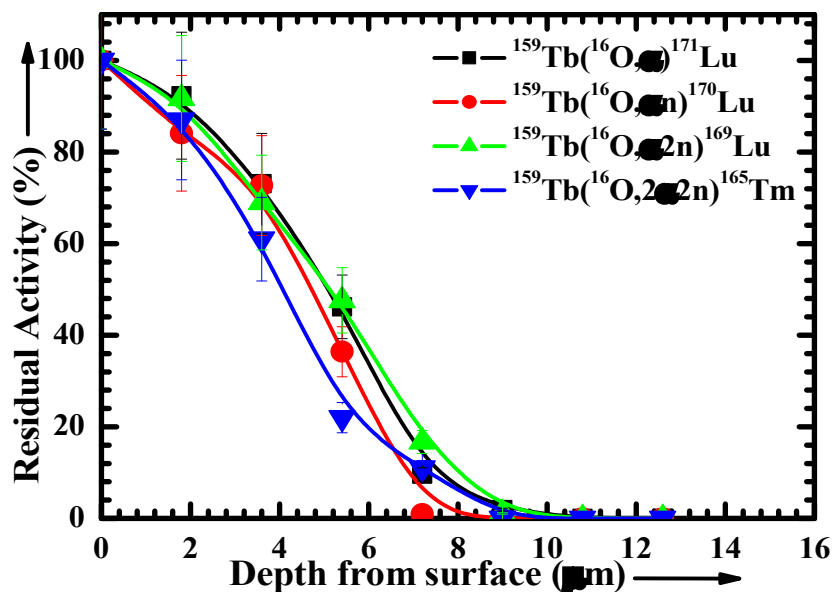


Fig 6 Calibration curves of reaction products
 $^{171}, ^{170}, ^{169}\text{Lu}, ^{165}\text{Tm}$ in Terbium material

4.3.2 TLA INVESTIGATIONS IN SPECTROSCOPICALLY PURE (\approx 95-99 %) THULIUM MATERIAL USING OXYGEN BEAM

The activity induced in the material surface using heavy ions will be contained within much narrower thickness as compared to that of light ions leading to higher sensitivity in the measurement of surface wear. Since Thulium-169 bombarded in a nuclear reactor can later serve as a radiation source in portable X-ray devices, it has also found its applications in microwave equipment. Due to its property, fluorescence at low levels, it is also used in personal radiation dosimeters. Through stack foil activation, an attempt has been made to calculate residual activity induced in Thulium-169 material using heavy ions of ^{16}O from industrial perspective. The yield curves of the isotopes; $^{182,181}\text{Ir}$, $^{182,181}\text{Os}$, $^{181,178}\text{Re}$, ^{175}Hf & ^{172}Lu have been obtained from the activity of pure Thulium-169 material, after irradiated by ^{16}O , populated at different incident energies across different depths of the target material through various reaction channels. The yield curves of the reaction products, is obtained from the activity measurement of the foils and a plot of the yield of the isotope against

the depth at which the foil is located. The stopping power of ^{16}O has been used to obtain the incident energy on each foil.

4.3.2.1 MEASUREMENT OF CROSS-SECTION AND YIELD CURVES

The yield per micron thickness against the depth as well as incident energy for several nuclides is shown in Figures. (7-9). Yield curves have been further used to deduce the activity curves. The residual activities induced, after removal of certain depths of material, have been calculated graphically with the help of obtained yield curves. The calibration curves thus obtained using reaction products, $^{182,181}\text{Ir}$, $^{182,181}\text{Os}$, $^{181,178}\text{Re}$, ^{175}Hf & ^{172}Lu from the plot of percentage of remaining activity against the removal of depth of material and are shown in Figures (10-12). Residual activity of various reaction products populated via various xn, pxn and α xn channels were found to have contribution upto $\approx 14\mu\text{m}$ depth from the surface [11]. Spectroscopic details of final reaction products post irradiation have been presented in Table 4.12.

Table 4.12 Measured cross-sections at different energies for reaction products identified in $^{16}\text{O} + ^{169}\text{Tm}$ through xn reaction channels for application in TLA [16].

SYSTEM: $^{16}\text{O} + ^{169}\text{Tm}$			
SL NO	Energy (MeV)	^{182}Ir	^{181}Ir
1	71.7 ± 1.0	3.28 ± 0.7	
2	74.9 ± 0.9	42.3 ± 7.2	28.7 ± 12.5
3	78.7 ± 0.9	59.8 ± 13.9	110 ± 15.6
4	82 ± 0.8	86.4 ± 14.8	170.4 ± 28.4
5	85.8 ± 0.8	47.6 ± 7.7	250.1 ± 67.7
6	88.9 ± 0.4	35.2 ± 3.2	316.3 ± 5.4
7	91.6 ± 0.4	13.7 ± 3.2	229.8 ± 39.6
8	94.6 ± 0.4	8.47 ± 1.4	183.8 ± 27.2

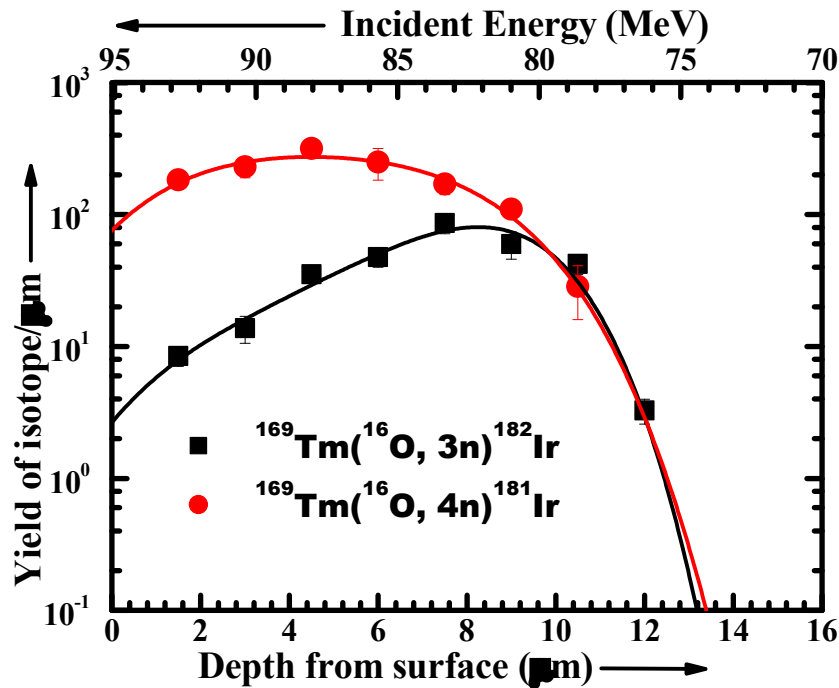


Fig 7 Yield curves of reaction products $^{182,181}\text{Ir}$ in Thulium material

Total cross-section for reaction products $^{182,181}\text{Ir}$ obtained through 3n & 4n channels respectively in Thulium material is measured by summing up of all individual cross-sections obtained at varying depths ranging from 0-16 microns and at varying energy range from 70-95 MeV of Oxygen beam. Total cross-section values for $^{182,181}\text{Ir}$ is 349.8 & 1515.47 mbarns respectively as represented in Table 4.12. As discussed in earlier sections, cross-section is measure of interaction probability between incident ion and material resulting in final yield of specific reaction product obtained. In fig 7, yield curves have been obtained with polynomial order of 4 for smooth fitting. Maximum yield has been observed for reaction product ^{181}Ir obtained through 4n reaction channel. Table 4.13 represents cross-section details of 2 reaction products obtained by irradiation of Thulium material with ^{16}O beam in the energy range of 70-95 MeV in pxn reaction channels which can be used for TLA investigation purpose in various industrial applications. Fig 8, illustrates plot of yield obtained through cross-section measurements for products $^{182,181}\text{Os}$ in p2n and p3n channels of Thulium material respectively. Total cross-section values for $^{182,181}\text{Os}$ is 1053.47 & 1062.38 respectively as represented in Table

4.13. Maximum yield has been observed for reaction product ^{181}Os obtained through p3n reaction channel.

Table 4.13 Measured cross-sections at different energies for reaction products identified in $^{16}\text{O} + ^{169}\text{Tm}$ through pxn reaction channels for application in TLA [16].

System: $^{16}\text{O} + ^{169}\text{Tm}$				
SL NO	Energy (MeV)	$^{182}\text{Os}^{\text{cum}}$	$^{182}\text{Os}^{\text{ind}}$	$^{181}\text{Os}^{\text{cum}}$
1	71.7 ± 1.0	4.58 ± 1.4	1.26 ± 0.6	2.72 ± 0.4
2	74.9 ± 0.9	82.7 ± 10	39.98 ± 5.1	4.81 ± 1.2
3	78.7 ± 0.9	139.4 ± 22.9	78.8 ± 13.8	32.81 ± 4.3
4	82 ± 0.8	155.6 ± 20.7	68.15 ± 8.3	129 ± 16.3
5	85.8 ± 0.8	107.4 ± 14.4	59.2 ± 7.5	198.02 ± 23.3
6	88.9 ± 0.4	71.5 ± 9.9	35.84 ± 6.2	250.09 ± 31.3
7	91.6 ± 0.4	29.3 ± 4.1	15.45 ± 4.4	153.8 ± 17.8
8	94.6 ± 0.4	18.4 ± 3.7	9.85 ± 2.7	173.1 ± 22.8

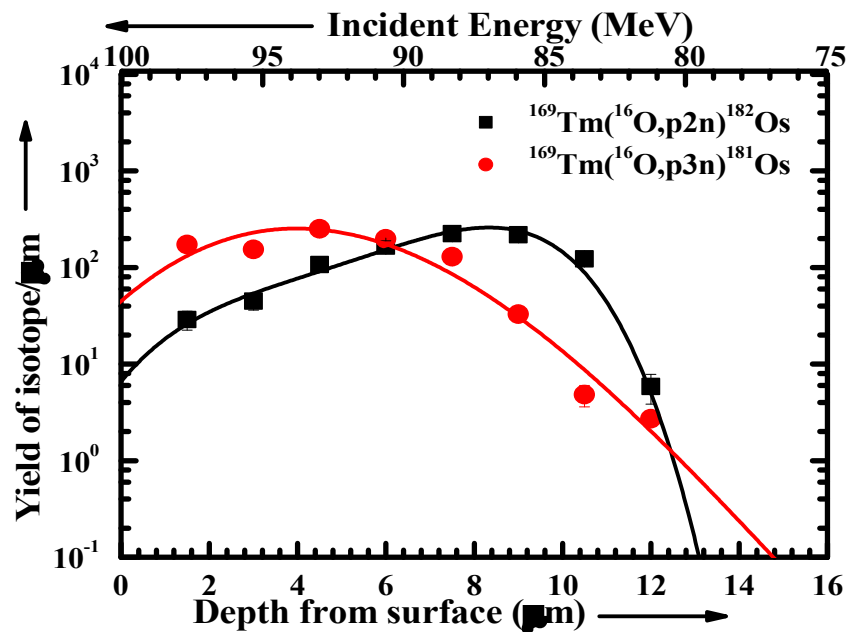


Fig 8 Yield curves of reaction products $^{182,181}\text{Os}$ in Thulium material

Table 4.14 Measured cross-sections at different energies for reaction products identified in $^{16}\text{O} + ^{169}\text{Tm}$ through Alpha reaction channels for application in TLA [16].

System: $^{16}\text{O} + ^{169}\text{Tm}$					
SL NO	Energy (MeV)	^{181}Re	^{178}Re	^{175}Hf	^{182}Lu
1	71.7 ± 1.0	2.6 ± 0.7			
2	74.9 ± 0.9	5.35 ± 0.7			
3	78.7 ± 0.9	137.3 ± 28.7	1.74 ± 0.2		14.9 ± 2.1
4	82 ± 0.8	391.4 ± 83	5.2 ± 0.8		20.5 ± 2.6
5	85.8 ± 0.8	594 ± 90.6	9.02 ± 1.2	0.57 ± 0.1	31.3 ± 3.9
6	88.9 ± 0.4	607.9 ± 86.7	27.34 ± 5.3	2.53 ± 0.4	30.2 ± 3.7
7	91.6 ± 0.4	526.2 ± 78.8	32.14 ± 3.7	2.96 ± 0.5	28.3 ± 3.1
8	94.6 ± 0.4	441.9 ± 66.9	34.31 ± 0.6	4.62 ± 0.6	28.1 ± 3.3

Table 4.14 represents cross-section details of 4 reaction products obtained by irradiation of Thulium material with ^{16}O beam in the energy range of 70-95 MeV in alpha reaction channels which can be used for TLA investigation purpose in various industrial applications. Fig 9 illustrates yield obtained through cross-section measurements for reaction products $^{181, 178}\text{Re}$ in $2p2n$, $\alpha3n$; ^{175}Hf in $2\alpha pn$ & ^{172}Lu in $3\alpha n$ reaction channels of Thulium material respectively. Total cross-section values for $^{181, 178}\text{Re}$; ^{175}Hf & ^{172}Lu is 2707.05 & 114.55; 10.68 & 143.59 respectively as represented in Table 4.14 Maximum yield has been observed for reaction product ^{181}Re obtained through $p3n$ reaction channel.

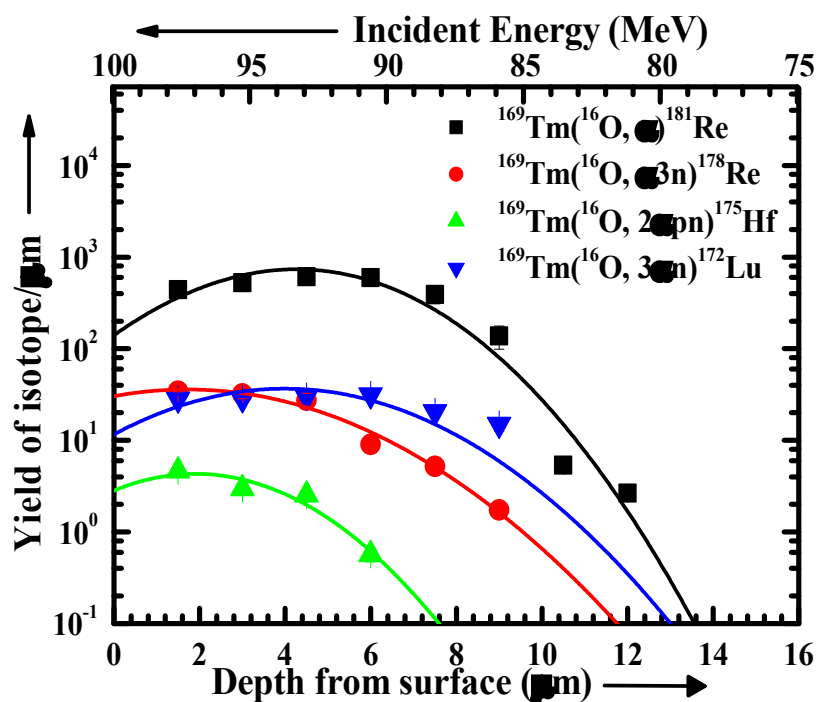


Fig 9 Yield curves of reaction products $^{181,178}\text{Re}$, ^{175}Hf , ^{172}Lu in Thulium material

4.3.2.2 MEASUREMENT OF ACTIVITY AND CALIBRATION CURVES

The integral area under the yield curves gives the total yield of isotopes. Figs (10-12) represent the total residual activity induced in Thulium material. It can be seen from the figures that various points have been obtained at regular intervals of increasing depth along with with the reduced activity. The remnant activity induced is then computed by fitting a polynomial function to the yield curve after removal of certain thickness and then by applying integration to the polynomial function with respect to depth of the material removed from the surface. Graphical plot of percentage of remaining activity against the depth of the material removed from the surface gives calibration curves as shown in Figs (10-12). The maximum surface activity induced in Thulium material for given energy range through various reactions post irradiation of material has been found to be $\approx 13\mu\text{m}$ [11].

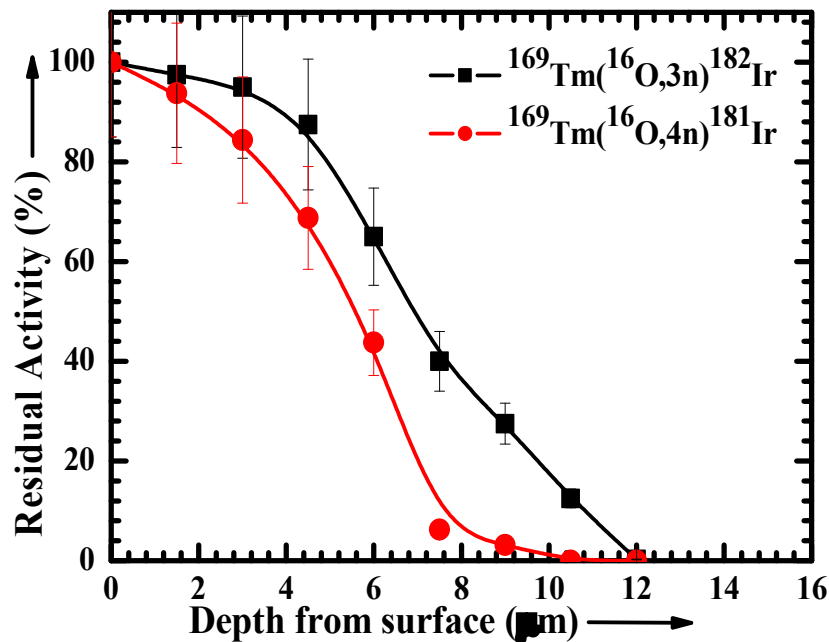


Fig 10 Calibration curves of reaction Products $^{182,181}\text{Ir}$ in Thulium material

Fig 10 illustrates plot of residual activity obtained through cross-section measurements for reaction products $^{182,181}\text{Ir}$ in 3n and 4n reaction channels of Thulium material respectively. Maximum activity has been observed in xn channels reaction products is approximately ranging upto 12 microns. At surface of material, it is obvious that beam will transfer all its intensity and as it traverses through thickness of nearly 13 microns, it will keep on attenuating unless it reaches zero. Fig 10 represents the distribution of activity for 2 reaction products ^{182}Ir & ^{181}Ir individually highlighted in black & red curves respectively from 100% intensity upto 0%. Fig 11 illustrates plot of residual activity obtained through cross-section measurements for reaction products $^{182,181}\text{Os}$ in p2n and p3n reaction channels of Thulium material respectively. Maximum activity has been observed for a reaction product is approximately ranging upto 12 microns. In Fig 11, distribution of activity for 2 reaction products ^{182}Os & ^{181}Os individually highlighted in black curve with squares & red curves with circles as data points respectively from 100% intensity upto 0%. Detailed distribution of intensity of residual activity induced ranging from

0-12 microns of thickness in Thulium material for reaction products obtained through pxn reaction channels has been presented in table 4.16.

TABLE 4.15 Residual Activity range distribution range in Thulium material for xn reaction channels using ^{16}O beam in energy range 70-95 MeV as presented in fig 10 [11].

Thickness Range (μm)	ACTIVITY INDUCED (%)	
	^{182}Ir	^{181}Ir
0	100	100
1.5	97.5	93.75
3	95	84.375
4.5	87.5	68.75
6	65	43.75
7.5	40	6.25
9	27.5	3.125
10.5	12.5	0
12	0.25	0

TABLE 4.16 Residual Activity range distribution range in Thulium material for pxn reaction channels using ^{16}O beam in energy range 70-95 MeV as presented in fig 11 [11].

Thickness Range (μm)	ACTIVITY INDUCED (%)	
	^{182}Os	^{181}Os
0	100	100
1.5	97.92	91.3
3	91.67	78.26
4.5	83.33	56.52
6	70.83	34.78
7.5	54.17	17.39
9	35.42	4.35
10.5	8.33	0.87
12	0	0

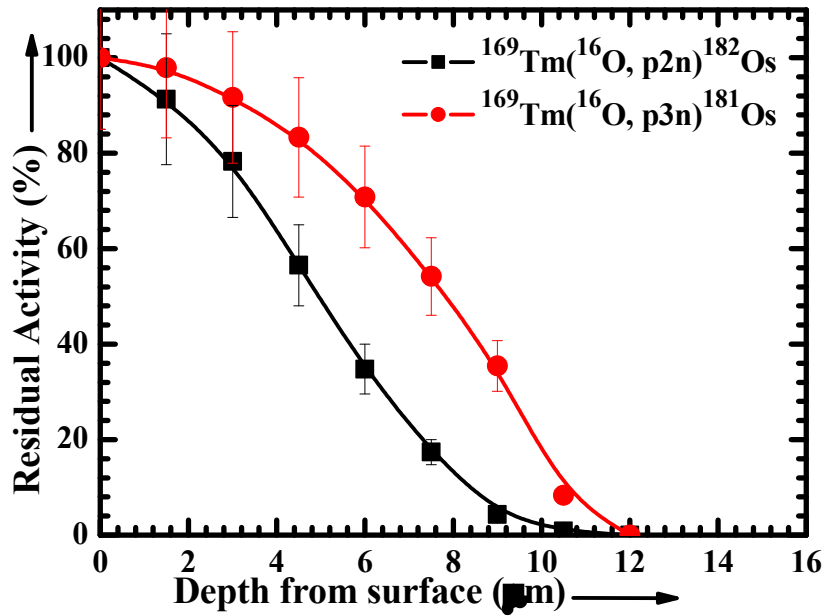


Fig 11 Calibration curves of reaction products $^{182,181}\text{Os}$ in Thulium material

Fig 12 illustrates residual activity obtained through cross-section measurements for reaction products $^{181, 178}\text{Re}$ in α and $\alpha 3n$ channels and ^{175}Hf & ^{172}Lu in $2\alpha n$ & $3\alpha n$ reaction channels of Thulium material respectively. Maximum activity has been observed for a reaction product is approximately ranging upto 9 microns. Here, the distribution of activity for 4 reaction products $^{181, 178}\text{Re}$, ^{175}Hf & ^{172}Lu individually highlighted in black, red, green & blue curves alongwith squares, circles, triangles and inverted triangles symbols respectively as data points from 100% intensity upto 0%. Least range of residual activity depth induced is observed for ^{175}Hf , as after 6 microns of thickness, residual activity starts approaching towards zero. In other all 3 products, residual activity induced starts approaching towards zero after a depth of 9 microns thickness. Detailed distribution of intensity of residual activity induced ranging from 0-12 microns of thickness in Thulium material for reaction products obtained through alpha reaction channels has been presented in table 4.17.

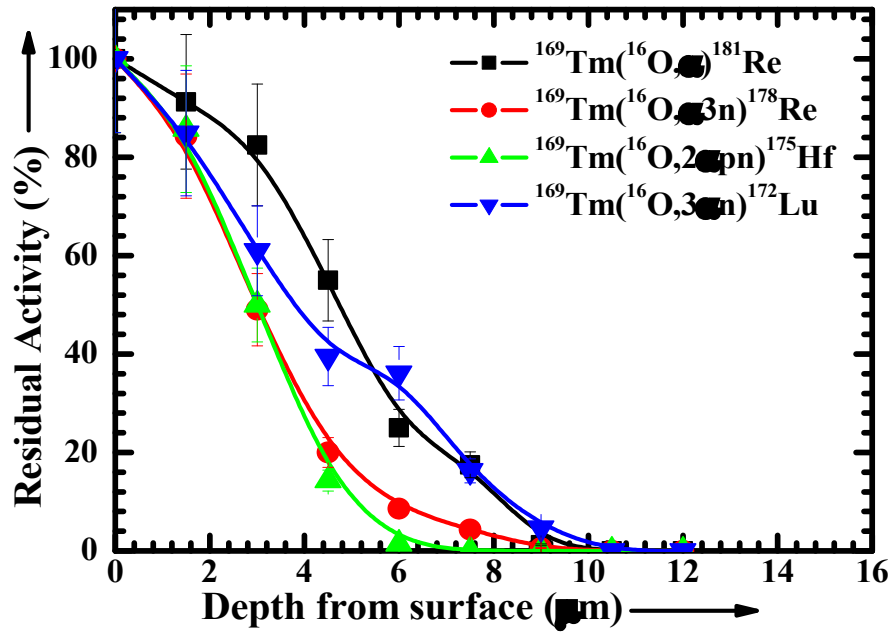


Fig 12 Calibration curves of reaction products
 $^{181,178}\text{Re}$, ^{175}Hf , ^{172}Lu in Thulium material

TABLE 4.17 Residual Activity range distribution range in Thulium material for alpha reaction channels using ^{16}O beam in energy range 70-95 MeV as presented in Fig 12 [11].

Thickness Range (microns)	ACTIVITY INDUCED (%)			
	^{181}Re	^{178}Re	^{175}Hf	^{172}Lu
0	100	100	100	100
1.5	91.25	84.29	85.71	84.9
3	82.5	49	50	61
4.5	55	20	14.3	39.5
6	25	8.6	1.4	36.1
7.5	17.5	4.3	0	16.27
9	1.25	0.57	0	4.65
10.5	0	0	0	0
12	0	0	0	0

4.3.3 TLA INVESTIGATIONS IN SPECTROSCOPICALLY PURE (\approx 95-99 %) TANTALUM MATERIAL USING OXYGEN (HEAVY ION) BEAM

Nuclear energy from fusion is the key to fulfil rising energy demands and tantalum is used in the form coatings, dopant or alloying element not only in fusion reactors but also across many vital industries due to its anti-corrosive and thermal properties. In our study, experiments have been carried out using stack foil activation made up of Tantalum material backed by aluminium catchers of appropriate thickness. Experimental details, energy of heavy ion beam & thicknesses of stacks have been discussed in the previous sections. HI beam was used for activity measurement as light ion beams were not available at accelerator centre i.e. IUAC, New Delhi. Surface activity induced across thickness of Tantalum foils have been measured for all the final reaction products obtained through various reactions post irradiation.

4.3.3.1 MEASUREMENT OF CROSS-SECTION AND YIELD CURVES

Measured cross-sections for various reaction products have been used to obtain yield curves. Plot for variation of yield against the depth from the surface has been obtained for generating the yield curves. Incident energy on each foil has been calculated using stopping power of ^{16}O beams. Yields of different isotopes obtained from the intensity of γ -lines are $^{194, 193, 192}\text{Tl}$, $^{193, 192}\text{Hg}$ and $^{192, 191, 190}\text{Au}$ across different energies and varying depths have been plotted in Fig (13-15). Nuclides shown in these represent the variation of yield per micron thickness against the depth as well as incident energy. The yield curve represents the yield of an isotope per unit thickness at a certain depth of Tantalum material. Integral area from the front surface to the final depth from where the given isotope production starts (i.e. threshold of the reaction) has been utilised to compute the net yield of particular isotope in the thick target by absorption of ^{16}O induced reactions [12]. The area under the curve gives the total yield of the isotope generated in thin target by absorption of energetic ^{16}O beams

Table 4.18 Measured cross-sections at different energies for reaction products identified in $^{16}\text{O} + ^{181}\text{Ta}$ through xn reaction channels for application in TLA [17].

System: $^{16}\text{O} + ^{181}\text{Ta}$							
SL NO	Energy (MeV)	$^{194\text{m}}\text{Tl}$	$^{194\text{g}}\text{Tl}$	$^{193\text{m}}\text{Tl}$	$^{193\text{g}}\text{Tl}$	$^{192\text{m}}\text{Tl}$	$^{192\text{g}}\text{Tl}$
1	76 ± 1.1	2 ± 0.2	2 ± 0.2	0.1 ± 0.0	26 ± 3.8		
2	80 ± 1.5	6 ± 0.8	6 ± 0.8	0.2 ± 0.0	45 ± 6.8	22 ± 3.2	22 ± 3.2
3	85 ± 1.2	4 ± 0.5	4 ± 0.5	0.2 ± 0.0	68 ± 10.2	61 ± 9.1	61 ± 9.1
4	87 ± 1.0	3 ± 0.4	3 ± 0.4	0.3 ± 0.0	46 ± 6.9	44 ± 6.5	44 ± 6.5
5	88 ± 1.6	2 ± 0.2	2 ± 0.2	0.1 ± 0.0	44 ± 6.5	91 ± 13.7	91 ± 13.7
6	93 ± 1.1	2.5 ± 0.3	2 ± 0.3	0.1 ± 0.0	35 ± 5.2	184 ± 27.6	184 ± 27.6
7	97 ± 1.0	2.0 ± 0.3	1.5 ± 0.3	0.1 ± 0.0	15 ± 2.3	171 ± 25.5	171 ± 25.5
8	99 ± 0.9	1 ± 0.1	1 ± 0.1	0.1 ± 0.0	17 ± 2.5	222 ± 33.3	222 ± 33.3

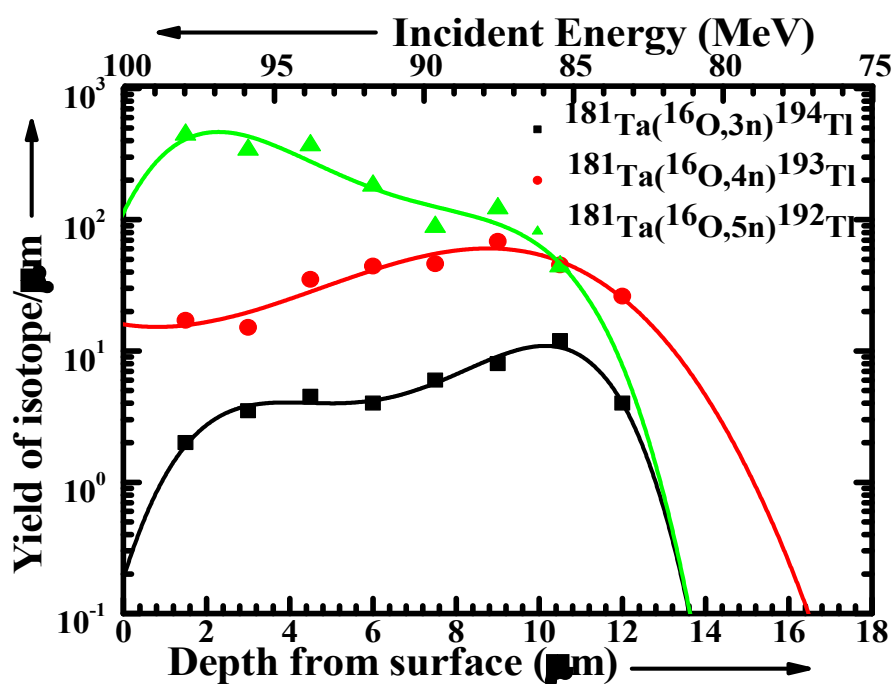


Fig 13 Yield Curves of isotopes $^{194}, ^{193}, ^{192}\text{Tl}$ in Tantalum material

Total cross-section for reaction products $^{194}, ^{193}, ^{192}\text{Tl}$ obtained through 3n, 4n & 5n reaction channels respectively in Tantalum material is measured by summing up of all individual cross-sections obtained at varying depths ranging from 0-18 microns and at varying energy range from 70-100 MeV incident Oxygen beam. Total cross-section values for $^{194}, ^{193}, ^{192}\text{Tl}$ is 50.6, 341.5 & 1827.8 respectively as represented in Table 4.18. As discussed in earlier sections; cross-section is measure of interaction probability between incident ion and material resulting in final yield of specific reaction product obtained. In fig 13 yield curves have been obtained with polynomial order of 4 for smooth fitting. Maximum yield has been observed for reaction product ^{192}Tl obtained through 5n reaction channel.

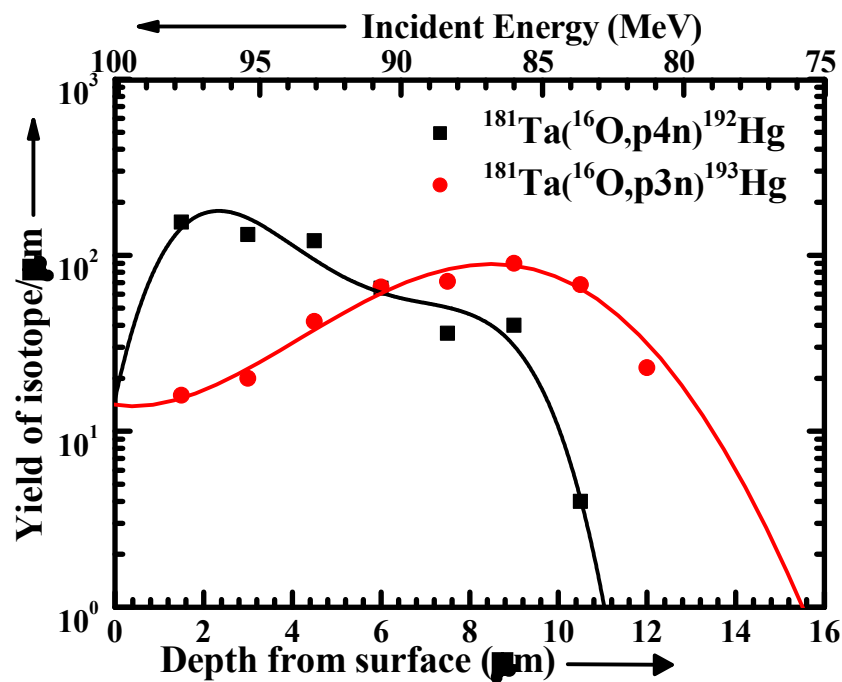


Fig 14 Yield Curves of isotopes $^{193}, ^{192}\text{Hg}$ in Tantalum material

Fig 14 illustrates plot of yield obtained through cross-section measurements for reaction products $^{193}, ^{192}\text{Hg}$ in p3n and p4n reaction channels of Tantalum material respectively. Total cross-section values for $^{193}, ^{192}\text{Hg}$ is 457.5 & 620.2 respectively as represented in Table 4.19 Maximum yield has been observed for reaction product ^{192}Hg obtained through p4n reaction channel.

Table 4.19 Measured cross-sections at different energies for reaction products identified in $^{16}\text{O} + ^{181}\text{Ta}$ through pxn reaction channels for application in TLA [17].

System: $^{16}\text{O} + ^{181}\text{Ta}$				
SL NO	Energy (MeV)	$^{193\text{g}}\text{Hg}$	$^{193\text{m}}\text{Hg}$	^{192}Hg
1	76 ± 1.1	23 ± 3.5		
2	80 ± 1.5	47 ± 7	21 ± 2.1	4 ± 0.5
3	85 ± 1.2	60 ± 8.9	30 ± 3.0	40 ± 6.0
4	87 ± 1.0	49 ± 7.4	22 ± 2.2	36 ± 5.5
5	88 ± 1.6	42 ± 6.2	24 ± 2.3	65 ± 9.8
6	93 ± 1.1	29 ± 4.4	13 ± 1.3	121 ± 18.2
7	97 ± 1.0	12 ± 1.7	8 ± 0.7	131 ± 6
8	99 ± 0.9	10 ± 1.5	6 ± 0.5	154 ± 23.2

Table 4.20 Measured cross-sections at different energies for reaction products identified in $^{16}\text{O} + ^{181}\text{Ta}$ through alpha reaction channels for applications in TLA [17].

System: $^{16}\text{O} + ^{181}\text{Ta}$						
SL NO	Energy (MeV)	$^{191\text{g}}\text{Hg}$	$^{191\text{m}}\text{Hg}$	$^{192\text{g}}\text{Au}$	$^{191\text{g}}\text{Au}$	$^{190\text{g}}\text{Au}$
1	76 ± 1.1					
2	80 ± 1.5			2 ± 0.2		
3	85 ± 1.2			10 ± 1.5		8 ± 1.3
4	87 ± 1.0			12 ± 1.8	2 ± 0.3	6 ± 0.8
5	88 ± 1.6	3 ± 0.5	0.3 ± 0.0	31 ± 4.6	2 ± 0.3	23 ± 3.5
6	93 ± 1.1	5 ± 0.7	3 ± 0.5	46 ± 6.9	3 ± 0.5	20 ± 2.9
7	97 ± 1.0	7 ± 0.9	8 ± 1.2	63 ± 9.5	14 ± 2.1	40 ± 5.9
8	99 ± 0.9	14 ± 2.1	18 ± 2.7	50 ± 7.5	22 ± 3.2	21 ± 3.2

There are total 4 reaction products initiated through reaction ^{16}O beam with Tantalum material through alpha reaction channels. To ensure feasibility of TLA investigation in materials, one of the essential factors necessary for feasibility of analysis is having good cross-section values. As mentioned in above table, one of the reaction products i.e. ^{191}gHg obtained through one of the alpha reaction channels is having maximum cross-section value 66.9 barns which is even below 100 barns. As discussed in earlier sections that cross-section is the measure of probability of interaction of material with incident ion beam, reaction product ^{191}gHg has been neglected in current analysis due to such low cross-section value.

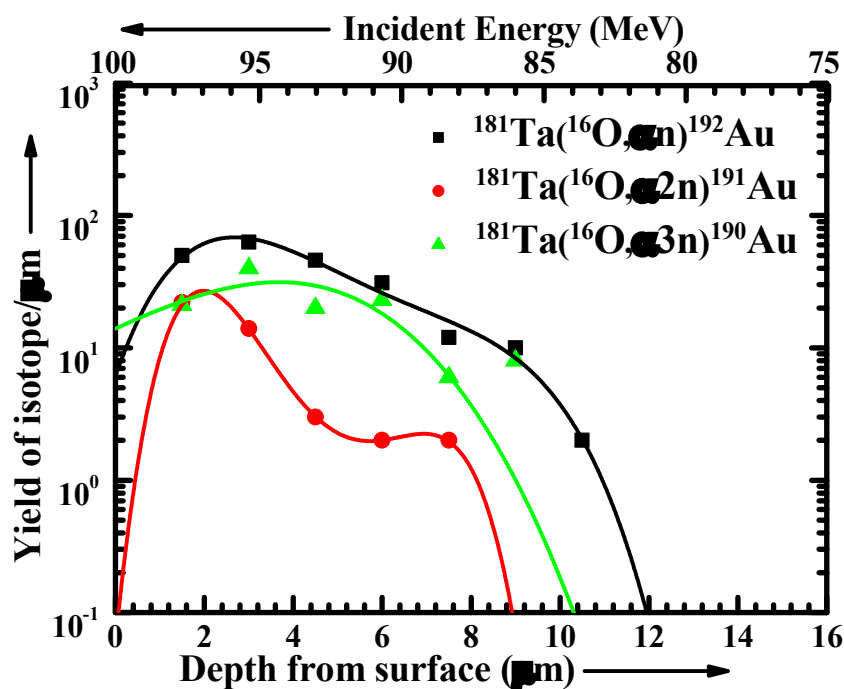


Fig 15 Yield Curves of isotopes $^{192, 191, 190}\text{Au}$ in Tantalum material

Fig 15 illustrates plot of yield obtained through cross-section measurements for reaction products $^{192, 191, 190}\text{Au}$ in αn , $\alpha 2n$ and $\alpha 3n$ reaction channels of Tantalum material respectively. Total cross-section values for $^{192, 191, 190}\text{Au}$ is 246, 49.4 & 135.6 (mbarns) respectively as represented in Table 4.20

Maximum yield has been observed for reaction product ^{192}Au obtained through an reaction channel.

4.3.3.2 MEASUREMENT OF ACTIVITY AND CALIBRATION CURVES

The integral area under the yield curves gives the total yield of isotopes. Fig (16-18) represents the total residual activity induced in tantalum material. It can be seen from the figure that various points have been obtained at regular intervals of increasing depth alongwith with the reduced activity. The remnant activity induced is then computed by fitting a polynomial function to the yield curve after removal of certain thickness and then by applying integration to the polynomial function with respect to depth of the material removed from the surface. Graphical plot of percentage of remaining activity against the depth of the material removed from the surface gives calibration curves as shown in Fig (16-18). The maximum surface activity induced in Tantalum material for given energy range through various reactions post irradiation of material has been found to be $\approx 12\text{-}16\ \mu\text{m}$ [12].

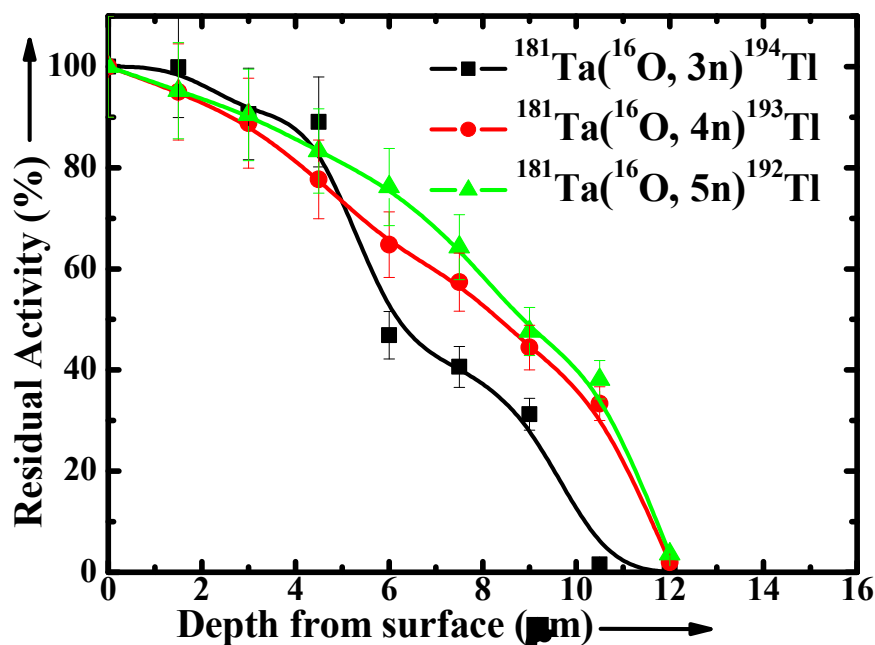


Fig 16 Calibration Curves of isotopes
 $^{194}, ^{193}, ^{192}\text{Tl}$ in Tantalum material

Fig 16 illustrates plot of residual activity obtained through cross-section measurements for reaction products $^{194,193, 192}\text{Tl}$ in 3n, 4n and 5n reaction channels of Tantalum material respectively. Maximum activity has been observed in xn channels reaction products is approximately ranging upto 12-16 microns. Fig 16 represents the distribution of activity for 3 reaction products ^{194}Tl , ^{193}Tl & ^{192}Tl individually highlighted in black squares, red circles & green triangle curves respectively from 100% intensity upto 0%.

TABLE 4.21 Residual Activity range distribution range in Tantalum material for xn reaction channels using ^{16}O beam in energy range 70-100 MeV [12].

Thickness Range (μm)	ACTIVITY INDUCED (%)		
	^{194}Tl	^{193}Tl	^{192}Tl
0	100	100	100
1.5	95.24	95	99.9
3	90.48	88.8	90.625
4.5	83.33	77.7	89.06
6	76.19	64.81	46.87
7.5	64.3	57.4	40.62
9	47.62	44.44	31.25
10.5	38.09	33.33	1.56
12	3.57	2	0

TABLE 4.22 Residual Activity range distribution range in Tantalum material for pxn reaction channels using ^{16}O beam in energy range 70-100 MeV [12].

Thickness Range (μm)	ACTIVITY INDUCED (%)	
	^{193}Hg	^{192}Hg
0	100	100
1.5	88.89	97.37
3	62.96	92.1
4.5	44.44	84.21
6	25.93	68.42
7.5	16.67	54
9	9.25	28.95
10.5	0.93	14.47
12	0	2.63

For pxn reaction channels, products obtained through p3n & p4n reaction channels viz; ^{193}Hg & ^{192}Hg , residual activity induced has been observed to be approximately 12 microns as shown in Fig 17. The maximum cross-section for both of these reaction products ranges above 450 mbarns. Half-lives of ^{193}Hg & ^{192}Hg 3.8 hrs & 4.85 hrs respectively. Having good cross-sectional values and measurable half-life, these reaction products can be used as trace elements for actual thin layer activated wear, erosion or corrosion measurements for industrial applications using Tantalum material. Distribution of activity across thickness ranging from 0-16 microns in reaction products $^{193}, ^{192}\text{Hg}$ has been presented in Table 4.22

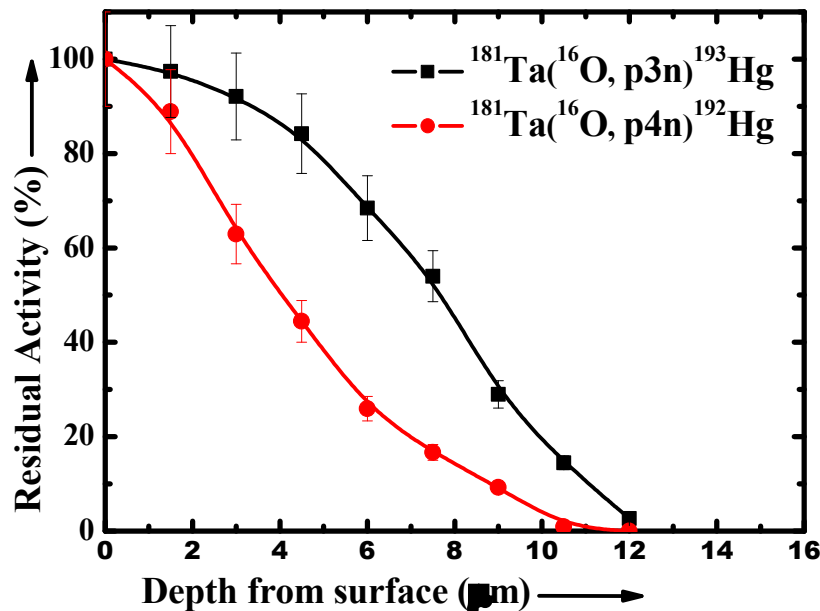


**Fig 17 Calibration Curves of isotopes
 $^{193}, ^{192}\text{Hg}$ in Tantalum material**

For αxn reaction channels, products obtained through αn , $\alpha 2\text{n}$ & $\alpha 3\text{n}$ reaction channels viz; ^{192}Au , ^{191}Au & ^{190}Au , residual activity induced has been observed to be approximately in range of 9-11 microns as shown in fig 18. The maximum cross-section for these reaction products ranges from 50 mbarns - 250 mbarns. Distribution of activity across thickness ranging from 0-12 microns in reaction products $^{192}, ^{191}, ^{190}\text{Au}$ has been presented in Table 4.23

TABLE 4.23 Residual Activity range distribution range in Tantalum material for alpha reaction channels using ^{16}O beam in energy range 70-100 MeV [12].

Thickness Range (μm)	ACTIVITY INDUCED (%)		
	^{192}Au	^{191}Au	^{190}Au
0	100	100	100
1.5	93.3	69.2	91.7
3	63.3	30.8	61.1
4.5	55	13.85	33.3
6	38.33	7.7	16.7
7.5	10	1.5	5.6
9	6.7	0	1.4
10.5	1.7	0	0

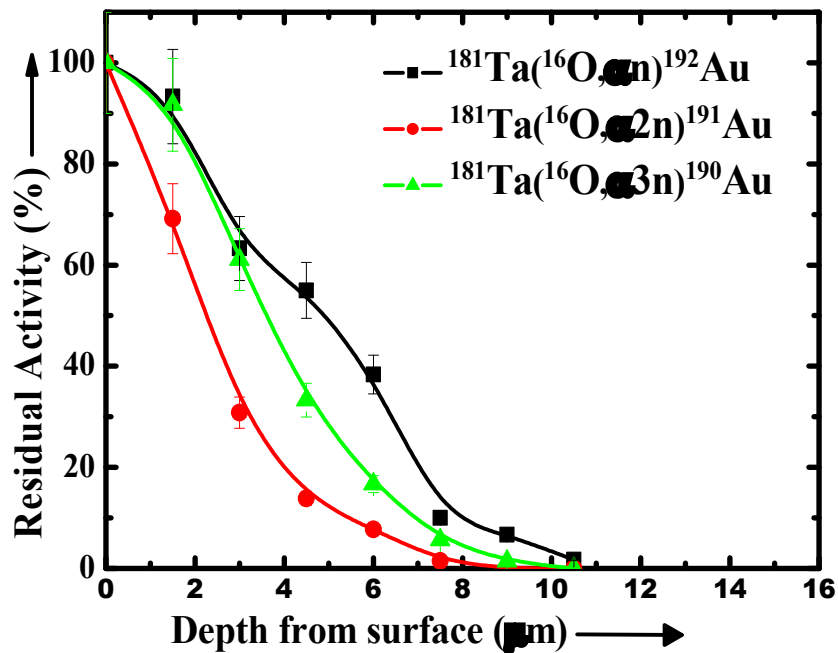


Fig 18 Calibration Curves of isotopes $^{192}, ^{191}, ^{190}\text{Au}$ in Tantalum material

4.3.4 COMPARATIVE STUDY IN DIFFERENT RARE EARTH MATERIALS USING OXYGEN (HEAVY ION) BEAM

As discussed earlier that, there are very few studies reported for TLA investigations using HI beams till date. In the present work, three different systems, i.e. $^{16}\text{O} + ^{159}\text{Tb}$, $^{16}\text{O} + ^{169}\text{Tm}$, $^{16}\text{O} + ^{181}\text{Ta}$ have been studied to check feasibility of TLA investigations and attempt has been made to make a comparative analysis between all these materials by observing activity induced in common reaction channels in almost same activation energy region and similar set of standard operating conditions. Furthermore, range in which these studies are carried out completely forms a new set of data for TLA investigation purposes which can be further used for practical TLA based studies.

4.3.4.1 MEASUREMENT OF CROSS-SECTIONS & YIELD CURVES

The yield curves for various isotopes; $^{172,171,170}\text{Ta}$, $^{171,170}\text{Hf}$, 171,170 , ^{169}Lu populated through different reaction for $^{16}\text{O} + ^{159}\text{Tb}$ and $^{182,181}\text{Ir}$, ^{181}Os , ^{181}Re for $^{16}\text{O} + ^{169}\text{Tm}$ and 194,193 , ^{192}Tl , $^{193,192}\text{Hg}$, 192,191 , ^{190}Au for $^{16}\text{O} + ^{181}\text{Ta}$ material have been obtained at different energies and different depths of target materials. The yield per micron thickness against the depth as well as incident energy for several isotopes is shown in Figs. (19–27). For comparative analysis, we have plotted the xn, pxn & xn channels for different systems. In Figs. (19–21), xn channels (where n = 3, 4, 5) for all the three systems have been plotted. The activity induced in xn channels for Terbium is ranging from 8–12 μm ; 13–14 μm for Thulium and 14–16 μm for Tantalum respectively. In case of pxn channels activity induced in Terbium is up to 14 μm ; 16 μm for both Thulium and Tantalum shown in Figs. (22–23). For alpha reaction channels (where n = 1, 2 3) activity induced for Terbium ranging from 8 to 12 μm ; 9–16 μm for Tantalum as shown in Figs. (24–27). In the present work, residual activity of various reaction products populated via various channels were found to have contribution ranging from ≈ 8 to 16 μm depth from the

surface [18]. In Figs (19-21), comparative analysis of yield distribution for different reaction products obtained from xn reaction channels in Terbium, Thulium and Tantalum material respectively have been presented. Comparative analysis of reaction products viz; ^{172}Ta , ^{182}Ir , & ^{194}Tl obtained through 3n reaction channels in Terbium, Thulium and Tantalum material respectively is presented in Fig 19. As discussed in earlier sections, yield of the reaction is the quantifiable measure of probability of interaction of beam with the material at respective depths and energy. From the Fig 19, it is clear that maximum rate of interaction is observed in Thulium and Tantalum material in the given energy range. Maximum probable range of interaction in these materials varies upto 14 microns while in case of Terbium material the range of interaction is limited only upto approximately 11 microns having least probability of interaction and yield as compared with other rare earth materials while operating in same set of standard conditions. In Fig 20, comparative analysis between yield of reaction products viz; ^{171}Ta ; ^{181}Ir & ^{193}Tl obtained through 4n reaction channels of Terbium, Thulium and Tantalum material respectively has been presented. In this case, maximum rate of interaction is observed in Thulium and Tantalum material in the given energy range. Maximum probable range of interaction in these materials varies upto 17 microns while in case of Terbium material the range of interaction is limited only upto approximately 10 microns having least range of yield as compared with other rare earth materials while operating in same set of standard conditions. The range of maximum yield and interaction obtained for reaction products through 4n reaction channels are higher as compared to that of range of yield and interaction obtained through 3n reaction channels in the same material [10-12]. Fig 21 illustrates plot of yield obtained through cross-section measurements for comparative analysis of different rare earth materials for reaction products viz ^{171}Ta & ^{193}Tl in 5n reaction channels of Terbium and Tantalum material respectively. From the Fig. 21 it is clear maximum rate of interaction is observed in Tantalum material in the given energy range. Maximum probable range of interaction in these materials varies upto 14 microns while in case of Terbium material the range of interaction is

limited only upto approximately 10 microns having least range of yield as compared with Tantalum material while operating in same set of standard conditions. The range of maximum yield and interaction obtained for reaction products through 5n reaction channels are higher as compared to that of range of yield and interaction obtained through 3n & 4n reaction channels within the same material. In Figs (22-23), comparison for yield distribution in different reaction products among the above mentioned materials has been presented obtained through pxn reaction channels. Fig 22 illustrates plot of yield obtained through cross-section measurements for comparative analysis of different rare earth materials for reaction products viz ^{171}Hf ; ^{181}Os & ^{193}Hg in p3n reaction channels of Terbium, Thulium and Tantalum material respectively. From the Fig. 22 it is clear maximum rate of interaction is observed in Thulium and Tantalum material in the given energy range. Maximum probable range of interaction in these materials varies upto 18 microns while in case of Terbium material the range of interaction is limited only upto approximately 13 microns having least range of yield as compared with other rare earth materials. Measurable cross-section for obtaining range of interaction in above mentioned materials ranges from 10 mbarns upto 1000 mbarns for reaction products obtained through p3n reaction channels [10-12]. For reaction products viz ^{170}Hf & ^{192}Hg obtained through p4n reaction channels, comparative analysis of yield distribution between Terbium & Tantalum materials respectively has been presented in Fig 23. Maximum rate of interaction is observed in Tantalum material in the given energy range. Maximum probable range of interaction in these materials varies upto 13 microns while in case of Terbium material the range of interaction is limited only upto approximately 11 microns having higher yield but less range as compared with Tantalum material. Measurable cross-section for obtaining range of interaction in above mentioned materials ranges approximately from 10 mbarns upto 1000 mbarns for reaction products obtained through p4n reaction channels [10-12].

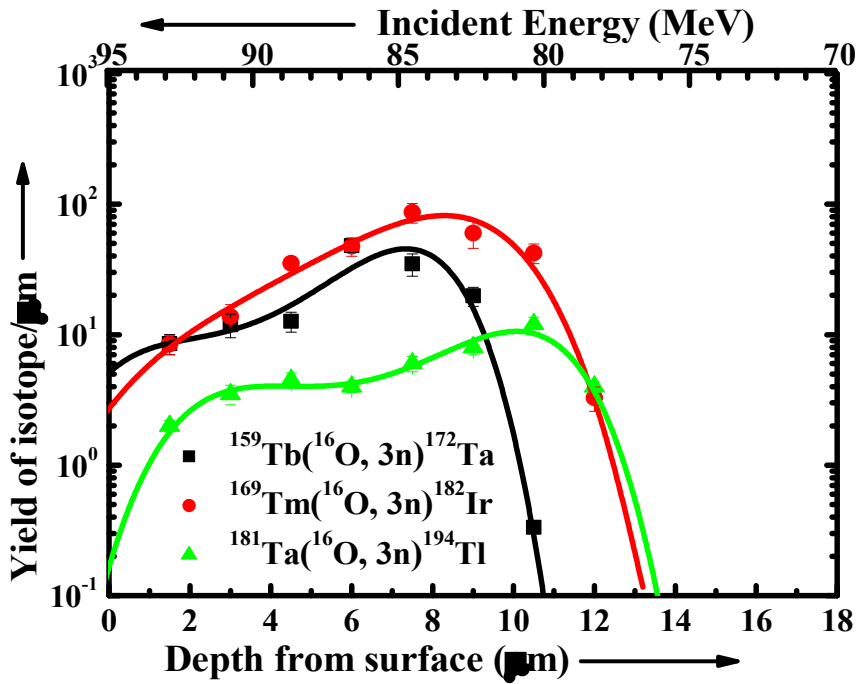


Fig. 19. Relative Yield curves of isotopes ^{172}Ta , ^{182}Ir , ^{194}Tl from Tb, Tm & Ta material

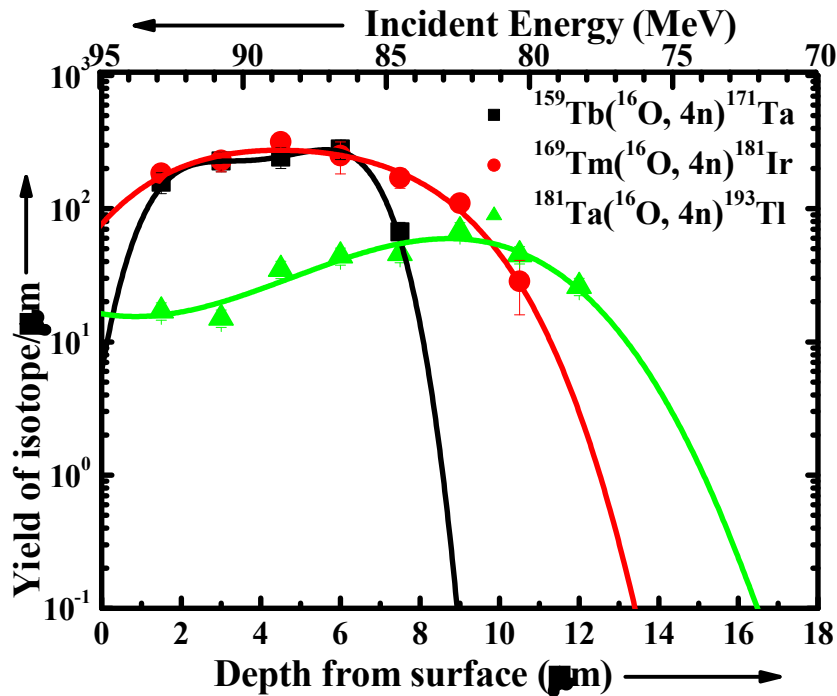


Fig. 20. Relative Yield curve of isotopes ^{171}Ta , ^{181}Ir , ^{193}Tl from Tb, Tm & Ta material.

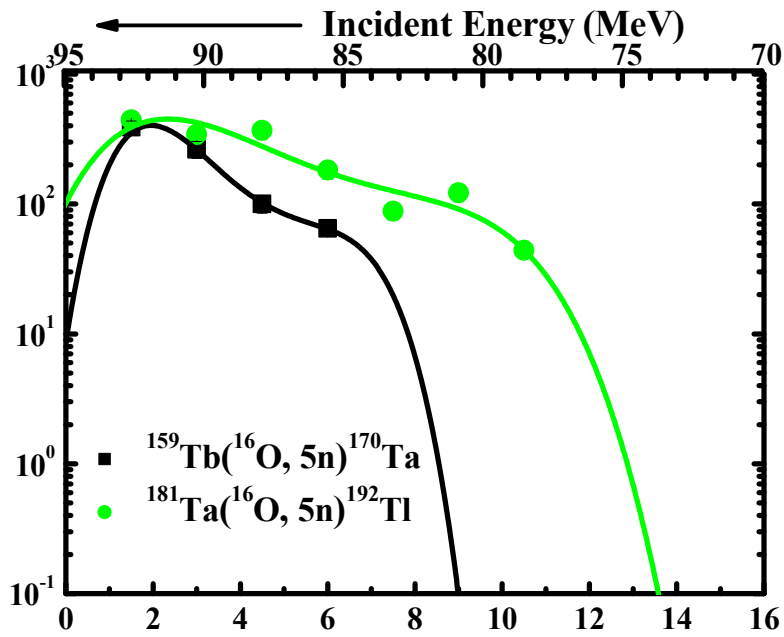


Fig. 21. Relative Yield curves of isotopes ^{170}Ta & ^{192}Tl from Tb & Ta material.

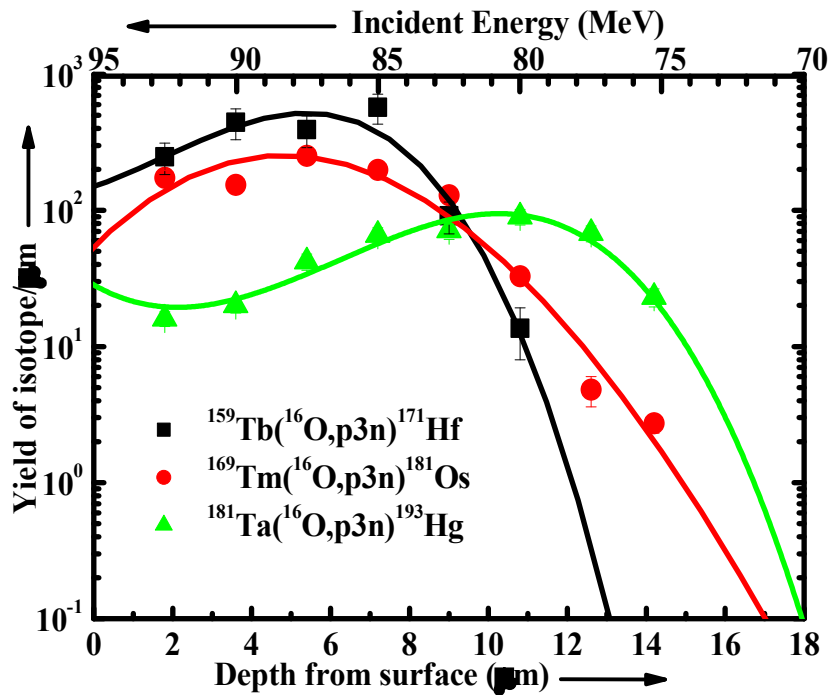


Fig. 22. Relative Yield curves of isotopes ^{171}Hf , ^{181}Os & ^{193}Hg from Tb, Tm & Ta material.

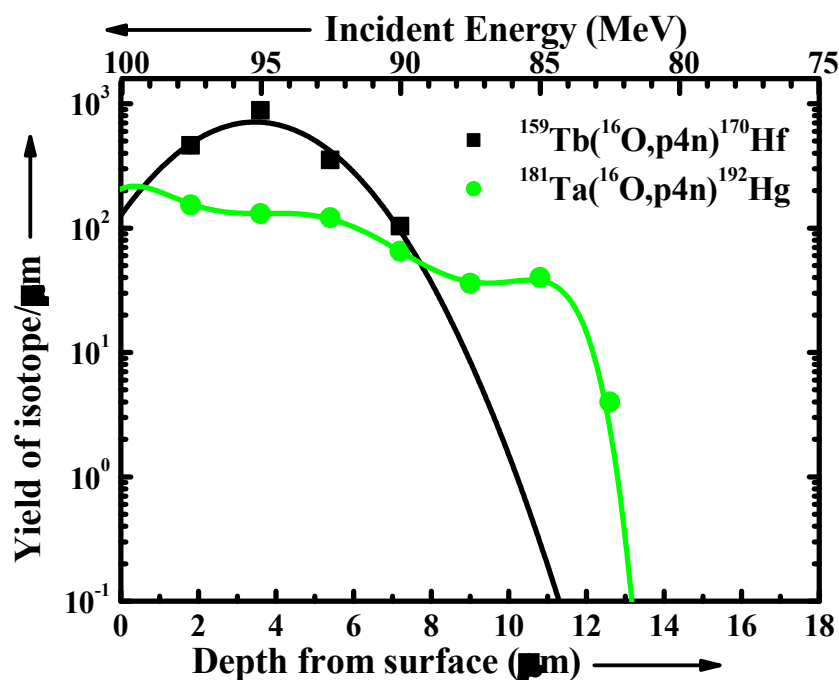


Fig. 23. Relative Yield curves of isotopes ^{170}Hf & ^{192}Hg from Tb & Ta material.

Figs. (24-26), represent comparison for yield distribution in different reaction products among the above mentioned materials obtained through alpha reaction channels. Fig 24 illustrates plot of yield obtained through cross-section measurements for comparative analysis of different rare earth materials for reaction products viz ^{171}Lu & ^{181}Re in alpha reaction channels of Terbium and Thulium material respectively. Maximum rate of interaction is observed in Terbium material in the given energy range as presented in Fig 24. Maximum probable range of interaction in these materials varies upto 16 microns while in case of Thulium material the range of interaction is limited only upto approximately 12 microns Measurable cross-section for obtaining range of interaction in above mentioned materials ranges approximately from 100 mbarns upto 1000 mbarns for reaction products obtained through alpha reaction channels [10-12]. Fig 25 illustrates yield distribution for reaction products viz ^{170}Lu & ^{192}Au in an reaction channel of Terbium and Tantalum material respectively. Maximum rate of interaction is observed in Tantalum material in the given energy range as presented in Fig 25. Maximum probable

range of interaction in these materials varies of upto 16 microns while in case of Terbium material, the range of interaction is limited only upto approximately 10 microns. Measurable cross-section for obtaining range of interaction in above mentioned materials ranges approximately from 10 mbarns upto 100 mbarns for reaction products obtained through αn reaction channel [10-12]. Fig 26 illustrates measurements for comparative analysis for reaction products viz ^{169}Lu & ^{191}Au in $\alpha 2n$ reaction channels of Terbium and Tantalum material respectively. Maximum rate of interaction is observed in Tantalum material in the given energy range. Maximum probable range of interaction in these materials varies of upto 11 microns while in case of Terbium material, the range of interaction is limited only upto approximately 9 microns. Measurable cross-section for obtaining range of interaction in above mentioned materials ranges approximately from 1 mbarns upto 100 mbarns for reaction products obtained through $\alpha 2n$ reaction channels [10-12]. Fig 27 illustrates plot of yield obtained through cross-section measurements for comparative analysis for reaction products viz ^{178}Re & ^{190}Au in $\alpha 3n$ reaction channels of Thulium and Tantalum material respectively. Maximum rate of interaction is observed in Tantalum material in the given energy range.

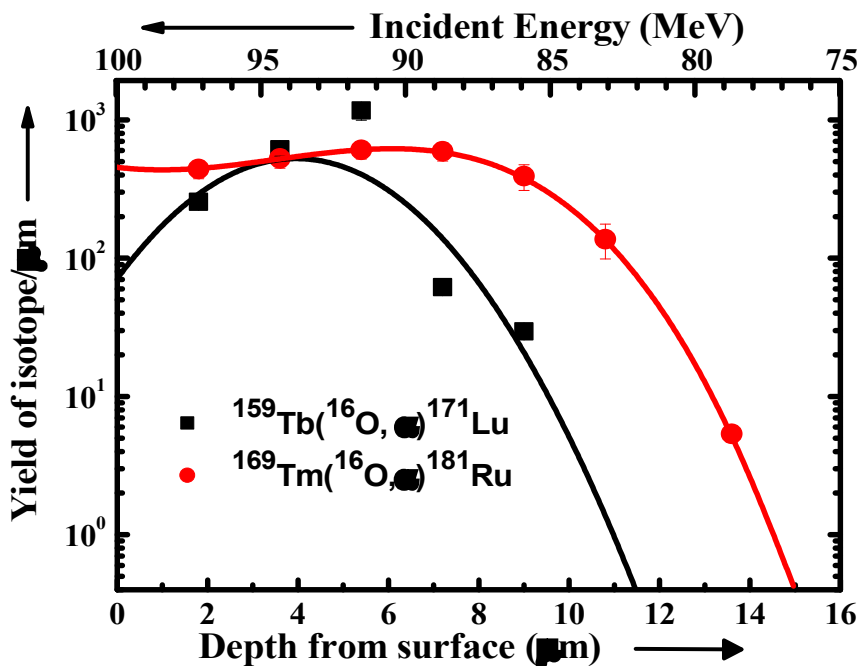


Fig. 24. Relative Yield curves of isotopes ^{171}Lu & ^{181}Re from Tb & Tm material.

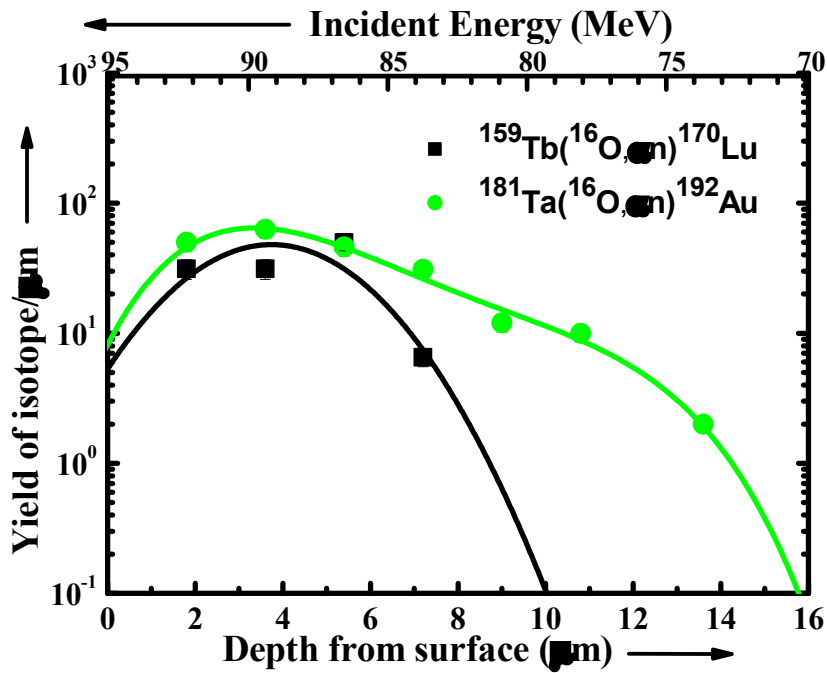


Fig. 25. Relative Yield curves of isotopes ^{170}Lu & ^{192}Au from Tb & Ta material.

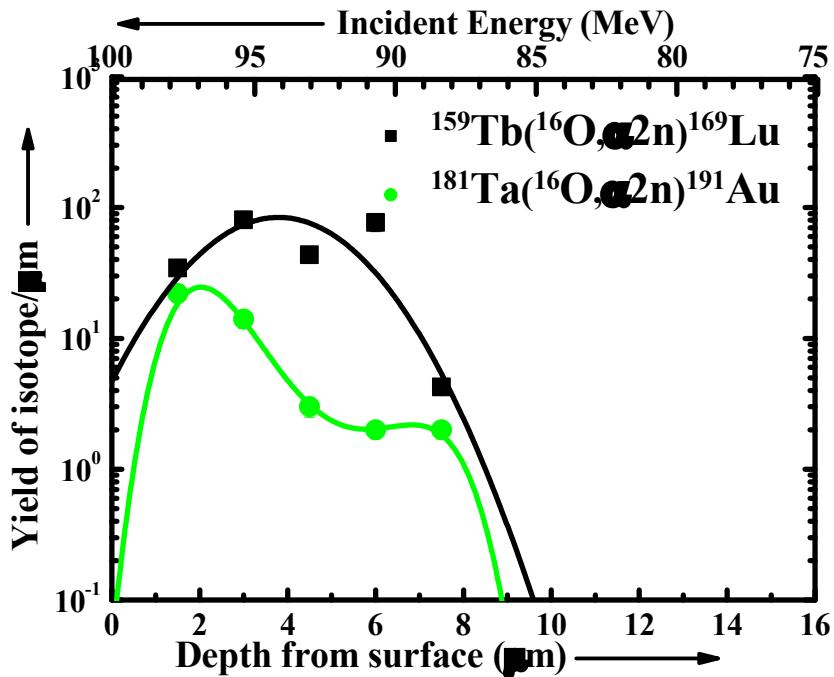


Fig. 26. Relative Yield curves of isotopes ^{169}Lu & ^{192}Au from Tb & Ta material.

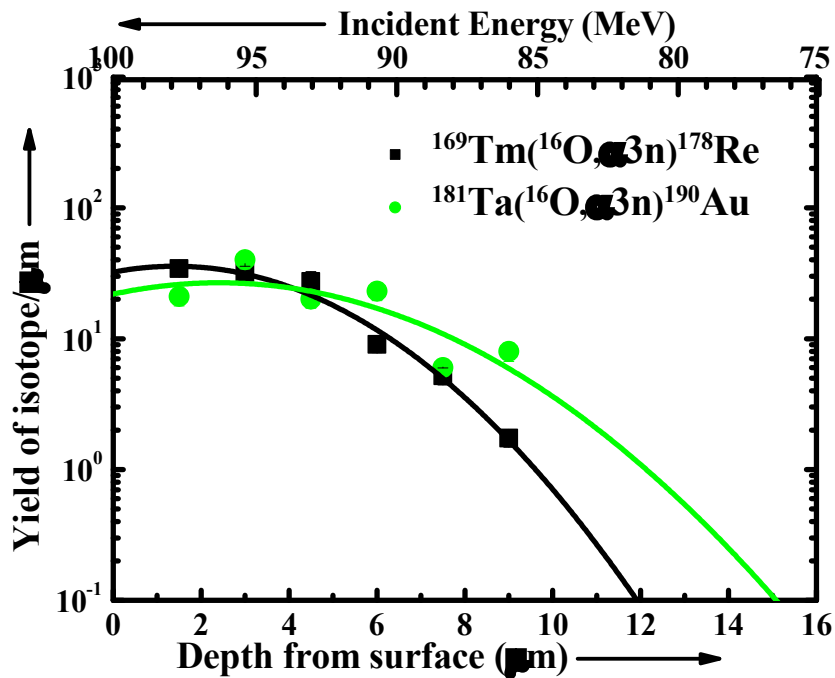


Fig. 27. Relative Yield curves of isotopes ^{178}Re & ^{190}Au from Tm & Ta material.

Maximum probable range of interaction in these materials varies of upto 15 microns while in case of Thulium material, the range of interaction is limited only upto approximately 12 microns. Measurable cross-section for obtaining range of interaction in above mentioned materials ranges approximately from 10 mbarns upto 80 mbarns for reaction products obtained through $\alpha 3n$ reaction channels [10-12]. For convenience of obtaining range and interaction of yield, curves have been fitted with polynomial fitting of order 3-4 for all the reaction products obtained xn, pxn & alpha reaction channels.

4.3.4.2 MEASUREMENT OF ACTIVITY INDUCED & CALIBRATION CURVES

Yield curves have been further used to deduce the calibration curves. The residual activities induced, $^{172,171,170}\text{Ta}$, $^{171,170}\text{Hf}$, $^{171,170,169}\text{Lu}$ have been plotted for Terbium and $^{182,181}\text{Ir}$, ^{181}Os , ^{181}Re for Thulium and $^{194,193,192}\text{Tl}$, $^{193,192}\text{Hg}$, $^{192,191,190}\text{Au}$ for Tantalum material after removal of certain depths of material. The calibration curves thus obtained using reaction products, from the plot of

percentage of remaining activity against the removal of depth of material are shown in Figs. 28–36. As indicated in Figs. 19–27, the total yield of the isotope in the given material may be obtained from the integral area under the yield curves. After the removal of certain depth of material (decreasing the thickness corresponding to the each foil of the stack one by one) the percentage of the remaining activity is computed graphically and the calibration curves so deduced from the yield curves are shown in Figs. 28–36. As a matter of fact, these calibration curves may be considered to correspond to pure metals bombarded with 110 MeV ^{16}O heavy ions normal to the beam direction. It may also be noticed from (Figs. 28–36) that the rate of change of activity per unit thickness is more for the higher slope curve i.e., the errors associated in higher slope curve will be less. The overall error has been estimated from the errors of cross-section in generating the calibration curves and the activity measurement of the irradiated samples and has been found less than 15%. Statistical errors has been deduced and fitted with a fourth-order polynomial function, where the uncertainty from the fitting is found to be \approx 3% for the energy range of interest [18].

TABLE 4.24 Residual Activity range distribution range in Terbium, Thulium & Tantalum materials for 3n reaction channels using ^{16}O beam in energy range 70-110 MeV [18].

Thickness Range (μm)	ACTIVITY INDUCED (%)		
	$^{159}\text{Tb}(^{16}\text{O},3\text{n})^{172}\text{Ta}$	$^{169}\text{Tm}(^{16}\text{O},3\text{n})^{182}\text{Ir}$	$^{181}\text{Ta}(^{16}\text{O},3\text{n})^{194}\text{Tl}$
0	100	100	100
1.5	96.67	97.5	95.24
3	86.67	95	90.48
4.5	83.33	87.5	83.33
6	60	65	76.19
7.5	26.67	40	64.3
9	10	27.5	47.62
10.5	0	12.5	38.09
12	0	2	3.57

Fig 28 illustrates plot of range of activity distribution obtained through cross-section measurements for comparative analysis of different rare earth materials for reaction products viz ^{172}Ta ; ^{182}Ir & ^{194}Tl in 3n reaction channels of Terbium, Thulium and Tantalum materials respectively. It is evident that at surface maximum transfer of kinetic energy takes place resulting in maximum activity induced. Hence residual activity induced approaches from (100 to 0) % as depth of material increases from 0 to 12 microns. The activity distribution is in steps of each 1.5 microns removed ranging from 0-12 microns. The amount of residual activity induced and maximum depth achieved in the energy range of 70-95 MeV of Oxygen beam on respective materials has been presented in Table 4.24. As yield for Thulium and Tantalum material obtained through cross-section measurement is higher, it can be observed that range of residual activity induced is also higher. In case of Thulium and Tantalum the maximum range of activity induced is upto 12 microns while in case Terbium material maximum range has been observed upto 10 microns approximately.

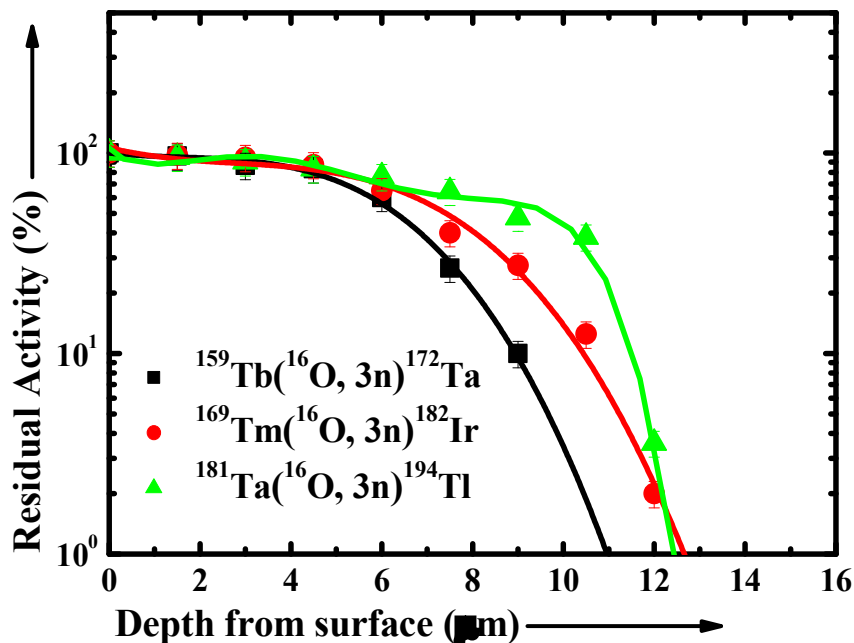


Fig. 28. Calibration curves of isotopes ^{172}Ta , ^{182}Ir , ^{194}Tl from Tb, Tm & Ta materials at incident energies ranging from 95 to 70 MeV.

Fig 29 illustrates plot of range of activity distribution obtained through cross-section measurements for comparative analysis of different rare earth materials for reaction products viz ^{171}Ta ; ^{181}Ir & ^{193}Tl in 4n reaction channels of Terbium, Thulium and Tantalum materials respectively. The activity distribution is in steps of each 1.5 microns removed ranging from 0-16 microns. The amount of residual activity induced and maximum depth achieved in the energy range of 70-95 MeV of Oxygen beam on respective materials has been presented in Table 4.25 As yield for Thulium and Tantalum material obtained through cross-section measurement is higher, it can be observed that range of residual activity induced is also higher. In case of Thulium and Tantalum the maximum range of activity induced is 12 & 15 microns respectively while in case terbium material maximum range has been observed upto 9 microns approximately.

TABLE 4.25 Residual Activity range distribution range in Terbium, Thulium & Tantalum materials for 3n reaction channels using ^{16}O beam in energy range 70-110 MeV [18].

Thickness Range (μm)	ACTIVITY INDUCED (%)		
	$^{159}\text{Tb}(^{16}\text{O},4\text{n})^{171}\text{Ta}$	$^{169}\text{Tm}(^{16}\text{O},4\text{n})^{181}\text{Ir}$	$^{181}\text{Ta}(^{16}\text{O},4\text{n})^{193}\text{Tl}$
0	100	100	100
1.8	92.86	93.75	95
3.6	76.19	84.375	88.8
5.4	26.67	68.75	77.7
7.2	14.28	43.75	64.81
9	1.19	6.25	57.4
10.8	0	3.125	44.44
12.6	0	0	33.33
14	-	-	2

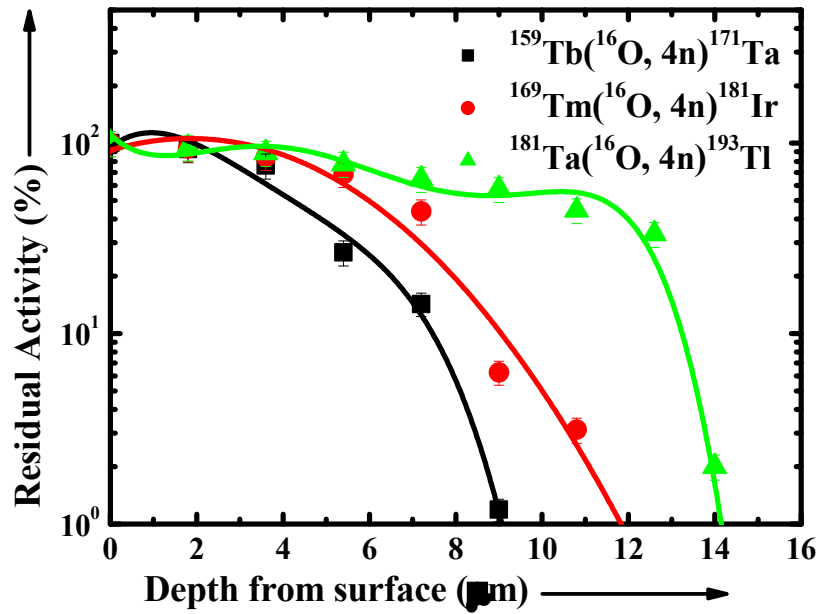


Fig. 29. Calibration curves of isotopes ^{171}Ta , ^{181}Ir , ^{193}Tl from Tb, Tm & Ta materials at incident energies ranging from 95 to 70 MeV.

TABLE 4.26 Residual Activity range distribution range in Terbium, & Tantalum materials for 5n reaction channels using ^{16}O beam in energy range 70-110 MeV [18].

Thickness Range (μm)	ACTIVITY INDUCED (%)	
	$^{159}\text{Tb}(^{16}\text{O}, 5n)^{170}\text{Ta}$	$^{181}\text{Ta}(^{16}\text{O}, 5n)^{192}\text{Tl}$
0	100	100
1.8	61.9	99.9
3.6	28.57	90.625
5.4	4.76	89.06
7.2	2.38	46.87
9	0	40.62
10.8	0	31.25
12.6	0	1.56

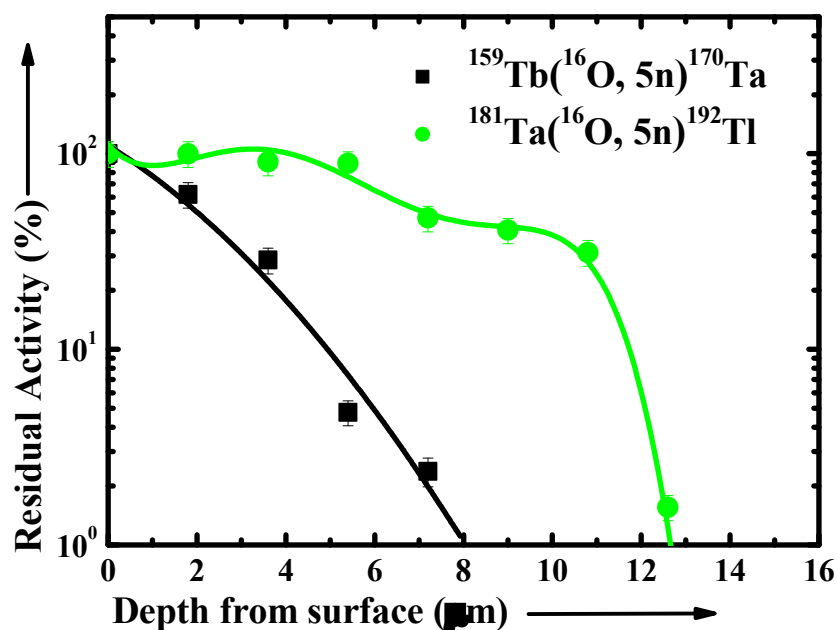


Fig. 30. Calibration curves of isotopes ^{170}Ta & ^{194}Tl from Tb & Ta materials at incident energies ranging from 95 to 70 MeV.

Fig 30 illustrates plot of range of activity distribution obtained through cross-section measurements for comparative analysis of different rare earth materials for reaction products viz ^{170}Ta & ^{192}Tl in 5n reaction channels of Terbium and Tantalum material respectively. The activity distribution is in steps of each 1.8 microns removed ranging from 0-16 microns. The amount of residual activity induced and maximum depth achieved in the energy range of 70-95 MeV of Oxygen beam on respective materials has been presented in Table 4.26 As yield for Tantalum material obtained through cross-section measurement is higher, it can be observed that range of residual activity induced is also higher. In case of Tantalum the maximum range of activity induced is 13 microns while in case of Terbium material, maximum range has been observed upto 8 microns approximately. Fig 31 illustrates plot of range of activity distribution obtained through cross-section measurements for comparative analysis of different rare earth materials for reaction products viz ^{171}Hf ; ^{181}Os & ^{193}Hg in p3n reaction channels of Terbium, Thulium and Tantalum material respectively. The activity distribution is in steps of each 1.8 microns removed ranging from 0-13 microns. The amount of residual activity

induced and maximum depth achieved in the energy range of 70-100 MeV of Oxygen beam on respective materials has been presented in Table 4.27. As yield for Thulium and Tantalum material obtained through cross-section measurement is higher, it can be observed that range of residual activity induced is also higher. In case of Thulium and Tantalum the maximum range of activity induced is nearly 13 microns respectively while in case of Terbium material maximum range has been observed upto 10 microns approximately.

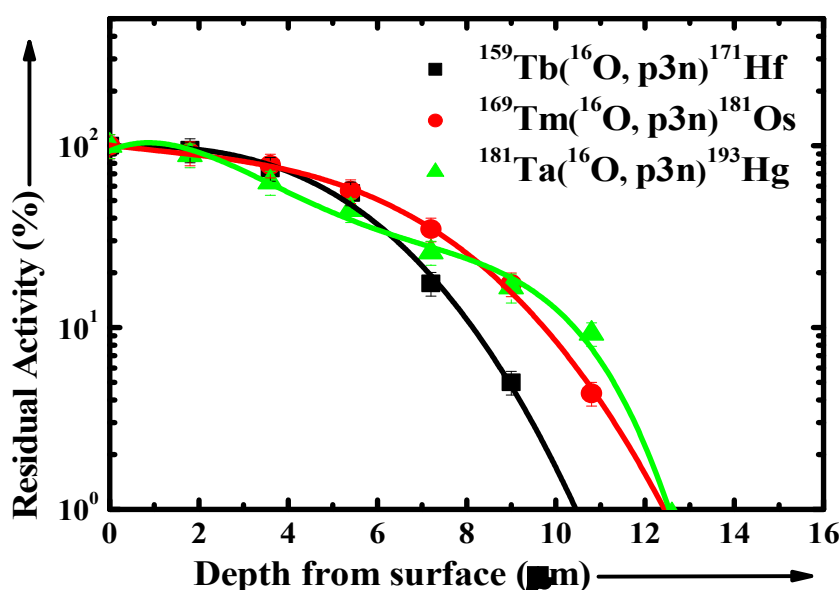


Fig. 31. Calibration curves of isotopes ^{171}Hf , ^{181}Os & ^{193}Hg from Tb, Tm & Ta materials at incident energies ranging from 100 to 70.

TABLE 4.27 Residual Activity range distribution range in Terbium, Thulium & Tantalum materials for p3n reaction channels using ^{16}O beam in energy range 70-110 MeV [18].

Thickness Range (μm)	ACTIVITY INDUCED (%)		
	$^{159}\text{Tb}(^{16}\text{O},4\text{n})^{171}\text{Ta}$	$^{169}\text{Tm}(^{16}\text{O},4\text{n})^{181}\text{Ir}$	$^{181}\text{Ta}(^{16}\text{O},4\text{n})^{193}\text{Tl}$
0	100	100	100
1.8	92.86	93.75	95
3.6	76.19	84.375	88.8
5.4	26.67	68.75	77.7
7.2	14.28	43.75	64.81
9	1.19	6.25	57.4
10.8	0	3.125	44.44
12.6	0	0	33.33

TABLE 4.28 Residual Activity range distribution range in Terbium & Tantalum materials for p4n reaction channels using ^{16}O beam in energy range 70-110 MeV [18].

Thickness Range (μm)	ACTIVITY INDUCED (%)	
	$^{159}\text{Tb}(^{16}\text{O}, \text{p4n})^{170}\text{Hf}$	$^{181}\text{Ta}(^{16}\text{O}, \text{p4n})^{192}\text{Hg}$
0	100	100
1.5	87.5	97.37
3	68.75	92.1
4.5	18.75	84.21
6	6.25	68.42
7.5	0	54
9	0	28.95
10.5	0	14.47
12	0	2.63

Fig 32 illustrates plot of range of residual activity obtained through cross-section measurements for comparative analysis of different rare earth materials for reaction products viz ^{170}Hf & ^{192}Hg in p4n reaction channels of Terbium and Tantalum material respectively. The activity distribution is in steps of each 1.5 microns removed ranging from 0-15 microns. The amount of residual activity induced and maximum depth achieved in the energy range of 70-95 MeV of Oxygen beam on respective materials has been presented in Table 4.28. As yield for Tantalum material obtained through cross-section measurement is higher, it can be observed that range of residual activity induced is also higher. In case of Tantalum the maximum range of activity induced is 14 microns while in case of Terbium material, maximum range has been observed upto 9 microns approximately.

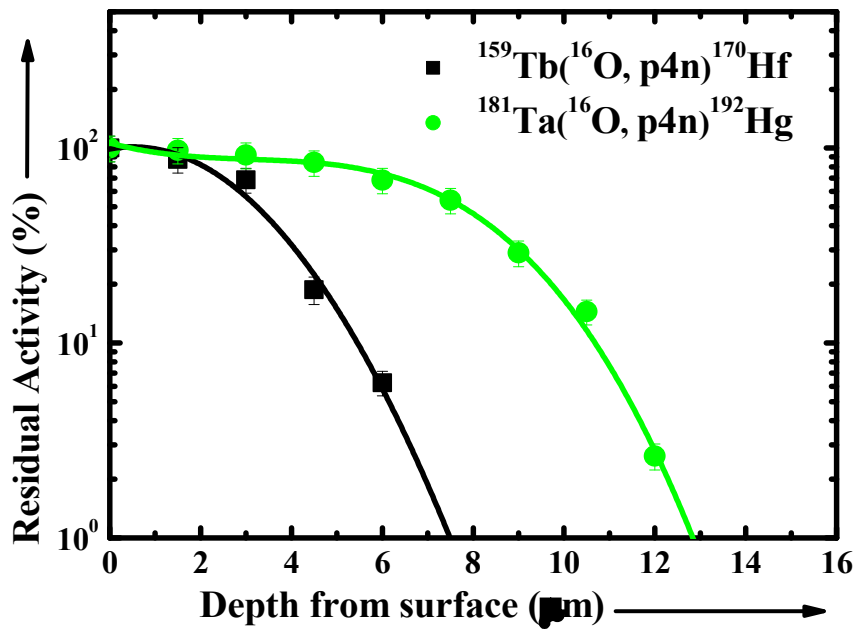


Fig. 32. Calibration curves of isotopes ^{170}Hf & ^{192}Hg from Tb & Ta materials at incident energies ranging from 100 to 70 MeV

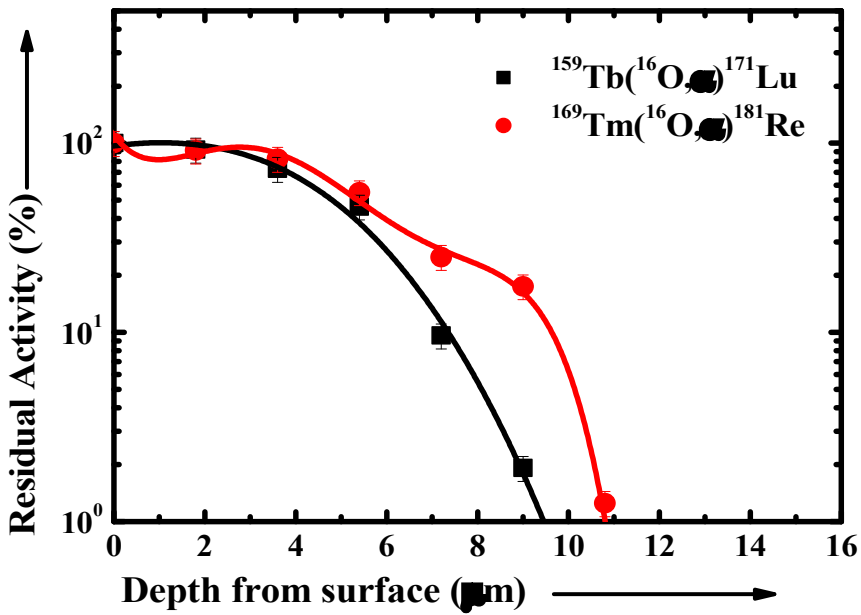


Fig. 33. Calibration curves of isotopes ^{171}Lu & ^{181}Re from Tb & Tm materials at incident energies ranging from 95 to 65 MeV.

Fig 33 illustrates plot of range of residual activity distribution obtained through cross-section measurements for comparative analysis of different rare earth materials for reaction products viz ^{171}Lu & ^{181}Re in 2p2n reaction channels of Terbium and Thulium material respectively. The activity distribution is in steps of each 1.8 microns removed ranging from 0-15 microns. The amount of residual activity induced and maximum depth achieved in the energy range of 70-95 MeV of Oxygen beam on respective materials has been presented in Table 4.29. As yield for Thulium material obtained through cross-section measurement is higher, it can be observed that range of residual activity induced is also higher. In case of Thulium, the maximum range of activity induced is 11 microns while in case of Terbium material, maximum range has been observed upto 9 microns approximately.

TABLE 4.29 Residual Activity range distribution range in Terbium & Thulium materials for 2p2n reaction channels using ^{16}O beam in energy range 70-110 MeV [18].

Thickness Range (μm)	ACTIVITY INDUCED (%)	
	$^{159}\text{Tb}(^{16}\text{O},2\text{p}2\text{n})^{171}\text{Lu}$	$^{169}\text{Tm}(^{16}\text{O},2\text{p}2\text{n})^{181}\text{Re}$
0	100	100
1.8	92.3	91.25
3.6	73.1	82.5
5.4	46.2	55
7.2	9.62	25
9	1.92	17.5
10.8	0	1.25
12.6	0	0

Fig 34 illustrates plot of range of residual activity distribution obtained through cross-section measurements for comparative analysis of different rare earth materials for reaction products viz ^{170}Lu & ^{192}Au in αn reaction channels of Terbium and Tantalum material respectively. The activity distribution is in

steps of each 1.8 microns removed ranging from 0-15 microns. The amount of residual activity induced and maximum depth achieved in the energy range of 70-95 MeV of Oxygen beam on respective materials has been presented in Table 4.30. As yield for Tantalum material obtained through cross-section measurement is higher, it can be observed that range of residual activity induced is also higher. In case of Tantalum, the maximum range of activity induced is 14 microns while in case of Terbium material, maximum range has been observed upto 8 microns approximately.

TABLE 4.30 Residual Activity range distribution range in Terbium & Tantalum materials for αn reaction channels using ^{16}O beam in energy range 70-110 MeV [18].

Thickness Range (μm)	ACTIVITY INDUCED (%)	
	$^{159}\text{Tb}(^{16}\text{O}, \alpha n)^{170}\text{Lu}$	$^{181}\text{Ta}(^{16}\text{O}, \alpha n)^{192}\text{Au}$
0	100	100
1.8	84.1	93.3
3.6	72.7	63.3
5.4	36.4	55
7.2	0.9	38.33
9	0	10
10.8	0	6.7
12.6	0	1.7

Fig 35 illustrates plot of range of residual activity distribution obtained through cross-section measurements for comparative analysis of different rare earth materials for reaction products viz ^{169}Lu & ^{191}Au in αn reaction channels of Terbium and Tantalum material respectively. The activity distribution is in steps of each 1.8 microns removed ranging from 0-15 microns. The amount of residual activity induced and maximum depth achieved in the energy range of 70-95 MeV of Oxygen beam on respective

materials has been presented in Table 4.31 The maximum range of activity induced is 9 microns in case of both Terbium and Tantalum material for above mentioned reaction products.

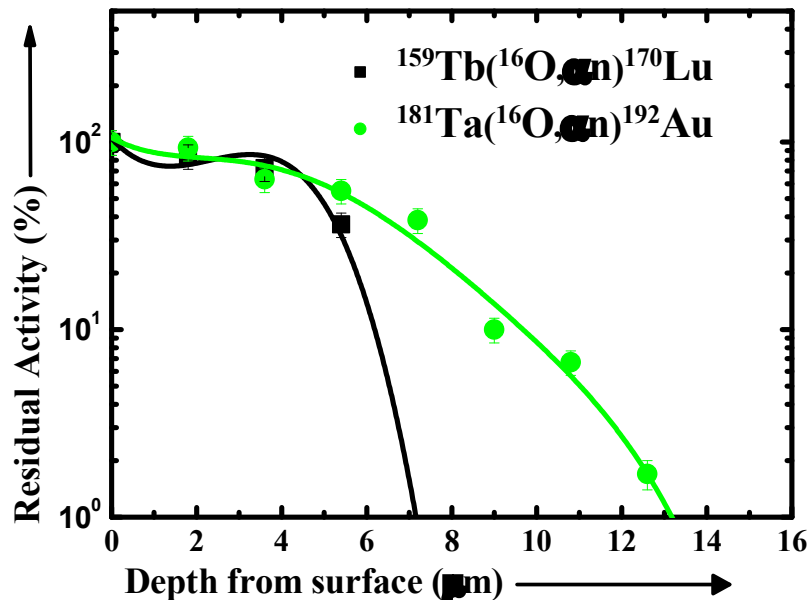


Fig. 34. Calibration curves of isotopes ^{170}Lu & ^{192}Au from Tb & Ta materials at incident energies ranging from 100 to 65 MeV.

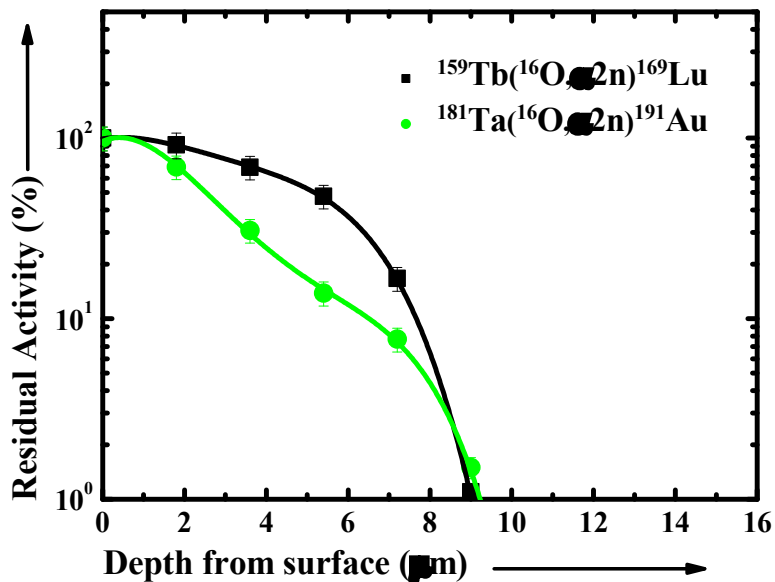


Fig. 35. Calibration curves of isotopes ^{169}Lu & ^{192}Au from Tb & Ta materials at incident energies ranging from 100 to 75 MeV.

TABLE 4.31 Residual Activity range distribution range in Terbium & Tantalum materials for $\alpha 2n$ reaction channels using ^{16}O beam in energy range 70-110 MeV [18].

Thickness Range (μm)	ACTIVITY INDUCED (%)	
	$^{159}\text{Tb}(^{16}\text{O}, \alpha 2n)^{169}\text{Lu}$	$^{181}\text{Ta}(^{16}\text{O}, \alpha 2n)^{191}\text{Au}$
0	100	100
1.8	91.7	69.2
3.6	69	30.8
5.4	47.61	13.85
7.2	16.7	7.7
9	1.1	1.5
10.8	0	0
12.6	0	0

TABLE 4.32 Residual Activity range distribution range in Thulium & Tantalum materials for $\alpha 3n$ reaction channels using ^{16}O beam in energy range 70-110 MeV [18].

Thickness Range (μm)	ACTIVITY INDUCED (%)	
	$^{169}\text{Tm}(^{16}\text{O}, \alpha 3n)^{178}\text{Re}$	$^{181}\text{Ta}(^{16}\text{O}, \alpha 3n)^{190}\text{Au}$
1.5	100	100
3	84.29	75
4.5	49	43
6	20	27
7.5	8.6	11
9	4.3	5.7
10.5	0.57	1
12	0	0.58

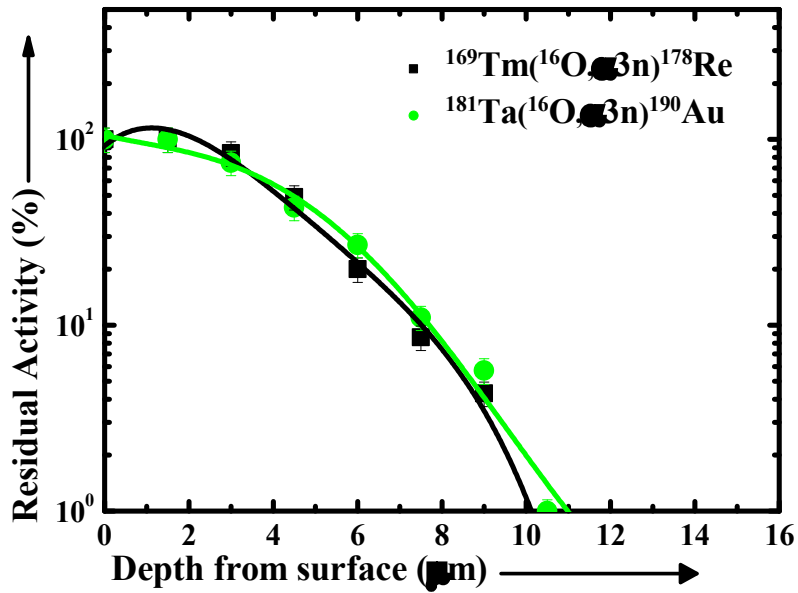


Fig. 36. Calibration curves of isotopes ^{178}Re & ^{190}Au from Tm & Ta materials at incident energies ranging from 100 to 70 MeV.

Fig 36 illustrates plot of range of residual activity distribution obtained through cross-section measurements for comparative analysis of different rare earth materials for reaction products viz ^{178}Re & ^{190}Au in $\alpha 3n$ reaction channels of Thulium and Tantalum material respectively. The activity distribution is in steps of each 1.5 microns removed ranging from 0-15 microns. The amount of residual activity induced and maximum depth achieved in the energy range of 70-95 MeV of Oxygen beam on respective materials has been presented in Table 4.32. The maximum range of activity induced is 10 microns in case of Thulium and in case of Tantalum material; maximum activity depth achieved in same set of standard operating conditions is 11 microns for above mentioned reaction products.

4.4 TLA REACTIONS INITIATED USING ALPHA ION BEAM

4.4.1 TLA INVESTIGATIONS IN NATURAL NICKEL MATERIAL USING ALPHA ION BEAM

Nickel based alloys and coatings have evolved mature subject of research and development from tribological applications point of view due to excellent anti wear & corrosion resistant properties. Attempts have been made to measure

the activity in irradiated natural Ni material induced by α -particles in the energy range 10-40 MeV followed by stack foil activation technique. Activity induced has been determined through the cross-sections obtained from various reactions for $^{58}\text{Ni}(\alpha, p)^{61}\text{Cu}$, $^{58}\text{Ni}(\alpha, pn)^{60}\text{Cu}$, $^{60}\text{Ni}(\alpha, p2n)^{61}\text{Cu}$, $^{60}\text{Ni}(\alpha, n)^{63}\text{Zn}$, $^{60}\text{Ni}(\alpha, 2n)^{62}\text{Zn}$, $^{61}\text{Ni}(\alpha, 3n)^{62}\text{Zn}$ and $^{61}\text{Ni}(\alpha, 2n)^{63}\text{Zn}$ in $\alpha+^{\text{nat}}\text{Ni}$ interaction at different beam energies [19].

To measure the cross-sections of various reaction products in $\alpha+^{\text{nat}}\text{Ni}$ interactions at $\approx 10\text{--}40$ MeV and subsequently used to study the amount of residual activity induced in natural Ni materials, experiments were performed at the Variable Energy Cyclotron Centre (VECC), Kolkata, India. For irradiation, natural Nickel targets were prepared by rolling technique. A stack consisting of 8 target foils made up of $^{\text{nat}}\text{Ni}$ material each backed by aluminium catcher of appropriate thickness obtained by energy loss calculation from SRIM/TRIM was impinged by a 40 MeV α -beam. The approximate thickness of $^{\text{nat}}\text{Ni}$ foils were 1.13, 1.8, 1.15, 0.9, 1.33, 1.19, 1.05 & 1.63 mg/cm^2 respectively each backed by aluminium catcher of approximate thickness of 1.3, 2.8, 1.47, 1.18, 1.41, 1.22, 1.24 & 2.23 mg/cm^2 . The total irradiation time was ≈ 12 h with a beam current ≈ 100 nA. The average beam energy on a given target foil and degrader was calculated by using the code SRIM based on stopping power and range calculations. A pre-calibrated HPGe detectors coupled with multichannel analyzer system has been used for post irradiation analysis. The overall error has been estimated from the errors of cross-section in generating the calibration curves and the activity measurement of the irradiated samples and has been found $\leq 15\%$. Statistical errors has been deduced and fitted with a fourth-order polynomial function, where the uncertainty from the fitting is found to be $\approx 3\%$ for the energy range of interest. Errors introduced due to solid angle defect are found to be less than $\leq 2\%$. The human errors introduced due to non-uniformity and inaccurate determination of foil thickness at various positions has been found to be $\approx 1\%$. The errors from the fluctuations in the beam current were found to

be $\approx 3\%$. Errors introduced due to attenuation in beam current while traversing through thickness of foil has been found to be $\leq 2\%$ [19].

To measure the range/depth of activity induced in Ni material, the cross-sections for $^{58}\text{Ni}(\alpha, p)^{61}\text{Cu}$, $^{58}\text{Ni}(\alpha, pn)^{60}\text{Cu}$, $^{60}\text{Ni}(\alpha, p2n)^{61}\text{Cu}$, $^{60}\text{Ni}(\alpha, n)^{63}\text{Zn}$, $^{60}\text{Ni}(\alpha, 2n)^{62}\text{Zn}$, $^{61}\text{Ni}(\alpha, 3n)^{62}\text{Zn}$ and $^{61}\text{Ni}(\alpha, 2n)^{63}\text{Zn}$ reactions have been measured by using the activation technique followed by off-line γ spectroscopy.

4.4.2 MEASUREMENT OF CROSS-SECTION AND YIELD CURVES

The yield curves for various isotopes; $^{61,60}\text{Cu}$ & $^{63,62}\text{Zn}$ populated through different reaction for $^{58, 60, 61 \text{ nat}}\text{Ni}$ material with α beam have been obtained at different energies and different depths. The stopping power of different materials has been used to obtain the incident energies on different samples. Area under the yield curves across different energies ranging from 10-40 MeV was integrated to obtain the residual curves. The yield per micron thickness against the depth as well as incident energy for residual isotopes viz; $^{61,60}\text{Cu}$, ^{63}Zn & ^{62}Zn is shown in Figs (37-39). For proper polynomial fit of the experimental data, theoretical cross-section values (obtained from PACE 4) have been included below 25 MeV for reactions [$^{58}\text{Ni}(\alpha, pn)$; $^{60}\text{Ni}(\alpha, p2n)$; $^{60}\text{Ni}(\alpha, n)$; $^{60}\text{Ni}(\alpha, 2n)$; $^{61}\text{Ni}(\alpha, 3n)$; $^{61}\text{Ni}(\alpha, 2n)$]. Total cross section values mentioned in Table 4.32 have been used for obtaining yield curves.

The yield curves for various isotopes; $^{61,60}\text{Cu}$ & $^{63,62}\text{Zn}$ populated through different reaction for $^{58, 60, 61 \text{ nat}}\text{Ni}$ material with α beam have been obtained at different energies and different depths. The stopping power of different materials has been used to obtain the incident energies on different samples. Area under the yield curves across different energies ranging from 10-40 MeV was integrated to obtain the residual curves. The yield per micron thickness against the depth as well as incident energy for residual isotopes viz; $^{61,60}\text{Cu}$, ^{63}Zn & ^{62}Zn is shown in Figs (37-39). For proper polynomial fit of the experimental data, theoretical cross-section values (obtained from PACE 4)

have been included below 25 MeV for reactions [$^{58}\text{Ni}(\alpha, \text{pn})$; $^{60}\text{Ni}(\alpha, \text{p2n})$; $^{60}\text{Ni}(\alpha, \text{n})$; $^{60}\text{Ni}(\alpha, \text{2n})$; $^{61}\text{Ni}(\alpha, \text{3n})$; $^{61}\text{Ni}(\alpha, \text{2n})$]. Total cross section values mentioned in Table 4 have been used for obtaining yield curves.

Table 4.33 Spectroscopic properties of isotopes $^{60}, ^{61}\text{Cu}$ & $^{62}, ^{63}\text{Zn}$ used in Stack Foil Activation technique [19-20].

SL NO	Reaction	Residue	Half-life	γ -ray energies(keV)	Cross-Section (mb)
1	$^{58}\text{Ni}(\alpha, \text{p})$	^{61}Cu	3.33 h	283.0, 656.0	1453
2	$^{58}\text{Ni}(\alpha, \text{pn})$	^{60}Cu	23.7 min	826.3, 1332.5	897.1
3	$^{60}\text{Ni}(\alpha, \text{p2n})$	^{61}Cu	3.33 h	283.0, 656.0	301
4	$^{60}\text{Ni}(\alpha, \text{n})$	^{63}Zn	38.47 min	669.86, 926.27	30.2
5	$^{60}\text{Ni}(\alpha, \text{2n})$	^{62}Zn	9.186 h	548.4, 596.7	92.4
6	$^{61}\text{Ni}(\alpha, \text{3n})$	^{62}Zn	9.186 h	548.4, 596.7	13.5
7	$^{61}\text{Ni}(\alpha, \text{2n})$	^{63}Zn	38.47 min	669.86, 926.27	406

Total cross-section for reaction products $^{61}, ^{60}\text{Cu}$ obtained through αp & αpn reaction channels respectively in $^{\text{nat}}\text{Ni}$ material is measured by summing up of all individual cross-sections obtained at varying depths ranging from 0-30 microns and at varying energy range from 10-40 MeV incident alpha ion beam. Total cross-section values for $^{61}, ^{60}\text{Cu}$ is 1453, & 897.1 mbarns respectively as represented in Table 4.33 In fig 37 yield curves have been obtained with polynomial order of 4 for smooth fitting. Maximum yield has

been observed for reaction product ^{61}Cu obtained through αp reaction channel [19]. Fig 38 illustrates plot of yield obtained through cross-section measurements for reaction products $^{63, 62}\text{Zn}$ in αn and $\alpha 2n$ reaction channels of $^{nat60}\text{Ni}$ material and ^{61}Cu obtained through $\alpha p 2n$ respectively. Total cross-section values for $^{63, 62}\text{Zn}$ is 30.2 & 92.4 respectively as represented in Table 4.33 Maximum yield has been observed for reaction product ^{62}Zn obtained through $\alpha p 2n$ reaction channel [19]. Fig 39 illustrates plot of yield obtained through cross-section measurements for reaction products $^{63, 62}\text{Zn}$ in $\alpha 2n$ and $\alpha 3n$ reaction channels of $^{nat61}\text{Ni}$ material respectively. Total cross-section values for $^{63, 62}\text{Zn}$ is 406 & 13.5 respectively as represented in Table 13. Maximum yield has been observed for reaction product ^{63}Zn obtained through $\alpha 2n$ reaction channel. As cross-section measured for reaction product ^{62}Zn is very less, it can be neglected in considering for TLA kind of studies [19].

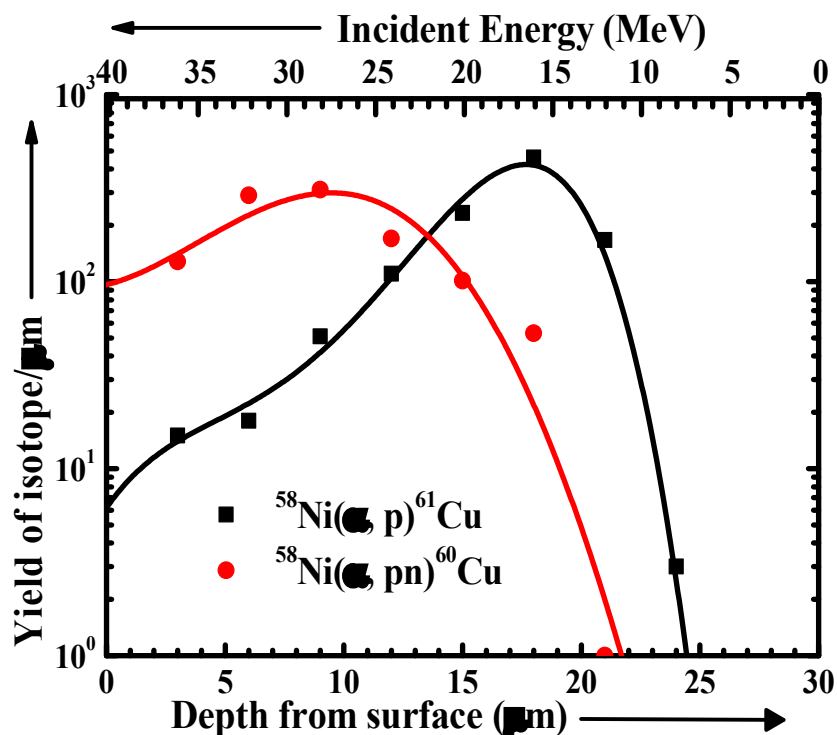


Fig 37 Relative Yield curves for ^{58}Ni Material

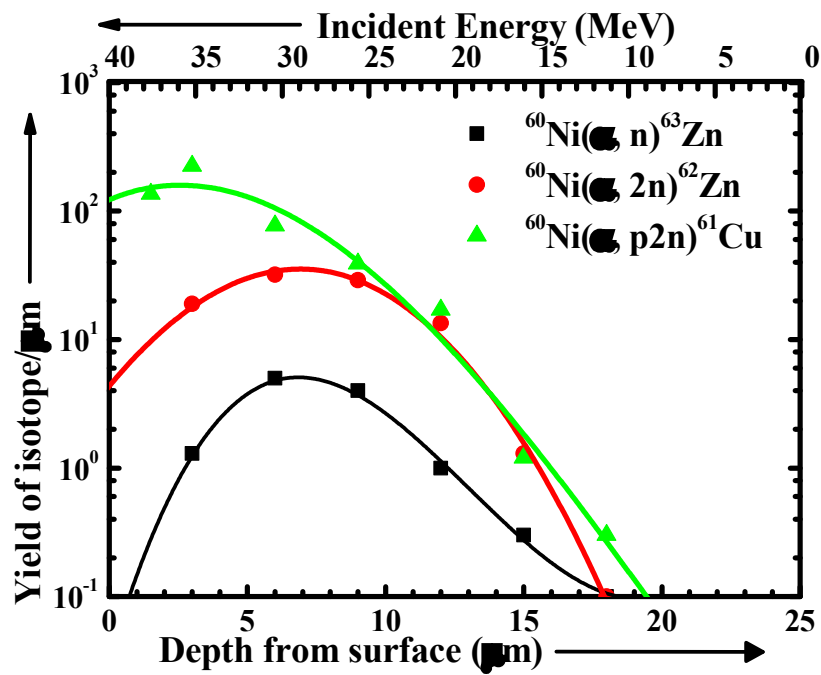


Fig 38 Relative Yield curves for ^{60}Ni Material

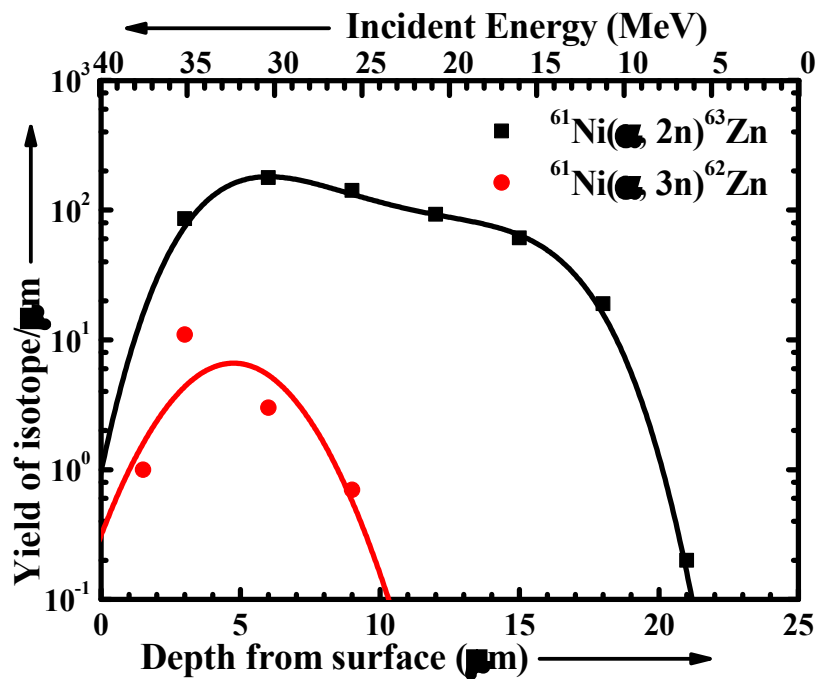


Fig 39 Relative Yield curves for ^{61}Ni Material

4.4.3 MEASUREMENT OF ACTIVITY AND CALIBRATION CURVES

Plot for amount of residual activity induced in $^{58, 60, 61 \text{ nat}}\text{Ni}$ material has been deduced with the help of total cross-section measured values from yield curves. The residual activity induced through α beams with energy range 10-40 MeV in $^{58}\text{Ni}(\alpha, p)^{61}\text{Cu}$; $^{58}\text{Ni}(\alpha, pn)^{60}\text{Cu}$; $^{60}\text{Ni}(\alpha, n)^{63}\text{Zn}$; $^{60}\text{Ni}(\alpha, 2n)^{63}\text{Zn}$; $^{61}\text{Ni}(\alpha, 2n)^{63}\text{Zn}$ & $^{61}\text{Ni}(\alpha, 3n)^{62}\text{Zn}$ has been shown in Figs (38-40). The total yield of the isotope in the given material may be obtained from the integral area under the yield curves. The percentage of remaining activity is computed graphically using polynomial fit by decreasing the thickness corresponding to each foil of stack one by one as shown in Figs (40-42). It has been observed that the activity induced in Ni is ranging upto $\approx 26\mu\text{m}$ [19-20]. Fig 40 illustrates plot of residual activity obtained through cross-section measurements for reaction products $^{61, 60}\text{Cu}$ in αp & αpn reaction channels of material respectively. Maximum activity observed for a reaction products obtained through reactions with $^{\text{nat}58}\text{Ni}$ is approximately ranging upto 26 microns in ^{61}Cu . Fig 41 illustrates plot of residual activity obtained through cross-section measurements for reaction products $^{63, 62}\text{Zn}$ & ^{61}Cu in αn & $\alpha 2n$ & $\alpha p 2n$ reaction channels of $^{\text{nat}60}\text{Ni}$ material respectively. Maximum activity observed for a reaction products obtained through reactions with $^{\text{nat}58}\text{Ni}$ is approximately ranging upto 25 microns in ^{61}Cu [19-20]. Fig 42 illustrates plot of residual activity obtained through cross-section measurements for reaction products $^{63, 62}\text{Zn}$ in $\alpha 2n$ & $\alpha 3n$ reaction channels of $^{\text{nat}61}\text{Ni}$ material respectively. Maximum activity observed for a reaction products obtained through reactions with $^{\text{nat}61}\text{Ni}$ is approximately ranging upto 21 microns in ^{63}Zn . As discussed earlier cross-section measured for ^{62}Zn is very less in few tens of mbarns, residual activity induced is also very low and it can be neglected for TLA based studies [19-20].

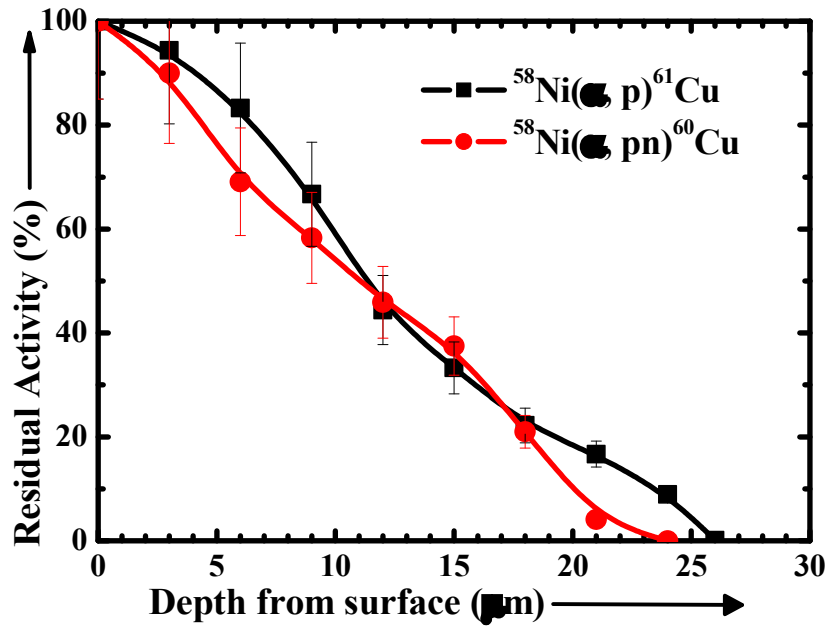


Fig 40 Calibration curves for ^{58}Ni at incident energies ranging from 10-40 MeV

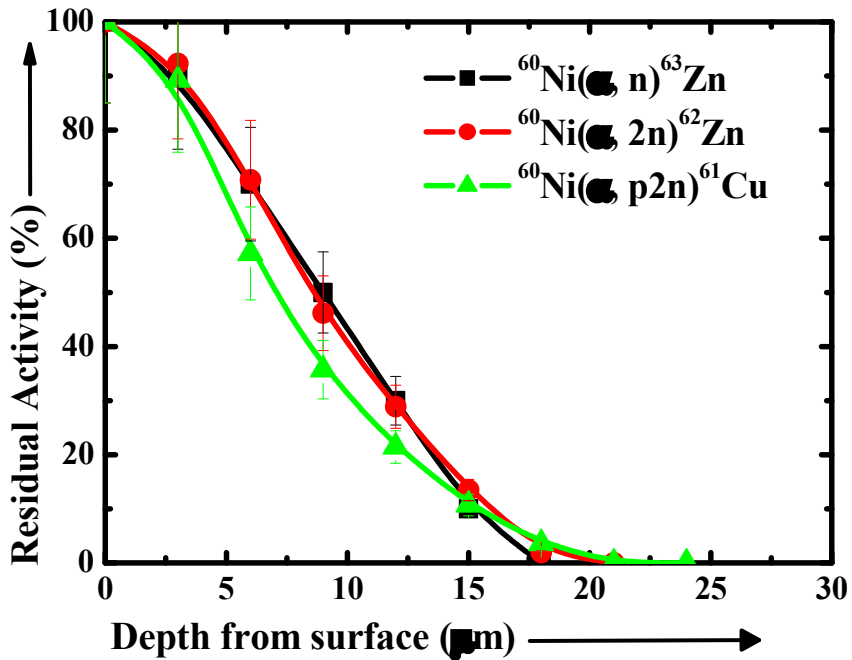


Fig 41 Calibration curves for ^{60}Ni at incident energies ranging from 10-40 MeV

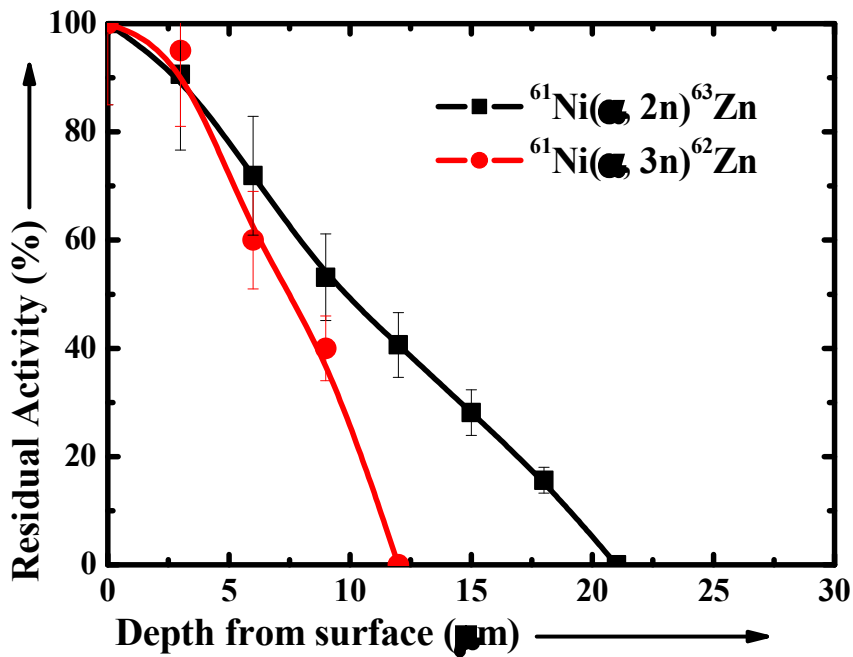


Fig 42 Calibration curves for ^{61}Ni at incident energies ranging from 10-40 MeV.

As Nickel has significant importance in terms of applications across various critical industries in the form of coatings & alloys, in the present work stack foil activation technique had been explored employing α beam with energy ranging from 10-40 MeV in $^{\text{nat}}\text{Ni}$ targets. As shown in Figs (40-42) the maximum residual activity induced is found to be 26 μm from the depth of the surface. As $^{61,60}\text{Cu}$ are populated through (α, p) & (α, pn) reactions while irradiating the same $^{\text{nat}}\text{Ni}$ target, the activity induced in ^{60}Cu via (α, pn) reaction is observed to be less by 3 μm i.e nearly 23 μm as compared to that of ^{61}Cu obtained through (α, p) reaction. The least amount of activity induced is found to be 21 μm in case of ^{63}Zn populated through $\alpha, 2n$ reaction on $^{\text{nat}}\text{Ni}$ target. ^{62}Zn populated through two different reactions with natNi targets i.e. $\alpha, 2n$ & $\alpha, 3n$ via ^{60}Ni & ^{61}Ni target materials is having activity contribution ranging $\approx 12-20 \mu\text{m}$. In the present study activity induced through all possible reactions in natNi material has been reported. As ^{62}Zn has comparatively longer half-life of nearly 10hrs, the experimental data obtained can be used further as a future scope employing TLA for investigating surface wear and

erosion phenomena at earlier stages in critically important industries like nuclear plants, power plants & other process industries applications where small failure would lead to catastrophic effects.

4.5 RESULTS & DISCUSSIONS

The maximum activity induced through various reaction products & respective channels for Terbium, Thulium, Tantalum materials with oxygen beam has been presented in Table 4.34-4.36 respectively.

Table No 4.34 Maximum surface activity induced in Terbium material with ^{16}O [10]

Reaction Residue	Reaction Channel	Max Activity (μm)
^{172}Ta	3n	13
^{171}Ta	4n	12
^{170}Ta	5n	13
^{171}Hf	p3n	13
^{170}Hf	p4n	13
^{171}Lu	2p2n	12
^{170}Lu	αn	11

Table No 4.35 Maximum surface activity induced in Thulium material with ^{16}O [11]

Reaction Residue	Reaction Channel	Max Activity (μm)
^{182}Ir	3n	12
^{181}Ir	4n	12
^{182}Os	p3n	12
^{181}Os	P4n	12
^{181}Re	2p2n	12

Table No 4.36 Maximum surface activity induced in Tantalum material with ^{16}O [12]

Reaction Residue	Reaction Channel	Max Activity (μm)
^{194}Tl	3n	13
^{193}Tl	4n	13
^{192}Tl	5n	13
^{193}Hg	p3n	14
^{192}Hg	p4n	13
^{192}Au	αn	11
^{191}Au	α2n	10
^{190}Au	α3n	8

Present work also reports maximum surface activity induced in natural nickel material through various reaction residues & reaction channels due to its anti-corrosive significance & applications in wide range of industries in Table No 4.37.

Table No 4.37 Maximum surface activity induced in Nickel material with α -beam [19]

Reaction Residue	Reaction Channel	Max Activity (μm)
^{61}Cu	α, p	26
^{60}Cu	α, pn	25
^{61}Cu	$\alpha, p2n$	18
^{63}Zn	α, n	20
^{62}Zn	$\alpha, 2n$	22
^{62}Zn	$\alpha, 2n$	21
^{63}Zn	$\alpha, 3n$	12

All the materials investigated for surface activity measurements have great significance from industrial applications point of view. Results obtained with various materials are completely a new set of cross-section, energy, ion beam & activity measurements which may be helpful in development of many customized tribological set-ups for measurement of surface degradation. Usually, TLA involves of measuring only one specific reaction residue of interest having higher cross-section values and measurable half-life. Current work reports all the possible cross-sections of reaction products obtained through initiation of nuclear reaction with HI Oxygen and Alpha beam, which can be further used for multidisciplinary applications or fields of research. Details of some such applications will be presented in next chapter Conclusions & Future Scope.

REFERENCES

- [1] Imam Kambali and Hari Suryanto, “*Journal of Engineering and Technological Sciences*”, 48 (4) (2016) 482–494.

- [2] IAEA report on The thin layer activation method and its applications in industry.
- [3] Devendra P. Singh, Vijay R. Sharma, Abhishek Yadav, Pushpendra P. Singh, Unnati, M. K. Sharma, H. D. Bhardwaj, B. P. Singh and R. Prasad, “*Journal of Nuclear Physics, Material Sciences, Radiation and Applications*”, (JNPMSRA), Vol. 1, No. 1, (2013) pp. 13–24.
- [4] M.S Uddin, M Hagiwara, F Tarkanyi, F Ditroi and M Baba, “*Applied Radiation and Isotope*”, Vol. 60, Issue 6, June 2004, pp. 911-920.
- [5] M.S Uddin, M Hagiwara, F Tarkanyi, F Ditroi and M Baba, “*Applied Radiation and Isotope*”, Vol. 63, Issue 3, September 2005, pp. 367-374.
- [6] M. M. Gunther, A. Britz, R. J. Clarke, K. Harres, G. Hoffmeister, F. Nurnberg, A. Otten, A. Pelka, M. Roth, and K. Vogt, “*Review of Scientific Instruments*” 84, 073305 (2013).
- [7] J. Lamovec, V. Jovic, D. Randjelovic, R. Aleksic, V. Radojevic, “*Thin Solid Films*”, Vol. 516, Issue 23, 1 October 2008, pp. 8646-8654.
- [8] Jothi Sudagar, Jianshe Lian and Wei Sha, “*Journal of Alloys and Compounds*”, Vol. 571, 15 September 2013, pp. 183-204.
- [9] Krishnan K H, John S, Srinivasan K, Praveen J, Ganesan M and Kavimani P; “*Metallurgical and Materials Transactions A*”, 2006, Vol 37, p 1917-1926.
- [10] D. P. Singh, Varun.V. Savadi, S.K.Joshi, Ishfaq Majeed, Md. Shuaib, V. R. Sharma, A. Yadav, P. P. Singh, Unnati, M. K. Sharma, R. Kumar, B. P. Singh and R. Prasad, “*Materials Today: Proceedings*”, 17P1 (2019) pp. 266-270.
- [11] Varun .V. Savadi, D. P. Singh, S.K.Joshi, Ishfaq Majeed, Md. Shuaib, V. R. Sharma, A. Yadav, P. P. Singh, Unnat, M. K. Sharma, R. Kumar, B. P. Singh and R. Prasad, “*Materials Today: Proceedings*”, 17P1 (2019) pp. 96-100.
- [12] Varun .V. Savadi, D. P. Singh, S.K.Joshi, Ishfaq Majeed, Md. Shuaib, V. R. Sharma, A. Yadav, P. P. Singh, Unnat, M. K. Sharma, R. Kumar, B. P. Singh and R. Prasad, “*Indian Journal of Pure and Applied Physics*”, Vol.57 (2019) pp. 566-569.

- [13] Ziegler; James F; Biersack, Jochen P. “SRIM-2008, Stopping Power and Range of Ions in Matter”.
- [14] Varun V Savadi, D P Singh, S K Joshi, A Yadav, P P Singh, M K Sharma, Unnati, M M Mustafa, B P Singh & R. Prasad, “*Indian Journal of Pure & Applied Physics*”, Vol. 59, May 2021, pp. 386-390.
- [15] Manoj Kumar Sharma , Unnati, B.P. Singh, Rakesh Kumar, K.S. Golda, H.D. Bhardwaj, R. Prasad, “*Nuclear Physics A*”, 776 (2006) 83–104.
- [16] Manoj Kumar Sharma, Unnati, B. K. Sharma, B. P. Singh, H. D. Bhardwaj, Rakesh Kumar, K. S. Golda, and R. Prasad, “*PHYSICAL REVIEW C*”, 70, 044606 (2004).
- [17] Devendra P. Singh, Unnati, Pushpendra P. Singh, Abhishek Yadav, Manoj Kumar Sharma, B. P. Singh, K. S. Golda, Rakesh Kumar, A. K. Sinha, and R. Prasad, “*PHYSICAL REVIEW C*”, 80, 014601 (2009).
- [18] Varun Vijay Savadi, D.P. Singh, S.K. Joshi, I. Majeed, Md. Shuaib, V.R. Sharma, A. Yadav, R. Kumar, P.P. Singh, Unnati, M.K. Sharma, S. Pandey, B.P. Singh, R. Prasad, “*Nuclear Inst. and Methods in Physics Research B*”, 479 (2020) 102–109.
- [19] Varun V Savadi, D P Singh, S K Joshi, A Yadav, P P Singh, M K Sharma, Unnati, M M Mustafa, B P Singh & R. Prasad, “*Indian Journal of Pure & Applied Physics*”, Vol. 59, May 2021, pp. 386-390.
- [20] Yadav A, Singh P P, Sharma M K, Singh D P, Unnati, Singh, B P & Prasad R, *Phys Rev C*, 78 (2008) 044606.

CHAPTER 5

CONCLUSIONS AND FUTURE PERSPECTIVES

5.1 CONCLUSIONS

Modern machineries and equipments used in industrial technologies require efficient and reliable monitoring tools & techniques to assess performance precisely. TLA is a very powerful monitoring technique used for registering in-situ loss in material rates with increased accuracy and sensitivity. In the present work, investigations have been carried out to measure and analyse feasibility of TLA in rare earth materials Terbium and Thulium alongwith strategically important materials like Tantalum and Nickel having wide range of industrial applications using HI beam. Experiments with these materials were initially carried out to measure nuclear interactions and reaction dynamics near and above CB through irradiations. This data obtained post irradiation has been used to explore and identify appropriate reaction products suitable for TLA applications. Activation of Terbium, Thulium and Tantalum materials has been achieved by bombarding ^{16}O beam obtained through accelerator at IUAC, New Delhi, India. Activation of natural Nickel material has been achieved by bombarding Alpha beam obtained through accelerator at VECC, Kolkata, India. The range of activation energy for Terbium, Thulium & Tantalum materials through Oxygen beam is approximately 70-110 MeV. For Natural nickel material range of activation energy is approximately from 10-40 MeV through Alpha beam. TLA is usually achieved by tracing one specific reaction having good cross-section, yield and measurable half-life values to monitor wear, erosion or corrosion rates in materials subjected to various industrial applications. As present work is focussed towards investigating the feasibility of TLA studies in above mentioned materials, all the nuclear reactions initiated through interaction of beams in material have

been recorded for cross-section measurements, yields and to determine remnant activity through calibration curves. In system $^{16}\text{O}+^{159}\text{Tb}$; 9 reaction products have been identified obtained through xn, pxn & alpha reaction channels. Reaction products ^{172}Ta , ^{171}Ta & ^{170}Ta are obtained through xn reaction channels where (n= 3, 4 & 5) respectively. Reaction products ^{171}Hf & ^{170}Hf are obtained through pxn reaction channels where (n= 3 & 4) respectively. Reaction products ^{171}Lu , ^{170}Lu , ^{169}Lu & ^{165}Tm are obtained through α , αn , $\alpha 2\text{n}$ & $2\alpha 2\text{n}$ reaction channels respectively. In case of $^{16}\text{O} + ^{169}\text{Tm}$ system; 8 reaction products have been identified which are obtained through xn, pxn & alpha reaction channels. Reaction products ^{182}Ir & ^{181}Ir are obtained through xn reaction channels where (n= 3 & 4) respectively. Reaction products ^{182}Os & ^{181}Os are obtained through pxn reaction channels where (n= 2 & 3) respectively. Reaction products ^{181}Re , ^{178}Re , ^{175}Hf & ^{172}Lu are obtained through α , $\alpha 3\text{n}$, $2\alpha\text{pn}$ & $3\alpha\text{n}$ reaction channels respectively. In system $^{16}\text{O} + ^{181}\text{Ta}$; 9 reaction products have been identified obtained through xn, pxn & alpha reaction channels. Reaction products ^{194}Tl , ^{193}Tl & ^{192}Tl are obtained through xn reaction channels where (n= 3, 4 & 5) respectively. Reaction products ^{193}Hg , ^{192}Hg & ^{191}Hg are obtained through pxn reaction channels where (n= 3, 4 & 5) respectively. Reaction products ^{192}Au , ^{191}Lu & ^{190}Au are obtained through αn , $\alpha 2\text{n}$ & $\alpha 3\text{n}$ channels respectively. For $\alpha + ^{58, 60, 61}\text{Ni}$, there are 4 reaction products identified viz; ^{61}Cu , ^{60}Cu , ^{63}Zn & ^{62}Zn through different alpha reaction channels. In all 29 reactions have been identified in above mentioned materials using Oxygen and Alpha ion beam. The experimentally measured cross-sections have been compared with the predictions of the theoretical model code PACE4. Uncertainties in measurement of cross-section values for all reactions by taking into account various errors are observed to be below $\leq 15\%$. All these reactions have measurable amount of cross-section, yield and half-life values which serves as an important input for execution of TLA based studies in alloys and composites having above mentioned materials in the form of elemental composition.

Measurement and analysis of depth distribution of the residual activity induced, obtained through calibration curves can be used further for evaluation of wear, erosion, corrosion and abrasion rates in above mentioned materials having applications in wide range of industries couple with TLA set-up. TLA can be achieved through two modes as discussed as;

Direct Measurements: Through this monitoring of wear rates due dry friction, abrasion and erosion can be measured in materials and components of specific interest. Sensitivity ranging from few tens to several hundred micrometers can be achieved by this method.

Indirect Measurements: This method is usually employed to evaluate the performance of lubricating fluids and components which are functioning in flowing mediums. Materials, equipments used in transportation, automobiles and process industries can be evaluated using this method employing TLA with sensitivity ranging upto few nanometers.

Range of depth achieved and energy of ion beam are one of the primary factors to be considered for TLA studies. Range of ion beam interactions is calculated using SRIM (Stopping Range Ions in Matter) by measuring dE/dX value which corresponds to range of energy loss across thickness of specific material. Thickness of stack (samples of target material) for experiments has been calculated using SRIM / TRIM software. Investigations carried in Terbium material conclude total 9 reaction products which can be used for TLA based studies. Out of these 9 reaction products, ^{171}Lu , ^{177}Hf & ^{170}Hf have very good yield with total cross-sections 2396.8, 2217.21 & 1917 mbarns & measurable half-lives 8.24 days, 12.1 hrs & 16.01 hrs respectively. Maximum range of residual activity induced or depth of activation achieved in these reaction products using oxygen beam with energy range 70-95 MeV has been observed upto approximately 13 microns. Investigations carried in Thulium material conclude total 8 reaction products which can be used for TLA based studies. Out of these 8 reaction products, ^{181}Re , ^{182}Os & ^{181}Os have very good yield with total cross-sections 2707.05, 1053.47 & 1062.38 mbarns & measurable half-lives of 19.9 hrs, 22.1 hrs & 105 min respectively.

Maximum range of residual activity induced or depth of activation achieved in these reaction products using oxygen beam with energy range 70-95 MeV has been observed upto approximately 12 microns. Investigations carried in Tantalum material conclude total 9 reaction products which can be used for TLA based studies. Out of these 9 reaction products, ^{192}Tl , ^{192}Hg & ^{193}Hg have very good yield with total cross-sections 1827.8, 620.2 & 457.5 mbarns & measurable half-lives 10.6 min, 4.85 hrs & 11.8 hrs respectively. Maximum range of residual activity induced or depth of activation achieved in these reaction products using oxygen beam with energy range 70-110 MeV has been observed upto approximately 15-16 microns. Investigations carried in natural Nickel material conclude total 4 reaction products which can be used for TLA based studies. Out of these 4 reaction products, ^{61}Cu , ^{60}Cu & ^{63}Zn have very good yield with total cross-sections 1453, 897.1 & 406 mbarns & measurable half-lives 3.33 hrs, 23.7 min & 38.47 min respectively. Maximum range of residual activity induced or depth of activation achieved in these reaction products using oxygen beam with energy range 70-110 MeV has been observed upto approximately 26 microns.

Emerging technologies in industrial sectors such as transportation, space, defense and energy requires reliable and improvised techniques for investigating and monitoring rate of losses due to material interactions. Hence, TLA serves as a high-resolution tool for estimation of surface degradation mechanisms. New materials can be tested for evaluating performing characteristics to be used in the form of coatings, lubricants etc. customized bench test rigs can be designed which optimizes evaluation of functionality of various components or systems in automobile sectors. Complex machinery components having tribological losses can be monitored efficiently using TLA. TLA is well established for investigation of wear, erosion, corrosion in automobile components like piston, cylinder performance. In past few years, significant research has been carried out to make use of this technique in other various industrial applications.

In present work, all reactions initiated through activation in above mentioned materials are by using heavy ion beams. Literature available for activation studies in materials using heavy ion beams is limited. Furthermore, from the identified reaction products, remaining 20 reaction products identified are also having good yield, cross-section values and half-lives values which serves as a feasible input for future based TLA studies in these materials having wide range of industrial applications. Sensitivity, precision and accuracy upto nanometers range can be achieved through UTLA method based upon recoil implantation into near surface of materials. Finally to conclude, investigations carried out for various reaction products forms a strong database for setting up actual TLA experiments using heavy ion beams as activation source not just limited to mechanical applications, but also for other industrial applications like medicine technology, accelerator technology etc and with motivation to carry out further more and more studies by using heavy ion beams obtained through modern accelerators.

5.2 FUTURE SCOPE

Investigations carried out in the present work specifically with Tantalum material through stack foil activation using oxygen beams can be further used as a database obtained through 9 reaction events to measure degradation of cutting tools which are formed through Tantalum Carbides. Precise measurement of wear, temperature deformation and grain growth properties can be observed through TLA based studies. Tantalum fabricated sheets and plates are widely used in chemical process equipments such as cladding, pressure tanks, valves, heat exchangers etc. due to superior corrosion resistance. Loss of material in such industrial applications can be monitored very effectively using TLA studies. Tantalum alloys in the form of fabricated sheets, plates, rods wires etc with alloy compositions containing 3-11% tantalum have proven to be very successful in resistance to corrosion by hot gases which allows higher operating temperatures and thus efficiency and fuel economy in jet engines and rocket nozzles. Using TLA thermal resistance and

corrosion resistance of tantalum alloys in such critical applications can be monitored very precisely through TLA. Advancement and boost towards clean and green technologies have resulted in production of hybrid engines which are efficient, economic and eco-friendly while operating. One of major applications of Terbium which has been investigated in current work is in hybrid engines. These engines function on electric motors which are based on permanent magnets. These magnets usually belong to rare earth category which needs to retain their magnetism at high temperatures. Terbium alongwith neodymium and dysprosium produces such magnets. Applications of such magnets are in the electric motors of wind-turbines, where high temperatures are also generated. The properties of such magnets and resistance to high temperature conditions in wind turbine applications can be monitored using current set of database obtained through activation of Terbium using Oxygen beams. As discussed earlier there are total 8 reaction residues identified with terbium through activation. Wide spread use of nickel due to anti-corrosive and temperature resistant properties make it one of most preferred alloying elements for applications such as pipelines of desalination plants, chemical & process industries and also in many structural applications. Accurate and precise monitoring of performance of nickel and nickel alloys can be determined using the current database obtained through activation of Ni with alpha beams. One of prominent applications is to determine corrosion-resistance in desalination tubes used in desalination plants and marine applications. Apart from such identified critical applications, TLA based investigations reported in present work can also be extended in frontiers of medical technology, nuclear physics, reactor applications, space and defense etc.



Activity induced in different rare earth materials using heavy ion oxygen beam; thin layer activation analysis

Varun Vijay Savadi^a, D.P. Singh^{a,*}, S.K. Joshi^a, I. Majeed^b, Md. Shuaib^b, V.R. Sharma^c, A. Yadav^d, R. Kumar^e, P.P. Singh^f, Unnati^g, M.K. Sharma^h, S. Pandeyⁱ, B.P. Singh^b, R. Prasad^b

^a Department of Physics, University of Petroleum & Energy Studies, Dehradun, Uttarakhand 248007, India

^b Department of Physics, Aligarh Muslim University, Aligarh (UP)-202 002, India

^c Departamento de Aceleradores, Instituto Nacional Investigaciones Nucleares, Apartado Postal 18-1027, Mexico

^d Department of Physics, Jamia Millia Islamia, New Delhi 110025, India

^e Inter University Accelerator Center, New Delhi 110067, India

^f Department of Physics, Indian Institute of Technology Ropar, Rupnagar, Punjab 140 001, India

^g Department of Physics, University of Delhi, New Delhi 110 007, India

^h Department of Physics, S. V. College, Aligarh 202001, India

ⁱ Department of Mechanical Engineering, University of Petroleum & Energy Studies, Dehradun, Uttarakhand -48007, India

ARTICLE INFO

Keywords:

Activation technique

Yield

Cross section measurements

Heavy ions

Thin layer activation technique

ABSTRACT

Activities have been measured in spectroscopically pure rare earth materials viz; Terbium, Thulium and Tantalum, based on the remnant radioactivity induced in the material, when bombarded by ^{16}O beam in the energy range from 70 MeV to 110 MeV. The cross sections of a number of isotopes populated through various reaction channels have been measured by the stacked foil activation technique. To measure the activity, yields of the radioactive isotopic products $^{172,171,170}\text{Ta}$, $^{171,170}\text{Hf}$, $^{171,170,169}\text{Lu}$, $^{182,181}\text{Ir}$, $^{182,181}\text{Os}$, ^{181}Re , $^{194,193,192}\text{Tl}$, $^{193,192}\text{Hg}$, and $^{192,191,190}\text{Au}$ have been determined using the measured cross-sections and subsequently used to measure the activity in these materials which has been found up to 8–16 μm .

1. Introduction

Recent advancement in science and technology has led to a positive shift towards establishment and growth of industries such as heavy engineering, conventional and/or nuclear power plants, manufacturing & processing industries. It is well known that these industries are substantially influenced by surface phenomenon such as wear, corrosion and erosion of materials [1–4]. The functioning of the conventional power plants at elevated temperatures for increased efficiency and demand is often coupled with challenges such as degradation of structural materials subjected to extreme temperature and pressure operating conditions [2–4]. Electric power industry and plants have been reported an estimated loss of around 150 million US\$ in a year in terms of efficiency, forced outages and repair costs due to solid particle erosion [5]. Installation of offshore wind plants due to climate change has gained importance over a couple of years. The materials used in monopile foundation and its components are subjected to varying wind currents leading to surface degradation and wear. Determination of reliable wear measurement methods for such fluctuating conditions in

offshore wind plants is an emerging challenge [6]. The pipelines in the nuclear power plants are often subjected to accelerated flow corrosion and thinning of welds at heat affected zones leading to failure of systems [7]. Various conventional non-destructive methods and techniques are available but with limitations to measure the surface defects occurring in various industries like; aerospace, manufacturing, process industries, military and defence, nuclear industry etc. [8]. Some of the commonly adopted methods are visual inspection, microscopy, radiography, dye penetrant, ultrasonic, magnetic particle testing, eddy current for metals, acoustic emission testing etc [9]. In case of visual inspection and microscopy only macroscopic and small surface flaws can be detected. Radiography and dye penetrant testing are not suitable for porous materials. For ultrasonic testing material subjected under test necessarily needs to be good conductor of sound. Magnetic particle testing is applicable to its best only with ferromagnetic materials. Eddy current is limited only for metals and acoustic emission involves cost implications for testing of a component [9]. In of the studies it was concluded that gravimetric method for determination of surface degradation could yield accurate results but is very time consuming [10].

* Corresponding author.

E-mail address: dpsingh19@gmail.com (D.P. Singh).

New developments and sustainable solutions in medical field such as artificial joints replacement are gaining significant importance. In one of the recent studies, wear evaluation of artificial joints subjected to more than several million cycles [11]. Assessment of non-contacting optical methods was carried out and successfully developed technique for measurement of wear up to 0.0001 mg in ceramics [12]. Studies employing gravimetric analysis for measurement of wear in knee implants subjected to as many as 3 million cycles [13]. A very high sensitive and reliable tool technique is required to investigate the near surface phenomenon.

For a couple of years, Thin Layer Activation (TLA) using charged particles has been preferred over conventional surface phenomena measurement methods due to many advantages [14–17]. With the help of TLA, surface degradation of multiple components can be measured in a single go without influencing the operating conditions of system. It is also economically more feasible with increased level of sensitivity and reduced amount of radioactivity leading to easy handling of samples. The precision of TLA ranges from several hundred micrometers to few tens of nanometers [15–17]. With the availability of cutting edge research in the accelerator technology, it is now possible to activate the desired surface of the material with the help of light and/or heavy charged particles such as proton, deuterons, alpha particles, oxygen beams, etc [18–20]. Since the charge particles quickly lose their kinetic energy as a consequence of intense interaction with the target atoms in a very thin layer, it is known as thin layer activation. TLA mechanism can be achieved either by activity loss measurement or collected activity measurement [18–20]. Activity has been measured using heavy ions up to 110 MeV in a Cu target for determination of surface wear induced in a very thin layer (up to nanometers) [21]. Studies conducted in titanium alloys using TLA with different beams viz; (nitrogen, carbon and light ions) lead to conclusion that wear measurement by TLA are more precise than conventional gravimetric analysis in titanium and chromium alloys [22]. TLA was employed for measurement of wear induced in piston ring and cylinder of automobile [23]. Wear analysis employing TLA with the help of light ions (proton, deuteron and alpha particles) in molybdenum was carried out, which is used as alloying elements in steel to increase corrosion resistance [24]. In of the studies, TLA was employed to study pseudoelasticity effect on nickel-titanium alloys used for orthodontic applications [25]. In one of the investigation conducted, it was concluded that platinum and platinum alloys can be activated in a very thin layer with most suitable radio-isotopes being ^{197}Au & ^{196}Au [26]. Recent studies conducted in neobium alloys could be employed in TLA by measuring cross sections as niobium alloys are commonly used in industries like nuclear and medicine [27]. In one of the studies conducted, calibration curves were deduced indicating amount residual activity induced in Rhodium & Rhodium alloys [28]. For investigation of wear and erosion specimens containing tungsten it was concluded that ^{183}Re and ^{184}Re are the most suitable ones by employing TLA [29]. see Table 1–3.

In the present work, we have used the TLA method to study the surface wear activation in different rare earth materials of interest. Tantalum and Terbium have been classified as rare earth materials of significant importance due to their wide range of applications and mechanical properties [30]. Terbium, Thulium & Tantalum have wide range of applications in electronics, medicine and heavy engineering works [30–33]. Tb^{3+} state is very significant in number of applications. Terbium being classified as one of the rare earth materials of significance has wide range of applications. It is being used predominantly in electronics industries, smart appliances due to its luminescence property. Tb^{3+} ions can be used to check for the presence of microbes. Terbium chloride is applied to the test area, which is then illuminated with UV light. Within minutes, any live endospores present will glow green. Terbium in the form alloying element with iron is very useful in magneto-optics for recording data. Terbium coupled with neodymium and dysprosium is capable of producing magnets which are widely used in electric motors of hybrid engines and wind turbines functioning at

Table 1
Spectroscopic properties of isotopes $^{172,171,170}\text{Ta}$, $^{171,170}\text{Hf}$, and $^{171,170,169}\text{Lu}$ for application in thin layer activation technique.

Isotope	Half-life	γ -ray		Reaction	σ_{max} (mb)
		Energy (keV)	Abundance%		
^{172}Ta	36.8 m	875.3	22	$^{159}\text{Tb} (^{16}\text{O}, 3n)^{172}\text{Ta}$	136.144
^{171}Ta	23.3 m	723.3	25	$^{159}\text{Tb} (^{16}\text{O}, 4n)^{171}\text{Ta}$	1140.33
^{170}Ta	6.76 m	860.2	25	$^{159}\text{Tb} (^{16}\text{O}, 5n)^{170}\text{Ta}$	925.09
^{171}Hf	12.1 h	1076.5	40	$^{159}\text{Tb} (^{16}\text{O}, p3n)^{171}\text{Hf}$	2217.61
^{170}Hf	16.1 h	620.7	18	$^{159}\text{Tb} (^{16}\text{O}, p4n)^{170}\text{Hf}$	1917.72
^{171}Lu	8.24 d	631.2	24	^{159}Tb	2396.98
^{170}Lu	2.01 d	1280.1	23	$(^{16}\text{O}, 2p2n)^{171}\text{Lu}$	137.64
^{169}Lu	34.06 m	1037.13	23	$^{159}\text{Tb} (^{16}\text{O}, \alpha n)^{170}\text{Lu}$ $^{159}\text{Tb} (^{16}\text{O}, \alpha 2n)^{169}\text{Lu}$	269.65

Table 2
Spectroscopic properties of isotopes $^{182,181}\text{Ir}$, $^{182,181}\text{Os}$ and ^{181}Re for application in thin layer activation technique.

Isotope	Half-life	γ -ray		Reaction	σ_{max} (mb)
		Energy (keV)	Abundance %		
^{182}Ir	36.8 m	273.1	43	$^{169}\text{Tm} (^{16}\text{O}, 3n)^{182}\text{Ir}$	349.8
^{181}Ir	23.3 m	107.6	15.9	$^{169}\text{Tm} (^{16}\text{O}, 4n)^{181}\text{Ir}$	1515.47
^{182}Os	6.76 m	180.22	34.7	^{169}Tm	1053.47
^{181}Os	12.1 h	238.68	44	$(^{16}\text{O}, p2n)^{182}\text{Os}$ ^{169}Tm	1062.38
^{181}Re	16.1 h	365.59	57	$(^{16}\text{O}, p3n)^{181}\text{Os}$ ^{169}Tm $(^{16}\text{O}, 2p2n)^{181}\text{Re}$	3142.95

Table 3
Spectroscopic properties of isotopes $^{182,181}\text{Ir}$, $^{182,181}\text{Os}$ and ^{181}Re for application in thin layer activation technique.

Isotope	Half-life	γ -ray		Reaction	σ_{max} (mb)
		Energy (keV)	Abundance%		
^{194}Tl	33 m	636.1	99	$^{181}\text{Ta} (^{16}\text{O}, 3n)^{194}\text{Tl}$	50.6
^{193}Tl	21.5 m	365,244	90.1, 15.2	$^{181}\text{Ta} (^{16}\text{O}, 4n)^{193}\text{Tl}$	341.5
^{192}Tl	10.8 m	422.9	31.1	$^{181}\text{Ta} (^{16}\text{O}, 5n)^{192}\text{Tl}$	1827.8
^{193}Hg	3.8 h	381.6, 861.1	11, 13	$^{181}\text{Ta} (^{16}\text{O}, p3n)^{193}\text{Hg}$	457.5
^{192}Hg	4.85 h	274.8	50.4	$^{181}\text{Ta} (^{16}\text{O}, p4n)^{192}\text{Hg}$	620.2
^{192}Au	4.92 h	295.5, 316.5	22.7, 58	$^{181}\text{Ta} (^{16}\text{O}, \alpha n)^{192}\text{Au}$	246
^{191}Au	3.18 h	282.9, 399.8	6.3, 4.5	$^{181}\text{Ta} (^{16}\text{O}, \alpha 2n)^{191}\text{Au}$	49.4
^{190}Au	42.83 m	295.9, 301.9	71, 25.1	$^{181}\text{Ta} (^{16}\text{O}, \alpha 3n)^{190}\text{Au}$	135.6

elevated temperatures. Terbium is also used as a dopant for materials in solid-state devices and optical fibers [31]. Tm^{3+} ions emit a strong blue luminescence when excited. Thulium is used to dope yttrium aluminum garnets (YAG) used in lasers. Thulium is also used in alloys with other rare earth metals [32]. Tantalum is highly corrosion resistant due to the formation of an oxide film. It is an excellent conductor of heat and electricity. The metal has a melting point exceeded only by tungsten and rhenium. Ta is used in the electronics industry for capacitors and high power resistors. It is also used to make alloys to increase strength, ductility and corrosion resistance. The metal is used in dental and surgical instruments and implants, as it causes no immune response [33]. Tantalum and tantalum alloys could be the futuristic potential materials used for space nuclear mission due to their excellent stability and mechanical properties at elevated temperatures [34]. Tantalum, Terbium and Thulium belong to rare earth materials which can play a very pivotal role in areas of nations security, development and

economy. Tantalum has been listed as one of the most critical material for India's manufacturing sector by 2030 in a study conducted by think-tank council on Energy, Environment and Water. Tantalum could also be a potential substitute for emerging uses in new mining and nano technology [30].

2. Experimental details

To estimate the activity in the thin layer of various materials, measured cross-section of various reaction products were used. Experiments were carried at Inter University Accelerator Center (IUAC), New Delhi which houses a 15 UD Pelletron accelerator facility. Heavy ions Oxygen beam having charged state of 7^+ obtained from accelerator has been used for sample activation. Terbium, Thullium & Tantalum targets (spectroscopically pure ranging from 95 to 99.99%) were irradiated by oxygen beam. For measurement of cross-sections of various reaction products & further to deduce the activity induced in the form of wear in various materials, activation technique has been employed as it is one of the simplest and powerful method. In this technique, energetic beam of appropriate energy is impinged on stack of targets backed up by Al-catchers of appropriate thickness. Activity induced in the target catcher foil assembly are measured by using off-line Gamma Spectroscopy. Present paper discusses irradiation of three target materials viz; ^{159}Tb , ^{169}Tm & ^{181}Ta with $^{16}\text{O}^{7+}$ in General Purpose Scattering Chamber (GPSC) of 1.5 m diameter, having in-vacuum transfer facility (ITF). By using this facility, time lapse between the stop of the irradiation and counting of the samples may be considerably reduced facilitating recording of induced activities having short half-lives. Total charge collected in the Faraday Cup, placed behind the target catcher foil assembly was used to determine the flux of incident ions. High Purity Germanium (HPGe) detector of 100 c.c. active volume coupled to a PC through CAMAC based FREEDOM software was used to record the activities produced in the samples after irradiation. Errors in these measurements are quite low as it is coupled with high resolution HPGe detectors making it possible to separate out the activities of different reaction products decaying by γ -rays of nearly same energies accurately.

Self supporting targets of ^{159}Tb spectroscopically (99.99% pure) having thickness ≈ 1.7 mg/cm² backed by Al-catchers of thickness ≈ 2 mg/cm² were prepared by rolling method. Targets of ^{169}Tm spectroscopically $\approx 100\%$ having ≈ 0.65 mg/cm² thickness were deposited on Al-backing of 1.5 mg/cm² thickness, using high vacuum-evaporation technique. Tantalum targets of ^{181}Ta of thickness ≈ 1.5 mg/cm² were deposited by eletro deposition technique on Al-backing of thickness ≈ 1 –1.5 mg/cm². In case of ^{159}Tb , two stacks containing four samples each were irradiated at energies 90 & 95 MeV respectively. In case of first stack, the thickness of four Tb samples were $\approx 1.65, 1.68, 1.57$ and 1.62 mg/cm² while corresponding catcher thickness were $\approx 1.71, 1.82, 1.69$ & 1.87 mg/cm² respectively. In case of second stack, the thickness of four Tb samples were $1.67, 1.72, 1.64$ and 1.81 mg/cm² while corresponding catcher thickness were $1.74, 1.86, 1.78$ & 1.94 mg/cm² respectively. The energy range covered in irradiating first stack of terbium was from 90 MeV to 65.5 MeV with intermediate energy points obtained at 83.2 MeV & 75.2 MeV respectively. Energy range covered in irradiating second stack of terbium was from 95 MeV to 69.3 MeV with intermediate energy points obtained at 87.2 MeV & 78.7 MeV respectively. In case of ^{169}Tm , two stacks containing four samples each were irradiated at energies 92 & 95 MeV respectively. In case of first stack thickness of Tm samples were $\approx 0.83, 0.69, 0.57$ and 0.63 mg/cm² while corresponding catcher thickness were $1.42, 1.36, 1.29$ & 1.33 mg/cm² respectively. In case of second stack thickness of Tm samples were $\approx 0.71, 0.69, 0.73$ and 0.64 mg/cm² while corresponding catcher thickness were $1.41, 1.38, 1.47$ & 1.29 respectively. After irradiation energy range covered was from 95 MeV to 71 MeV Further in case of ^{181}Ta , three stacks, with four foils, three foils and one foil respectively, were irradiated at $\approx 100, 98$ & 88 MeV beam energies to

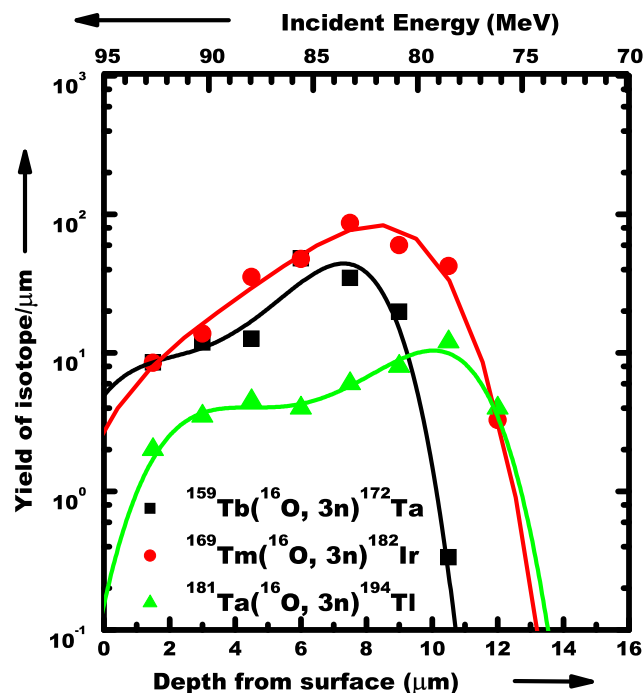


Fig. 1. Relative Yield curves of isotopes ^{172}Ta , ^{182}Ir , ^{194}Tl from Tb, Tm & Ta material.

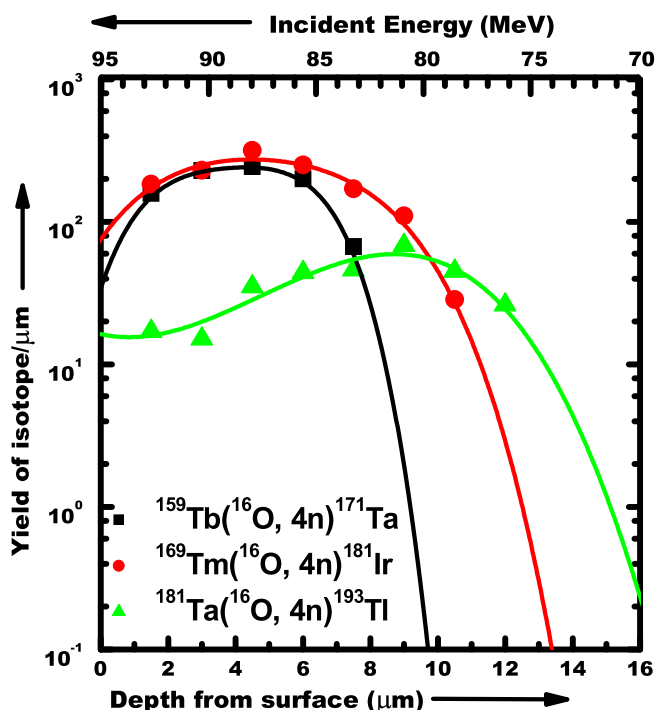


Fig. 2. Relative Yield curve of isotopes ^{171}Ta , ^{181}Ir , ^{193}Tl from Tb, Tm & Ta material.

cover a wide energy range. In the first stack, the thicknesses of four Ta samples were $\approx 1.25, 1.43, 1.42$ and 1.22 mg/cm² while the thicknesses of corresponding Al-catchers were $\approx 1.16, 1.76, 2.01$ and 1.24 mg/cm² respectively. In the second stack, the thicknesses of three Ta samples were $\approx 1.28, 2.03$ and 1.76 mg/cm² while the thicknesses of corresponding Al-catchers were $\approx 1.81, 1.65,$ and 1.47 mg/cm² respectively. However, in the third one containing single foil, the thickness of Ta sample was ≈ 1.22 mg/cm² while the thickness of corresponding Al-catcher was ≈ 1.29 mg/cm². Backing with Al-catchers helped to serve as

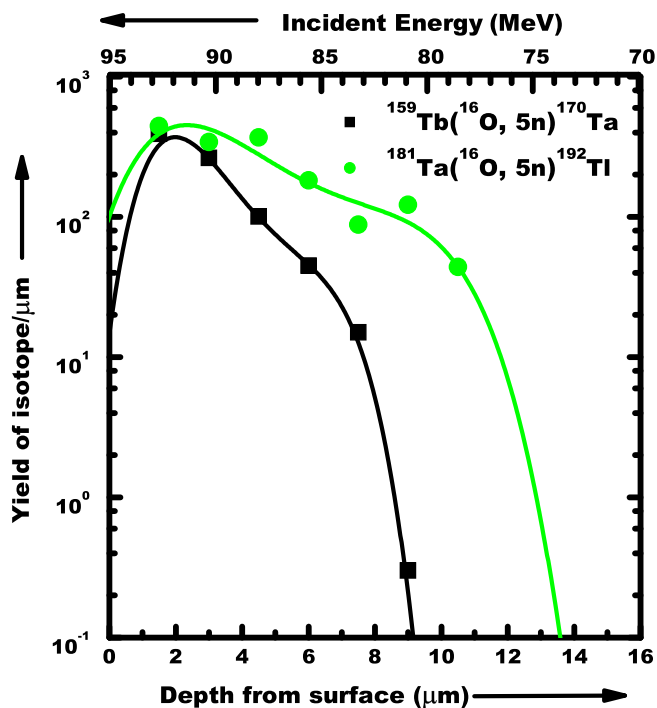


Fig. 3. Relative Yield curves of isotopes ^{170}Ta & ^{194}Tl from Tb & Ta material.

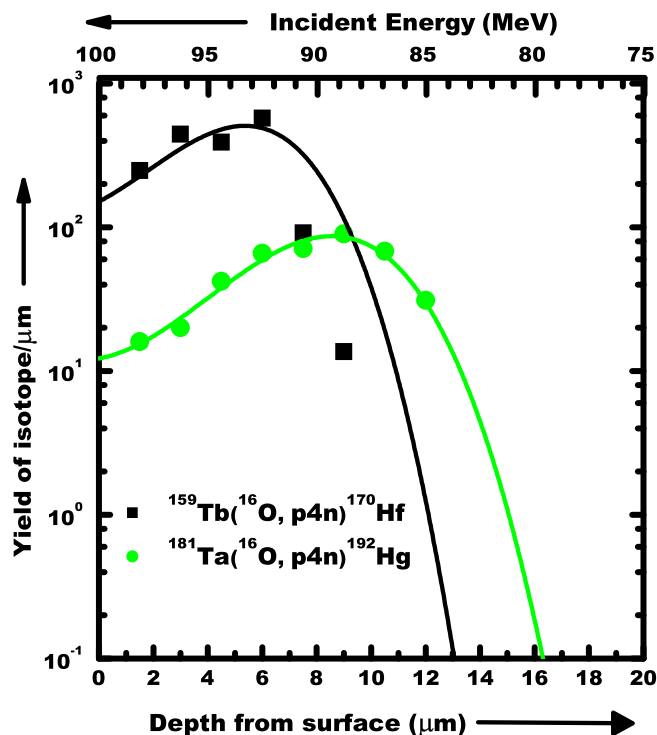


Fig. 5. Relative Yield curves of isotopes ^{170}Hf & ^{192}Hg from Tb & Ta material.

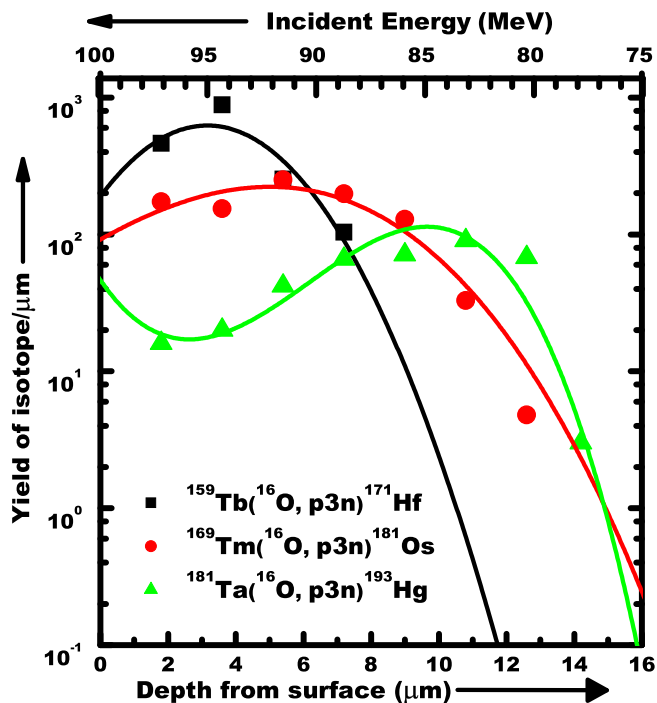


Fig. 4. Relative Yield curves of isotopes ^{171}Hf , ^{181}Os & ^{193}Hg from Tb, Tm & Ta material.

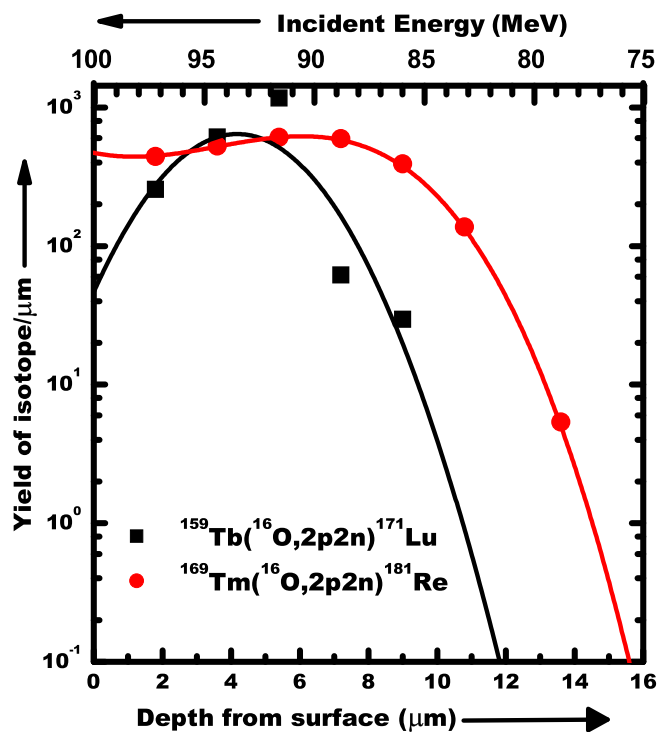


Fig. 6. Relative Yield curves of isotopes ^{171}Lu & ^{181}Re from Tb & Tm material.

both energy degrader as well as catcher for residues recoiling out of target foil during the irradiations. α -transmission method was used to measure the thickness of each target. Measurement of energy lost by 5.487 MeV α -particles obtained from standard ^{241}Am source, while passing through the material of target is used to employ this technique. The targets were cut into the size of $1.2 \times 1.2 \text{ cm}^2$ were pasted on Al-holders having concentric hole of 1.0 cm diameter. Successive targets of the stack get irradiated at different energies. The energies of the incident ion on successive targets have been calculated using stopping

power values obtained from code SRIM based on the range-energy formulations. The stacks were placed normal to the beam direction, so that the recoiling products could be trapped in the catcher foil placed just behind the target and there would be no loss of activity. Beam current varying from ≈ 30 to 50 nA was used and the irradiations were carried out for ≈ 8 – 12 h duration for each stack.

After the irradiation of the materials in different stacks, targets/material samples along with catcher foils was taken out from the GPSC

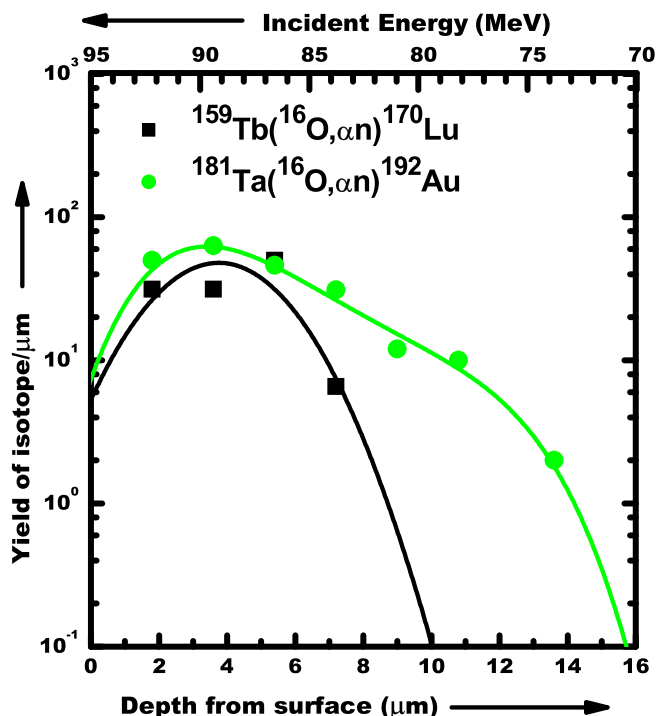


Fig. 7. Relative Yield curves of isotopes ^{170}Lu & ^{192}Au from Tb & Ta material.

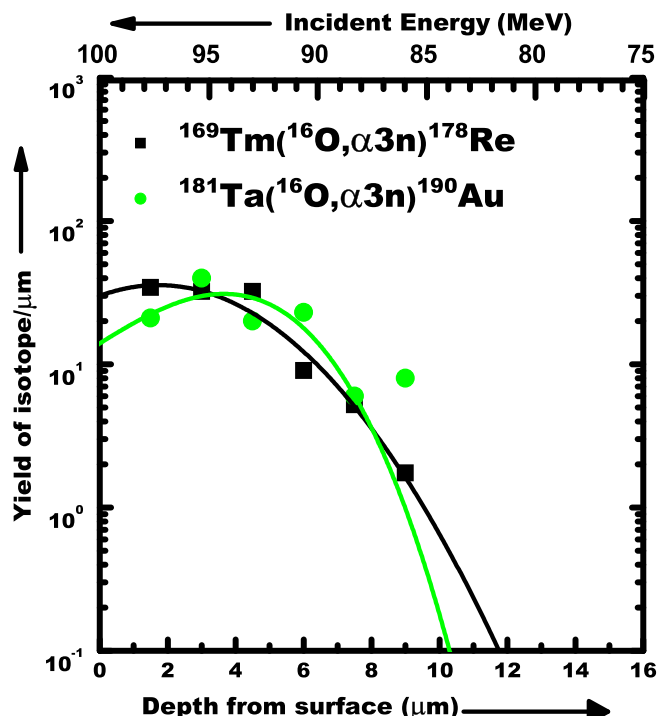


Fig. 9. Relative Yield curves of isotopes ^{178}Re & ^{190}Au from Tm & Ta material.

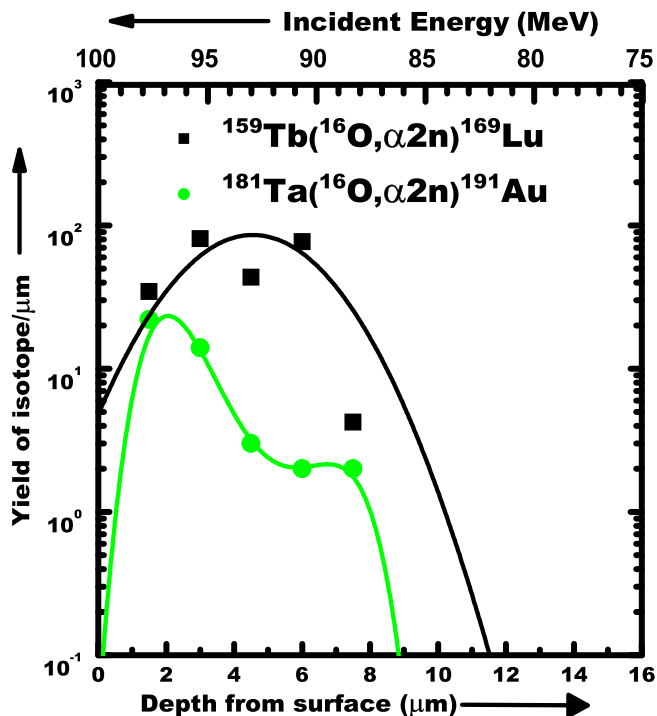


Fig. 8. Relative Yield curves of isotopes ^{169}Lu & ^{192}Au from Tb & Ta material.

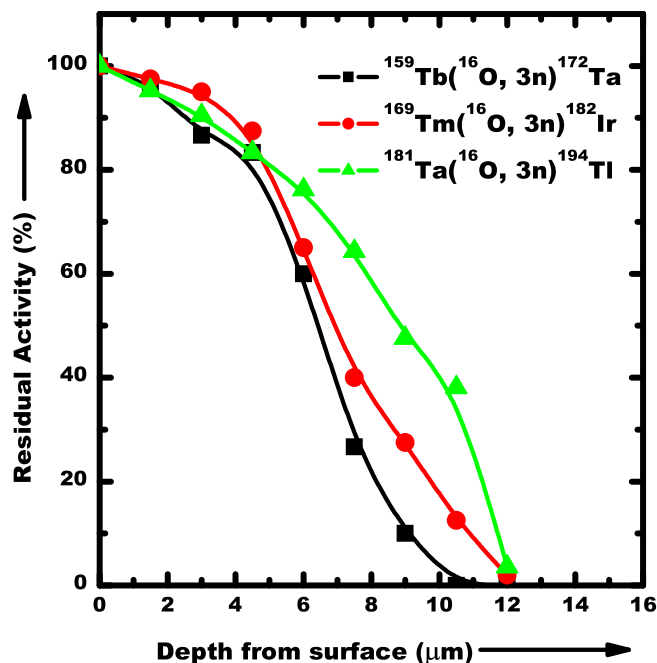


Fig. 10. Calibration curves of isotopes ^{172}Ta , ^{182}Ir , ^{194}Tl from Tb, Tm & Ta materials at incident energies ranging from 95 to 70 MeV.

with the help of ITF. The evaporation residues populated in each target-catcher foil assembly were identified by (characteristic γ -rays). The activities induced in the irradiated samples were recorded using HPGe γ -ray spectrometer. The HPGe detector was pre-calibrated both for energy as well as efficiency by using various standard γ sources i.e., ^{60}Co and ^{152}Eu of known strengths. To obtain the residual activity measured cross sections of various reaction products were plotted at varying energies versus thickness of the target. Residual activity was calculated using remnant activity obtained from measured cross-section versus

varying thickness of the target material. Further details regarding the experiment are given elsewhere [35–37].

3. Measurement & analysis

3.1. Measurement of cross-section and yield curves

The yield curves for various isotopes; $^{172,171,170}\text{Ta}$, $^{171,170}\text{Hf}$, 171,170 , ^{169}Lu populated through different reaction for $^{16}\text{O} + ^{159}\text{Tb}$ and

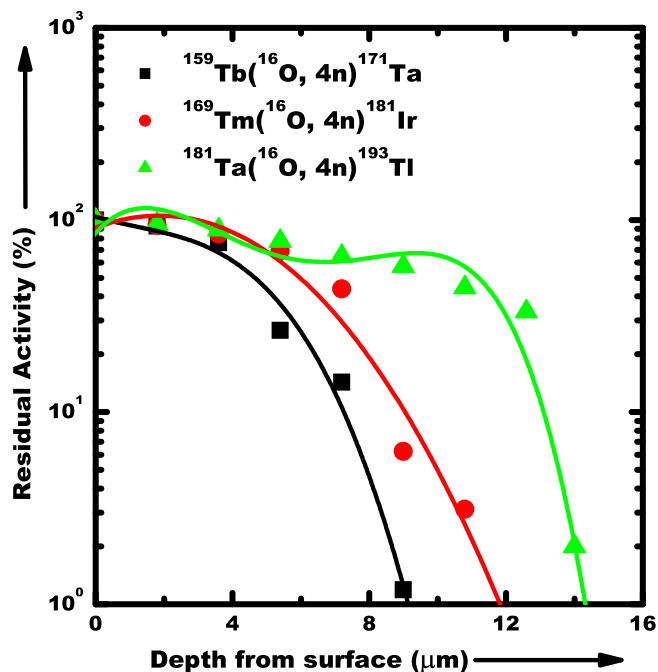


Fig. 11. Calibration curves of isotopes ^{171}Ta , ^{181}Ir , ^{193}Tl from Tb, Tm & Ta materials at incident energies ranging from 95 to 70 MeV.

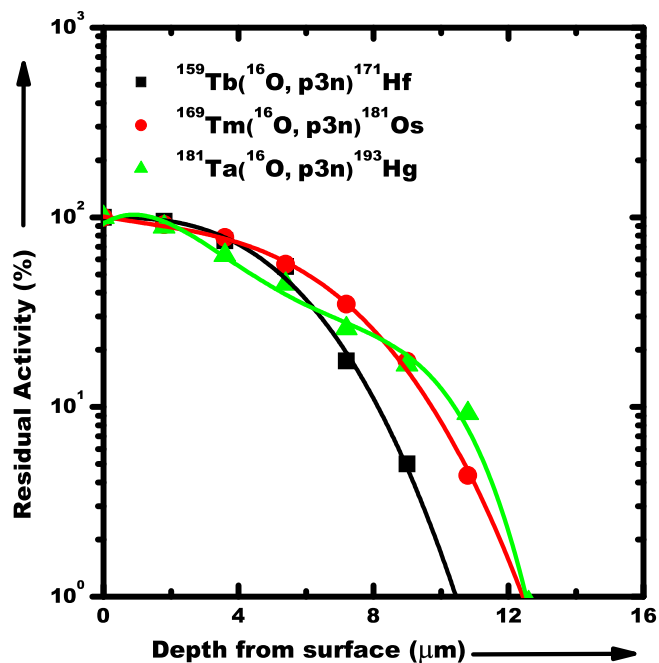


Fig. 13. Calibration curves of isotopes ^{171}Hf , ^{181}Os & ^{193}Hg from Tb, Tm & Ta materials at incident energies ranging from 100 to 65.

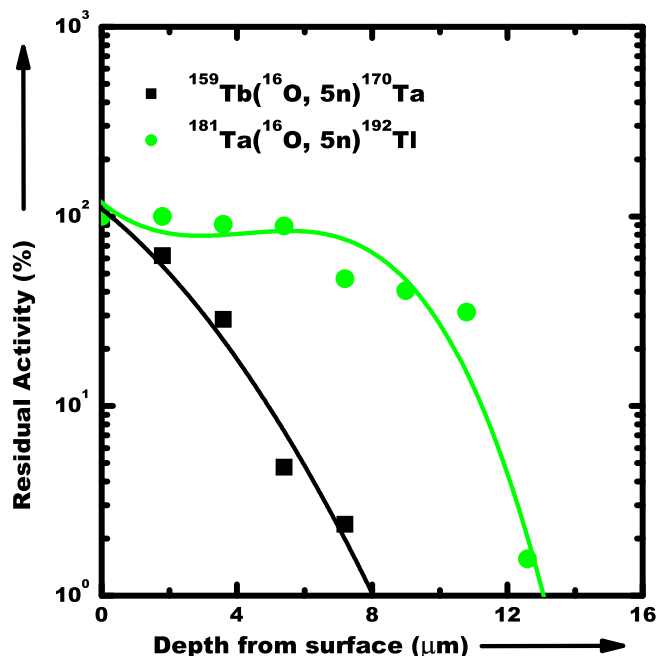


Fig. 12. Calibration curves of isotopes ^{170}Ta & ^{194}Tl from Tb & Ta materials at incident energies ranging from 95 to 65 MeV.

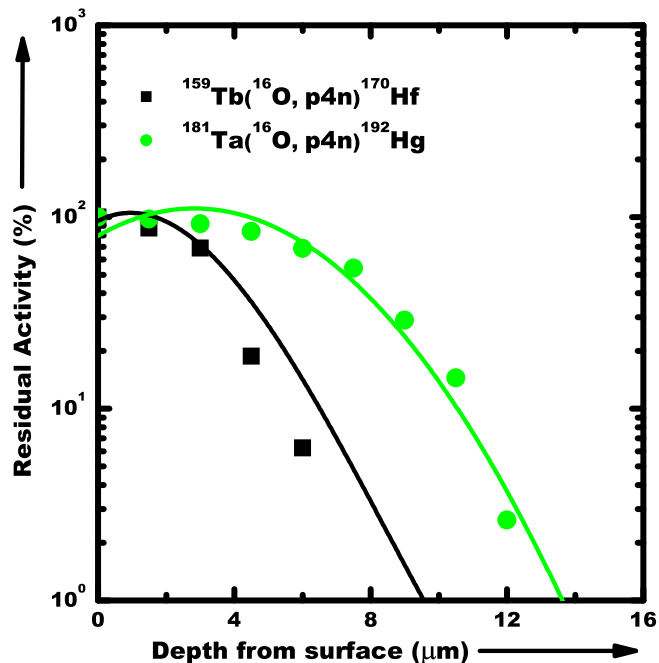


Fig. 14. Calibration curves of isotopes ^{170}Hf & ^{192}Hg from Tb & Ta materials at incident energies ranging from 100 to 65 MeV.

$^{182,181}\text{Ir}$, ^{181}Os , ^{181}Re for $^{16}\text{O} + ^{169}\text{Tm}$ and 194,193 , ^{192}Tl , $^{193,192}\text{Hg}$, 192,191 , ^{190}Au for $^{16}\text{O} + ^{181}\text{Ta}$ material have been obtained at different energies and different depths of target materials. The stopping power of different materials have been used to obtain the incident energy on each material sample in the respective stack. Area under the yield curves across different energies ranging from 70–110 MeV was integrated to obtain the residual curves for all three systems. The yield per micron thickness against the depth as well as incident energy for several isotopes are shown in Figs. 1–9. For convenience, we have

plotted the xn, pxn & α xn channels for different systems for comparative analysis. In Figs. 1–3, xn channels (where $n = 3, 4, 5$) for all the three systems have been plotted. The activity induced in xn channels for terbium is ranging from 8–12 μm ; 13–14 μm for thulium and 14–16 μm for tantalum respectively. In case of pxn channels activity induced in terbium is up to 14 μm ; 16 μm for both thulium and tantalum shown in Figs. 4 and 5. For α xn channels (where $x = 1, 2, 3$) activity induced for terbium ranging from 8 to 12 μm ; 9–16 μm for tantalum as shown in Figs. 6–9. In the present work, residual activity of various reaction

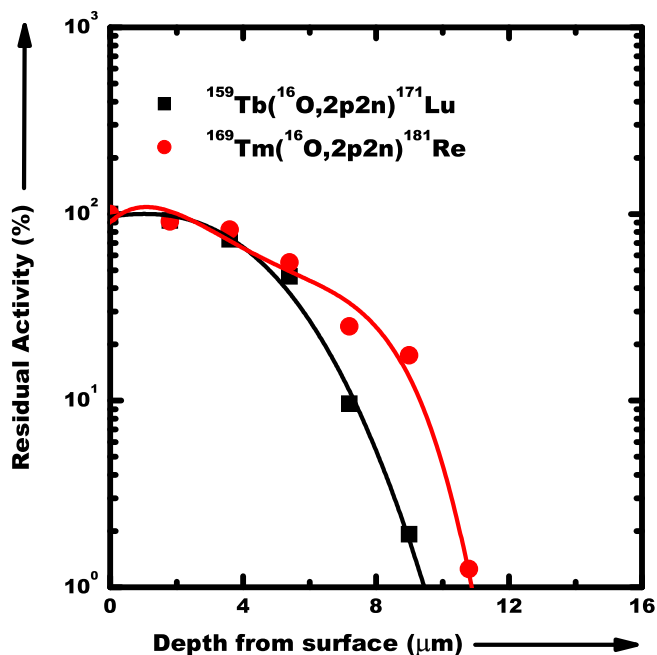


Fig. 15. Calibration curves of isotopes ^{171}Lu & ^{181}Re from Tb & Tm materials at incident energies ranging from 95 to 65 MeV.

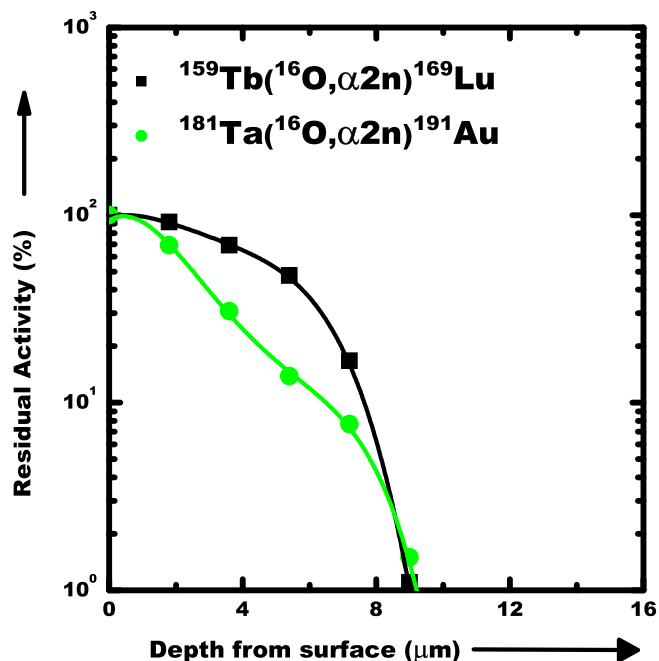


Fig. 17. Calibration curves of isotopes ^{169}Lu & ^{192}Au from Tb & Ta materials at incident energies ranging from 100 to 65 MeV.

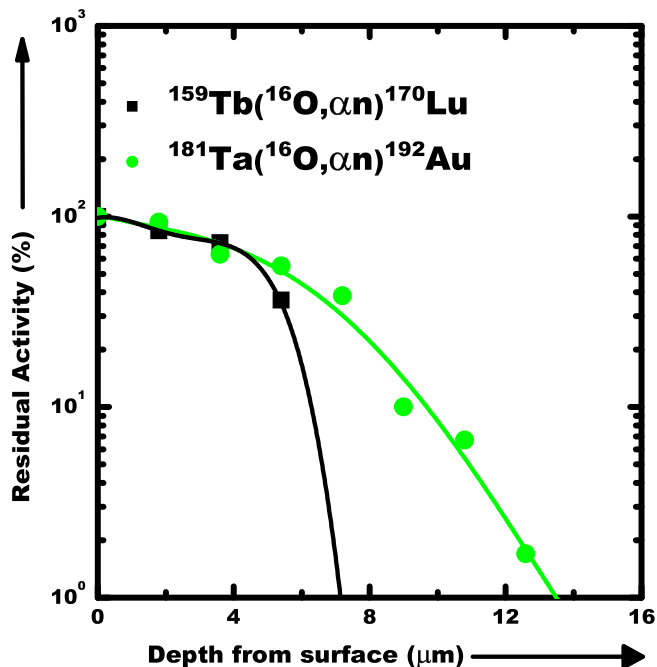


Fig. 16. Calibration curves of isotopes ^{170}Lu & ^{192}Au from Tb & Ta materials at incident energies ranging from 100 to 65 MeV.

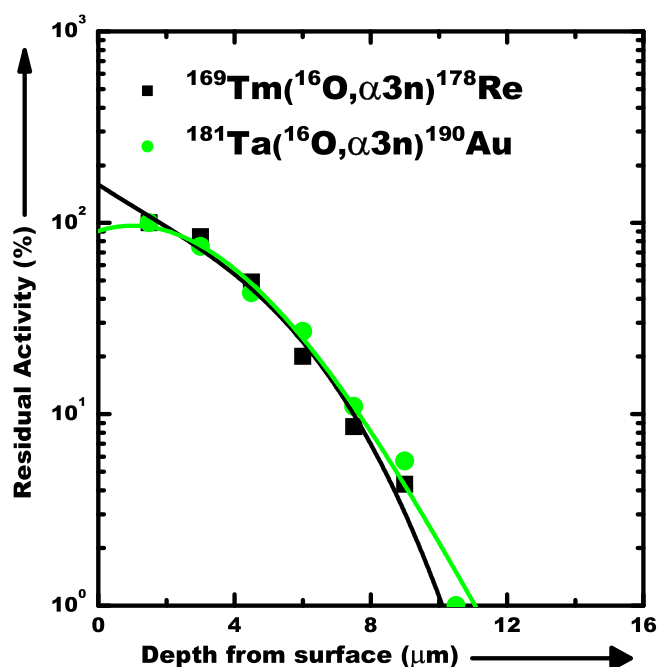


Fig. 18. Calibration curves of isotopes ^{178}Re & ^{190}Au from Tm & Ta materials at incident energies ranging from 100 to 70 MeV.

products populated via various channels were found to have contribution ranging from ≈ 8 to $16 \mu\text{m}$ depth from the surface.

3.2. Calibration curves

Yield curves have been further used to deduce the calibration curves. The residual activities induced, $^{172,171,170}\text{Tm}$, $^{171,170}\text{Hf}$, $^{171,170,169}\text{Lu}$ have been plotted for Terbium and $^{182,181}\text{Ir}$, ^{181}Os , ^{181}Re for Thulium and $^{194,193,192}\text{Tl}$, $^{193,192}\text{Hg}$, $^{192,191,190}\text{Au}$ for Tantalum material after removal of certain depths of material, have been calculated graphically with the help of obtained yield curves. The calibration

curves thus obtained using reaction products, from the plot of percentage of remaining activity against the removal of depth of material are shown in Figs. 10–18.

As indicated in Figs. 1–9, the total yield of the isotope in the given material may be obtained from the integral area under the yield curves. After the removal of certain depth of material (decreasing the thickness corresponding to the each foil of the stack one by one) the percentage of the remaining activity is computed graphically and the calibration curves so deduced from the yield curves are shown in Figs. 10–18. As a matter of fact, these calibration curves may be considered to correspond to pure metals bombarded with 110 MeV ^{16}O heavy ions normal to the

beam direction. It may also be noticed from (Figs. 10–18) that the rate of change of activity per unit thickness is more for the higher slope curve i.e., the errors associated in higher slope curve will be less. The overall error has been estimated from the errors of cross-section in generating the calibration curves and the activity measurement of the irradiated samples and has been found $\leq 15\%$.

4. Conclusion

An attempt has been made to explore the TLA technique for various rare earth materials viz; Terbium, Thulium & Tantalum. With the help of cross section and varying energies, yield of different materials have been determined. Further, these yield curves have been used to deduce the calibration curves by plotting remnant activity versus thickness of the target material. A systematic has been observed that with increase in mass of target, activity induced also increases. The cross section generated data may be utilised for various applications of selected materials as discussed earlier. The maximum activity has been induced in case of xn & pxn channels for all materials ranging 12–16 microns, while in case of α xn channels, for all materials, it has been observed ranging from 8–13 μm . On the basis of analysis, it has been observed that maximum activity induced is found in Tantalum material up to 16 μm , while in Thulium Terbium it has been found 14 μm & 13 μm respectively when bombarded by the oxygen ion in almost same energy region.

Acknowledgments

The authors are thankful to the Director of IUAC, New, Delhi, India, for providing facilities to carry out the experiments. D. P. Singh thanks to SERB-DST for providing financial support through Project No. ECR/2017/000641 under the early Career Research Award. Support from University of Petroleum & Energy Studies (UPES), Dehradun for conducting this work is gratefully acknowledged.

References

- [1] Vikas Chawla, et al., *J. Miner. Mater. Characteriz. Eng.* 10 (4) (2011) 367–385.
- [2] A.S. Khanna, Introduction to high temperature oxidation and corrosion, ASM International, pp 1–322, ISBN 0-87170-762-4, SAN: 204-7586, 2002.
- [3] P.V. Ananthapadmanabhan, et al., *Surf. Coat. Technol.* 49 (1991) 62–66.
- [4] John Stringer et al.: Proceedings International conference on corrosion 'CONCORN', December 3–6, Mumbai, India, pp 13–23, 1997.
- [5] Kevin J. Stein, et al., *Wear* 224 (1999) 153–159.
- [6] Aziah North, et al., *IEEE Underwater Technol. (UT)* 1874 (1861) 2019.
- [7] Tomarov, et al., *Therm. Eng.* 66 (2) (2019) 138–147 ISSN 0040-6015.
- [8] Dwivedi et al.: *Materials Today: Proceedings* 5, 3690–3698.
- [9] Report on NDT; ndt.net, 7th European Conference on Non-destructive Testing, 2018.
- [10] Daniyal, et al., *J. Build. Pathol. Rehabil.* 5 (2020) 1.
- [11] Zikai Hua, et al., *Wear Test Apparatus for Friction and Wear Evaluation Hip Prostheses* (2019), <https://doi.org/10.3389/fmech.2019.00012>.
- [12] Green, et al., *Part H: Journal of Engineering in Medicine* 229 (3) (2015) 245–254, <https://doi.org/10.1177/0954411915577119>.
- [13] Anke Turger, et al., *BioMed. Eng. OnLine* 12 (2013) 84.
- [14] Imam Kambali, et al., *J. Eng. Technol. Sci.* 48 (4) (2016) 482–494.
- [15] IAEA report on The thin layer activation method and its applications in industry.
- [16] Devendra P. Singh, et al., *J. Nucl. Phys., Mater. Sci., Radiat. Appl. (JNPMSRA 1)* (2013) 13–24.
- [17] Syed M. Qaim, et al., *Radiochim. Acta* 104 (9) (2016) 601–624.
- [18] D.P. Chowdhury et al.: *Radiochim. Acta* 100, 139–145 (2012)/ract. (2011).1889.
- [19] Jayashree Biswal, et al., *Nucl. Instrum. Methods Phys. Res. B* 399 (2017) 69–73.
- [20] R. Verma et al., BARC Report External BARC/2016/E/004.
- [21] D.P. Chowdhury, et al., *Nucl. Instr. Meth. Phys. Res. B* 211 (2003) 288–296.
- [22] G. Dearnaley, et al., *Surf. Coatings Technol.* 201 (2007) 8070–8075.
- [23] E. Corniani, et al., *Wear* 267 (2009) 828–832.
- [24] F. Ditroi, et al., *Nucl. Instrum. Methods Phys. Res. B* 290 (2012) 30–38.
- [25] M. Cioffi, et al., *Acta Biomater.* 1 (2015) 717–724.
- [26] F. Tarkanyi, et al., *Nucl. Instrum. Methods Phys. Res. B* 226 (2004) 473–489.
- [27] F. Ditroi, et al., *Nucl. Instrum. Methods Phys. Res. B* 373 (2016) 17–27.
- [28] F. Ditroi, et al., *Nucl. Instrum. Methods Phys. Res. B* 269 (2011) 1963–1972.
- [29] F. Tarkanyi, et al., *Nucl. Instrum. Methods Phys. Res. B* 252 (2006) 160–174.
- [30] Kirti Kumar et al; *Mineral Economics*; 10.1007/s13563-019-00189-0 (2019).
- [31] Terbium. Chemicool Periodic Table. Chemicool.com. 2012. Web. 3/2/2019.
- [32] Thulium. Chemicool Periodic Table. Chemicool.com. 2015. Web. 3/2/2019.
- [33] Tantalum. Chemicool Periodic Table. Chemicool.com. 2012. Web. 3/2/2019.
- [34] Chad E. Duty et al.: Proceedings of the Space Nuclear Conference, Paper 1183 (2005).
- [35] Devendra P. Singh, et al., *Phys. Rev. C* 80 (2009) 014601.
- [36] Manoj Kumar Sharma, et al., *Phys. Rev. C* 70 (2004) 044606.
- [37] Manoj Kumar Sharma et al., *Nucl. Phys. A* 776 (2006) 83–104.



Experimental Investigations of Alpha Particle Irradiation of Natural Nickel

Varun V Savadi^a, D P Singh^{a*}, S K Joshi^a, A Yadav^b, P P Singh^c, M K Sharma^d, Unnati^e, M M Mustafa^f, B P Singh^g & R. Prasad^g

^aDepartment of Physics, University of Petroleum & Energy Studies, Dehradun-248 007, India

^bDepartment of Physics, Jamia Milia Islamia, New Delhi -110 025, India

^cDepartment of Physics, IIT, Ropar, Rup Nagar, Punjab-140 001, India

^dDepartment of Physics, S V College, Aligarh-202 001, India

^eDepartment of Physics, University of Delhi, New Delhi -110 067, India

^fDepartment of Physics, University of Calicut, Thenjipalam, Kerala-673 635, India

^gDepartment of Physics, Aligarh Muslim University, Aligarh (UP)-202 002, India

Received 8 July 2020; accepted 25 March 2021

Attempts have been made to measure the activity in irradiated natural Ni material induced by α -particles in the energy range 10-40 MeV followed by stack foil activation technique. Activity induced has been determined through the cross-sections obtained from various reactions for $^{58}\text{Ni}(\alpha, p)^{61}\text{Cu}$, $^{58}\text{Ni}(\alpha, pn)^{60}\text{Cu}$, $^{60}\text{Ni}(\alpha, p2n)^{61}\text{Cu}$, $^{60}\text{Ni}(\alpha, n)^{63}\text{Zn}$, $^{60}\text{Ni}(\alpha, 2n)^{62}\text{Zn}$, $^{61}\text{Ni}(\alpha, 3n)^{62}\text{Zn}$ and $^{61}\text{Ni}(\alpha, 2n)^{63}\text{Zn}$ in $\alpha^{+nat}\text{Ni}$ interaction at different beam energies has been found to vary from 10-26 microns.

Keywords: nickel & nickel alloys; gamma spectroscopy; stack foil activation; yield; cross-section measurements; beam of alpha particles.

1 Introduction

Over a couple of decades there has been a growing concern to investigate the potential damage induced due to erosion in machinery and other related equipment in processing industries¹⁻³. Surface degradation phenomenon such as wear, erosion, corrosion *etc.* are inevitable processes influencing industrial performance and efficiency. The functionality of materials, used in power generation plants and other processing industries with increased efficiency, is a field of current interest to meet the global energy demands¹⁻⁵. Machinery, equipment and components utilised in various industries like; oil & gas, power plants and others are often subjected to slurry erosion leading to wear of materials pose a critical issue on performance, dependability and service life of components. Wear induced due to material erosion is often coupled with capital expenses and accountable for overall performance and service life of the industry²⁻⁶. The process of wear influencing corrosion & vice versa is highly interdependent and could lead to catastrophic & economic losses in modern types of machineries used in marine applications, chemical plants *etc.* often subjected to tribo-chemical interactions⁷. Selection of appropriate materials and various techniques leading to increased

efficiency and service life of the industry components is a matter of concern in near future. A noble method of coating technique popularized as the “Electro-less Coating” was developed with its widespread applications across every domain of industry⁸. Over a last couple of decades, interestingly nickel based alloys and coatings have evolved mature subject of research and development from tribological applications point of view due to excellent anti wear & corrosion resistant properties⁹⁻¹⁴. Further, various non-destructive techniques available till date are used for measuring the surface defects and phenomenon like corrosion & erosion but are having their own limitations of testing¹⁵⁻¹⁶. Charged particle activation analysis is a nuclear non-destructive tool in which, a beam of appropriate energy is made to impinge on a very thin layer of material surface by light & heavy ions. Further total cross-sections obtained for various reaction products after employing stack foil activation at varying depths is used for estimation of surface wear in materials. In charged particle activation, very thin layer of surface is activated for measurements and is mostly preferred over conventional techniques due to its high precision and accuracy with recent advancement in accelerator technology¹⁷⁻²⁰. Studies performed with help of stack foil activation have been of great use in determining surface wear induced in many components which can be measured simultaneously while being in

situ-operations with precision ranging from micrometers to nanometres¹⁷⁻²⁰. Recent boost in accelerator technology has now made it possible to measure surface degradation on desired surface of component by using appropriate charged particles either by using stack foil activation followed by offline γ -spectroscopy or by indirect measurement method²¹⁻²³. Several such studies have been carried out on many materials & alloys such as nickel titanium, platinum, rhodium niobium & copper *etc* applicable in large number of industries²⁴⁻³⁶. In the present work, stack foil activation is employed in natural nickel material to estimate the activity induced. Analysis of the amount of activity induced has been determined through the cross-sections obtained from various reaction channels with energy ranging from 10-40 MeV. It has been observed that the activity induced in Ni is found to vary from 10-26 microns³⁷⁻³⁸. Different reaction residues obtained from various α -channels in current experiment have very good half-lives and total cross-section values which can further be explored for research and industrial applications.

2 Experiment Details

To measure the cross-sections of various reaction products in α +^{nat}Ni interactions at \approx 10–40 MeV³⁹ and subsequently used to study the amount of residual activity induced in natural Ni materials, experiments were performed at the Variable Energy Cyclotron Centre (VECC), Kolkata, India. For irradiation, natural nickel targets were prepared by rolling technique. A stack consisting of 8 target foils made up of ^{nat}Ni material each backed by aluminium catcher of appropriate thickness obtained by energy loss calculation from SRIM/TRIM was impinged by a 40 MeV α -beam. The approximate thickness of ^{nat}Ni foils were 1.13, 1.8, 1.15, 0.9, 1.33, 1.19, 1.05 & 1.63 mg/cm² respectively each backed by aluminium catcher of approximate thickness of 1.3, 2.8, 1.47, 1.18, 1.41, 1.22, 1.24 & 2.23 mg/cm². The total irradiation time was \approx 12 h with a beam current \approx 100 nA. The average beam energy on a given target foil and degrader was calculated by using the code SRIM based on stopping power and range calculations. A pre-calibrated HPGe detectors coupled with multi-channel analyzer system has been used for post irradiation analysis. The overall error has been estimated from the errors of cross-section in generating the calibration curves and the activity measurement of the irradiated samples and has been found \leq 15%. Statistical errors has been deduced and

fitted with a fourth-order polynomial function, where the uncertainty from the fitting is found to be \approx 3% for the energy range of interest. Errors introduced due to solid angle defect is found to be less than \leq 2% as demonstrated by Gardener *et al.*⁴⁰. The human errors introduced due to non-uniformity and inaccurate determination of foil thickness at various positions has been found to be \approx 1%. The errors from the fluctuations in the beam current were found to be \approx 3%. Errors introduced due to attenuation in beam current while traversing through thickness of foil has been found to be \leq 2%⁴¹.

3. Measurement & Analysis

To measure the range/depth of activity induced in Ni material, the cross-sections for ⁵⁸Ni(α , p)⁶¹Cu, ⁵⁸Ni(α , pn)⁶⁰Cu, ⁶⁰Ni(α , p2n)⁶¹Cu, ⁶⁰Ni(α , n)⁶³Zn, ⁶⁰Ni(α , 2n)⁶²Zn, ⁶¹Ni(α , 3n)⁶²Zn and ⁶¹Ni(α , 2n)⁶³Zn reactions have been measured by using the activation technique followed by off-line γ spectroscopy³⁹.

3.1. Measurement of Yield Curves:

The yield curves for various isotopes; ^{61,60}Cu & ^{63,62}Zn populated through different reaction for ^{58, 60, 61 nat}Ni material with α beam have been obtained at different energies and different depths. The stopping power of different materials has been used to obtain the incident energies on different samples. Area under the yield curves across different energies ranging from 10-40 MeV was integrated to obtain the residual curves. The yield per micron thickness against the depth as well as incident energy for residual isotopes viz; ^{61,60}Cu, ⁶³Zn & ⁶²Zn is shown in Figs. 1-3(a). For proper polynomial fit of the experimental data, theoretical cross-section values (obtained from PACE 4) have been included below 25 MeV for reactions [⁵⁸Ni(α , pn); ⁶⁰Ni(α , p2n); ⁶⁰Ni(α , n); ⁶⁰Ni(α , 2n); ⁶¹Ni(α , 3n); ⁶¹Ni(α , 2n)]. Total cross section values mentioned in Table 1 have been used for obtaining yield curves.

3.2. Calibration curves:

Plot for amount of residual activity induced in ^{58, 60, 61 nat}Ni material has been deduced with the help of total cross-section measured values from yield curves. The residual activity induced through α beams with energy range 10-40 MeV in ⁵⁸Ni(α , P)⁶¹Cu; ⁵⁸Ni(α , Pn)⁶⁰Cu; ⁶⁰Ni(α , n)⁶³Zn; ⁶⁰Ni(α , 2n)⁶³Zn; ⁶¹Ni(α , 2n)⁶³Zn & ⁶¹Ni(α , 3n)⁶²Zn has been shown in Figs.1-3(b). The total yield of the isotope in the given material may be obtained from the integral area under the yield curves. The percentage of remaining activity is computed graphically using polynomial fit by decreasing the

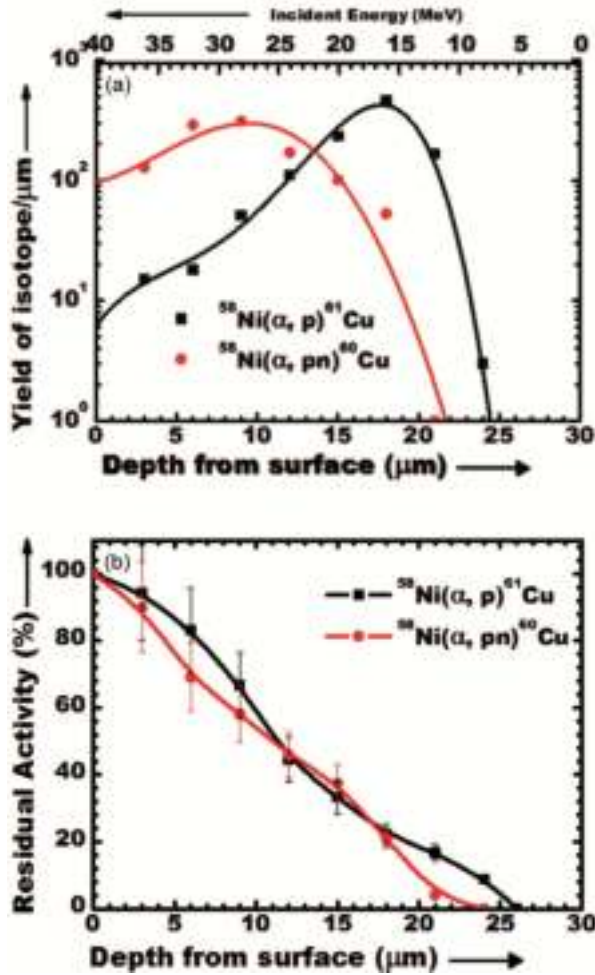


Fig. 1(a-b)—Relative Yield curves for ^{58nat}Ni Material; b—Calibration curves for ^{58nat}Ni at incident energies ranging from 10-40 MeV

thickness corresponding to each foil of stack one by one as shown in Figs. 1-3(b). It has been observed that the activity induced in Ni is ranging upto ≈ 26μm.

Measurement of cross-sections and residual activity induced are expressed in Eqs 1-4. Total thickness of ^{nat}Ni material is assumed to be x_t mg/cm² irradiated by α beam having 90° angle of incidence, then activity induced in total thickness of material where, $x_i(i=1, 2, \dots, 8)$ (mg/cm²) is given by Eqⁿ (1).

$$x_t = x_1 + x_2 + \dots x_n = \sum_{i=1}^n x_i \quad \dots (1)$$

It is obvious that as the beam traverse across the thickness x_1 to x_n , it continuously keeps on losing energy as a result of which total cross-section obtained will vary according to the beam energy and thickness which is stated in Eqⁿ (2.1).

$$A_n = NI\sigma_1x_1S + NI\sigma_2x_2S + \dots NI\sigma_nx_nS \quad \dots (2.1)$$

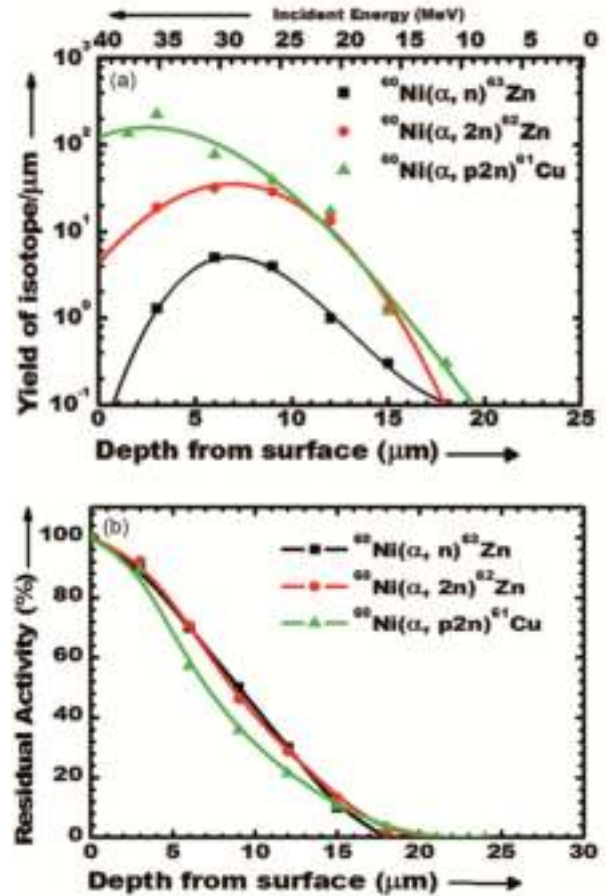


Fig. 2(a-b) — Relative Yield curves for ^{60nat}Ni Material; b—Calibration curves for ^{58nat}Ni at incident energies ranging from 10-40 MeV

Further Eqⁿ (2.1) is reduced to Eqⁿ (2.2) when the cross-sections obtained across the varying thickness remains almost constant.

$$= NIS \sum_{i=1}^n \sigma_i x_i \quad \dots (2.2)$$

Amount of activity induced is directly dependent on the total cross-section values obtained across different beam energy and varying thickness in a given stack of metallic foil. In case of remnant activity measurement has to be carried for a particular thickness x_1 as compared to total thickness x_n , it can be expressed with Eqⁿ (3) in which ratio A_{n-1}/A_n is independent of N, I and t_i for a particular isotope.

$$\frac{A_{n-1}}{A_n} = \frac{\sum_{i=2}^n \sigma_i x_i}{\sum_{i=1}^n \sigma_i x_i} \quad \dots (3)$$

Further if the cross-section values obtained remains constant through the entire thickness x_t of the material, then eqⁿ (3) can be further deduced and expressed by eqⁿ(4) in which activity produced is simply proportional to the depth.

Table I — Spectroscopic properties of isotopes $^{60,61}\text{Cu}$ & $^{62,63}\text{Zn}$ used in Stack Foil Activation technique.

Reaction	Residue	Half-life	γ -ray energies (keV)	Natural abundance (%)	Total Cross-Section (mb)
$^{58}\text{Ni}(\alpha, p)$	^{61}Cu	3.33 h	283.0, 656.0	68.007	1453
$^{58}\text{Ni}(\alpha, pn)$	^{60}Cu	23.7 min	826.3, 1332.5	68.007	897.1
$^{60}\text{Ni}(\alpha, p2n)$	^{61}Cu	3.33 h	283.0, 656.0	26.223	301
$^{60}\text{Ni}(\alpha, n)$	^{63}Zn	38.47 min	669.86, 926.27	26.223	30.2
$^{60}\text{Ni}(\alpha, 2n)$	^{62}Zn	9.186 h	548.4, 596.7	26.223	92.4
$^{61}\text{Ni}(\alpha, 3n)$	^{62}Zn	9.186 h	548.4, 596.7	1.140	13.5
$^{61}\text{Ni}(\alpha, 2n)$	^{63}Zn	38.47 min	669.86, 926.27	1.140	406

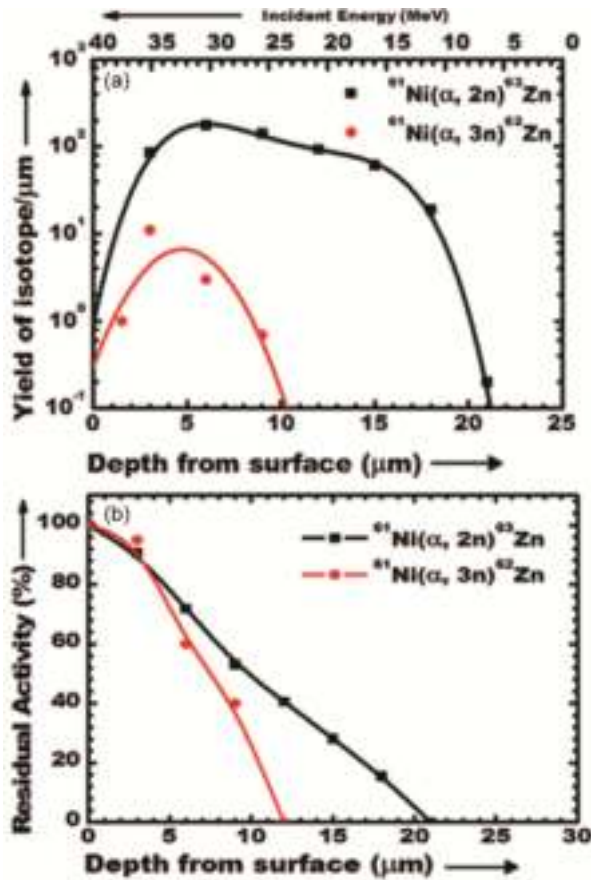


Fig. 3a-b — Relative Yield curves for $^{60}\text{natNi}$ Material; b-Calibration curves for $^{58}\text{natNi}$ at incident energies ranging from 10-40 MeV

$$\frac{A_{n-1}}{A_n} = \frac{\sum_{i=2}^n x_i}{\sum_{i=1}^n x_i} = \frac{\sum_{i=2}^n x_i}{x_t} \quad \dots (4)$$

However with the change in cross-section values across the thickness of stack foil activated metallic sample calibration curves are obtained in accordance with Eqⁿ(3).

4 Conclusion

As Nickel has significant importance in terms of applications across various critical industries in the form of coatings & alloys, in the present work stack

foil activation technique had been explored employing α beam with energy ranging from 10-40 MeV in $^{\text{nat}}\text{Ni}$ targets. As shown in Figs. 1-3(b) the maximum residual activity induced is found to be 26 μm from the depth of the surface. As $^{61,60}\text{Cu}$ are populated through (α, p) & (α, pn) reactions while irradiating the same $^{\text{nat}}^{58}\text{Ni}$ target, the activity induced in ^{60}Cu via (α, pn) reaction is observed to be less by 3 μm i.e nearly 23 μm as compared to that of ^{61}Cu obtained through (α, p) reaction. The least amount of activity induced is found to be 21 μm in case of ^{63}Zn populated through $\alpha, 2n$ reaction on $^{\text{nat}}^{61}\text{Ni}$ target. ^{62}Zn populated through two different reactions with $^{\text{nat}}\text{Ni}$ targets i.e. $\alpha, 2n$ & $\alpha, 3n$ via ^{60}Ni & ^{61}Ni target materials is having activity contribution ranging \approx 12-20 μm . In the present study activity induced through all possible reactions in $^{\text{nat}}\text{Ni}$ material has been reported. As ^{62}Zn has comparatively longer half-life of nearly 10hrs, the experimental data obtained can be used further as a future scope employing TLA for investigating surface wear and erosion phenomena at earlier stages in critically important industries like nuclear plants, power plants & other process industries applications where small failure would lead to catastrophic effects.

Acknowledgements

The authors are thankful to the Director, VECC, Kolkata, India, for providing facilities to carry out the experiments. D. P. Singh thanks to SERB-DST for providing financial support through Project No. ECR/2017/000641 under the early Career Research Award. Support from University of Petroleum & Energy Studies (UPES), Dehradun for conducting this work is gratefully acknowledged.

References

- 1 Davis J R, Surface Engineering for Corrosion and Wear Resistance, (Materials Park OH), *ASM Int*, (2011) 54.
- 2 Tarjan I & Debreczeni E, Theoretical and experimental investigation on the wear of pipeline caused by hydraulic transport 2nd International conference on Hydraulic Transport of Solids in Pipes, *BHRA*, (1972).

- 3 Bain A G & Bonnington S T, Interview—slurry pipelines: exciting technology entering period of renaissance accepted The Hydraulic Transport of Solids by Pipeline, (Pergamon: Oxford), (1970).
- 4 Charles M E, Transport of solid by pipelines, Proc Hydrotransport-I BHRA Proc Hydrotransport-I, (1979).
- 5 Tan Y, Zhang H, Dongmin Y, Jiang S, Song J & Sheng Y, *Tribol Int*, 46 (2012) 137.
- 6 Gupta R, Singh S N & Seshadri V, Basics in Minerals Processing Accelerated wear rate test rig for the predicting of erosion in slurry pipelines 19th NCFMFP, IIT Bombay, (1992) C1.1.
- 7 Lee C K, *Surf Coat Technol*, 202 (2008) 4868.
- 8 Sahoo P & Das S K, *Mater Des*, 32 (2011) 1760.
- 9 Balaraju J N & Rajam K S, *Surf Coat Technol*, 195 (2005) 154.
- 10 Huang L, Gao Y, Zheng Z J & Li H, *Gongneng Cailiao*, 38 (2007) 683.
- 11 He S Z, Huang X M, Zheng H M, Li P, Lin Z P, Shan C L & Mocaxue X, 29 (2009) 362.
- 12 Shaffer S J & Rogers M J, *Wear*, 263 (2007) 1281.
- 13 Klingenberg M L, Brooman E W & Naguy T, *Plat Surf Finish*, 92 (2005) 42.
- 14 Zou Y, Cheng Y, Cheng L & Liu W, *Mater Trans*, 51 (2010) 277.
- 15 Report on NDT; ndt.net, 7th European Conference on Non-destructive Testing.
- 16 Daniyal Md & Akhtar Sabih, *J Build Pathol Rehabilitat*, 5 (2019) 1.
- 17 Imam K & Hari S, *J Eng Technol Sci*, 48 (2016) 482.
- 18 IAEA report on The thin layer activation method and its applications in industry.
- 19 Singh D P, Sharma V R, Yadav A, Singh P P, Sharma U M K, Bhardwaj H D, Singh B P & Prasad R, *J Nucl Phys, Material Sciences, Radiation and Applications*, (2013) 13.
- 20 Qaim S M, Spahn I, Scholten B & Neumaier B, *Radiochim Acta*, 104 (2016) 601.
- 21 Chowdhury D P, Datta J & Reddy A V R, *Radiochim Acta*, 99 (2011) 1.
- 22 Biswal J, Thakre G D, Pant H J, Samantray J S, Arya P K, Sharma S C & Gupta A K, *Nucl Instr Meth Phys Res B*, 399 (2017) 69.
- 23 Verma R, Swain K K, Remya D P S, Dalvi A A, Nicy A, Ghosh M, Chowdhury D P, Datta J & Dasgupta S, BARC Report External BARC/2016/E/004.
- 24 Chowdhury D P, *Nucl Instr Meth Phys Res B*, 211 (2003) 288.
- 25 Dearnaley G, Asher J, Peacock A T, Allen S J & Watkins R E J, *Surf Coat Technol*, 201 (2007) 8070.
- 26 Corniani E, Jech M, Ditroi F, Wopelka T & Franek F, *Wear*, 267 (2009) 828.
- 27 Tarkanyi F, Ditroi F, Hermanne A, Takacs S & Ignatyuk A V, *Nucl Instr Meth Phys Res B*, 280 (2012) 45.
- 28 Gilliland C M, Ceccone D G & Cigada C R A, *Acta Biomater*, 1 (2005) 717.
- 29 Tarkanyi F, Ditroi F, Takacs S, Csikai J, Hermanne A, Uddin, Hagiwara M & Baba M, *Nucl Instr Meth Phys Res B*, 226 (2004) 473.
- 30 Ditroi F, Takacs S, Haba H, Komori Y & Aikawa M, *Nucl Instr Meth Phys Res B*, 385 (2016) 1.
- 31 Ditroi F, Tarkanyi F, Takacs S, Hermanne A, Yamazaki H, Baba M, Mohammadi A & Ignatyuk A V, *Nucl Instr Meth Phys Res B*, 269 (2011) 1963.
- 32 Tarkanyi F, Takacs S, Szelecsenyi F, Ditroi F, Hermanne A & Sonck M, *Nucl Instr Meth Phys Res B*, 252 (2006) 160.
- 33 Savadi V V, Singh D P, Joshi S K, Majeed I, Shuaib Md, Sharma V R, Yadav A, Kumar R, Singh P P, Unnati, Sharma M K, Pandey S, Singh B P & Prasad R, *Nucl Instr Meth Phys Res B*, 479 (2020) 102.
- 34 Savadi Varun V, Singh D P, Joshi S K, Majeed I, Shuaib Md, Sharma V R, Yadav A, Singh P P, Unnati, Sharma M K, Kumar R, Singh B P & Prasad R, *Mater Today*, 17 (2019) 96.
- 35 Savadi Varun V, Singh D P, Joshi S K, Majeed I, Shuaib Md, Sharma V R, Yadav A, Singh P P, Unnati, Sharma M K, Kumar R, Singh B P & Prasad R, *Mater Today*, 17P1 (2019) 266.
- 36 Singh D P, Savadi Varun V, Majeed I, Shuaib Md, Sharma V R, Yadav A, Singh P P, Unnati, Sharma M K, Kumar R, Singh B P & Prasad R, *Indian J Pure Appl Phys*, 57 (2019) 566.
- 37 Nandi S, Reddy J P, Kumar D & Singh K, Springer Nature Singapore Pte Ltd, (2020).
- 38 Viswanathan R & Bakker W, *J Mater Eng Perform*, 10 (2001) 96.
- 39 Yadav A, Singh P P, Sharma M K, Singh D P, Unnati, Singh B P & Prasad R, *Phys Rev C*, 78 (2008) 044606.
- 40 Gardner R P & Verghese K, *Nucl Instr Meth*, 93 (1971) 163.
- 41 Ernst J, Iowski R, Klampfl H, Machner H, T Mayer-Kuckuk & R Schanz, *Z Phys A*, 308 (1982) 301.



Thin Layer Activation analysis in $^{16}\text{O} + ^{169}\text{Tm}$ system at low energies

Varun .V. Savadi¹, D. P. Singh^{1*}, S.K.Joshi¹, Ishfaq Majeed², Md. Shuaib², V. R. Sharma³, A. Yadav⁴, P. P. Singh⁵, Unnati⁶, M. K. Sharma⁷, R. Kumar⁴,
B. P. Singh² and R. Prasad²

¹Department of Physics, University of Petroleum and Energy Studies, Dehradun-248 007, India

²Nuclear Physics Laboratory, Department of Physics, Aligarh Muslim University, Aligarh-202 002, India

³Departamento de Aceleradores, Instituto Nacional Investigaciones Nucleares, Apartado Postal 18-1027, C.P. 11801 Ciudad de Mexico, Mexico

⁴NP-Group Inter University Accelerator Centre, Aruna Asaf Ali Marg, New Delhi-110 067, India

⁵Department of Physics, Indian Institute of Technology Ropar, Rupnagar, Punjab-140 001, India

⁶Department of Physics, University of Delhi, New Delhi-110 067, India

⁷Physics Department, S. V. College, Aligarh-202001, India

Abstract

In this paper authors have explored the use of Thin Layer Activation in a material formed by the irradiation of heavy ion beams on the particular target of interest and its further applications from industrial point of view. Activity depth distributions resulting from the irradiation of Thulium-169 by heavy ion Oxygen-16 beams have been calculated. A pre-calibrated high purity germanium detector was used for radioactive counting of samples. The measured cross-sections for different radio-isotopes have been used to deduce the practical yields for several reaction products; $^{182, 181}\text{Ir}$, $^{182, 181}\text{Os}$, $^{181, 178}\text{Re}$, ^{175}Hf , ^{172}Lu from the intensity of characteristic γ -lines at different energies of ^{16}O beam in the energy range ≈ 70 -100 MeV employing stacked foil activation technique. Calibration curves obtained from various reaction products have been determined with the help of yield curves. The main purpose of this work is to study the surface wear with increased sensitivity by applying heavy ion in thin layer activation technique.

© 2018 Elsevier Ltd. All rights reserved.

Selection and peer-review under responsibility of the scientific committee of the International Conference on Advanced Materials, Energy & Environmental Sustainability, ICAMEES2018

Keywords: Thin layer activation; Activation Technique; Surface loss; Wear; Corrosion; Erosion.

* D.P.Singh Tel.: +91 9927668776

E-mail address: dpsingh19@gmail.com

2214-7853© 2018 Elsevier Ltd. All rights reserved.

Selection and peer-review under responsibility of the scientific committee of the International Conference on Advanced Materials, Energy & Environmental Sustainability, ICAMEES2018

1. Introduction

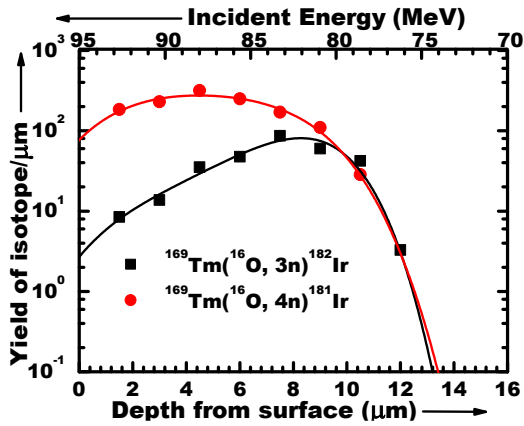
With the recent advancements in the field of science and technology, surface phenomenon such as wear, erosion and corrosion, influencing various industrial applications, are the topics of current interest [1-3]. Thin layer activation (TLA) is one of the important techniques widely used for material performance studies such as wear, corrosion, erosion etc. In this technique, referred as the corrosion monitoring method, a small section of material is exposed to an energetic beam of charged particles, so as to produce the activity surface layer. The measurement of activity in the surface layer of the materials is of prime importance ranging from few tens of nano-meters to several hundreds of micro-meter. Surface loss even in few nano-meters could be a major hindrance for smooth functioning engineering systems in various industries [4]. Accurate and high precision techniques, used to study surface phenomenon, result in considerable savings for industry in general. Various conventional techniques like gravimetric, mechanical, chemical and optical methods are found to have their own limitations in case of practical environments due to limited sensitivity range and time consuming [4-9]. TLA technique is powerful technique which employs a beam of charged particles to a very thin layer (\approx micro-meter) of materials surface. A material surface, of interest, is so chosen and the activity induced in the thin layer of the material surface may be observed [10-20] by monitoring of γ -activity in the thin layer of the material. The activity induced in the material surface using heavy ions will be contained within much narrower thickness as compared to that of light ions leading to higher sensitivity in the measurement of surface wear. Since Thulium-169 bombarded in a nuclear reactor can later serve as a radiation source in portable X-ray devices, it has also found its applications in microwave equipment. Due to its property, fluorescence at low levels, it is also used in personal radiation dosimeters. In the present work attempt has been made to calculate residual activity induced in Thulium-169 materials employing heavy ions of Oxygen-16 from industrial perspective.

2. Experimental Details

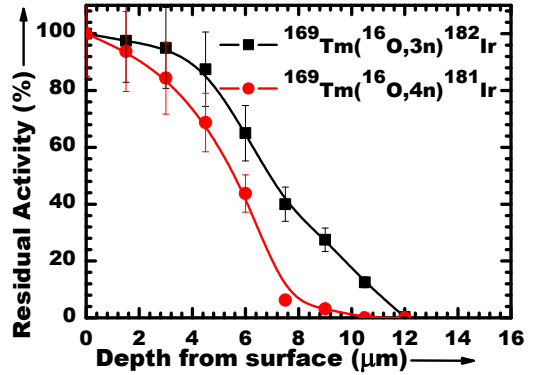
The experiment were performed [21] using a beam of $^{16}\text{O}^{7+}$ delivered from the 15UD-Pelletron Accelerator at the Inter-University Accelerator Centre (IUAC), New Delhi, India. Targets of spectroscopically pure ^{169}Tm ($\approx 99.99\%$) of thickness $\approx 1.5 \text{ mg/cm}^2$ were prepared by rolling technique at the target laboratory of IUAC. To trap the recoiling products produced via different reaction processes, aluminium catchers of appropriate thickness were placed after each target. Irradiations were carried out at energy $\approx 95, 92$ & 87 MeV with a constant beam current $\approx 30\text{-}50 \text{ nA}$ for $\approx 8\text{-}10$ hrs in the general purpose scattering chamber containing in-vacuum transfer facility. The activities produced in the material were recorded using high purity Germanium detector of 100 c.c. active volume coupled to a PC through CAMAC based FREEDOM software. The detector was pre-calibrated with various standard γ -sources, such as ^{60}Co , ^{133}Ba , and ^{152}Eu , of known strengths. In the present work, nuclear reaction cross-sections for several reaction products populated via reaction channels; $^{182}\text{Ir}(3n)$, $^{181}\text{Ir}(4n)$, $^{182}\text{Os}(p2n)$, $^{181}\text{Os}(p3n)$, $^{181}\text{Re}(2p2n)$, $^{178}\text{Re}(\alpha 3n)$, $^{175}\text{Hf}(2\alpha pn)$ & $^{172}\text{Lu}(3\alpha n)$ have been measured in the irradiation of Thulium-169 by Oxygen-16 from threshold ($\approx 70 \text{ MeV}$) to well above it ($\approx 100 \text{ MeV}$). These cross-sections are used for the determination of practical yields and further for the measurement of activity for application in TLA technique.

Table 1. List of final reaction products along with their spectroscopic properties.

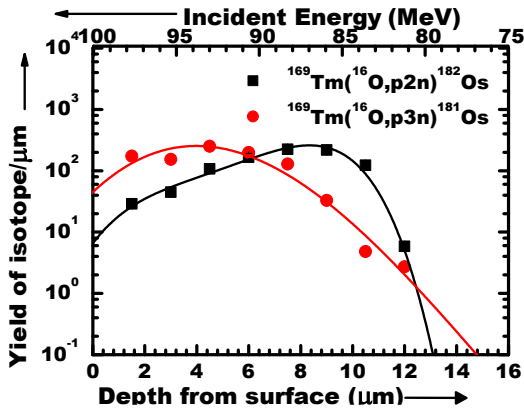
Isotope	Half-Life	γ -ray	
		E_{γ} (keV)	I_{γ} (%)
^{182}Ir	36.8 min	273.1	43
^{181}Ir	23.3 min	107.6	15.9
^{182}Os	6.76 min	180.22	34.7
^{181}Os	12.1 hrs	238.68	44
^{181}Re	16.1 hrs	365.59	57
^{178}Re	8.24 days	237.19	54
^{175}Hf	2.01 days	343.4	87
^{172}Lu	34.06 min	1093.6	63.5



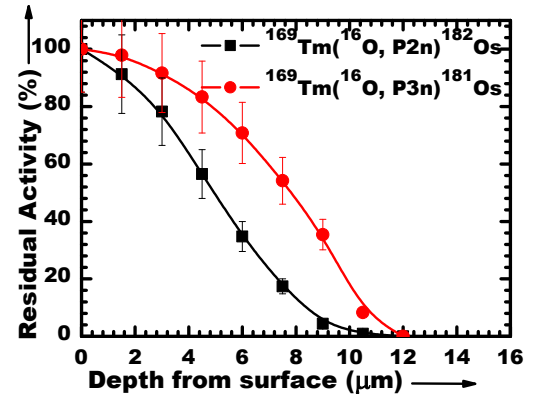
figs 1(a):Yield curves of reaction products $^{182,181}\text{Ir}$



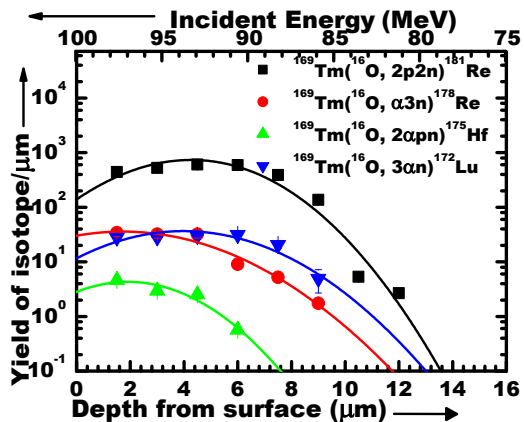
figs 2(a): Calibration curves of reaction products $^{182,181}\text{Ir}$



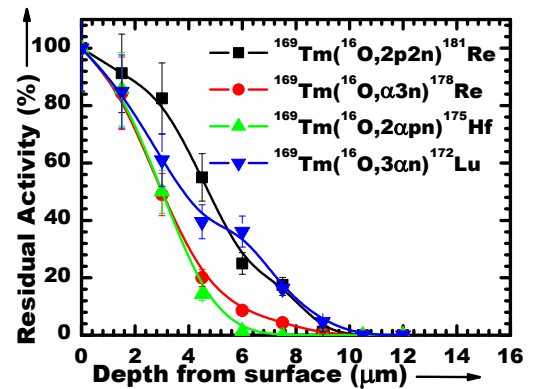
figs 1(b): Yield curves of reaction products $^{182,181}\text{Os}$



figs 2(b): Calibration curves of reaction products $^{182,181}\text{Os}$



figs 1(c): Yield curves of reaction products $^{182,178}\text{Re}$, ^{175}Hf , ^{172}Lu



figs 2(c): Calibration curves of reaction products $^{182,178}\text{Re}$, ^{175}Hf , ^{172}Lu

3. Measurement of activity

3.1. Yield curves

The yield curves of the isotopes; $^{182,181}\text{Ir}$, $^{182,181}\text{Os}$, $^{181,178}\text{Re}$, ^{175}Hf & ^{172}Lu have been obtained from the activity of pure Thulium-169 material, after irradiated by Oxygen-16, populated at different incident energies across different depths of the target material through various reaction channels. The yield curves of the reaction products, is obtained from the activity measurement of the foils and a plot of the yield of the isotope against the depth at which the foil is located. The stopping power of Oxygen-16 has been used to obtain the incident energy on each foil. The total yield can be calculated by integrating the area under the yield curves across different energies ranging from 70-110 MeV. The yield per micron thickness against the depth as well as incident energy for several nuclides is shown in Figures. 1(a-c). In the present work, residual activity of various reaction products populated via various xn, pxn and α xn channels were found to have contribution upto $\approx 14\mu\text{m}$ depth from the surface. The remnant activity induced in the Tm material for several nuclides populated through various xn, pxn and α xn channels are as given in Figures. 2 (a-c).

3.2. Calibration curves

Yield curves have been further used to deduce the activity curves. The residual activities induced, after removal of certain depths of material, have been calculated graphically with the help of obtained yield curves. The calibration curves thus obtained using reaction products, $^{182,181}\text{Ir}$, $^{182,181}\text{Os}$, $^{181,178}\text{Re}$, ^{175}Hf & ^{172}Lu from the plot of percentage of remaining activity against the removal of depth of material and are shown in fig 2(a-c). As a matter of fact, these calibration curves may be considered to correspond to pure metals irradiated with Oxygen-16 of 70-100 MeV

4. Conclusion

The potential use of the TLA technique in measuring the surface loss in materials due to wear has been described with particular reference to Thulium and its reaction products populated through various reaction channels at different energies across different depths from surface. Activity depth distribution calculated using TLA employing heavy ions gives precise estimation of the residual activity induced in the material. Due to its higher sensitivity and accuracy it has clear advantage in studying surface wear of different materials as compared to that of conventional methods being used. With recent availability of accelerators technology, heavy ions coupled with TLA for investigating surface studies for various materials is possible.

Acknowledgements

The authors are grateful to the Director of IUAC, New, Delhi, India, for providing facilities to carry out the experiments. D. P. Singh thanks to SERB-DST for providing financial support through Project No. ECR/2017/000641 under the early Career Research Award.

REFERENCES

- [1] FONTANA, M.G., "Corrosion Engineering", 3rd edition, McGraw Hill Book Company, Singapore (1987).
- [2] Non-destructive testing. December 1974
- [3] I.A.E.A. Report: Real-time nondestructive monitoring of wear and corrosion using the thin layer activation technique. IAEA, Vienna, May (1990).
- [4] J. Datta, J RadioanalNuclChem (2016) 308:329–334
- [5] Blondiaux, G., et. al.: Experiments to establish the optimum beam parameters for wear and corrosion measurements. Report WP9 IDRANAP 13-01/2001, European Commission of Excellence, Bucharest (2001).
- [6] Ziegler, J. F., et. al.: The stopping and range of ions in matter. SRIM – Version 2008.04 (2008).
- [7] D.P. Chowdhury et. al.; Nuclear Instruments and Methods in Physics Research B 103 (1995) 261-266.
- [8] D. P. Chowdhury, et. al.; Radiochim. Acta **99**, 1–7 (2011)
- [9] Devendra P. Singh, et. al.; Journal of Nuclear Physics, Material Sciences, Radiation and Applications (JNPMSRA) Vol. 1, No. 1 August 2013 pp. 13–24
- [10] A. Niiler, et. al.: Nucl. Instrum. Methods **138**, 179 (1976).
- [11] P. Leterrible, et. al.: Nucl. Instrum. Methods B **10/11**, 1054 (1985).
- [12] W. Scharfet. al.: Nucl. Instrum. Methods B **22**, 573 (1987).
- [13] T. Kosakoet. al.: Nucl. Instrum. Methods B **40/41**, 587 (1989).
- [14] M. Bouchacourtet. al.: Nucl. Instrum. Methods B **40/41**, 1199 (1989).
- [15] W. Neumannet. al.: Nucl. Instrum. Methods B **45**, 126 (1990).
- [16] B. Constantinescu et. al.: Nucl. Instrum. Methods B **89**, 83 (1994).
- [17] C. Stan-Sionet. al.: Nucl. Instrum. Methods B **93**, 326 (1994).
- [18] P. M. Racoltaet. al.: Nucl. Instrum. Methods B **127/128**, 949 (1997).
- [19] G. Laguzziet. al.: J. Radioanal. Nucl. Chem. **262**, 325 (2004).
- [20] F. Ditroi, S. Takacset. al.: Wear **261**, 1397 (2006).
- [21] Devendra P. Singh et. al.; Investigation of the role of break-up processes on the fusion of ^{16}O induced reactions; Physical Review C **80**, 014601 (2009).



Activity measurement in Terbium-159 material using heavy ion beams

D. P. Singh^{1*}, Varun.V. Savadi¹, S.K.Joshi¹, Ishfaq Majeed², Md. Shuaib², V. R. Sharma³, A. Yadav⁴, P. P. Singh⁵, Unnati⁶, M. K. Sharma⁷, R. Kumar⁴, B. P. Singh² and R. Prasad²

¹Department of Physics, University of Petroleum and Energy Studies, Dehradun-248 007, India

²Nuclear Physics Laboratory, Department of Physics, Aligarh Muslim University, Aligarh-202 002, India

³Departamento de Aceleradores, Instituto Nacional Investigaciones Nucleares, Apartado Postal 18-1027, C.P. 11801 Ciudad de Mexico, Mexico

⁴NP-Group Inter University Accelerator Centre, Aruna Asaf Ali Marg, New Delhi-110 067, India

⁵Department of Physics, Indian Institute of Technology Ropar, Rupnagar, Punjab-140 001, India

⁶Department of Physics, University of Delhi, New Delhi-110 067, India

⁷Physics Department, S. V. College, Aligarh-202001, India

Abstract

Experiment has been performed to study the activity produced in the irradiation of Terbium-159 material with Oxygen-16 heavy ion beams using thin layer activation technique. The yields of reaction products $^{172,171,170}\text{Ta}$, $^{171,170}\text{Hf}$ and $^{171,170,169}\text{Lu}$ populated via various reaction channels have been measured in the Coulomb barrier to the well above it. A pre-calibrated high purity germanium detector has been used for γ -counting of material. The yield curves obtained from the study of intensity of characteristics γ -lines at different energies of heavy ion beam have been further used to determine the calibration curves of the obtained reaction products. An attempt has been made to study surface wear in terbium by applying heavy ion thin layer activation technique with increased sensitivity.

© 2018 Elsevier Ltd. All rights reserved.

Selection and peer-review under responsibility of the scientific committee of the International Conference on Advanced Materials, Energy & Environmental Sustainability, ICAMEES2018

Keywords: Thin layer activation; Activation Technique; Surface loss; Wear; Corrosion; Erosion.

* D.P.Singh Tel.: +91 9927668776

E-mail address: dpsingh19@gmail.com

© 2018 Elsevier Ltd. All rights reserved.

Selection and peer-review under responsibility of the scientific committee of the International Conference on Advanced Materials, Energy & Environmental Sustainability, ICAMEES2018

1. Introduction

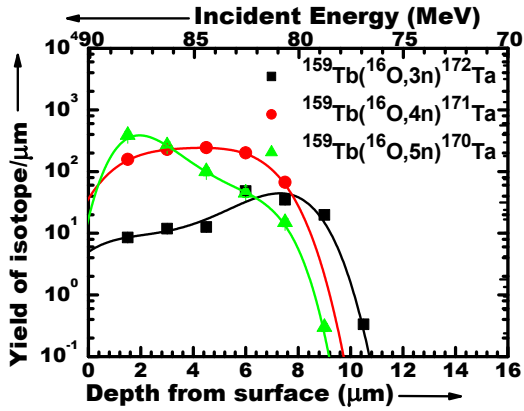
Industries such as Chemical processing plants, Thermal power plants, Nuclear power plants & Reactors and heavy equipment are substantially influenced by surface phenomenon such as wear, erosion and corrosion [1]. Due to extreme working conditions and larger impact in case of failure, monitoring and safety becomes priority. Over the last few decades, many new and improvised tools and techniques have evolved for studying surface performance occurring in different materials. Amongst the various methods available, Thin layer activation (TLA) technique has much greater potential due to its increased sensitivity [2,3]. Surface degradation process such as corrosion, erosion and wear are studied by TLA method in which several reaction products of interest may be utilised [4]. The principle basis of TLA is the creation of appropriate reaction products in a given material at a well-defined depth over a selected area. Light ion beams like proton, deuteron, ^3He or ^4He particles etc., of suitable energy [5-7] are generally used to populate a thin layer of activities ranging from several micro-meters to a few hundred micro-meters. With the advent of Heavy ion accelerators, it has now been possible to study the surface wear studies in different materials of interest using heavy ion reactions [8-18]. Since terbium is being used in solid state devices applied in nuclear plants; low energy light bulbs and mercury lamps; in medical X-ray imaging with reduced exposure time and also in laser devices in the form of terbium salts, we have considered this material for study over different energy ranges.

2. Experimental Details

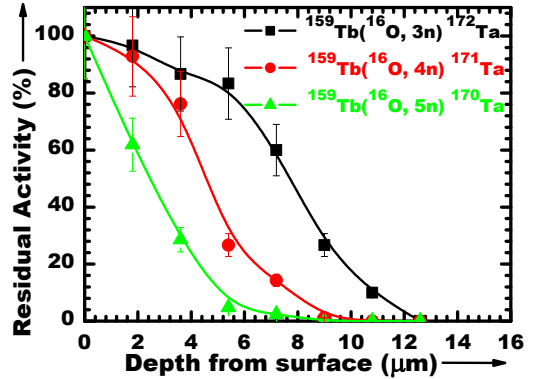
Experiment were performed [19] using Oxygen-16 beams delivered from the Pelletron Accelerator at the Inter-University Accelerator Centre (IUAC), New Delhi, India. Targets of spectroscopically pure ^{159}Tb ($\approx 99.99\%$) of thickness $\approx 1.8 \text{ mg/cm}^2$ were prepared at the target laboratory of IUAC, using the rolling technique. To trap the recoiling products produced via different reaction processes. Required thickness of aluminium to be used as energy degraders was computed from stopping power data using SRIM (2008 Version). Irradiations were carried out at energies of ≈ 90 and 95 MeV with a constant beam current $\approx 50 \text{ nA}$ for ≈ 10 hrs in the General Purpose Scattering Chamber, which has an in-vacuum transfer facility. The activities produced after irradiation was recorded using High Purity Germanium (HPGe) detector calibrated with various standard gamma sources. Various reaction residues were identified by detecting their characteristic γ -lines. A list of identified residues and their spectroscopic properties are shown in Table 1. In the present work, reaction cross-sections for several reaction products populated via different reaction channels; $^{172}\text{Ta}(3n)$, $^{171}\text{Ta}(4n)$, $^{170}\text{Ta}(5n)$, $^{171}\text{Hf}(p3n)$, $^{170}\text{Hf}(p4n)$, $^{171}\text{Lu}(2p2n)$, $^{170}\text{Lu}(\alpha n)$, $^{169}\text{Lu}(\alpha 2n)$ & $^{165}\text{Tm}(2\alpha 2n)$ have been measured in $^{16}\text{O}+^{159}\text{Tb}$ system from threshold ($\approx 70 \text{ MeV}$) to well above it ($\approx 100 \text{ MeV}$). Cross-sections obtained for various isotopes populated through various reaction channels across different energies are used to calculate the total yield and residual activity induced for application in thin layer activation technique.

Table 1. List of final reaction products along with their spectroscopic properties.

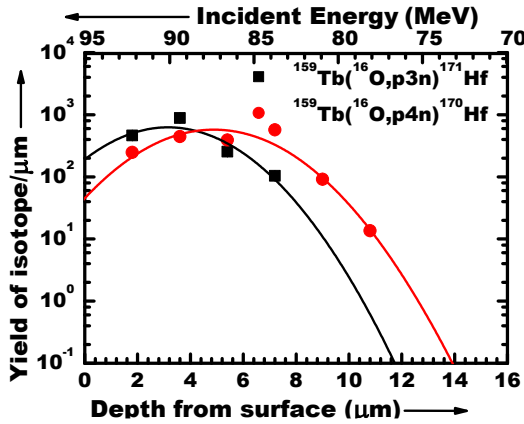
Isotope	Half-Life	γ -ray	
		E_γ (keV)	I_γ (%)
^{172}Ta	36.8 min	875.3	22
^{171}Ta	23.3 min	723.3	25
^{170}Ta	6.76 min	860.2	25
^{171}Hf	12.1 hrs	1076.5	40
^{170}Hf	16.1 hrs	620.7	18
^{171}Lu	8.24 days	631.2	24
^{170}Lu	2.01 days	1280.10	23
^{169}Lu	34.06 min	1037.13	23



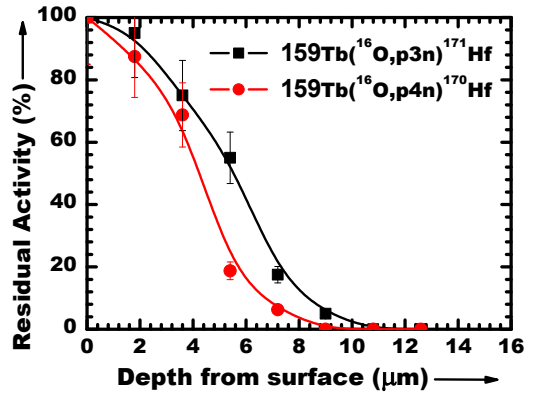
figs 1(a): Yield curves of reaction products $^{172,171,170}\text{Ta}$



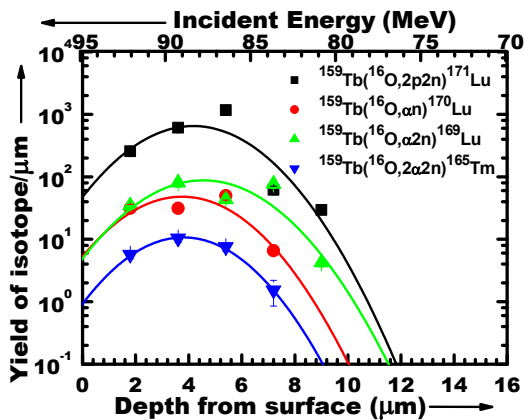
figs 2(a): Calibration curves of reaction products $^{172,171,170}\text{Ta}$



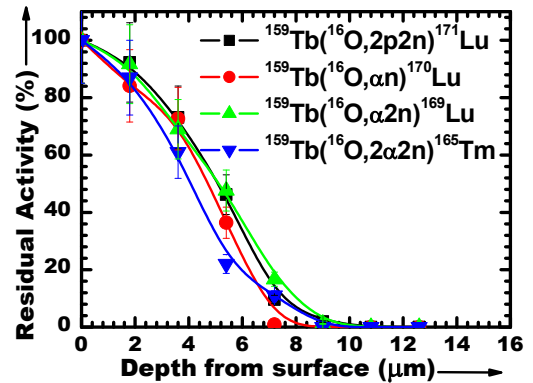
figs 1(b): Yield curves of reaction products $^{171,170}\text{Hf}$



figs 2(b): Calibration curves of reaction products $^{171,170}\text{Hf}$



figs 1(c): Yield curves of reaction products $^{171, 170, 169}\text{Lu}, ^{165}\text{Tm}$



figs 2(c): Calibration curves of reaction products $^{171, 170, 169}\text{Lu}, ^{165}\text{Tm}$

3. Measurement of activity

3.1. Yield curves

The yield curves of the isotopes, i.e., the variation of yield against the depth from the surface, are generated by a stacked-foil irradiation using thin metal foils. The yield of the isotopes produced in each foil of the stack is obtained from the activity measurement of the foils and a plot of the yield of the isotope against the depth at which the foil is located generates the yield curve. The activities induced in each foil of the stack were used to deduce the yields of the isotopes of interest. The stopping power of ^{16}O beams has been used to obtain the incident energy on each foil. The yields of $^{172,171,170}\text{Ta}$, $^{171,170}\text{Hf}$, $^{171,170,169}\text{Lu}$ and ^{165}Tm isotopes have been obtained, from the intensity of characteristic γ -lines, at different energies of Oxygen-16 beams, i.e., at different depths from the experiment carried out for the measurement of the cross-sections of the reactions. The yield per micron thickness against the depth as well as incident energy for several nuclides is shown in Figures. 1(a-c). In order to compute the net yield of a particular isotope in the thick material by the absorption of Oxygen-16 beams, the integral area of the curve from the front surface to the final depth from where the given isotope production starts (threshold of reaction) has been obtained. As can be seen from these figures, the different isotopes of a given element have different yields depending on the reaction channel and the Q-value for the reaction. The area under the curves gives the total yield of the isotope generated in the thick target by absorption of energetic Oxygen beams. In the present work, residual activity of radio-isotopes populated via various xn, pxn and α xn channels were found to have contribution upto $\approx 13\mu\text{m}$ depth from the surface. The remnant activity induced in the target Tb material for several nuclides populated through various xn, pxn and α xn channels are as represented in Figures. 2 (a-c).

3.2. Calibration curves

The total yield of the isotope in the given material may be obtained from the integral area under the yield curves. As can be seen from Figs.1(a-c), the percentage of the remaining activity after the removal of certain thickness of material is then computed by fitting a polynomial function to the yield curve and then applying integration to the polynomial function as per removal of depth of material from the surface. The calibration curve is then obtained by plotting the percentage of the remaining activity against the depth of material removed from the surface and the calibration curves so deduced from the yield curves are shown in Figs. 2(a-c). As a matter of fact, these calibration curves may be considered to correspond to pure metals bombarded with Oxygen ion of 70-100 MeV.

4. Conclusion

Thin layer activation technique is one of the important nuclear techniques based on the production of a radioisotope in the surface of a material by a charged particle induced nuclear reaction, followed by an estimation of the loss of the activity which is a measure of the surface loss of materials in the range of nanometer to hundreds of micrometer in the fields of wear, corrosion or erosion. The technique has been found to be a very useful tool in the basic scientific research and industrial applications. Its sensitivity, potentiality, capability, adaptability and versatility in metallic and non-metallic materials have been established by numerous reported works to date. Therefore, a database compilation of reliable cross sections of nuclear reactions will be highly useful for generation of calibration curves for TLA applications. In the present work an attempt has been made to develop the TLA technique using ^{16}O incident beam to determine the surface wear in the micron order in Ta material. The calibration curves with percentage of residual activity against the removal of thickness may be utilized to investigate surface wear of materials used in various industrial applications. The investigations of surface wear data of such materials used in power reactors and other applications are useful from point of view operational performance and safety of nuclear power plants.

Acknowledgements

The authors are grateful to the Director of IUAC, New, Delhi, India, for providing facilities to carry out the experiments. D. P. Singh thanks to SERB-DST for providing financial support through Project No. ECR/2017/000641 under the early Career Research Award.

REFERENCES

- [1] FONTANA, M.G., “Corrosion Engineering”, 3rd edition, McGraw Hill Book Company, Singapore (1987).
- [2] I.A.E.A. Report: Real-time nondestructive monitoring of wear and corrosion using the thin layer activation technique. IAEA, Vienna, May (1990).
- [3] O. Lacroix: Nuclear Instruments and Methods in Physics Research A 369 (1996) 427-430
- [4] Ziegler, J. F., et. al.: The stopping and range of ions in matter. SRIM – Version 2008.04 (2008).
- [5] D.P. Chowdhury et. al.; Nuclear Instruments and Methods in Physics Research B 103 (1995) 261-266
- [6] D. P. Chowdhury, et. al.; Radiochim. Acta **99**, 1–7 (2011)
- [7] Devendra P. Singh, et. al.; Journal of Nuclear Physics, Material Sciences, Radiation and Applications (JNPMSRA) Vol. 1, No. 1 August 2013 pp. 13–24
- [8] A. Niiler, et. al.: Nucl. Instrum. Methods **138**, 179 (1976).
- [9] P. Leterrible, et. al.: Nucl. Instrum. Methods B **10/11**, 1054(1985).
- [10] W. Scharf et. al.: Nucl. Instrum. Methods B **22**, 573(1987).
- [11] Kosako, T., Nishimura, K.: Nucl. Instrum. Methods B 40/41, 587(1989).
- [12] Bouchacourt, M., Marsigne, C., Dubail, A., Blondiaux, G., De-brun, J. L.: Nucl. Instrum. Methods B 40/41, 1199 (1989)
- [13] Neumann, W., Stalder, C.: Nucl. Instrum. Methods B 45, 126(1990).
- [14] B. Constantinescu et. al.: Nucl. Instrum. Methods B **89**, 83 (1994).
- [15] C. Stan-Sionet. al.: Nucl. Instrum. Methods B **93**, 326 (1994).
- [16] P. M. Racolta et. al.: Nucl. Instrum. Methods B **127/128**, 949 (1997).
- [17] G. Laguzziet. al.: J. Radioanal. Nucl. Chem. **262**, 325 (2004).
- [18] F. Ditroi, S. Takacset. al.: Wear **261**, 1397 (2006).
- [19] Devendra P. Singh et. al.; Investigation of the role of break-up processes on the fusion of ^{16}O induced reactions; Physical Review C 80, 014601 (2009).

Thin layer activation analysis of ^{16}O induced reactions for surface wear studies in some natural isotopes

Varun Vijay Savadi^a, Ishfaq Majeed^b, Mohd Shuaib^b, Vijay Raj Sharma^c,

Abhishek Yadav^d, Devendra P Singh^{a*}, Pushpendra P Singh^e, Unnati^f,

Manoj Kumar Sharma^g, Rakesh Kumar^d, B P Singh^b & R Prasad^b

^aDepartment of Physics, University of Petroleum and Energy Studies, Dehradun 248 007, India

^bNuclear Physics Laboratory, Department of Physics, Aligarh Muslim University, Aligarh 202 002, India

^cDepartamento de Aceleradores, Instituto Nacional Investigaciones Nucleares,

Apartado Postal 18-1027, C.P. 11801 Ciudad de Mexico, Mexico

^dNP-Group Inter University Accelerator Centre, Aruna Asaf Ali Marg, New Delhi 110 067, India

^eDepartment of Physics, Indian Institute of Technology Ropar, Rupnagar 140 001, India

^fDepartment of Physics, University of Delhi, New Delhi 110 067, India

^gPhysics Department, S V College, Aligarh 202 001, India

Received 8 April 2019

In the present work, the residual activity induced in ^{181}Ta targets bombarded with ^{16}O beam in the energy range ≈ 70 -100 MeV have been measured. Stacked foil activation has been employed to measure the cross-sections of the several radio-isotopes populated through different nuclear reaction across various energies. Yields of the radio-isotopic products such as $^{194,193,192}\text{Tl}$, $^{193,192}\text{Hg}$, $^{192,191,190}\text{Au}$ have been obtained with the help of the characteristic γ -lines. Further, calibration curves are deduced by observing remnant activity induced across different depths in the target material. As a result an attempt has been made to employ thin layer activation technique with increased sensitivity for the study of surface wear.

Keywords: Activation technique, Thin layer activation, Surface loss, Ion beam nuclear reaction, Corrosion, Erosion

1 Introduction

Over the past decades many methods have been developed for investigation of surface phenomenon such as wear, corrosion and erosion in different materials. Thin layer activation (TLA) like gravimetry, metallography, electrical resistance etc. are some of the conventional techniques which are still in practice^{1,2}. However, it is difficult to make in-situ applications of these conventional methods when the structures are too big or are not easily accessible. A desirable technique is still in need in case of complex structures which can produce radioactivity in confined parts without affecting the ongoing operations². TLA technique is one of the most extensively used methods nowadays, since it measures radio-activities at very shorter depths in material more precisely. It can be achieved using beams of light ions like proton, deuteron and alpha particles³⁻⁵. The principle of TLA usually involves activation of desired

radio-isotopic nuclide in the material of interest at required depths and selected area^{6,7}. With the advent and availability of heavy ion accelerators, it is now possible to produce heavy ion beams like ^{12}C , ^{14}N and ^{16}O etc. Range of activity induced using TLA may vary from micrometers to nanometers depending upon the types of incident beam and materials used⁸⁻¹⁸. The sensitivity of TLA technique is high due to the capability of low level radio-activity measurement performed by gamma spectrometry. With the help of such sensitive and effective methods one can detect, measure and monitor the surface phenomenon more precisely. Tantalum is widely used in many industrial applications as an important construction material being highly anti-corrosive and inert to most of acid attacks. Further, it is also used in making capacitors and transistors alongwith medicinal applications such as dental, surgical instruments and implants without affecting the immune system¹⁹⁻²⁰. By employing TLA technique with heavy ions beams, we have made an attempt to study the surface activity induced in

*Corresponding author (E-mail: dpsingh19@gmail.com)

tantalum material. Nuclear energy from fusion is one of the key forms to fulfil the ever increasing demand with almost negligible green house effects. Since tantalum is an important material not only for the fission reactor but also for fusion reactors as well, we have chosen it as a material for analysis in the present work.

2 Experimental Details

Experiments were carried out²¹ using 15 UD-Pelletron tandem van-de-graaf type accelerator at the Inter University Accelerator Centre (IUAC), New Delhi, India. Heavy ion oxygen beam with charge state of 7^+ was projected on tantalum targets. Targets of spectroscopically pure 99.99% tantalum of ≈ 1.5 mg/cm^2 thickness were prepared using rolling technique at target laboratory. Tantalum targets were irradiated for about 8-10 hrs with three different beam energies *viz.* 100, 98 and 88 MeV with a constant current of ≈ 50 nA in the general purpose scattering chamber (GPSC) consisting in-vacuum transfer facility. The activities produced after irradiation were recorded using a pre-calibrated (with various standard γ -sources, such as ^{60}Co , ^{133}Ba , and ^{152}Eu , of known strengths), High purity germanium (HPGe) detector of 100 c.c. active volume coupled to a PC through CAMAC based FREEDOM software. The various radio isotopes populated through various reaction channels have been identified using gamma spectroscopy through characteristic γ -lines followed by decay curve analysis. In Table 1 the reaction residues populated with various reaction channels xn, pxn and α xn etc. have been listed along with spectroscopic properties. The cross sections of various reaction products for the $^{16}\text{O} + ^{181}\text{Ta}$ system are measured in energy range 70 MeV - 100 MeV. Practical yields have been obtained using these cross sections and further applied in TLA for measuring the activity induced.

Table 1 – List of final reaction products along with their spectroscopic properties.

Isotope	Half-life	E_γ (keV)	I_γ (%)
^{192}Tl	10.8 m	422.9	31.1
^{193}Tl	21.6 m	365, 244	90.1, 15.2,
^{194}Tl	33 m	636.1	99
^{192}Hg	4.85 h	274.8	50.4
^{193}Hg	3.8 h	381.6, 861.1	11.0, 13.0
^{190}Au	42.83m	295.9, 301.9	71.0, 25.1
^{191}Au	3.18 h	283.9, 399.8	6.3, 4.5
^{192}Au	4.94 h	295.5, 316.5	22.7, 58.0

3 Measurement of Cross-Section

3.1 Yield curves

Measured cross-sections for various reaction products by activation ion technique have been used to obtain yield curves. Plot for variation of yield against the depth from the surface has been obtained for generating the yield curves. Incident energy on each foil has been calculated using stopping power of ^{16}O beams. The yields of different isotopes obtained from the intensity of characteristic γ - lines are $^{194,193,192}\text{Tl}$, $^{193,192}\text{Hg}$ and $^{192,191,190}\text{Au}$ across different energies and varying depths are plotted in Fig. 1.

Nuclides shown in Figs 1(a-c) represent the variation of yield per micron thickness against the depth as well as incident energy. The yield curve

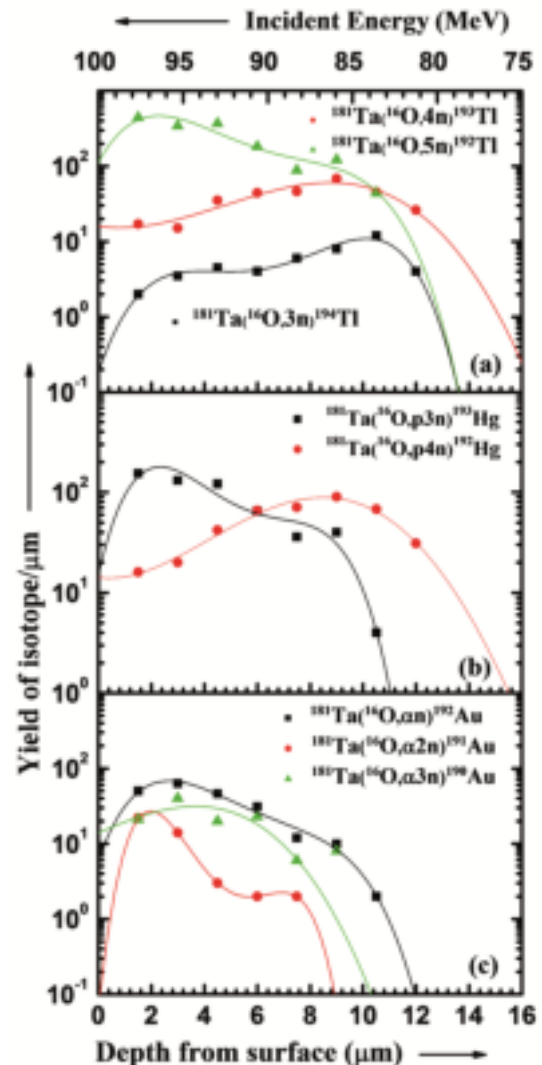


Fig. 1 – Yield curves of isotopes (a) $^{194,193,192}\text{Tl}$ (b) $^{193,192}\text{Hg}$ & (c) $^{192,191,190}\text{Au}$ from Ta material.

represents the yield of an isotope per unit thickness at a certain depth of the metal. Integral area of the curve from the front surface to the final depth from where the given isotope production starts (i.e., threshold of reaction) has been utilised to compute the net yield of particular isotope in the thick target by absorption of ^{16}O induced beams. It can be seen from Figs 1(a-c) depending on the Q-value and various reaction channels the yields of different isotopes are also different. The area under the curves gives the total yield of the isotope generated in the thin target by absorption of energetic ^{16}O beams. In the present work, residual activity of radio-isotopes populated via various xn, pxn and α xn channels were found to have contribution up to $\approx 12\ \mu\text{m}$ depths from the surface.

3.2 Calibration curves

The integral area under the yield curves gives the total yield of the isotopes. Fig. 2(a-c) represents the

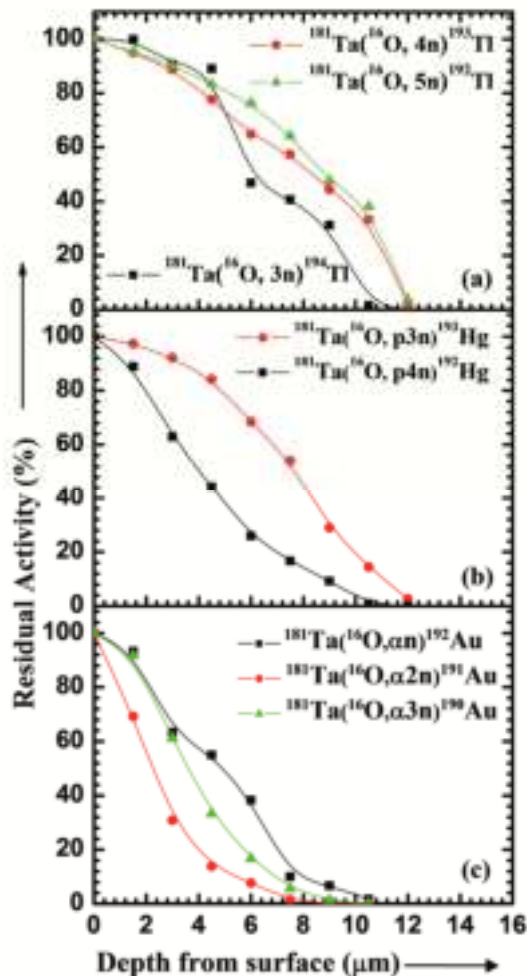


Fig. 2 – Calibration curves of isotopes (a) $^{194,193,192}\text{Tl}$ (b) $^{193,192}\text{Hg}$ & (c) $^{192,191,190}\text{Au}$ from Ta material.

total residual activity induced in material. It can be seen from the figure that various points have been obtained at regular intervals of increasing depth along with the reduced activity. The remnant activity induced is then computed by fitting a polynomial function to the yield curve after removal of certain thickness and then by applying integration to the polynomial function with respect to depth of material removed from the surface. Plot of percentage of remaining activity against the depth of material removed from the surface gives calibration curves as shown in Fig. 2(a-c). As a matter of fact, these calibration curves may be considered to correspond to pure metals bombarded with ^{16}O ion of 70-100 MeV.

4 Conclusions

Sensitivity of TLA technique is very high compared to conventional methods. Any small amount of γ -activity can be easily detected without making any changes in ongoing operation. Due to its high sensitivity and precision it can be applied to monitor loss of materials under real operation conditions. The precision range using TLA technique may vary from few nanometers to hundreds of micrometers in the fields of wear, corrosion or erosion. Most of industrial applications involve working parameters such as pressure and temperature especially process industries. Since, temperature and pressure being intensive property and γ -emission remaining unaffected with these parameters TLA can be easily employed in various industries. Its sensitivity, potentiality, capability, adaptability and versatility in metallic and non-metallic materials have been established by numerous reported works to date. Therefore, a database compilation of reliable cross sections of nuclear reactions will be highly useful for generation of calibration curves for TLA applications. In the present work an attempt has been made to develop the TLA technique using ^{16}O incident beam to determine the surface wear in the micron order in Ta material. With the help of calibration curves and residual activity induced one can easily estimate the surface phenomenon process such as wear, corrosion or erosion of materials used for construction in various industrial applications. Failure in detection of even a small amount of loss of material due to surface phenomenon in industries like nuclear, process and heavy machineries could lead to catastrophic losses. A highly precise and sensitive technique like TLA can be employed in such conditions to investigate the surface phenomenon.

Acknowledgement

The authors are grateful to the Director of IUAC, New, Delhi, India, for providing facilities to carry out the experiments. DPS thanks DST for providing financial support through Project No. ECR/2017/000641 under the early career research award.

References

- 1 FONTANA M G, Corrosion Engineering, 3rd Edn, McGraw Hill Book Company, Singapore (1987).
- 2 I A E A, Real-time non-destructive monitoring of wear and corrosion using the thin layer activation technique, IAEA, Vienna, (1990).
- 3 Chowdhury D P, Datta J, Reddy A V R & Dasgupta S, *Nucl Instr Meth Phys Res B*, 103 (1995) 261.
- 4 Chowdhury D P, Datta J & Reddy A V R, *Radiochim Acta*, 99 (2011) 1.
- 5 Singh D P, Sharma V R, Yadav A, Singh P P, Unnati, Sharma M K, Singh B P & Prasad R, *J Nucl Phys*, 1 (2013).
- 6 Blondiaux G, Dragulescu E, Racolta P M & Stroosnijder R, *Experiments to establish the optimum beam parameters for wear and corrosion measurements*, Report WP9 IDTRANAP 13-01/2001, European Commission of Excellence, Bucharest (2001).
- 7 Ziegler J F, Ziegler M D & Biersack J P, *The stopping and range of ions in matter*, SRIM – Version 2008 (2008) 04.
- 8 Niiler A & Stephen E, *Nucl Instr Meth*, 138 (1976) 179.
- 9 Leterrible P, Blondiaux G, Valladon M, Debrun J L, Ducreux M & Guerrand M, *Nucl Instr Meth, B*, 10/11 (1985) 1054.
- 10 Scharf W & Andrzej N, *Nucl Instr Meth B*, 22 (1987) 573.
- 11 Kosako & Kazuo N, *Nucl Instr Meth B*, 40 (1989) 587.
- 12 Bouchacourtet M, Marsigne C, Dubail A, Blondiaux G & Debrun J L, *Nucl Instr Meth B*, 40/41 (1989) 1199.
- 13 Neumann W & Michel R, *Nucl Instr Meth B*, 45 (1990) 126.
- 14 Constantinescu B, Vasilescu A, Radtke M & Reinholz U, *Nucl Instr Meth B*, 89 (1994) 83.
- 15 Stan-Sion C, Huggle, Nolte E, Blinov A & Dumitru M, *Nucl Instr Meth B*, 93 (1994) 326.
- 16 Racolta P M, Popa-Simil L & Alexandreanu B, *Nucl Instr Meth B*, 127/128 (1997) 949.
- 17 Laguzzi G, Luvidi L, De Cristofaro N & Stroosnijder M F, *J Radioanal Nucl Chem*, 262 (2004) 325.
- 18 Ditroi F, Mahunka I, Takacs S & Seif E N, *Wear*, 261 (2006) 1397.
- 19 <https://www.titanmf.com/technical-resources/>
- 20 Tantalum Chemicool Periodic Table, Chemicool.com.
- 21 Singh D P, Unnati, Singh Pushpendra P, Yadav A, Sharma M K, Singh B P, Golda K S, Kumar Rakesh, Sinha A K & Prasad R, *Phys Rev C*, 80 (2009) 014601.



PLAGIARISM CERTIFICATE

1. We **Dr D. P. Singh** (Internal Guide), **Dr Shyam Pandey** (Co Guide/ External Guide) certify that the Thesis titled Investigation of "**Thin Layer Activation Studies in Strategically Important Rare Earth Materials**" submitted by Scholar **Mr Varun Vijay Savadi** having **SAP ID 500073886** has been run through a Plagiarism Check Software and the Plagiarism Percentage is reported to be **7%**.
2. Plagiarism Report generated by the Plagiarism Software is attached.

A handwritten signature in blue ink, appearing to read 'D. P. Singh', with a horizontal line underneath.

Signature of the Internal Guide

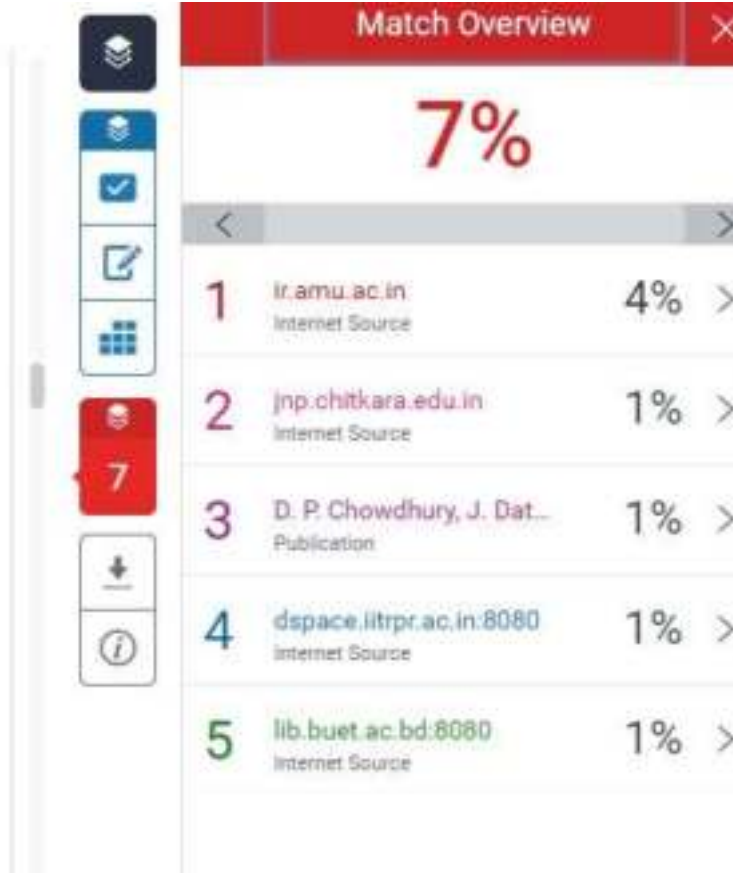
A handwritten signature in green ink, appearing to read 'Shyam Pandey', with a horizontal line underneath.

Signature of External Guide/Co Guide

A handwritten signature in black ink, appearing to read 'Varun Savadi', with a horizontal line underneath.

Signature of the Scholar

similar manner to Van-de Graff generators. Accelerator at IUAC is also known as Tandem Accelerator due to additional feature of utilizing its accelerating voltage twice before the particles interact with material. **Once the terminal is fully charged to high voltage,** any appropriate ion beam can be used to accelerate. Figure 3.1 is a schematic representation of the Pelletron accelerator. Working of acceleration of particles through Pelletron can be understood as follows [1-3].



Match Overview		
7%		
<hr/>		
1	ir.amu.ac.in Internet Source	4% >
2	jnp.chitkara.edu.in Internet Source	1% >
3	D. P. Chowdhury, J. Dat... Publication	1% >
4	dspace.iiitpr.ac.in:8080 Internet Source	1% >
5	lib.buet.ac.bd:8080 Internet Source	1% >